Catalytic Wet Air Oxidation of Phenol in a Trickle Bed Reactor: Kinetics and Reactor Modelling

Dissertation presented by

Athanasios Eftaxias

To obtain the degree:
Doctor in Chemical Engineering
of the Rovira i Virgili University

Escola Tècnica Superior de Enginyeria Química
Departament d'Enginyeria Química
Universitat Rovira i Virgili
Tarragona

December 2002

Universitat Rovira i Virgili
Escola Tècnica Superior d'Enginyeria Química

Catalytic Wet Air Oxidation of Phenol in a Trickle Bed Reactor: Kinetics and Reactor Modelling

Memoria presentada por

Athanasios Eftaxias

para optar al Grado de
Doctor en Ingeniería Química

Tesis dirigida por el Dr. Frank Stüber

Miembros tribunal de tesis

Presidente Dr. Manel Poch
Secretario Dr. Jaume Jiralt
Vocales
Dr. Fernando Beltran
Dr. Henri Delmas
Dr. Faical Larachi
Suplentes
Dr. Josep Font
Dr. Agusti Fortuny

Evaluadores externos (Doctorado Europeo)
Dra. Isabelle Polaert
Dra. Styliani Agatzini-Leonardou

Diciembre 2002

El Dr. Frank Stüber, Professor Titular del Departament d'Enginyeria Química de l'Escola Tècnica Superior d'Enginyeria Química, de la Universitat Rovira i Virgili de Tarragona,

Faig constar que el present treball, amb el títol

CATALYTIC WET AIR OXIDATION OF PHENOL IN A TRICKLE BED REACTOR: KINETICS AND REACTOR MODELLING,

que presenta el doctorand n' ATHANASIOS EFTAXIAS per optar al grau de Doctor en Enginyeria Química, ha estat dut a terme sota la meva immediata direcció, i que tots els resultats obtinguts són fruit del treball i l'anàlisi realitzat per l'esmentat doctorand.

I per a què es faci saber i tingui els efectes que correspongui, signo aquesta certificació.

Tarragona, 2 decembre de 2002

Dr. Frank Stüber
Professor Titular d'Enginyeria Química

Acknowledgements

This work owes a lot to the ideas, suggestions, help and encouragement of many people, to whom I would like to express my sincere gratitude.

In the first place, to my supervisor Dr. F. Stüber for his patience, guidance and critical spirit through out this time. Definitely, I will miss his questions and observations from now on.

Within the Chemical Reaction Engineering & Process Intensification Group, to Dr. J. Font who, through numerous discussions, clarified many of my doubts. Furthermore, to Dr. A. Fortuny, who helped me to overcome many laboratory obstacles and to Dr. A. Fabregat who has been attendant to provide the material support necessary for the realisation of this work.

I am also indebted to Dr. F. Larachi for his attention and hospitality during and beyond my visit at his research group. His advice has been highly appreciated.

I would also like to acknowledge the kindness of Dr. M. Poch, Dr. J. Giralt, Dr. F. Beltran, Dr. H. Delmas and Dr. F. Larachi, for accepting to participate in the examining committee of this PhD. thesis, as well as Dr. J. Font and Dr. A. Fortuny who are the substitute members of the committee. Also I am thankful to Dr. I. Polaert and Dr. S. Agatzini for accepting to elaborate the reports that enabled this work to opt for European PhD. award, and for their comments regarding the manuscript.

Of course I cannot forget of my *classmates*. In the first place those with whom I shared laboratory, G. Sahin, M. Paradowska (and her nordic spirit), and M.E. Suarez, or office Dr. A. Morato, A. Manyes and X. Rodríguez. Although we have often discussed about pumps during the coffee break, not always we were drinking coffee and not always we were talking about pumps.

Also I would like to mention those people that still ask me "when are you going to be around?" : Bassilis, Stelios, Xristos, Giorgos, Argiris and also Demitris and Giannis.

Evidently, my brothers and my parents are also asking the same question. Their encouragement has been very important for me.

Last, but not least, Silvia, Tarragona would not have been so pleasant without her.

Resumen

El tratamiento y el reciclaje de efluentes acuosos es de máximo interés para conseguir un desarrollo sostenible de las actividades humanas. La necesidad de aprovechar en un futuro cercano las aguas residuales de procesos industriales de un modo eficaz ha reforzado la investigación sobre métodos de bajo coste para su recuperación, dado que las tecnologías existentes ya no son universalmente aplicables. La oxidación catalítica por vía húmeda (CWAO) es uno de los procesos emergentes más prometedores particularmente para el tratamiento de aguas contaminadas con materia orgánica, en concentraciones medio altas, y/o biotóxica. Sin embargo, la implementación del método es adecuada siempre que se use un catalizador activo y estable. Con este propósito, la actividad catalítica y la estabilidad del carbón activo se ha comprobado en la CWAO usando como compuesto modelo el fenol. En condiciones de temperatura y presión moderadas el carbón activo ha demostrado ser un material catalítico barato, que a la vez, es estable, mas activo en la conversión de fenol, además produciendo menor cantidad de productos de oxidación parcial tóxicos que los catalizadores soportados convencionales. Durante la CWAO del fenol, numerosos productos intermedios se forman, por lo que el conocimiento de la cinética de su oxidación es fundamental para el diseño, modelización y escalado fiable del proceso a escala de planta piloto o incluso industrial. Debido a la insuficiencia de los clásicos métodos de optimización para llevar acabo la estimación de parámetros en modelos de alta complejidad, el uso de algoritmos estocásticos se ha probado con éxito, permitiendo el desarrollo de modelos cinéticos más avanzados que los que se implementan actualmente en el campo de la CWAO. El desarrollo de modelos cinéticos complejos es escaso en la literatura actual, así como los estudios que tratan los aspectos químicos y de ingeniería del proceso de la CWAO. Sin embargo, hay una necesidad clara para el desarrollo simultaneo de los aspectos químicos y de ingeniería de la tecnología. Consequentemente, en paralelo se ha enfocado en la modelización de un reactor de goteo (TBR), según el estado de arte actual en el campo de estos reactores. Es demostrado que estos reactores son más adecuados que los reactores agitados con catalizador en suspención para la CWAO de compuestos orgánicos que tienden a reacciones de polimerisación en fase liquida. Además se han probado dos distintos modos de operación, con flujo de gas y liquido cocorriente descendiente o ascendiente, y se ha demostrado que la primera forma de operación es la mas adecuada para este sistema. A continuación un modelo fenomenológico para el TBR ha sido desarrollado y programado. El modelo implementa la cinética previamente obtenida, y además se ha puesto énfasis en la incorporación de los efectos de mojado, y de transferencia de materia. La operación no isotérmica se ha estudiado también para investigar la posibilidad de operar de modo autotérmico, disminuyendo asi los costes de operación del proceso. La validación del modelo fenomenológico con los datos experimentales obtenidos en el TBR del laboratorio ha sido favorable. Posteriormente, este modelo ha sido utilizado como una herramienta fiable para el escalado del proceso. Los resultados obtenidos de la modelización del escalado permiten la extracción de recomendaciones sobre el diseño y la operación de unidades industriales, haciendo más fiable la aplicación del método a escala industrial.

x

Abstract

Wastewater treatment and re-use of industrial process water is a critical issue for the suitable development of human activities. The need for effective water recycling has reinforced the research on tailored low cost pollution abatement since the existing solutions are not longer universal. In particular, the emerging Catalytic Wet Air Oxidation (CWAO) process is one of the most promising technologies for the remediation of moderately concentrated and/or biotoxic water pollutants, when a stable and active catalyst can be provided. To this purpose, the catalytic activity and stability of active carbon was tested in the CWAO of the target compound, phenol, at mild conditions of temperature and pressure. The active carbon, which is a relatively inexpensive catalytic material is shown to be stable and to yield higher phenol destruction and less toxic partial mineralisation products, compared to a widely used copper oxide catalyst. During the CWAO of phenol, numerous partial oxidation products appeared and the knowledge of the kinetics that control their oxidation process is fundamental for the design, modelling and scale up of CWAO pilot plant or industrial units. Complex kinetic modelling was undertaken using both the classical gradient based method and a stochastic algorithm termed Simulated Annealing (SA). SA was shown to perform better in the identification of multiparameter kinetic reaction schemes, allowing to improve the kinetic modelling of CWAO beyond the actual state of art in this field. Detailed kinetic analysis of CWAO is scarce in the literature and the same situation holds for engineering studies. There is a clear need for the simultaneous development of process chemistry and engineering aspects. Consequently, we parallely focused on the state of art modelling of a Trickle Bed Reactor (TBR), being the priority candidate of best performing CWAO reactor. First, the ability of TBR in CWAO was affirmed by appropriate experimental comparison of batch slurry reactor and continuous fixed bed reactors operating either in the cocurrent downflow mode (TBR), or upflow mode (FBR) of the gas and liquid flow. A phenomenological transport-reaction model of the TBR was then developed and programmed. The TBR model implements the previously obtained oxidation kinetics and emphasis on important aspects of TBR, namely catalyst wetting, and mass transfer between the phases. Non-isothermal operation is also accounted for to face the need for autothermal operation, lowering the global process costs. The validation of the model was successfully done with the available experimental data from the laboratory TBR and thus provided a reliable tool for the scale up study of the CWAO process. The outcomings of this model aided scale up, allow to give recommendation on the design and operation of industrial units, thereby making more reliable the implementation of CWAO units on an industrial level.

Contents

List of Figures

List of Tables

Nomenclature

Latin Characters

a_s	Specific packing area m^2/m^3
A	reactor section area (m^2)
A_H	heat exchange area (m^2)
C_j	concentration of compound j $(mmol/L)$
c_p	heat capacity (J/KgK)
D_j^{eff}	effective diffusion coefficient of compound j (m^2/s)
D_j^{ad}	axial dispersion coefficient (m^2/s)
f	external wetting efficiency (f=f^d+f^s)
H	Henry constant
ΔH	Heat of adsorption (J/mol)
ΔH^v	Heat of evaporation (J/mol)
ΔH_j^f	Heat of formation of compound j (J/mol)
E_a	Activation energy (J/mol)
f	Wetting efficiency
$\mathbf{F}$	Vector containing the differences between experiment and model
$\mathbf{I}$	Unity Matrix
J	jacobian
k	Boltzman Constant
k_{gs}	gaseous oxygen-solid mass transfer coefficient (m/s)
k_{jls}	j-compound liquid solid mass transfer coefficient (m/s)
$k_{gl}a$	gaseous oxygen-liquid volumetric mass transfer coefficient (s^{-1})
$(ka)_{ll}$	static-dynamic liquid volumetric mass transfer coefficient (s^{-1})
K_0	Adsorption preexponential factor (L/mol)
k_0	Frequency factor (case dependent units)
m	mass (kg)
$\dot{m}$	mass flow rate (Kg/s)
n	number of model parameters
$\dot{n}$	molar flow rate (mol/s)
$N_p,\ N_e,\ N_c$	Number of points, experiments, compounds
N_o	number of total experimental observations $= N_p N_e N_c$
P	total pressure in the reactor (Pa)
P	probability
r	particle radial dimension (m)
r_c	column radius (m)
r_i	ith reaction rate $(mol/kg/s)$
r_p	catalyst particle diameter (m)
R	Universal gas constant (8.314 $J/molK$)
R_j	total production or destruction rate for compound j $(mol/kg/s)$
S	Objective function

Latin Characters	(continued)
t	Time (h)
T	Temperature (K)
T_a	ambient temperature (K)
T_0	Reactor inlet temperature (K)
U_H	heat exchanger overall heat transfer coefficient (W/m^2K)
U_w	reactor to wall overall heat transfer coefficient (W/m^2K)
u_l	liquid superficial velocity (m/s)
u_g	gas superficial velocity (m/s)
$\mathbf{V}$	Variance Matrix
$\dot{V}$	Volumetric flow rate (m^3/s)
x	parameter set
x	mole fraction
X	conversion
z	reactor axial dimension (m)

Greek Characters	
α	oxygen order
α	confidence
β	organic order
γ	ratio of liquid reactant flux to gas reactant flux to the catalyst particle
ϵ	liquid hold up
ϵ	catalyst particle porosity
η	effectiveness factor
λ	Effective axial conductivity (W/mK)
μ	Levenberg Marquardt parameter
ρ_b	bed density (kg/m^3)
ρ_l	liquid density (kg/m^3)
ρ_g	gas density (kg/m^3)
ρ_p	particle density (kg/m^3)
σ^2	variance
τ	Space time (h)
ϕ	evaporation rate pro reactor length $(mol/m/s)$

Superscripts	
d	dynamic liquid
g	gas or dry zone
s	static liquid
*	on catalyst surface

Subscripts	
0	at the entrance of the reactor
b	bed
e	equilibrium
H_2O	water
i	reaction index
j	compound index
O_2	oxygen
p	particle
t	total
w	wall

Abreviations

AC	Active Carbon
AOP	Advanced Oxidation Process
ATR	Adiabatic Temperature Rise
COD	Chemical Oxygen Demand
CWAO	(Heterogeneous) Catalytic Wet Air Oxidation
Cu0803	Engelhard $10\% CuO - \gamma - Al_2O_3$ catalyst
4-HBA	4-Hydroxybenzoic acid
HPLC	High pressure liquid chromatography
L-H	Langmuir Hinshelwood
L-M	Levenberg Marquardt
L-M*	Levenberg Marquardt starting from the S-A solution
NN	Neural Network
P-L	Power Law
S-A	Simulated Annealing
TBR	Trickle Bed Reactor
TPO	Temperature Programmed Oxidation
SAE	Sum of Absolute Errors
SRSE	Sum of Relative Squared Errors
SSE	Sum of Squared Errors
WAO	Wet Air Oxidation

Part I

Introduction & Methodology

Chapter 1

Introduction

1.1 Wastewater Management

The sustainable water management is one of the critical issues to be addressed in the coming decades. Up to date, more than half of the available freshwater is appropriated for human uses [1], indicating a high degree of exploitation of the existing water resources. In the close future, the water resources may even suffer drastic variations on a local and/or global level, because of the foreseen population growth and climate changes. This fact, in combination with the water pollution caused by mankind activity, makes water re-use of outmost importance. However, one should keep in mind that, from a global point of view, the recycling of water is not environmentally benign if high energy input technologies are used for this purpose [2]. Thus, the development of efficient wastewater technologies with low energetic and operation costs is essential for all types of wastewater.

Wastewater can be divided into four broad categories, according to its origin, namely domestic, industrial, public service and system loss/leakage [3]. Among these, industrial wastewaters occupy a 42.4% of the total volume and domestic a 36.4%. The types of contaminants that can be present in the aquatic effluents have been summarised as:

- Suspended Solids, Dissolved inorganics

- Biodegradable Organics & Nutrients

- Priority Pollutants (carcinogeneous etc.), Pathogens, Refractory (non-biodegradable) Organics, Heavy Metals

In particular, increasing quantities of wastewater with a high organic load result from numerous industrial and domestic applications. The most common depolluting technology in this case is the conventional biological treatment. However, its application becomes impossible for streams that contain high organic load and/or bio-toxic compounds. For example, aqueous phenol solutions with concentrations exceeding 0.5 g/L should not be treated in biological plants, even though acclimatised cultives in laboratory tests have performed depollution of solutions with up to 2 g/L of phenol [4]. Phenol and phenol like compounds are frequently encountered in the end of pipe streams of several chemical

industries, such as petrochemical, pharmaceutical etc. The importance of these effluents is outlined by the high quantities that are eventually rejected in the environment despite the legislation restrictions, as shown in Table 1.1 for the United States in the year 2000 [5].

Table 1.1: Annual release of toxic phenol-like pollutants in the United States for the year 2000 [5]

Compound	Emision (ton/year)	Overall Ranking
Phenol	22	35
2,4-Dinitrophenol	11	50
Catechol	8.3	59
Aniline	5.8	70
Hydroquinone	1.9	95
Quinone	0.64	115
Pentachlorophenol	0.55	120
Chlorophenols	0.046	203
2-Nitrophenol	0.026	213
4-Nitrophenol	0.007	239

Alternative methods have been developed for the remediation of these effluents, the most important being the adsorption on activated carbon, the thermal incineration and the liquid phase chemical oxidation. Adsorption on activated carbon is very effective for a broad range of organic pollutants. It is well known that activated carbon has a large surface area and adsorbs significant quantities of pollutants [6], but it does not ultimately destroy them. An adequate strategy for the spent active carbon disposal or regeneration is required, harming strongly the operating cost of the method. Incineration is the other well established technology for the treatment of concentrated and toxic organic waste streams. Organic pollutants are burnt at atmospheric pressure and high temperatures between 1000^oC and 1700^oC [7]. Thus, incineration can offer almost complete pollutant destruction, although at very high energy costs, because an organic load above 25% is necessary to guarantee autothermal oxidation. Furthermore, this technique has been accused for the emission of toxic by-products such as dioxins and furans [8].

Liquid phase chemical oxidation methods promise to overcome the existing drawbacks of the above mentioned treatment methods by destroying the pollutant while being dissolved in the liquid phase. Several emerging liquid phase oxidation methods can be distinguished in terms of the different oxidants, catalysts and operating conditions selected. The non-catalytic Wet Air Oxidation (WAO) process uses a gaseous source of oxygen which is the most readily available oxidant. Molecular oxygen can be dissolved in sufficient quantities in the liquid phase, at relatively mild temperatures and pressures above 150^oC and 2 MPa to oxidise several organic pollutants [9, 10, 11]. Alternatively, more effective, but also more expensive oxidants, like hydrogen peroxide [12, 13, 14] and ozone [12, 15] have been tested, yielding good results at milder conditions.

The incorporation of a catalyst has also been considered in combination with all types of oxidants aiming to reduce the operating temperature and pressure, and/or to treat pollutants that cannot be destroyed during non-catalytic liquid phase oxidation processes. Homogeneous catalysts, such as copper ions in solution were very effective in oxidising several organics when air was used as oxidant [16]. The classical Fenton's reaction, which combines iron salts with hydrogen peroxide has also given good results for various organic pollutants [17]. Nonetheless, the addition of a homogeneous catalyst has the inherent disadvantage of the posterior catalyst removal from the treated effluent, because the metal ions are pollutants themselves in the range of concentrations used. Heterogeneous catalysts, on the other hand, do not need any extra separation step and are thus more attractive. Solid catalysts, mostly noble metals and base metal oxides, have been tested in combination with all types of oxidants. Less frequently, active carbon (AC) also has been chosen as a catalyst without any additional active phase [18, 19, 20, 21, 22]. The incorporation of heterogeneous catalysts has exhibited promising results in laboratory tests, but industrial applications have been hindered because of the lack of stable catalytic performance over sufficiently long periods. It has been demonstrated that catalyst deactivation can take place because of the active phase leaching [23], the formation of carbonaceous deposits [24] and, to a less extent, the catalyst sintering [25].

A different way to enhance oxidation, is the application of external energy sources, such as electrical/electrochemical [26, 27], radiation [12, 28] and ultrasound [29], to form very reactive $OH\cdot$ radicals. These methods seem to be mostly adequate for low flow rate and low concentration effluents and the successful removal of target pollutants has been reported even at ambient conditions. Obviously, in this case the heating cost is translated to the cost of producing the respective energy for each process. An ultimate distinction between the different methods is based on the operating conditions. If process temperature and pressure are higher than the critical pressure and temperature of water, then supercritical methods emerge. Supercritical processes are extremely effective, but suffer from corrosion, salt precipitation, as well as high energy requirements [30].

It is well known that the process performance and economics strongly relies on the sound reactor selection and design. Dudukovic [31], in a critical review of the current trends in catalytic reactor engineering, outlines the importance of the simultaneous development of both chemistry and engineering aspects for any emerging process. A better understanding of the reactor behaviour, would enable to improve the reactor operation and modelling tools, thus eventually minimising the operation costs and, more important, the scale up risks. The implementation of novel reactor concepts can result in significant improvements in process performance. For example, in supercritical water oxidation innovative reactor configurations, such as the MODAR and the transpiring wall reactors, overcome corrosion and salt precipitation problems [32]. To avoid multistep processes, Polaert et al. [33] have proposed a bifunctional reactor scheme for the adsorption of phenol over activated carbon, and the subsequent regeneration of the latter in the same unit, as shown in Fig. 1.1. TBR periodic operation, which was very effective for enhancing TBR performance [34], has also shown advantages in catalytic wet air oxidation reactions [35].
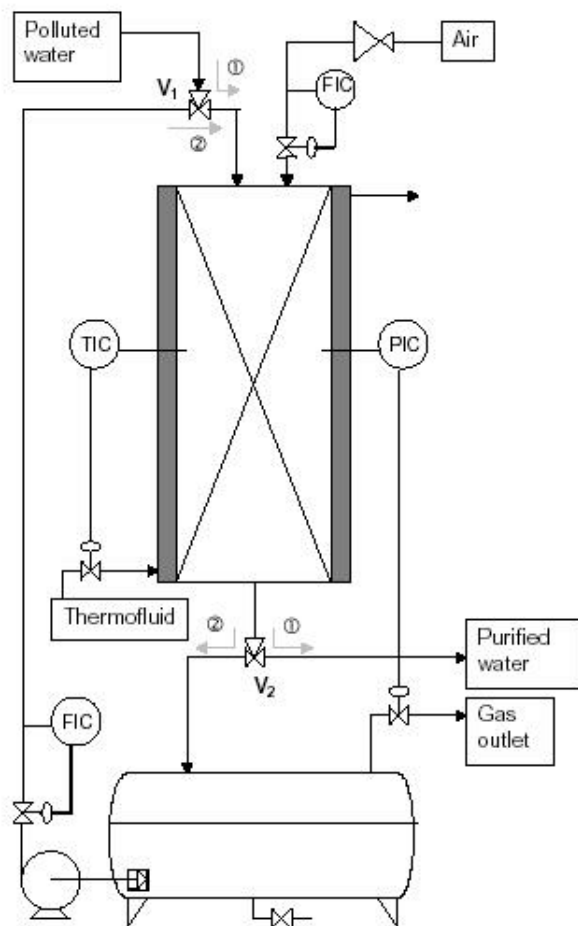
Figure 1.1: Bifunctional reactor for aqueous phenol adsorption and active carbon regeneration in the same unit [33].

The review of the related research work done in this field, suggests that the process selection should be tailored to the composition of the effluent, the desired conversion and the flow rate. A thorough study of the optimum range of application for each method is a rather difficult task, but future work should be driven in this direction. A first attempt by Andreozzi et al. [12], led to the technology map shown in Fig. 1.2, in which WAO appears to be the most suitable technology for wastewater containing between 20 and 200 g/L of COD (Chemical Oxygen Demand). The suitability of WAO would be further reinforced if a heterogeneous catalyst is successfully incorporated in the process. Thus, particular emphasis has to be dedicated to the study of the Catalytic Wet Air Oxidation (CWAO) process.
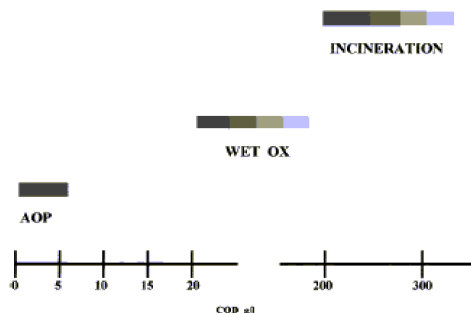
Figure 1.2: Suitability of water technologies according to COD contents [12].

1.2 Wet Air Oxidation Fundamentals

The Wet Air Oxidation process was originally developed by F.J.Zimmermann and its first industrial applications appeared in the late 1950s [9]. Currently, there are more than 200 plants operating around the world, the majority being dedicated to the treatment of sewage sludge. Other main fields of application consist in the regeneration of activated carbon and the treatment of industrial wastewater [36].

According to this method, the dissolved or suspended organic matter is oxidised in the liquid phase by some gaseous source of oxygen, that may be either pure oxygen, or air [11]. Typical operating conditions are in the range of 100-300^oC and 0.5-20 MPa. Some industrial applications, as summarised by Kolaczkowski et al. [36], Luck [13, 37] and Debellefontaine and Foussard [38], are given in Table 1.2. The main differences between the distinct processes consist in the reactor type used and the incorporation, or not, of a catalyst.

The most widely spread variation is the non-catalytic Zimpro process, which uses a cocurrent bubble column reactor, operating at temperatures between 147^oC - 325^oC and pressures of 2-21 MPa. A simplified flow diagram of the process is given in Fig. 1.3. The main components in the flow diagram are the separate gas and liquid feed lines, the heat exchanger unit, a gas liquid separator and a catalytic converter to destroy any volatile organics remaining in the gas phase. Alternative non-catalytic WAO processes are the Wetox process, that combines a series of agitated tank reactors, the Vertech process that uses the gravity to develop high pressures in a deep shaft reactor, the Kenox process which incorporates novel elements like static mixing and ultrasound energy and the oxyget process in which the liquid is fed in the reactor in form of droplets to eliminate oxygen transfer limitations.

WAO can achieve easily 90 to 95% conversion [38], which in general is not enough to meet effluent discharge regulations. Thus, most of WAO units are followed by biological
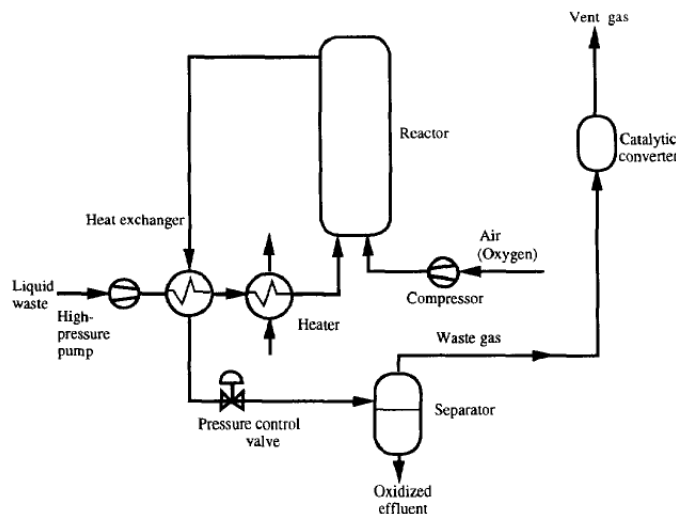
Figure 1.3: Simplified Zimpro process flow diagram.

treatment.

Despite its success in laboratory applications, catalytic WAO has yet not found the industrial recognition met with non-catalytic WAO. The main reasons, as pointed out earlier, are that the homogeneous catalysts have to be removed in a subsequent step, while the heterogeneous catalysts have to maintain their activity for sufficiently long periods. Homogeneous catalysts, such as Cu^{2+} or Fe^{2+} ions, are used in the Ciba-Geigy, LOPROX and WPO processes. The former uses Cu^{2+} ions at elevated temperatures (above $300^{o}C$) and is very successful in completely removing dioxins. In the reactor exit the catalyst is precipitated as copper sulphide and recycled to the reactor. The other two processes add Fe^{2+}, in more moderate conditions [13].

The heterogeneous Catalytic WAO (hereafter stated as CWAO) has scarcely found industrial applications. The NS-LC process uses a vertical monolith reactor with a $Pt - Pd/TiO_2 - ZrO_2$ catalyst. The operating conditions are $220^{o}C$ and $4 \ MPa$. The Osaka gas process uses a mixture of precious and base metals on titania or zirconia-titania supports. Typical operating conditions are $250^{o}C$ and $6.86 \ MPa$. The Kurita process uses nitrite instead of oxygen, and a similar catalyst (supported Pt), becoming more effective at lower temperatures, around $170^{o}C$.

Surprisingly, the industrial applications of CWAO operate at temperatures and pressures that are not significantly lower than those encountered in WAO. In addition, they use expensive noble metal catalysts. This contradicts with laboratory scale tests that have clearly proven the superior efficiency of CWAO at significantly lower temperatures and pressures [11], yielding less and more biodegradable partial oxidation products [39].

Given the potential of the CWAO, significant efforts have been driven in the three last

Table 1.2: Main industrial processes of Wet Air Oxidation

Process	Waste type	No Plants	Reactor Type	T (^{o}C)	P (MPa)	Catalyst
Zimpro	sewage sludge spent AC industrial	200 20 50	Bubble Column	280-325	20	none
Vertech	sewage sludge	1	deep shaft	<280	<11	none
Wetox	ns	ns	stirred tanks	200-250	4	none
Kenox	ns	ns	recirculation reactor	<240	4.5	none
Oxyget	ns	ns	tubular jet	<300	ns	none
Ciba-Geigy	industrial	3	-	300	ns	Cu^{2+}
LOPROX[1]	industrial	>1	Bubble column	<200	5-20	Fe^{2+}
NS-LC	ns	ns	Monolith	220	4	$Pt-Pd/$ TiO_2-ZrO_2
Osaka gas	coal gasifier coke oven cyanide sewage sludge	ns	Slurry Bubble Column	250	7	ZrO_2 or TiO_2 with noble or base metals
Kurita[2]	ammonia	ns	ns	>100	ns	supported Pt

ns: not specified

[1]This process uses organic quinone substances to generate hydrogen peroxide

[2]This process uses nitrite as oxidant

three decades to both develop active and stable catalysts for the process, and describe the reaction kinetics. Conversely, three phase catalytic reactor design and modelling for CWAO has received less attention, although some first trends have been reported.

An overview of the current state of art on CWAO catalysts, kinetics and reactor design is attempted to outline both the progress done in the field of CWAO and the open key aspects to be addressed by future research work.

1.3   Catalytic Wet Air Oxidation Catalysts

1.3.1   Active catalysts

The heterogeneous catalysts that have been employed in CWAO can be divided in two main groups, i.e. metal oxides (as well as mixtures of them) and supported noble metals [16, 40]. Active carbon, without any deposited active phase, has also exhibited catalytic activity [18, 19].

Noble Metals

Noble metals have been very effective in the treatment of different pollutants such as phenols [41, 42, 43, 20, 44], carboxylic acids, including refractory acetic acid, [46, 43, 45, 48, 47, 50, 49, 51, 52, 53], ammonia [54, 55, 56] and kraft effluents [57, 58, 59, 60, 61]. Pd, Pt and Ru have received most attention although Ir or Rh have also been tested [48, 46, 52]. Table 1.3 summarises the applications of noble metal catalysts in the CWAO.

Table 1.3: Process data of CWAO using noble catalysts

Noble Metal	Support	Substrate	T (^oC)	P MPa	Ref.
Pt	$\gamma - Al_2O_3$	acetic acid	>200		[53]
Ru, Ir, Pd, Ag, base metals	CeO_2, TiO_2, ZrO_2	acetic acid	200	2	[46]
Pt	$\gamma - Al_2O_3$	maleic acid	>120	>0.4	[62]
Ru	CeO_2	maleic acid	>160	2	[63]
Ru	TiO_2	succinic acid	>150	5	[49]
Pt	C	carboxylic acids	>20	>0.1	[45]
Pt	C	carboxylic acids	200	0.69	[51]
Pt	$\gamma - Al_2O_3$, resin	carboxylic acids	80	0.1	[64]
Ir	C	butiric acid	200	0.69	[52]
Pt, Ru, Rh	TiO_2, CeO_2, C	phenol/acrylic acid	170	2	[48]
Pt	$\gamma - Al_2O_3$	phenol	> 155	2	[44]
Pt, Ag,	MnO_2/CeO_2	phenol	>80	0.5	[42]
Pt-Ru	C	phenol	>35		[41]
Ru	C, CeO_2/C	phenol	160	2	[43]
Pt	C	p-chlorophenol	170	2.6	[20]
Pt, Ru, Pd, Rh	CeO_2	ammonia	>150	2	[54]
Pd	C	ammonia	280	2	[56]
Pt	SDB resin	ammonia	>110	<0.28	[65]
Pt, Ru, Pd, Ir	TiO_2, CeO_2, C	ammonia	>150	1.5	[55]
Pt-Ru	C	trichloroethene	>90	>0.2	[66]
Ru	TiO_2, ZrO_2	Kraft effluent	190	5.5	[60]
Ru	TiO_2	Kraft effluent	190	8	[61]
Pd, $Pd - Pt$	$\gamma - Al_2O_3$, ALON^{TM}	Kraft Effluent	>80	1.84	[57]
$Pd - Pt - Ce$	$\gamma - Al_2O_3$	Kraft effluent	>130	> 1.5	[67, 58, 59]

From Table 1.3 it can be deduced that numerous noble metal catalysts are available,

but for different pollutants different metals may present optimum results. For example, in the case of acetic acid oxidation, Barbier et al. [46] state that the catalytic activity decreases in the order $Ru > Ir > Pd$, while for the oxidation of p-chlorophenol, Qin et al. [20] found out that catalytic activity decreases in a *reverse* order $Pt > Pd > Ru$. Occasionally, synergistic effects in bimetallic catalysts improve catalyst activity and/or selectivity. Better N_2 selectivity was achieved during ammonia oxidation when a mixed $Ru - Pd/CeO_2$ catalyst was used [54]. Promoters have also been used with noble metal catalysts. An Ag promoted Pt over MnO_2/CeO_2 catalyst enhanced the CWAO of phenol compared to the non promoted catalyst [42].

The noble metal support also influences significantly catalyst performance. Metal oxides, like alumina, ceria, titania and zirconia, as well as active carbon or high specific area graphite have been mainly studied. In the treatment of Kraft bleach effluents increasing the support surface area had a positive effect on catalyst activity [60]. The dispersion of the active phase was also shown to be important for the CWAO of phenol, as demonstrated by a comparative study of two Pt/Al_2O_3 catalysts prepared in different manners [44]. Finally, the deposition of noble metals on hydrophobic supports, i.e. certain active carbons [56], or styrene divinyl benzene co-polymer [65], is very effective for the destruction of volatile pollutants such as ammonia.

Metal Oxides

The other broad family of catalysts used in CWAO is the pure or mixed metal oxides. Copper oxide, alone or combined with other oxides, has received special attention in the CWAO of aqueous effluents [90, 98, 99, 101, 82]. Phenol was successfully oxidised by a commercial Harshaw Cu0803 T1/8 catalyst, comprising 10% copper oxide supported over alumina [90, 82]. Baldi et al. [98] and Goto and Smith [99] tested a commercial CuO/ZnO catalyst to oxidise Formic acid while Levec et al. [101] used a catalyst combining Cu, Mn and La oxides supported on Al_2O_3 and ZnO to oxidise acetic acid. In the early nineties, other commercial catalysts comprising CuO, ZnO and $\gamma - Al_2O_3$ [96, 81], or CoO [80, 97] were successfully employed by Pintar and Levec to oxidise phenol and substituted phenols.

Ceria oxide, manganese-ceria mixed oxides and promoted ceria catalysts have also exhibited high activities. In the eighties, Imamura and co-workers (as summarised by [16]) developed Mn/Ce oxide catalysts for the CWAO of ammonia, which proved to be very effective for most organic compounds. De Leitenburg et al. [102] reported that ternary mixed oxides with ceria zirconia and MnO_x or CuO performed better than ceria, or ceria - zirconia catalysts alone. Hamoudi et al. found that that CeO/MnO catalysts can effectively oxidise phenol [24, 87, 104] and 4-chloroguaiacol [105]. Later, Chen et al. [88] showed that a Mn/Ce ratio of 6/4 was the most active for phenol oxidation. The performance of the catalyst was further improved by the incorporation of potassium [86], although this modification mainly affected catalyst stability, and will be discussed later.

Metal oxide catalysts not based on copper or cerium have been tested in fewer cases. The use of ferric oxide gave reproducible results for the oxidation of acetic acid under

Table 1.4: Process data of CWAO using metal oxide catalysts

Oxide	Support	Substrate	T (^oC)	P MPa	Ref.
Cu/Cr oxides		phenol	>127	0.32	[69, 68, 70]
$Cu/Cr/Ba/Al$ oxides		phenol	127	0.8	[71]
$Co,\ Fe,\ Mn,\ Zn$ oxides with Cu oxides	$\gamma - Al_2O_3$	phenol	140	0.9	[23]
CuO	$\gamma - Al_2O_3$	phenol	>120	>0.6	[72, 73]
CuO	$\gamma - Al_2O_3$	phenol	140	0.9	[74]
$Cu/Ni/Al$ oxides		phenol	140	0.9	[75, 76, 77, 78]
$CuO/ZnO/CoO$	cement	phenol	>130	7	[79]
$CuO/ZnO/CoO$	cement	phenol	>150	(*)	[80]
CuO/ZnO	$\gamma - Al_2O_3$	phenol	>105	>0.15	[81]
CuO	$\gamma - Al_2O_3$	phenol	>113	>0.44	[82]
CuO/CeO_2		phenol	130	0.73	[83, 84]
$K - MnO_2/CeO_2$		phenol	110	0.5	[86, 85]
MnO_2/CeO_2		phenol	>80	>0.2	[24, 87, 88]
CuO	C	phenol	>160	>2.6	[89]
CuO	$\gamma - Al_2O_3$	phenol	>95	>0.1	[90, 91]
$MnO_2,\ Co_2O_3$		phenol	>170	>1.3	[92]
$Ni - oxide$		phenol	>15	-	[93]
$Cu/Zn/Cr/Ba/Al$ oxides		phenol	>110	>0.1	[94]
$MnO_2,\ Co_2O_3$		p-chlorophenol	>170	>1.3	[95]
$CuO/ZnO/CoO$	cement	p-chlorophenol p-nitrophenol	>150	(*)	[97]
CuO/ZnO	$\gamma - Al_2O_3$	p-chlorophenol p-nitrophenol	>105	>0.15	[96]
CuO/ZnO		formic acid	>200	4	[98, 99]
Fe_2O_3		acetic acid	>252	>6.7	[100]
$Cu/Mn/La$	$ZnO - Al_2O_3$	acetic acid	>250	(*)	[101]
$Ce/Zr/Cu$ oxides or $Ce/Zr/Mn$		acetic acid	>245	>5	[102]
MnO/CeO		acetic acid	247	1	[16]
		n-butilamine	220		
		PEG	220		
		pyridine	270		
		ammonia	263		
MnO_2/CeO_2		alcohol distilery waste	>180	>0.5	[103]

*These tests were performed in a liquid full reactor saturated with oxygen.

severe conditions ($T > 250^oC, P > 6.7MPa$), while the copper based catalysts suffered severe deactivation [100]. More recently, nickel oxide catalysts have been used to remove effectively phenol in atmospheric pressure conditions [93].

Active carbon

Most commonly, AC has been used as a catalyst support [66, 48, 43]. Only in the las five years, the AC without any additional active phase, was shown to possess a long term catalytic activity in the oxidation of phenol [18, 19, 20], that could even surpass that of a conventional copper oxide catalyst as shown in Fig. 1.4 [18]. Experiments currently in progress in our laboratory, indicate that AC is also active in the oxidation of m-xylene, o-cresol, o-chlorophenol and aniline, while nitrophenol, sulfolane and nitrobenzene are extremely refractory.
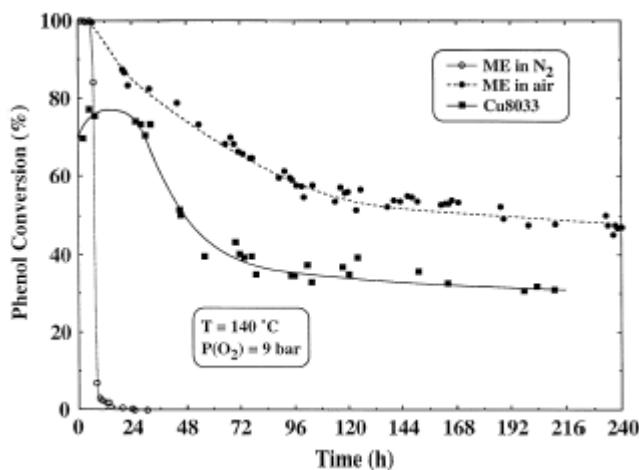
Figure 1.4: Comparison of phenol conversion profiles at 140^oC and 4.7 MPa using AC (ME) in nitrogen, air and Cu0803 in air [18].

The underlying mechanisms that are responsible for the catalytic activity of AC in CWAO are far from being well understood. To bring some light in this open aspect, a recopilation of the existing data of the CWAO of phenol over AC [18, 106, 107] is carried out and an attempt is done to relate these results to other studied systems that employ AC as a catalyst.

The most important conclusion is that the phenol oxidation over AC seems to proceed through the formation of a carbonaceous layer on the AC surface. It has been reported that during the CWAO of phenol over powdered AC in a semi batch slurry reactor it was impossible to balance the total carbon mass over the liquid and gas phase [107]. Also, a very low activation energy of about 40 kJ/mol was evaluated for phenol removal which is rather comparable to the 50 kJ/mol reported for the oxidative coupling reaction of phenol to form dimmers in the liquid phase catalysed by cuprous chloride [108]. Related

TBR studies using AC at 140^oC and oxygen partial pressure ranging from 0.1 to 0.9 MPa showed an initial increase of the AC weight of 20% at 0.9 MPa. Then, the AC weight (as well as the phenol conversion) continuously decreased to result in a loss of 33% after 10 days [106]. In the same run, a final reduction of the initial AC surface area of about 63% occurred, most probably due to blockage of micropores by some *organic* deposit.

A possible explanation of these results can be deduced from related studies. Active carbon is known to catalyse other reactions, like the SO_2 oxidation [109] or the oxidative dehydrogenation of ethylbenzene [110, 111, 112, 113]. For these reactions, the AC surface functional groups oxidise the substrate and are consequently reoxidised by oxygen in a redox cycle, in which the functional groups present on the AC surface participate.

In the gas phase oxydehydrogenation of ethylbenzene over AC, Pereira et al. [111, 112, 113] observed conversion and AC weight evolution in 3 day long runs that are similar to the trends observed by Fortuny et al. [106] for the CWAO of phenol. The former authors report the initial formation of coke deposit in the AC surface and found out by measurements of the total and micropore surface area that the formed coke layer completely blocked the micropores of AC. An elemental analysis of their carbons samples indicated a temporal change in its composition, i.e. a decrease of carbon content with a corresponding increase of oxygen and hydrogen at higher run times. Due to this composition change of the coke layer, the rate of gasification progressively became dominant, as the new oxygen containing surface groups formed with run time were shown by TPO analysis to be only effective in the coke gasification but not in its formation. Milder conditions of oxygen pressure and temperature delayed, but not avoided, both the consumption of AC and the shift of *active* surface groups to groups not available for the organic redox cycle. In the case of the phenol oxidation, the application of milder conditions (lower oxygen pressure) also had a positive effect on AC weight, as shown in Table 1.5, although in this case the activity towards phenol oxidation remained practically constant over 10 days.

Table 1.5: Infuence of the oxygen partial pressure on the carbon consumption [106].

P_{O_2} (MPa)	0.1	0.2	0.4	0.9
Consumption (%)*	-18	-3	16	33

*With respect to the initally loaded active carbon.

Two additional TBR runs of phenol oxidation were conducted at 0.9 MPa using either air with a phenol free feed or pure nitrogen with a phenol feed. Without phenol fed to the reactor, the combustion rate of AC is greatly enhanced leading to its total consumption after 9 days running. In the absence of oxygen, the phenol conversion dropped rapidly to zero after the adsorption step and no intermediates were found in the reactor effluent. Apparently, the oxygen containing surface groups of the AC alone are not capable of oxidising the adsorbed phenol in significant quantities.

Given the similarities between the findings of the work of Pereira et al. [111, 112, 113] and ours, the assumption of the formation of a coke-like layer and its participation in the liquid phase oxidation of phenol seems to be reasonable. According to the work

on the oxidative dehydrogenation of ethylbenzene, a redox cycle can be figured out to take place on the formed coke layer. However, differences certainly will arise compared to the oxidative dehydrogenation of ethylbenzene, because the oxidation of phenol is carried out in the liquid phase and seems to follow a much more complex mechanism. For instance, the rate of combustion of the AC is greatly enhanced in the liquid phase and the adsorption of water on the AC surface also should play an import role in the coke formation during the CWAO of phenol.

1.3.2 Catalyst stability

Up to date, the main drawback of CWAO, preventing it from a broad industrial application, consists in the catalyst deactivation, which occurs mainly due to active phase leaching or formation of carbonaceous deposits, during the oxidation process. The most prominent catalysts prone to leaching of the active phase are mixed oxides catalysts. Pintar and Levec [97] performed CWAO of nitrophenol and chlorophenol over a catalyst comprising CuO, ZnO and CoO in a liquid full fixed bed reactor and detected metal ions from all the above oxides in the solution. Similar trends were also observed for other copper catalysts like $CuO/\gamma - Al_2O_3$ [72, 75], bimetallic copper containing catalysts [23], copper on activated carbon [114, 116] or zeolites [117]. Under continuous operation, this decline leads to a continuous activity loss as clearly shown in Fig. 1.4. Thus, the development of more stable metal oxide catalysts can be pointed out as a critical issue in CWAO.

Recently, metal oxide catalysts with promising behaviour have been prepared. Alejandre et al. [76, 77, 78] developed mixed copper, nickel and aluminium oxide catalysts, which performed without any activity loss for 15 days on stream in a Trickle Bed Reactor. Hocevar et al. [83, 84], prepared different $CuO - CeO_2$ catalysts in which copper leaching was significantly reduced. For mixed Ce/Mn oxide catalysts, it was found that measurable amounts of Mn could dissolve [24, 48]. Active phase leaching was also reported for noble metal catalysts from during the CWAO of pulp mill effluents over Pd and Pt catalysts [59, 115].

Catalyst deactivation caused by the formation of carbonaceous deposit on the catalyst surface has been observed for several types of catalysts. Ceria oxide based catalysts have been found to suffer from this type of catalyst deactivation during tests carried out in agitated tank reactors [24, 87]. Further work demonstrated that carbonaceous deposits could be minimised by promoting the catalyst with Pt and Ag [87, 42]. More recently, it was found that less expensive potassium can also retard such formation [85, 86]. The carbonaceous deposit has to be related both to the nature of the organic pollutant and the reactor type used. The enhanced formation of such deposits has been confirmed by several authors in slurry reactors [81, 24], with a characteristic high liquid to catalyst ratio, that promotes the homogeneous polymerisation reactions. Consequently, comparative studies have shown that the extent of these parallel side reactions in the liquid phase are significantly reduced in Trickle Bed Reactors [80, 77, 107].

In the case of AC the catalytic activity during the CWAO of phenol at 140^oC was
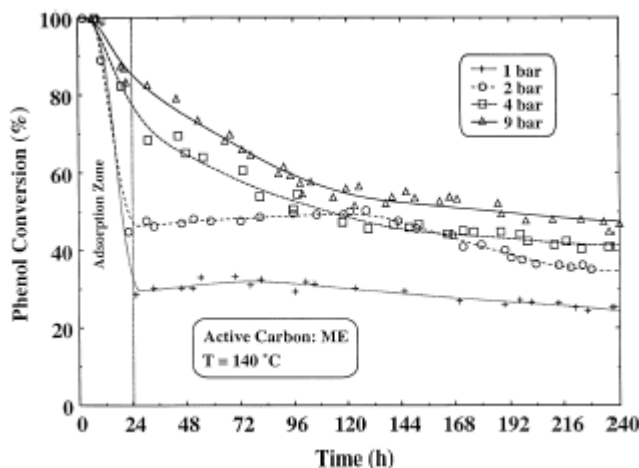
Figure 1.5: Phenol conversion dependence on the oxygen partial pressure using AC [106].

shown to be stable only for pressures below $0.4\ MPa$, while at higher pressures a constant decline was observed [106] (Fig. 1.5). The loss of AC catalytic activity was attributed to the simultaneous burnt out of the AC catalytic bed during the oxidation process. It was demonstrated that the rate of combustion of AC is considerably faster when, instead of the phenolic solution, a pure water solution is fed to the reactor [18]. Obviously the phenol oxidation and the carbon burn out are competitive reactions, and the phenol adsorbed on the AC surface protects the AC from being oxidised, as long as the concentration of O_2 is kept below a certain limit.

1.3.3 Overview

A wide range of supported noble metals, mixed metal oxides, as well as active carbon alone have been shown to exhibit catalytic activity for the oxidation of aqueous solutions of organic pollutants. Noble metal catalysts are very effective for the removal of refractory carboxylic acids, while for the less refractory phenolic pollutants, mixed metal oxides and active carbon yield good results. Catalyst deactivation has been found to occur either due to carbonaceous deposit formation, or due to active phase leaching. For both noble metal and mixed oxide catalysts analysis of the outlet solution for dissolved metals should be always carried out to measure the degree of stability of the catalyst. Long term runs in continuous reactor should also be tested to validate catalyst stability under continuous operation conditions. Such 10 day tests have shown that AC can yield constant phenol conversions, as long as oxygen partial pressure is below $0.4\ MPa$.

1.4 Reaction Mechanisms & Rate Equations in WAO and CWAO

To understand the CWAO process, the knowledge of the reaction kinetics is fundamental. The effort of research should focus on the establishment of both the reaction pathways followed during the oxidation reactions and the kinetic laws that can describe them. This knowledge, apart from giving a fundamental insight to CWAO can lead to significant improvements in the operation and design of CWAO units. Thus, in the following we attempt to give a review of the state of art of these aspects and point out fields for further research work.

1.4.1 Reaction Pathways

Pathways of phenol oxidation

The pathways and mechanism of CWAO reactions have been studied in detail only for pure compounds. Phenol and substituted phenols are commonly encountered in industrial effluents that are refractory to conventional biotreatment [5]. Also phenol has been shown to be more refractory than most of the substituted phenols [118], making it the ideal target compound for both WAO [119, 118, 120, 122, 123] and CWAO [94, 96, 81, 80, 97, 82, 90, 72, 73, 106, 18, 75, 76, 104, 48, 71, 68, 69, 70] conducted either in slurry, rotating basket or fixed bed reactor.

These studies demonstrated that phenol could be readily destroyed although its oxidation is followed by the formation of numerous organic intermediates. It is also well known that phenol oxidation occurs through a free radical chain mechanism [90, 81, 124, 125], that can take place in the homogeneous phase or on the catalyst surface. A simple but accepted mechanism for the CWAO of phenol has been proposed by [81]:

$$RH - OH + cat \quad \rightarrow \quad R \cdot H = O + \cdot H - cat \tag{1.1}$$
$$R \cdot H = O + O_2 \quad \rightarrow \quad RHO - OO \cdot \tag{1.2}$$
$$RHO - OO \cdot + RH - OH \quad \rightarrow \quad ROH - OOH + R \cdot H = O \tag{1.3}$$

In this mechanism $RH - OH$ corresponds to phenol, $R \cdot H = O$ corresponds to the phenoxy radical and $RHO - OO\cdot$ corresponds to the peroxy radical. Recently efforts are driven to develop more detailed radical reaction networks for the WAO of phenol, involving several tens of radical reactions, that should be more reliable in extrapolation beyond the fitted conditions [124].

In addition to the elementary mechanisms of phenol oxidation, it is important to assess the pathway leading to the formation of carbon dioxide. The existing reaction schemes available in the literature are generally based on the pioneer work of Devlin and Harris [119]. These authors in a study of the non-catalytic WAO of phenol, carried out a thorough analysis both to identify the most important intermediate compounds and

to propose the reaction network illustrated in Fig. 1.6. In can be seen that the phenol ring is firstly oxidised towards catechol and hydroquinone (hereafter joint to dihydric phenols) and benzoquinones. Subsequently, the ring breaks down forming low molecular weight carboxylic acids ($< C6$). Unsaturated acids, like maleic and acrylic acids seemed to be the main intermediates in the reaction path, while oxalic (including glyoxal and glyoxylic acid), formic and acetic acid were more stable, thus formed in higher quantities. Especially, acetic acid was found to accumulate in the system, so it could be considered as an end product. Malonic acid was determined in only small amounts while succinic and propanoic acids only appear in traces, under conditions of oxygen deficit.

Studies on the catalytic aqueous phenol oxidation showed a similar intermediate distribution in the presence of a solid catalyst. Ohta et al. [82] reported the formation of catechol, hydroquinone, maleic acid and oxalic acid, on a copper oxide catalyst. Fortuny et al. [73] using the same catalyst, identified in addition benzoquinone, malonic acid, acetic acid and formic acid. These authors calculated that the detected compounds account for more than 95% of the experimentally measured COD. Pintar and Levec [81] detected dihydric phenols and small quantities of benzoquinone, using a ZnO, CuO and $\gamma - Al_2O_3$ catalyst in a slurry reactor. Neither maleic, nor oxalic acid were detected, but instead acetic acid was present in considerable quantities. For this reactor it was found that phenol undergoes not only oxidation reaction but also polymerisation reactions in the homogenous liquid phase. In a related study using a liquid full differential packed bed reactor they identified additionally 1,4-dioxo-2-butene and maleic acid [80], although no polymers on the catalyst surface were detected. Oliviero et al. [43] using Ru supported on either CeO_2 or C also detected several of the compounds encountered by Devlin and Harris. They devide the detected compounds in $C6$: (benzoquinone and small amounts of dihydric phenols), $C4$: (maleic, succinic and small amounts of fumaric acid), $C3$: (acrylic acid, 3-hydroxy as well as 3-oxo propionic acid and small amounts of pyruvic acid) and refractory acetic acid. More recently Santos et al. [70], studied separately the oxidation of the main aromatic and carboxylic acid compounds mentioned above and proposed a scheme that distinguishes between the oxidation pathway of catechol, with that of hydroquinone. These authors concluded that during catechol oxidation alone only oxalic acid is formed, while hydroquinone undergoes a complex scheme that agrees with the Devlin and Harris mechanism.

Pathways of substituted phenols oxidation

WAO of substituted phenols seems to result in a similar intermediates distribution. Pintar and Levec [97] reported the formation of hydroquinone, benzoquinone, 1,4-dioxo-2-butene, maleic acid and carbon dioxide during p-nitrophenol and p-chlorophenol oxidation. At low conversions, however, short chain carboxylic acids were not detected. It should be mentioned that the reported intermediates are included in the Devlin and Harris mechanism for phenol degradation. It was also found that the concentration of Cl^- and NO_2^-/NO_3^- ions in the aqueous phase corresponds to the hydrocarbon conversion indicating that other cloro or nitro compounds are not formed.
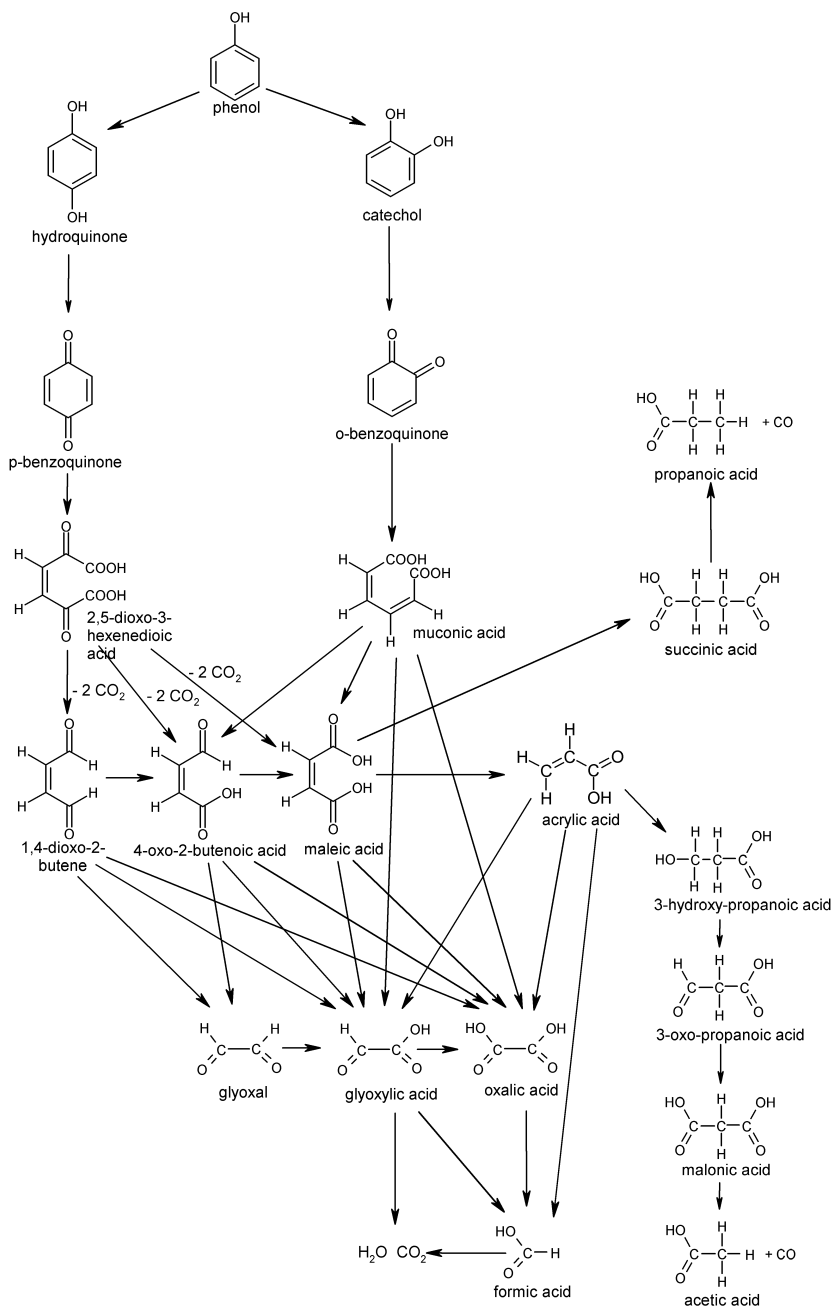
Figure 1.6: Reaction network for phenol CWAO according to Devlin and Harris [119].

Table 1.6: Reported intermediates during oxidative or thermal decomposition of carboxylic acids

Compound (Formula)	mu	ma	fu	su	bu	pr	ar	ae	gl	ox	fo	Ref
muconic ($C_6H_6O_4$)		*	*				+	+	*	*	*	[127]
maleic ($C_4H_4O_4$)			+	+			+	+	*	*	*	[127, 63, 62, 64]
fumaric ($C_4H_4O_4$)							+	+	*	*	*	[127]
succinic ($C_4H_6O_4$)								+				[49, 50]
butyric ($C_4H_8O_2$)					+			+				[52]
propionic ($C_3H_6O_2$)								+				[128, 51]
acrylic ($C_3H_4O_2$)								+			+	[127, 43]
acetic ($C_2H_4O_2$)												[129, 131, 100, 46, 47]
glyoxylic ($C_2H_2O_3$)										+		[129, 130]
oxalic ($C_2H_2O_4$)											+	[129, 130, 45, 98, 51]
formic (CH_2O_2)											+	[70]

(+): Produced under oxidative conditions. (∗): Produced also by thermal decomposition.

Qin et al. [20] studied the WAO oxidation of p-chlorophenol, and observed that in the absence of a catalyst, stable intermediates were formed because a p-chlorophenol conversion of 73.5% corresponded to only 42.9% of TOC reduction. In CWAO, this difference became smaller, in general being less than 10%. These authors report the additional formation of phenol and dichloro phenols, which were not detected in the study of Pintar and Levec [97]. Nevertheless, no phenol dimers were detected.

Neri et al. [126] studied the CWAO of p-coumaric acid over promoted ceria catalysts and they reported chain side oxidation leading to catechol, p-hydroxybenzaldehyde and p-hydroxybenzoic acid (and their hydroxylation products), as well as broken ring intermediates such as oxalic, formic and oxalacetic acid.

Pathways of carboxylic acids oxidation

The study of the WAO/CWAO of carboxylic acids is a very important issue because the oxidation of numerous organic compounds leads to the formation of carboxylic acids, before being mineralised to CO_2 and H_2O [11]. Table 1.6 summarises the carboxylic acids studied and the intermediates that were detected. In general, it should be pointed out that the studies have been performed at different conditions, resulting to different intermediate distribution.

For carboxylic acids both the oxidative degradation and the thermal decomposition, via decarbxylation roots, should take place, explaining the different intermediates observed. For example, during the maleic acid thermal decomposition no acetic acid is detected, the main product being formic acid. In an oxidative environment acetic acid is formed in quantities half of those of formic acid [129]. The presence of a catalyst also affects reaction pathways of maleic acid destruction, since no acetic acid formation is reported at all for Pt/C and $Pt/\gamma-Al_2O_3$ catalysts [64, 62].

In general, unsaturated carboxylic acids can be oxidised or decomposed more easily

than unsaturated one. When carboxylic acids with several carbon atoms are oxidised, low molecular weight acids are formed, mainly acetic, oxalic and formic acids. Acetic acid seems that, whenever it is formed, it is oxidised more slowly than the rest of carboxylic acids. Furthermore, in acetic acid oxidation studies no significant amounts of intermediates are reported. Oxalic acid has been shown to thermally decompose to formic acid, or to be oxidised towards carbon dioxide. Formic acid is usually considered to be oxidised forming carbon dioxide, although the formation of oxalic acid to some extend has also been reported [70].

Industrial effluent oxidation pathways

Industrial effluents are usually complex mixtures of several compounds, thus the possible intermediates that can be formed during their treatment is much broader. Nevertheless, for some wastes, namely Kraft bleach plant effluents [60, 61], and alcohol distillery liquors [103, 59], it has been shown that the main intermediates are also low molecular weight carboxylic acids among which acetic acid is the most persistent [120, 132].

1.4.2   Rate Equations & Rate Constants

The amount of efforts dedicated to identify the most probable reaction pathway of the CWAO is directly related to the sophistication of the developed reaction schemes. Usually, this gives rise to either progressively complex lumping or very detailed reaction pathways. Within these reaction schemes, it is possible to distinguish two main categories of rate equations that are used to mathematically describe the ongoing oxidation processes. For instance, simple power law (P-L) expressions have been typically pointed out for non-catalytic oxidation in the liquid phase, while Langmuir - Hinshelwood (L-H) expressions, including adsorption-desorption steps are necessary to describe solid catalysed oxidation reactions. These aspects are discussed in detail in the following sections.

Lumping & detail reaction schemes

Lumping schemes: The intermediates formed during WAO or CWAO reactions do not necessarily react at the same rate, some of them being even refractory to oxidation at the conditions employed. In addition, industrial effluents are mixtures of several compounds and their exact composition may not be well defined. Thus, there is a trend to conveniently lump intermediates in order to model the kinetics in terms of more general characteristics such as Chemical Oxygen Demand (COD) or Total Organic Carbon (TOC). This approach of direct degradation rates of the pseudo-compounds to carbon dioxide has performed well (e.g. [128, 129, 127] when the refractory intermediates are only formed in trace amounts. When this is not the case more advanced lumping strate-

gies can improve the model performance. The WAO scheme of most organic substrate has been frequently simplified to the lumped scheme given below [120, 132].

Organic Compounds $\longrightarrow$ $CO_2 + H_2O$

Acetic Acid
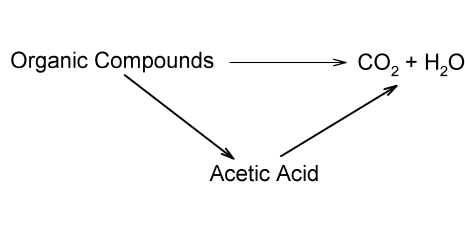
This scheme has been used in combination with power law kinetics to model the non-catalytic WAO of phenolic, activated sludge, black liquor and brewery waste [120] effluents. This scheme could also match experimental data for the CWAO of pulp mills [58] and petrochemical plant [133] effluents, although the rate constant of acetic acid oxidation did not obey the Arrhenius law. The authors attributed this behaviour to the extremely low rate of acetic acid degradation, which makes its calculation less precise. More recent lumping strategies could overcome this inconsistency, by simply omitting the reaction of acetic acid degradation [134]. This simpler scheme improved the fit with experimental results, avoiding any unreasonable parameter values. Belkacemi et al. further modified the scheme, lumping separately all the initial effluent compounds and the intermediate compounds detected, instead of only acetic acid, and the gas products [103]. The authors also replaced the simple power law kinetics by more adequate heterogeneous Langmuir - Hinshelwood expressions to successfully correlate data from CWAO studies, where the classical lumping strategy gave poor agreement with Arrhenius behaviour [133, 58]. Finally, this model was extended, by incorporating an additional lump of carbonaceous compounds, to properly account for the catalyst deactivation observed during CWAO in a slurry batch reactor [42].

Detailed schemes: Lumping schemes are very convenient to model effluent COD reduction, although they miss important information about the reaction pathways, which can be important. This defect can become critical because different pathways may dominate at different conditions. Then the distribution is not available to check for such intermediates formed that are known to be equally, or even more toxic than the initial pollutants themselves. Thus detailed reaction mechanisms that account for the partial oxidation products formed are a significant improvement in the kinetic modelling of CWAO.

However, up to date only a few studies on carboxylic acids have considered such an approach. For example, Beziat et al. [49] studied the CWAO of succinic acid and proposed the reaction scheme shown in Fig. 1.7. This scheme accounts explicitly for the formed intermediates, resulting in a high number of kinetic parameter, which transforms the following kinetic parameter estimation into a difficult task.

Extension of such a model, that includes all possible reaction connecting intermediates presently seems to be impossible for more complex systems. A reasonable solution is to
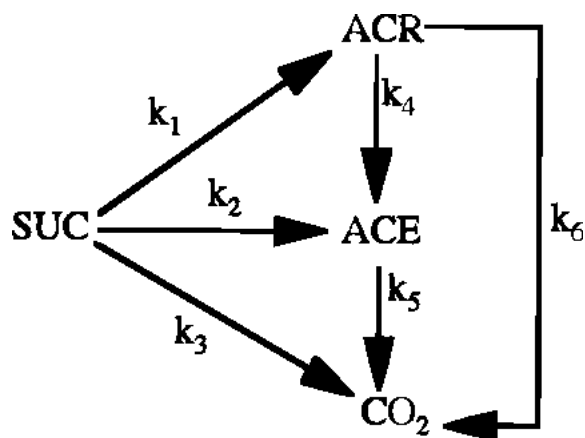
Figure 1.7: Reaction scheme for the oxidation of succinic acid. SUC: succinic acid, ACR: acrylic acid, ACE: acetic acid. [49]

select reaction networks that account only for influent reactions should be considered. In this view Eftaxias et al. [121] developed a model for the CWAO of phenol in a TBR that accounts for eight compounds considering only eight reactions.

Rate Expressions

Power Law Expressions: For non-catalytic oxidation the use of power law expressions has been typically pointed out. These equations are of the general form of Eq. 1.4.

$$r_{org} = k_0 \, exp(-E_a/RT) \, [C_{O_2}]^\alpha \, [C_{org}]^\beta \tag{1.4}$$

The values of the kinetic constants following Eq. 1.4 are summarised in Table 1.7, for both WAO and CWAO studies. For WAO usually a first order dependence on the organic substrate has been reported for phenol, substituted phenols [122, 118] and carboxylic acids, such as formic, oxalic, acetic and propionic acid [128, 129]. The same trends also hold for TOC or COD lumps [120, 118, 128, 129]. Unsaturated carboxylic acids, such as acrylic maleic and fumaric acid [127] show orders close to 1.5 and the authors attributed this fact to the existence of simultaneous reactions over two reactive centers in these molecules (double bond and carboxylic group), giving rise to an apparent reaction order increase.

Reported oxygen orders in general oscillate between 0 and 1. For phenol, Willms et al. [122] report an 0.5 order, while Joglekar et al. [118] state a first order. Shende and Levec [128, 129] give orders equal, or close to 0.5 for saturated carboxylic acids. On the other hand, for unsaturated carboxylic acids the orders could vary from 0.54 for acrylic and fumaric acid to 0.12 for maleic acid. The oxygen orders for TOC removal during oxidation of these acids were higher ranging between 0.3 and 1.

Activation energies depend on the particular compound studied, but they generaly take values in the interval for 70 to 160 kJ/mol the CWAO usually being in the down

limit. because of the free radical nature of the phenol and substituted phenols oxidation reaction, different activation energies have been reported for the induction and rapid propagation periods. According to Willms et al. [122] the activation energy was found to be 94 kJ/mol and 112 kJ/mol for each step respectively, while Joglekar et al. [118] reported much lower values of 22 kJ/mol and 50 kJ/mol These later values however should be questioned for mass transfer problems. in general, low molecular weight carboxylic acids are less reactive than ring compounds, resulting in high activation energies. On the other hand, thermal decomposition of unsaturated acids was found to have lower activation energies [127].

Power law equations have also been considered in CWAO kinetic studied. The CWAO of phenol usually yields a first order dependence on the substrate [91, 72, 92], although Ohta et al. [82] report a value of 0.44. For formic acid Baldi et al. [98] also obtained a first order dependence, as well as Klinghoffer et al. [53] in the case of acetic acid oxidation over $Pt/\gamma - Al_2O_3$. On the other hand, Gallezot et al. [47] and Beziat et al. [50], claimed a zero order for acetic acid and succinic acid using Ru/C and Ru/TiO_2 catalysts respectively. They justified these results by stating that these compounds are strongly adsorbed on the ruthenium surface. Furthermore, a -0.5 acetic acid order was obtained on a Ru/CeO_2 and it was argued that on this catalyst acetic acid adsorbs even stronger [46]. These latter findings suggest that the substrate adsorption on the catalyst surface can significantly affect the resulting reaction rate, making evident that in many CWAO cases L-H expressions should be implemented.

For most of the above studies the oxygen order lies within 0.4 and 0.65, i.e. close to 0.5 [46, 50, 47, 72, 82]. Nevertheless, Baldi et al. [98] obtained first order oxygen dependence for the CWAO of formic acid in a liquid full fixed bed reactor operating in the kinetic controlled regime. The reported activation energies may even vary for the same compound and catalyst. For phenol, most authors agree in values between 85 and 105 kJ/mol [82, 72, 92]. Conversely, Sadana et al. [91] reported a much higher value of 176 kJ/mol, for the steady state period. The values reported for carboxylic acids are between 81 and 155 kJ/mol [98, 46, 50, 47, 53], most values being higher than those for phenol oxidation, as was the case also in the non-catalytic WAO.

Langmuir-Hinshelwood kinetics

In describing heterogeneous catalytic reactions, Langmuir - Hinshelwood expressions have been proven very powerful. Surprisingly, they have found less application to CWAO kinetics. A wide scenario of L-H expressions can be developed, although the most popular used in CWAO accounts for the competitive adsorption of the organics on the same active site, omitting the existing adsorption of oxygen. The resulting expression is then given by Eq. 1.5:

$$r_i = k_0 \, exp(-E_a/RT) \frac{K_0 \, [C_{O_2}]^\alpha \, [C_{org.}]^\beta \, exp(-\Delta H_{org}/RT)}{1 + \sum K_{0j} C_j exp(-\Delta H_j/RT)} \tag{1.5}$$

Table 1.8 summarises the kinetic parameters reported for L-H kinetics. In these studies

Table 1.7: Kinetic parameters for WAO and CWAO of pure organic compounds following Power Law kinetics of Eq. 1.4.

Compound	Catalyst	$E_a^{(2)}$ (kJ/mol)	α	β	Ref.
Succinic Acid[3]	Ru/TiO_2	125	0.4	0	[50]
Fumaric acid	none	83.6	0.54	1.45	[127]
Maleic acid	none	99.2	0.12	1.45	[127]
Maleic acid	none	131.5	0	1	[62]
Propionic acid	none	150	0.5	1	[129]
3-HPA[1]	none	135	0.5	1	[129]
Acrylic acid	none	94.3	0.54	1.5	[127]
Acetic acid	none	178	0.5	1	[129]
Acetic acid	$Pt/\gamma Al_2O_3$	81	-	1	[53]
Acetic acid	Ru/C	100.5	0.65	0	[47]
Acetic acid	Ru/CeO_2	96.6	0.5	-0.5	[46]
Oxalic acid	none	137	0.5	1	[129]
Glyoxalic acid	none	97	1	1	[129]
Formic acid	none	149	0.5	1	[129]
Formic acid	CuO/ZnO	155	1	1	[98]
Phenol	none	22 / 50	1	1	[118]
Phenol	none	94 / 112	0.5	1	[122]
Phenol	none	113.2	-	1	[92]
Phenol	$CuO/\gamma - Al_2O_3$	276 / 176	1 / 0.5	1	[91]
Phenol	$CuO/\gamma - Al_2O_3$	85.3	0.55	0.44	[82]
Phenol	$CuO/\gamma - Al_2O_3$	85	0.5	1	[72]
Phenol	MnO_2	104.5	-	1	[92]
Phenol	Co_2O_3	96.3	-	1	[92]
Phenol	Cu^{2+}	85.2	-	1	[92]
p-chlorophenol	none	134.5 / 77	1	1	[118]
p-chlorophenol	none	91.9	-	1	[92]
p-chlorophenol	Cu^{2+}	75.5	-	1	[92]
o-chlorophenol	none	137.9/ 145	1	1	[118]
m-chlorophenol	none	72.1/ 130	1	1	[118]
p-methoxyphenol	none	157.9 / 71	1	1	[118]
o-methoxyphenol	none	133 / 133	1	1	[118]
o-cresol	none	130.4 / 190	1	1	[118]
m-cresol	none	86.4 / 48	1	1	[118]
o-ethylphenol	none	79.3 / 89	1	1	[118]
2,6-dimethylphenol	none	0 / 62	1	1	[118]
m-xylene	none	103 / 89.5	0.5	1	[122]

[1] 3-Hydroxypropionic acid

[2] when two values are given the correspond to: induction / steady state periods

[3] initial rate calculation

Table 1.8: Kinetic parameters obtained in CWAO of pure organic compounds using Langmuir Hinshelwood kinetics

Compound	Catalyst	E_a (kJ/mol)	ΔH (kJ/mol)	α	β	product adsorption	Ref.
Acetic acid	Ferric oxide	87.8	≈ 0	0.5	1	No	[101]
Acetic acid	Cu, Mn, La Al,Zn oxides	-	-	0.5	1	No	[100]
Succinic acid	Ru/TiO_2	-	-	-	1	Yes	[49]
Phenol	$CuOZnOCoO$	139	-62	0.5	1	No	[80]
Phenol	MnO_2/CeO_2	174	-109	-	1	Yes	[104]
Phenol	CuO/C	78.6	-	0.5	1	No	[89]
p-Chlorophenol	$CuOZnOCoO$	90	-24	0.5	1	No	[97]
p-Nitrophenol	$CuOZnOCoO$	89	-18	0.5	1	No	[97]

the substrate and the oxygen order have been successfully set equal to 1 and 0.5 respectively and have not been optimised. Several studies have considered that only the initial reactant, but not the products, adsorb on the catalysts surface. Nevertheless, it has been demonstrated that phenol adsorption on AC can be affected by the presence of dihydric phenols or benzoquinone, in the solution [135].

With this type of equation, first order dependence on the substrate has been obtained for all the substrates tested, i.e. acetic acid [100, 101], succinic acid [49], phenol [80, 104, 89] and substituted phenols [97]. The activation energy values of the range 78 to 90 kJ/mol, although high values between 140 and 170 kJ/mol have also been reported, without any specific trend depending on the compound. The corresponding heats of adsorption fall within the range -18 to -109 kJ/mol, although a value close to zero has also been reported for acetic acid oxidation over ferric oxide [100]. Among these studies Beziat et al. [49] took into account competitive adsorption of the succinic acid oxidation products, while Hamoudi et al. [104] took into account adsorption of oxidation products (included as a lump), as well as carbonaceous deposits.

Synergistic Effects and Reactor Type

Synergistic effects: It is likely that the oxidation rates of pure compounds are different when they are oxidised in the presence of other oxidisable compounds, which form active free radicals. For the WAO process, it has been reported that effluent recirculation had a positive effect on pollutant abatement, because it provides a free radical environment since the entrance to the reactor [136]. Santos et al. [70], in a detailed study, observed that the apparent reaction rates of phenol oxidation intermediates do not agree with those found when they are oxidised alone. Shende and Levec claim that synergistic effects occur depending on the conditions employed. They observed that mixtures of low molecular carboxylic acids are oxidised with rates different from the individual when the oxygen partial pressure was below 2.2 MPa [129]. This fact elucidate that reaction kinetic studies performed for individual compounds cannot always be applied to describe

their degradation in a complex mixture.

Effect of reactor type: Most kinetic studies of CWAO have been carried out in agitated slurry, or spinning basket reactors in semi batch operation. These reactors are characterised by a very high liquid to catalyst ratio. At these conditions, homogeneous polymerisation reactions are strongly enhanced and may lead to catalyst deactivation [81, 104], by irreversible adsorption of the formed condensation products. Consequently, measured substrate disappearance rates do not correspond to the true intrinsic oxidation kinetics. It has been reported that there exists a critical catalyst concentration, above which the homogeneous contribution is negligible [68]. Pintar and Levec [81] used a kinetic expression including a homogeneous and a heterogeneous contribution to match the phenol degradation profiles obtained in a batch reactor. However, the developed kinetic expression could not match the performance of a TBR, where the extend of the homogeneous side reactions is strongly reduced. In a comparative study between a batch slurry reactor and a TBR, Stüber et al. [107] found out that initial rate constants could be 50 times higher in the slurry reactor and attributed this difference to high rates of polymerisation reactions in the slurry system.

The conclusion is that for reaction systems that are prone to condensation reactions in the liquid phase, it is not recommended to extrapolate kinetics obtained in slurry reactors to model and design Fixed Bed Reactors. Alternative kinetic studies have been performed in liquid full fixed bed reactors [99, 100, 80, 97], or TBRs [72]. In the former, the liquid stream is pre-saturated with oxygen and then enters in the reactor. At these operating conditions, oxygen is the limiting reactant, thus the reactor has to be operated in the differential mode, to avoid oxygen depletion. The kinetics obtained in this type of reactor gave better results in the modelling of CWAO of carboxylic acids in a TBR [99, 100], but still predicted conversions 50% lower than the experimentally observed for the CWAO of phenol [79].

Conducting a kinetic study directly in a TBR has the advantage of low liquid to solid ratio, compared to the liquid full fixed bed reactor. In addition, a TBR can be operated in integral mode, so a wider range of conversions and concentrations can be covered. Nevertheless, one has to ensure that the reactor performance is exclusively controlled by kinetics, diminishing any external or internal mass transfer limitations. This is possible only for low rates of reaction, which is the case of CWAO, as the pollutant concentration is low because they are diluted in water.

1.4.3   Overview

In general the CWAO reactions follow a homogeneous - heterogeneous free radical mechanism. The pathway for complete mineralisation of phenol, and substituted phenols is complex leading to the formation of hydroquinone, catechol, benzoquinone and low molecular weight carboxylic acids.

Most of the CWAO kinetic studies have only focused on the degradation rates of pure compounds, or lumped pseudocompounds, such as COD or TOC. Even though

sophisticated lumping strategies achieve to model well COD and deactivation kinetics, they miss important information on the pathways prevailing at each conditions, and the distribution of intermediates of the resulting effluent.

In the modelling of CWAO reactions mainly P-L kinetics, and to a less extend L-H expressions, have been implemented. For the former rate type, first order for the substrate is often encountered, while the oxygen order mostly being close to 0.5. However, the applicability of power law kinetics occasionally leads to reaction orders that lack physical sense (e.g. negative), because of adsorption onto the catalyst surface. Thus the development of detailed kinetic models, using L-H expressions, should be considered as a priority item in future research work on in the field of CWAO.

1.5   Kinetic Multiparameter Estimation

The kinetic parameters presented previously are determined by fitting the rate expressions to available experimental data, that can be obtained either from batch, CSTR or Plug Flow reactors. For CSTR reactor the value of reaction rate can be directly determined, from the mass balance and the known inlet and outlet concentrations as well as the applied flow rates. Operation and control of such reactors in three phase catalytic systems can be complicated and many experiments are necessary to cover a broad conversion range. Batch and plug flow reactors provide concentration profiles versus time for batch reactor and space time for the plug flow reactor. Batch reactors have been mainly used for CWAO kinetic studies, as they can easily handle gas-liquid-solid (catalyst) systems. For these reactors an adequate reactor model is used to relate the obtained concentration profiles with the reaction kinetics. If no mass transfer limitations exist, and assuming ideal batch, or ideal plug flow operation we can obtain Eqs. 1.6 and 1.7 respectively:

$$\frac{dC}{dt} = -C_{cat}\,r \tag{1.6}$$

$$\frac{dC}{d\tau} = -\rho_l\,r \tag{1.7}$$

The experimental data can then be related to the reaction rate by means of the differential or the integral method, which are briefly described below.

1.5.1   Differential Methods

According to the differential method the derivatives dC/dt or $dC/d\tau$ are first evaluated from the experimental data and subsequently the reaction rate r is transformed by linearisation techniques. For example, the simple P-L rate equation of Eq. 1.4 can be linearised in the following way:

$$ln(r) = ln(k) + \alpha ln(C_{O_2}) + \beta ln(C_{org}) \tag{1.8}$$

$$ln(k) = ln(k_0) - E_a/RT \tag{1.9}$$

By plotting $ln(r)$ against substrate and oxygen concentration the unknown kinetic parameters k, α and β can be calculated. If data are available at different temperatures, by plotting the $ln(k)$ versus $1/T$, to obtain the well known Arrhenius plot, the calculation of the frequency factor and activation energy is possible. For more complex L-H kinetics Hougen and Watson proposed an adequate linearisation procedure that is described in chemical reaction engineering textbooks [137, 138].

The advantage of differential methods is that they do not need to define a priori initial guess values for the kinetic parameters. On the other hand, the graphical determination of the reaction rates and the two step linear regression lead to low precision estimates. Furthermore, they need a minimum calculation effort, thus they were very popular before

the computer era. However, this procedure has been criticised, as it may lead to erroneous results [139, 140]. Thus integral methods, coupled with nonlinear regression techniques are becoming very popular.

1.5.2   Integral Methods

According to the integral method an adequate rate equation is proposed to integrate Eq. 1.6 or 1.7. Then, the involved kinetic parameters are optimised by nonlinear regression methods to match experimental concentration profiles. Obviously in this case, a rate equation and additionally initial guess values of kinetic parameter values have to be postulated and model discrimination is done in terms of the best fit, the statistical significance of the involved parameters and finally their physical sense.

The estimation of kinetic parameters is a very delicate task and its quality depends on how carefully the fitting strategy was planed and executed. Several fitting strategies have been applied to study WAO or CWAO reactions. The simplest approach, is based on linearisation techniques as discussed before, has been mainly used in pioneer CWAO studies as for example those of Sadana and Katzer [91] and that of Baldi et al. [98] and [122, 118, 96, 81].

Because of the continuous improvements in computational power, integral methods coupled with nonlinear parameter estimation have replaced the differential methods. In particular, Gradient-based methods, have been widely employed in nonlinear parameter estimation [141]. Among these methods, the Levenberg-Marquardt (L-M) algorithm, of a quadratic convergence, is the most commonly used. The major drawback of this algorithm is that convergence to local minima frequently occurs when poor initial guess values are provided. For example, several thermodynamic parameters included in the DECHEMA data bank, which were obtained by local optimisation methods, were proved not to correspond to the best fit [142]. Although differential methods can be used to provide initial guess parameters, it is still recommended to test several initial guess parameter. However, finding of a suitable initial guess for all parameters in a complex reaction scheme is a critical, almost impossible task.

In WAO/CWAO studies the L-M, or other gradient methods, also have been widely employed to calculate reaction and adsorption parameters [72, 124, 59, 80, 97, 89, 104, 103]. To reduce regression complexity, the non-linear regression fitting is often applied to evaluate the apparent reaction constants for fixed temperature and oxygen partial pressures. Then, the activation energies, the heats of adsorption and the oxygen order are calculated in a subsequent step by means of conventional linear regression.

If complex reaction networks are considered, the number of involved parameters increases drastically. So it is expected that the classical L-M algorithm would fail to reach a reliable solution. For this reason, comparison with global optimisation methods should be considered. These methods permit to find the global minimum of the objective function, on cost of a significantly higher computational time. The global optimisation approaches use either deterministic (e.g. [143, 144]) or stochastic (e.g. [145, 146, 147]) methods. Deterministic methods guarantee convergence to the global minimum within the defined

parameter space. In general they identify the proximity of all local minima of the objective function, and consequently apply a gradient method to calculate them. However, the algebra behind this process is rather complex, thus, these methods usually require advanced programming skills.

The stochastic methods scan randomly the entire parameter space and they theoretically converge to the global minimum for infinite number of function evaluations. The main advantage of these algorithms is that they are less sensitive to the starting guess values compared to the classical gradient methods, and present less computational complexities. The application of stochastic methods for the estimation of kinetic parameters is scarce. Belohlav et al. [148] and Zamostny and Belohlav, [149] used a random search algorithm for the kinetic modelling of hydrogenation reactions. Moros et al. [150] and Wolf and Moros [151], used a genetic algorithm to provide initial parameter guess values for the subsequent application of local minimisation methods. Finally, Asprey and Naka, [139] in a review of the current state of art in kinetic parameter estimation, highlighted the simulated annealing as a powerful algorithm with numerous applications in combinatorial optimisation and as an excellent tool for nonlinear kinetic parameter estimation. In a more detailed comparison between this latter algorithm and the classical L-M method Eftaxias et al. [152] report that S-A is much more robust and can be used for more complex system that the L-M algorithm.

Thus, the inherent problems of the application of local optimisation algorithms to the modelling of complex reaction networks, can be overcomed by global optimisation methods. These methods, should not only achieve better mathematical solutions, but also provide kinetic parameters with statistical significance and physical meaning. However, gradient method application starting from the solution obtained by the stochastic algorithms has to be considered, because the calculation of the gradients provides useful information about the statistical significance of each of the parameters [153], as well as the discrimination of rival models which achieve similar fits [154].

1.5.3 Overview

Traditionally kinetic constants were obtained by linearisation techniques. Nevertheless, the continuously increasing computational power makes has made possible the application of nonlinear parameter estimation methods. The L-M algorithm, which is a gradient based method has, been widely used for this purpose in the field of WAO/CWAO, as well as elsewhere. The application of nonlinear parameter estimation methods has been shown to lead to more reliable estimates. Nevertheless, the classical local minimisation methods are foreseen to fail in the development of complex reaction networks, thus their application in the development of complex CWAO reaction networks may result problematic. Therefore, the use of global minimisation algorithms should be tested for the development of such detailed reaction kinetic schemes.

1.6   Multiphase Catalytic Reactors

The discovery of solid catalysts and their application to chemical processes in the early years of the twentieth century has led to a breakthrough of the chemical industry [138]. Despite the enormous progress in understanding and describing multiphase catalytic reactors in the last century, successful scale up, i.e. successful transfer of laboratory results to the design commercial units is not trivial and is mainly based on empirical approaches [155]. The complexity of the modelling of multiphase reactors comes from the fact that their modelling joins phenomena that take place in different length scales. Reaction kinetics are governed by molecular phenomena, external and internal transport processes are of Eddy or particle scale, while the fluid flow patterns through the reactor occur at the reactor scale. These phenomena can be described with different degrees of sophistication, as shown in Table 1.9 proposed by Dudukovic et al. [156]. Naturally, as the degree of sophistication increases, it is more time consuming to develop and solve the model equations. In general, it is recommended to use the same degree of sophistication for the different scales involved in the model.

Table 1.9: Levels of multiphase reactor modelling [156]

Molecular (reaction) scale			
Striclty empirical	Mechanism Based	Fundamental-Elementary	
Eddy or particle scale transport			
Empirical	Micromixing models	DNS[1] CFD[2]	
Empirical part of rate equation	Thiele Models	Rigorous	
Reactor Scale			
Ideal Reactors	Empirical models	Phenomenological models	CFD models
PFR, CSTR	Axial dispersion		

[1] Direct Numerical Solution [2] Computational Fluid Dynamics

The complexity of multiphase reactor modelling increases when they are used for solid catalysed reactions between a gaseous and a liquid reactant. This situation is very common in industrially relevant processes, such as hydrotreating and hydrogenation [157], but recent works point out the increasing use of multiphase reactors in selective oxidation [158], and wastewater treatment processes, i.e. in the CWAO process [159, 160, 161].

Several reactor types, with different characteristics, can be used to accommodate the solid catalyst and carry out multiphase catalytic reactions. Therefore, reactor type selection has to be examined for each reaction system, considering catalyst type, catalyst activity and stability, reactant and product properties and interfering reactions. In this view, the choice of a suitable reactor for the CWAO process is discussed in the first place.

1.6.1 Reactor Choice for the CWAO

Four main categories of gas-liquid-solid catalytic reactors can be distinguished: agitated slurry CSTR reactors, sparged catalyst reactors, like slurry bubble column and fluidised beds and finally fixed bed reactors. Mechanically agitated slurry reactors exhibit high heat and mass transfer rates, but stirring leads to high investment and operation costs and energy consumption. Furthermore, these reactors have a very low catalyst to liquid ratio, thus undesired parallel reactions may be enhanced. Sparged catalyst reactors exhibit heat transfer rates that are still higher than those of fixed bed reactors, but also a higher liquid to catalyst ratio. Furthermore, catalyst particles have to be separated from the exit liquid stream when continuous operation is desired. Fixed bed reactors have the lowest liquid to catalyst ratio, on cost of lower heat and mass transfer rates.

As it was shown earlier, during the CWAO of certain organic pollutants, like phenols, parallel polymerisation reactions occur when the liquid to catalyst ratio is high [107, 81]. For this reason agitated slurry and sparged catalyst reactors do not seem to be adequate for the CWAO of phenol. On the other hand, as the pollutants are diluted the intrinsic reaction rates are low, thus mass and heat transfer limitations should not be as important as in the case of pure reaction systems, for example for hydrogenation reactions. These facts suggest that fixed bed reactors are the priority choice for the CWAO of phenol.

There exist three basic modes of operation of gas - liquid - solid fixed bed catalytic reactors, depending on the direction of the gas and the liquid flow, as shown in Fig. 1.8. The Trickle Bed Reactor (TBR) is characterised by the cocurent downflow of both gas and liquid phases (shown in Fig. 1.8a), although the countercurrent operation of liquid downflow and gas upflow, (Fig. 1.8b) may be advantageous in special cases. The last configuration is that of cocurrent gas and liquid upflow, then termed packed bubble column (Fig. 1.8c).

The most frequently used in industry is the TBR as it allows a variety of flow regimes making it more flexible. Up flow reactors are used when it is necessary to assure complete external wetting of catalyst. Furthermore, they have been shown to permit better temperature control for extremely exothermic reactions [162]. Countercurrent operation allows to selectively remove by-products that may inhibit catalyst performance. The large experience on the operation of TBRs in industrial hydrotreatment processes, makes them the first choice for the performance of CWAO reactions.

1.6.2 Design Parameters of TBRs

In the TBR the liquid flows mainly over the catalyst particles in the form of rivulets, films and droplets. It is generally accepted that the liquid phase can be distinguished in dynamic (moving) and static (stagnant) zones, as schematically illustrated in Fig. 1.9. Prior to the reaction that takes place on the external and internal surface of the catalyst particles, the reactants and products have to diffuse from the gas or liquid phase to the active catalyst sites. Furthermore, the flow rates and the thermophyisical properties of the gas and liquid phase, influence the flow patterns, and the degree of backmixing of the liquid phase. Thus, the TBR is a result of complex interactions between the
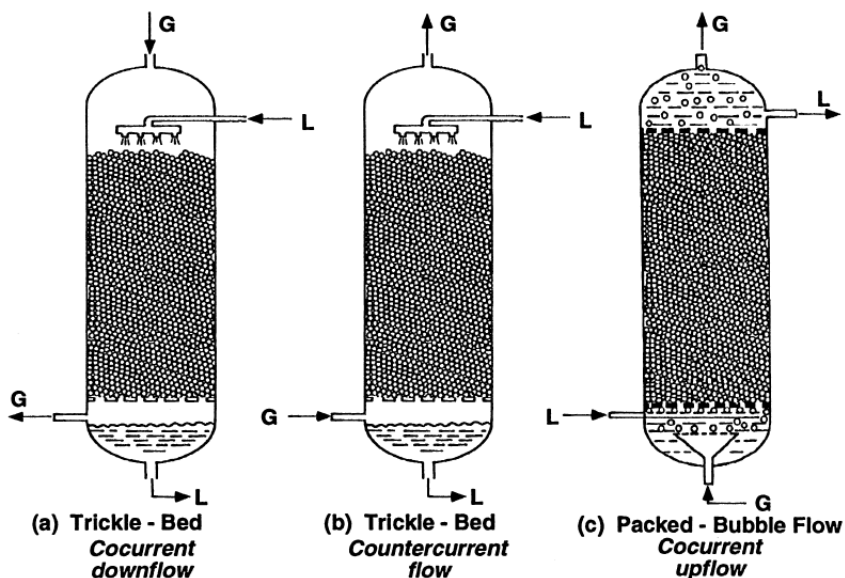
Figure 1.8: Packed bed reactors for gas-liquid-solid catalysed systems. (a) Trickle Bed Reactor with cocurrent downflow; (b) trickle bed with counrercurrent flow; (c) Packed bubble-flow reactor with cocurrent upflow. [156].

intrinsic reaction kinetics, the multiphase heat and mass transfer and the gas liquid hydrodynamics.

To account for the above phenomena several models have been developed involving several parameters. Such parameters are the catalyst wetting, the liquid holdup, the interface mass transfer coefficients (gas-liquid, liquid-solid and gas-solid), the intraparticle effective diffusion coefficient and the axial dispersion coefficient. These parameters depend on the hydrodynamic regime of the reactor (ie. the pattern of the gas-liquid flow) and the physical properties of the gas, liquid and solid. These parameters are discussed below.

Flow Regimes: Flow regimes are meant to describe the pattern of the two phase flow throughout the reactor, which considerably influences the hydrodynamic and the transfer properties in the reactor. Several flow patterns have been proposed, and several regime maps have been reported [164, 165, 138]. The differences between different investigations are cause by the different conditions and fluids used in each study, especially if foaming fluids are present in the liquid phase. However, for most industrial or laboratory applications of TBRs, with non-foaming liquids, operate in the in the trickle or pulse regime [165]. As already mentioned in the trickle regime the liquid trickles laminarly over the packing. At higher liquid and/or gas liquid velocities pulsing flow appears, while for low liquid velocities and high gas velocities the flow is in spray form.

The flow regime studies have been mainly carried at low pressure-temperature con-
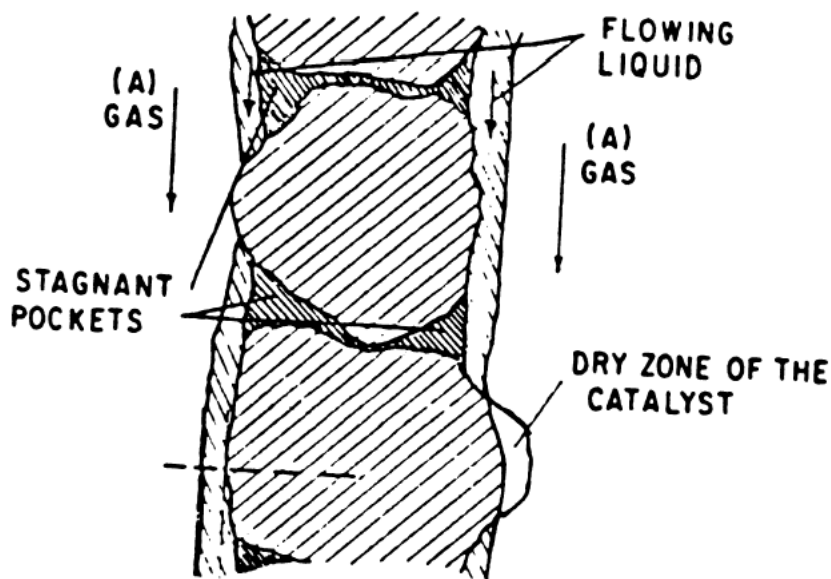
Figure 1.9: Trickle Flow in a catalyst bed [163].

ditions. As expected changes are observed at higher pressures and temperatures. Here, a simplified map accounting only for the transition of trickle to pulse regime at high pressure is presented in Fig. 1.10 [166].

The flow regimes that appear in up flow operation have also been monitored. In this case at low gas flow rates the bubble flow takes place. At high gas superficial velocities and low liquid spray flow appears, whereas at high gas and liquid velocities pulses appear [165].

Catalyst wetting: The wetting efficiency can be defined as the averaged fraction of the external particle surface that is covered by liquid as shown in Fig. 1.9. It should be mentioned that in most cases the particle is internally completely wetted by capillary effects, unless in the case of very exothermic reactions, where the reaction heat release can volatilise the liquid trapped in the pores [167]. The incomplete wetting of catalyst particles in TBRs has two causes [156]. The first one is because of liquid maldistributions on reactor scale, that leave certain portions of the bed poorly irrigated. This problem can be readily addressed through a proper design of liquid distributors, as well as proper packing procedure. However, incomplete catalyst wetting is inherently related to TBRs at low liquid flow rate, because there is not enough liquid to cover all the catalyst surface. The catalyst wetting can be improved, not only by increasing the liquid flow rate, but also by increasing the gas flow rate or operating pressure, because both factors increase shear stress on the gas-liquid interface, which spreads the liquid on the catalyst surface [168]. Conversely, the operation at elevated temperatures results in a decrease of catalyst wetting [156].
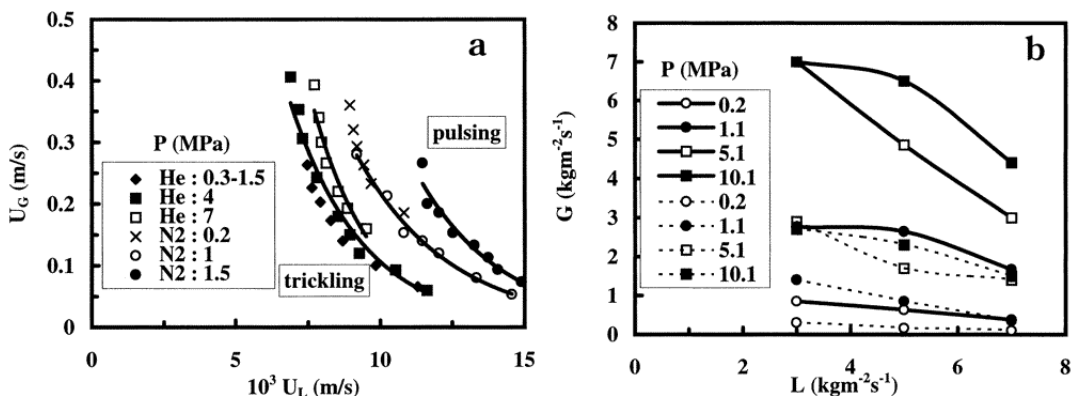
Figure 1.10: Effect of pressure and physical properties on trickle-to-pulse flow regime transition: (a) water/nitrogen and water/helium systems; (b) water/nitrogen system (continuous lines) and ethyleneglycol/nitrogen system (dotted lines). Lines represent the trends. (Taken from the review of: [166]).

The degree of catalyst wetting will have a significant effect on the achieved conversion and may condition the reactor operation. If the limiting reactant is in the liquid phase complete wetting enhances conversion, whereas, if the limiting reactant is in the gas phase, an incomplete wetting gives higher conversions [166]. To allow for complete wetting at given operating conditions of the TBR there are two possible options. 1) to operate the reactor in upflow mode and 2) to dilute the catalyst bed with fines [169]. In the former case the complete wetting is guaranteed as the reactor is flooded with liquid and when the reactor operates in the bubble flow regime the gas is flowing dispersed in the form of small bubbles. The latter option may not lead to 100% wetting at low liquid flow rates [170], but it has been shown that both configurations can yield similar conversions [169].

The comparison between upflow and down flow configuration for either gas or liquid reactant limitation is exemplarily shown in Fig. 1.11 for the hydrogenation of α-methylstyrene over $Pd/\gamma - Al_2O_3$. Under gas limited conditions (low hydrogen pressure) down flow operation with partial catalyst wetting resulted to higher α-methylstyrene conversions. This behaviour is inverted at higher hydrogen pressure, where the reaction turns liquid reactant limited and up-flow mode, results to higher conversions [169]. Khadilkar et al. [171] proposed a simple criterion to diagnose the operation mode that will achieve higher conversions. These authors defined the γ reactant flux ratio as follows:

$$\gamma = \frac{D_L^{eff}C_L}{\nu D_g^{eff}C_g} \tag{1.10}$$

Where D^{eff} is the effective diffusion coefficient of the reactant in the catalyst particle, C is the concentration, ν the stoichiometric coefficient and g and L correspond to the gas and liquid phase respectively. According to Khadilkar et al. [171], when $\gamma \gg 1$, the reaction is gas-reactant limited and downflow mode is preferred, in terms of conversion.
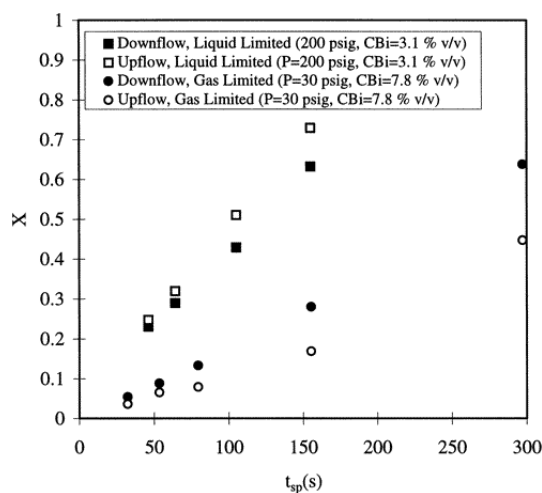
Figure 1.11: Comparison of conversion (X) at different space times t_{sp} between trickle-bed and upflow performance for the hydrogenation of α-methylstyrene to cumene over a $Pd/\gamma - Al_2O_3$ catalyst: (a) Gas-limited reaction; (b) liquid-limited reaction [169].

Conversely, for $\gamma \gg 1$, the system turns to liquid-reactant limited and the preferred operation mode is downflow. This criterion successfully applied in situations were both upflow and downflow operation had been tested.

Although the achievement of high reaction rates is usually desired, in certain situations this is not the case. For strongly exothermic reactions the reaction rate increase results to higher temperature rise in trickle bed operation, which can lead to temperature runaway [167], while upflow operation allows for better temperature control [162, 172, 173, 174]. For complex reactions, the final product distribution can also be affected by the operation mode and strategy. Stüber and Delmas [174], suggested a multistage upflow operation for the optimisation of the selectivity, while Chaudhari et al. [173], considering a single stage process, obtained higher selectivities in downflow operation.

Liquid hold up and pressure drop: The total liquid holdup is defined as the external (interparticle) and internal (intraparticle) fraction of the total volume of the reactor occupied by the liquid phase. For reasons of simplicity the external holdup will be simply termed as the liquid holdup. Liquid holdup can be further distinguished in dynamic and static holdup. The former corresponds to the liquid portion that flows through the reactor, while the latter is the stagnant liquid trapped in the void sections between the particles. Pressure drop is related to liquid holdup as the latter determines the effective void fraction, which is available for the gas phase, in the reactor. Dudukovic et al. [156] gave an excellent review of the qualitative dependence of liquid hold up and pressure drop on operating conditions. Some of the most interesting trends are the following:

- At a given gas density, the two-phase pressure drop increases with gas and liquid mass fluxes, superficial velocities and liquid viscosity. Liquid holdup increases with

liquid mass flux and superficial velocity and liquid viscosity, but decreases with increasing gas mass flux or superficial gas velocity.

- At given superficial velocities and as gas density is increased, the pressure drop increases while the liquid holdup decreases. When the pressures of gases of different molecular weights are set to have equal densities, identical pressure drops occur for the same fluid throughputs.

- Liquid holdups in PBCs in bubble flow are greater than in TBRs in trickle flow, whereas in pulse flow, they tend to be quite close in values. For design purposes, both the PBC and TBR can be treated as hydrodynamically similar in the pulse flow regime.

Liquid phase backmixing: Axial mixing can influence TBR performance in bench and pilot plant TBRs although they usually do not affect significantly performance of commercial units [163]. To account for axial dispersion the piston dispersion, or the piston dispersion-exchange model have been employed. The piston dispersion model considers that that the processes provoking backmixing exhibit the same functional relationship as the Fick Law [191]. However, the residence time distribution measurements in trickle beds have been described more realistically by the piston dispersion exchange model assumes mass transfer between dynamic liquid and stagnant zones [191, 177].

Mears (cited in [191, 157]) developed criteria for the estimation of axial dispersion effects. According to these criteria, the required reactor length, (L), to particle diameter, d_p, to hold the reactor length within a 5% of that calculated assuming ideal plug flow is:

$$\frac{L}{d_p} = \frac{20n}{Pe_L} ln\frac{C_{feed}}{C_{exit}} \tag{1.11}$$

where $Pe_L = d_p\, u_l/D_L^{ad}$, u_L the liquid superficial velocity, D^{ad} the axial dispersion coefficient and n the reaction order. Gianetto and Specchia [157] state that for beds around 20 times longer than the catalyst pellet size axial dispersion may be negligible.

Interphase mass transfer coefficients: Prior to the surface reaction, interphase mass transfer (also termed *External diffusion*) has to take place to bring the reactants to the catalyst particle. In agreement with Fig. 1.9 these interphase resistances can occur in the transport from gas to liquid, from liquid to solid, from gas to solid and from dynamic to static liquid. To model the mass transfer between phase mainly the simple 2 film theory has been used. This model locates all the resistances to the mass transfer in a small interphase layer and defines a mass transfer coefficient that correlates the concentration difference to the mass flux across the interphase.

For the gas to liquid resistance it can be written:

$$\frac{1}{K_L a_i} = \frac{1}{H k_g a_i} + \frac{1}{k_L a_i} \tag{1.12}$$

Were K_L, k_g and k_L are the overall, the gas side and the liquid side mass transfer coefficients, a_i is the gas-liquid specific interphase area H being the Henry constant.

For sparingly soluble gases, like oxygen in water, Hk_ga_i is reported to be at least one order of magnitude larger than k_La_i at the given gas and liquid rates used in TBRs [175]. Thus the overall coefficient is approximately equal to the liquid side coefficient, which is thus the limiting step in the mass transfer between the gas and the liquid phase. At a given gas density, liquid side volumetric mass transfer coefficient increases with increasing gas and liquid flow rates, as well as with increasing gas density [156].

Similarly, the liquid-solid mass transfer has been modelled in terms of the external catalyst surface a_s and a mass transfer coefficient k_s. k_s increases with increasing liquid superficial velocity, as can be judged from the correlations available in the literature [165, 166, 156]. However, these correlations do not state effect of the gas flow on k_s. On the other hand, the dependence of k_s on pressure is not yet understood and future research work should address this open aspect [156]. For upflow operation, Stüber et al. [176] have shown that liquid solid mass transfer coefficient at high pressures increases also with gas velocity, at very low liquid velocities.

For incomplete wetting, direct gas to solid mass transfer is sought to be very fast compared to the other mass transfer resistances, thus Herskowitz and Smith [175] suggest to consider equilibrium concentration on the gas-solid contact surface.

The criteria encountered in the literature for the detection of significant external mass transfer limitations compare the volumetric mass transfer rate to the reaction rate [191, 165, 138, 157]. When the true reaction rates are not *a priori* known, these criteria can be expressed in terms of the experimentally observed reaction rate (r^{obs}) that can be obtained for example by initial reaction rate measurements. It is generally accepted that there are no significant external mass transfer limitations if the following inequalities hold, both for gas-liquid (gl) and liquid-solid (ls) resistances:

$$\alpha_{gl} = \frac{r_{obs}\rho_b}{(k_{gl}a)C} < 0.05 \tag{1.13}$$

$$\alpha_{ls} = \frac{r_{obs}\rho_b}{(k_{ls}a_s)C} < 0.05 \tag{1.14}$$

where C is the concentration of the limiting reactant in the liquid phase.

Intraparticle diffusion: Intraparticle diffusion (also termed as *internal diffusion*) of reactants and products occurs in the catalyst pores. To account for internal diffusion an effectiveness factor η can be defined as the ratio of the observed (apparent) reaction rate for a catalyst particle, to the reaction rate that would be obtained if the concentration of the reactants in the entire particle were those at the particle surface. In the past, several analytical approximations have been developed for the calculation of η [165, 175]. Nonetheless, the increasing computational capacity of the current computers makes more attractive the numerical solution of the simultaneous diffusion-reaction equation for the catalyst particle [138], given below for spherical catalyst particles:

$$\frac{1}{r^2} \frac{d}{dr} \left(r^2 D_j^{eff} \left(\frac{dC_j}{dr} \right) \right) + \rho_p R_j \; = \; 0 \tag{1.15}$$

with boundary conditions at the center and the surface:

$$\left. \frac{dC_j}{dr} \right|_{r=0} \; = \; 0 \tag{1.16}$$

$$C_j(r = r_p) \; = \; C_j^* \tag{1.17}$$

To perform the above calculations the effective diffusion coefficient of the compound j in the catalyst particle has to be evaluated. This is usually calculated based on the diffusion coefficient of the respective compound in the bulk liquid phase and the porosity ϵ_p and tortuosity τ of the catalyst as follows [191]:

$$D_j^{eff} = \frac{D_j \epsilon_p}{\tau} \tag{1.18}$$

Effectiveness factor calculation presents some particular features for the case of TBRs. The fact that for low liquid flow rates catalyst particles can be partially wetted, leads to asymmetric reactant concentration on the catalyst surface. To properly deal with this situation, the calculation of an overall effectiveness factor is proposed averaging two effectiveness factors calculated for a fully wetted η^l and a completely dry η^g particles in the following way:

$$\eta = f\eta^l + (1 - f)\eta^g \tag{1.19}$$

If the limiting reactant is in the liquid phase η^g is simply considered to be zero, i.e. only the wetted part is considered to participate. On the other hand, if the gas reactant is limiting, then the liquid reactant concentration is considered to be uniform over the whole particle. This approach has been further modified accounting also for the stagnant liquid portion covering the catalyst (Fig. 1.12) given good results for the modelling of hydrogenation reactions [178, 173] and has been also extended to account for vapor side contribution in the case of volatile liquid reactants [179].

To diagnose the existence of internal diffusion limitations the Weisz - Prater criterion, modified for n-order reactions [138], can be used. In the first place the observed reaction rate, based on experimental data has to be determined. Then a quantity termed the Φ ratio can be calculated:

$$\Phi = \frac{(r_j \rho_p)_{obs} L_p^2}{C_j^* D_j^{eff}} \tag{1.20}$$

Where L_p is the ratio of catalyst volume to the catalyst surface. For n-order reactions, if $\Phi \ll 2/(n+1)$ it can be considered that internal diffusion limitations can be neglected.
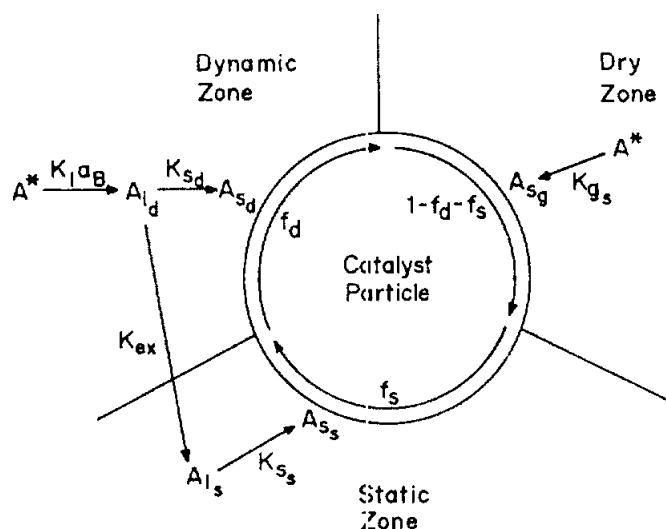
Figure 1.12: Spherical catalyst particle shown as divided in three zones [178].

Heat transfer: TBRs are often used to carry out exothermic reactions, thus heat transfer phenomena can be important. Since the reaction takes place in the catalyst particles, the reaction heat is released inside them. Thus, the heat has to be transferred to the bulk gas and liquid phases and, if the reactor is not operating under adiabatic conditions, to the environment. Intraparticle temperature gradients are not likely to occur in a TBR, unless liquid phase vaporisation takes place [191]. Thus, usually only radial heat transfer and the heat transfer to the wall reactor is taken into account [175]. Radial temperature gradients occur when the reactor diameter to reactor length ratio is high. The heat flux across the wall has to be considered, when the reactor does not operates adiabatically.

Property estimation: The TBR hydrodynamic and mass transfer parameters can be evaluated experimentally, as done by Stüber et al. [176]. However, it is unfeasible to do so every time a TBR operation is considered. Thus, for the calculation of the above magnitudes one has to rely on the numerous correlations that have been published in the literature. An excellent summary of these can be found in the recent review of Dudukovic et al. [156]. Unfortunately, as mentioned in the review, one cannot recommend a best universal correlation. Fig. 1.13 presents the experimental values and the respective predictions of established correlations for: (a) External liquid holdup in low and high interaction regime. (b) Liquid superficial velocity at trickle-pulse transition. (c) Pressure drop in trickle flow. (d) External liquid holdup in trickle flow. This panorama shows that significant deviations are possible, and this is the reason why industrial practise usually relies on *in house* correlations.

In the absence of such data, one should use the correlation obtained for systems and conditions as similar as possible to the ones under study. Fortunately, the air-water
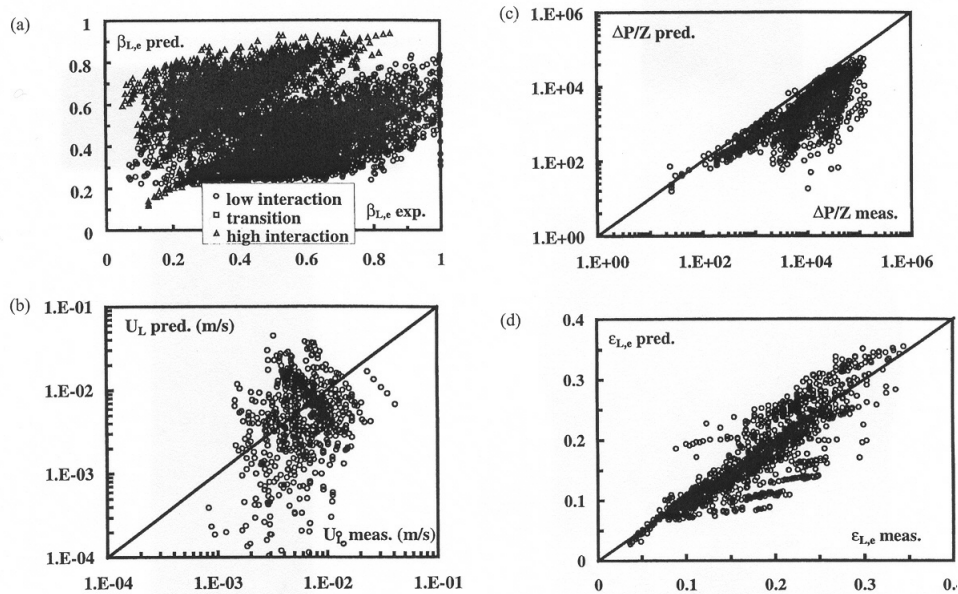
Figure 1.13: Error in hydrodynamic parameter estimation with well established correlations [156]. (a) External liquid holdup in low and high interaction regime. (b) Liquid superficial velocity at trickle-pulse transition. (c) Pressure drop in trickle flow. (d) External liquid holdup in trickle flow.

system is one of the most widely studied, although in most cases only at low pressure-temperature conditions. Conversely, CWAO reactions take place at high temperatures and pressures. The recent efforts to develop more reliable correlations, that should be also valid for high P-T conditions, are mainly based on phenomenological [180, 181, 182], CFD [183, 184], Neural Networks [185] and hybrid phenomenological-Neural Network approaches [186]. CFD based approaches should be more reliable, but their implementation is not trivial. Phenomenological models should be more reliable for extrapolation, when there are no significant non-linearities in the system studied. Neural Network approaches have the advantage that they are very good non-linear approximators and there is no need for simplifications that are done on phenomenological models. On the other hand, they are less reliable when they are used outside of their fitting range. Due to the high temperature-pressure conditions considered in this study phenomenological methods, when available have been preferred.

The high number of correlations available in the open literature would require a disproportional space to discuss them and only the correlations selected for this study will be discussed later in the Section 2.4.2. A detailed presentation of the latest correlations on the catalyst wetting, liquid holdup and pressure drop, gas - liquid and liquid solid mass transfer reader may refer to Duducovic et al. [156] and Al-Dahhan et al. [166]. The same authors also [175] present a review of correlations for the radial thermal conductiv-

ity and the wall heat transfer. Herskowitz and Smith [175] present several correlations for the calculation of the Peclet number, while Iliuta et al. [192] present data for the incorporation of the effect of the stagnant zones in the modelling of backmixing.

1.6.3 Trickle Bed Reactor Modelling

As already shown in Table 1.9 TBR models with different degrees of sophistication can be developed. The simplest approach is to neglect all mass transfer resistances and consider a pseudohomogeneous approach as proposed by Froment and Bischoff for packed bed reactors [138]. However, one has to take care to adequately adjust gas reactant concentration in the liquid phase, to be in equilibrium with the gas phase. The model equation is given by:

$$\frac{d(u_L C_j)}{dz} - R_j \rho_b = 0 \tag{1.21}$$

Where the u_L is the liquid superficial velocity, ρ_b is the bed density and R_j the overall reaction rate of the compound j, which for complex reaction networks is given by the sum of all the reaction rates r_i in which the compound j participates.

The assumption that mass transport is faster than chemical reaction does not hold in laboratory and industrial reactors with highly active catalysts. Thus, external and internal resistances have to be incorporated in the model as well as axial dispersion effects. Depending on the particularities of each case study, several models, characterised by progressing complexity, have been proposed [99, 164, 187, 165, 157, 178].

Of special interest for the modelling of CWAO process is the model developed by Goto and Smith [99] for the catalytic oxidation of formic acid. This isothermal one-dimensional model accounts for gas-liquid-solid external mass transfer, internal diffusion limitations and axial dispersion phenomena. The model is given by the following equations:

Reaction kinetics:

$$-R_{O_2} = k_{O_2} \eta \, C_{FA} C_{O_2} \tag{1.22}$$

Oxygen balance in the gas phase:

$$u_g \frac{d(C_{O_2})_g}{dz} + (k_L a_g)_{O_2} \left[(C_{O_2})_g / H_{O_2} - (C_{O_2})_L \right] = 0 \tag{1.23}$$

Oxygen balance in the liquid phase:

$$\epsilon_l D_{O_2}^{ad} \frac{d^2(C_{O_2})_L}{dz^2} - u_L \frac{d(C_{O_2})_L}{dz} + (k_L a_g)_{O_2} \left[(C_{O_2})_g / H_{O_2} - (C_{O_2})_L \right] -$$

$$(k_s a_s)_{O_2} \left[(C_{O_2})_L - (C_{O_2})_s \right] = 0 \tag{1.24}$$

Formic acid balance in the liquid phase:

$$\epsilon_l (D_{FA}^{ad} \frac{d^2(C_{FA})_L}{dz^2} - u_L \frac{d(C_{FA})_L}{dz} - (k_s a_s)_{FA} [(C_{FA})_L - (C_{FA})_s] = 0 \tag{1.25}$$

Liquid particle mass transfer for Oxygen:

$$(k_s a_s)_{O_2} \left[(C_{O_2})_L - (C_{O_2})_s \right] = (-r_{FA}) \tag{1.26}$$

Liquid particle mass transfer for formic acid:

$$(k_s a_s)_{FA} \left[(C_{O_2})_L - (C_{FA})_s \right] = (-r_{FA}) \tag{1.27}$$

The model does not consider the partial wetting, although it has been proven that the models that incorporate the effect of partial wetting perform better [188].

As TBRs are often used for highly exothermic reactions like hydrogenation or oxidation, the energy balance is required to determine the variation of the reactor temperature. A general approach, here modified to account for multiple reaction systems and heat transfer across the reactor wall, is given by Gianetto and Speccia [157]:

$$-\lambda \frac{d^2 T}{dz^2} + (u_l \rho_l c_{pl} + u_g \rho_g c_{pg}) \frac{dT}{dz} = \sum r_i^{app} (-\Delta H_i) - \frac{4 \, U_w \, (T_b - T_w)}{d_r} \tag{1.28}$$

Eq. 1.28 assumes that interface heat transfer is very fast, so that all phases have the same temperature. However, for extremely exothermic cases, temperature gradients between gas/liquid and solid phases can exist, and they should be incorporated in the model [189, 190].

Equation 1.28 does not account for the effect of liquid phase evaporation, which can be significant for the CWAO conditions. Van Gelder et al. [193] proposed two different approaches to quantify the solvent evaporation effect. The first one postulates that the gas phase is saturated with solvent vapor. Then, the amount of vapor that has to be evaporated is calculated to satisfy the vapor liquid equilibria for the given conditions. The other approach considers a liquid to gas flux, with a sufficiently volumetric mass transfer coefficient. Then, taking the vapor pressure of the solvent at the gas liquid interface equal to the saturated vapor pressure, the evaporating flux can be calculated. The latter approach requires less computational time because of a simplified numerical treatment.

It should be pointed out that the above discussion is limited to one dimensional approaches that are valid for reactors with high length to diameter ratio, or when the reaction is not highly exothermic. When this is not the case, as it can be in some industrial applications, the use one-dimensional models is not recommended [194].

1.6.4 Applications of TBRs in CWAO

The vast majority of CWAO studies, discussed in previous sections, deals with catalyst performance and reaction kinetics aspects. Less studies have focused on CWAO reactor operation, design and modelling. The studies of Tukac and Hanika [19], Tukac et al. [195], Santos et al. [68, 69] and Stüber et al. [107] focused on experimental observations of the TBR performance. The studies of Smith and co-workers [99, 100], Pintar et al. [79]
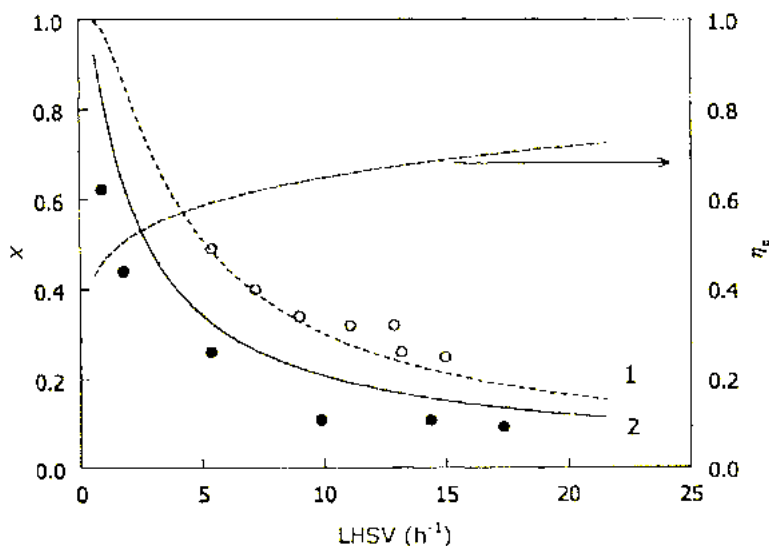
Figure 1.14: Phenol conversion (x) and wetting efficiency (η_c) vs liquid hourly space velocity. Temperature 168^oC , gas flow rate 38 L/H and total pressure 5 MPa. ($\circ$) random-packed bed, ($\bullet$) bed diluted with fines [195].

and Maugans and Akgerman [196] propose TBR models and compare their predictions to experimental observations. Finally, Larachi et al. [197] and Iliuta and Larachi [198] compared different gas - liquid - solid reactors by numerical simulations. The major findings of these studies are summarised below:

Experimental Observations: Non-idealities in TBRs operation during CWAO reactions have been reported by Tukac and Hanika [195], Tukac et al. [19] and Santos et al. [68]. The former studies [195, 19] reported that phenol conversion could decrease with increasing residence time and attributed this fact to the insufficient wetting of the catalyst particles. These non-idealities disappeared when they diluted the catalyst bed with inert fines, to increase catalyst wetting. Nonetheless, the obtained conversions were still to the obtained without catalyst dilution with fines, as shown in Fig.1.14. The authors justified this behaviour because of the enhanced oxygen mass transfer from the gas phase to the catalyst particle through the wet surface.

Santos et al. [68] performed experiments at different catalyst concentrations (i.e. catalyst dilution with inert particles of the same size) in a fixed bed up-flow reactor. They report the existence of a critical catalyst concentration, above which the reaction rate is of first order dependent on catalyst weight. For lower catalyst concentrations, the apparent reaction rate is no longer proportional to the catalyst concentration because the homogeneous contributions to the apparent reaction rate become significant.

Non-isothermal operation in CWAO reactors has been also studied by Tukac and Hanika [19]. These authors used an adiabatic TBR to oxidise a 5 g/L aqueous phenol solution. Adiabatic operation should give a temperature rise of 39^oC at complete phenol conversion. Experimentally, the conversion achieved was 25%, thus a temperature rise of 10^oC should be expected. Although it could be expected that the temperature rise should be lower, due to evaporation effects, it was found to be even higher than the expected, taking a value of 13^oC. This contrasts the observations for non catalytic WAO where the ATR in the reactors is significantly affected by water evaporation [38].

Modelling: Up to date only a few studies have been published aiming to predict integral reactor performance [99, 100, 79, 196]. Smith and co-workers modelled the oxidation of formic acid [99] and acetic acid [100] in a TBR. The reaction kinetics used in these studies were previously obtained operating the same reactor in a differential mode, i.e. with low catalyst loading. The reactor model they used is given by eq.1.22 - 1.27:

The respective gas to liquid and liquid to solid mass transfer coefficients were obtained by correlating experimental data at 25^oC and 0.1 MPa and can be found in [215]. The plug flow model was also considered by neglecting the axial dispersion terms. For the CWAO of formic acid [99], both models performed well giving errors between 0% and 5% with respect to experimental observations. As model predictions systematically overpredicted conversion the authors argued that these are caused by errors in physical property estimations, rather than inadequacy of the model. The relative importance of transport resistances according to this model, in decreasing order was: gas to liquid, intraparticle diffusion, liquid to particle and axial dispersion. The authors considered the fact that gas to liquid resistance was more important than intraparticle diffusion as a characteristic of TBR type. For the CWAO of acetic acid [100] higher deviations were observed at low liquid flow rates, which the authors attributed to channelling effects.

Pintar et al. [79] used the same model for the CWAO of phenol in a TBR. They used Langmuir Hinshelwood kinetics obtained from experiments in a differential liquid full packed bed reactor [80], with no internal diffusion resistances. Although they calculated the wetting efficiency between 0.6 and 0.7, they did not account for it in the model. Their simulations predicted phenol conversions more than 50% lower than the experimental ones. This could not be justified by simple mass transfer limitations, because even when they neglected all mass transfer resistances model prediction remained almost unaffected. To match experimental concentrations they multiplied the frequency factor of the rate equation by a factor of 3. According to the authors, this can be justified because the direct contact between gaseous oxygen and the catalyst, produces an increase in the number of active sites of the catalyst.

Very recently, Maugans and Akgerman [196], presented a TBR model for the CWAO, accounting for external and internal diffusion resistances and catalyst deactivation, although the reasons of the latter were not investigated. The reaction kinetics they used were previously obtained in a slurry reactor and the model performed well and the obtained profiles match experimental observations. It is interesting to note that in this case the batch kinetics were successfully transferred to the fixed bed reactor, contrary to the

case of Pintar and Levec [80] and Stüber et al. [107].

The issue of reactor screening has been attended from a theoretical standpoint. Larachi et al. [197] and Iliuta and Larachi [198] modelled the performance of different reactor types with non-deactivating and deactivating catalysts for the CWAO of phenol. They considered four different reactor types, namely Trickle Bed Reactor (TBR), Packed Bubble Column (PBC), Slurry Bubble Column (SBC) and Fluidised Bed (FLB). In all simulations the effectiveness factor was calculated by solving the diffusion-reaction equation in the pellet. The TBR and PBC model equations were an extension of Equations 1.23-1.27, with the incorporation of the transient terms, as well as the effect of mass transfer from the dynamic liquid to the stagnant liquid. For the SBC an additional equation was added to account for the longitudinal distribution of the solids. The simulation results indicated that under the conditions studied, the PBC outperforms the TBR, because the reaction conditions CAWO was liquid reactant limited so partial wetting is harmful. Further they state that higher conversions can be achieved if the feed is diluted before it enters in the reactor. Finally, it was shown that the TBR and the PBC were less prone to catalyst deactivation, while the SBC suffered more severe deactivation than the FLB.

1.6.5 Overview

Trickle Bed Reactors have been widely used in the chemical industry, to bring in contact gas and liquid reactants over a solid catalyst, so they are expected to play an important role for the industrial application of CWAO. The modelling of these reactors is not trivial and effects occurring in molecular, pellet and reactor scale should be joint in an adequate model. The studies dealing with the CWAO reactor performance outline the importance of the gas liquid mass transfer resistance. Thus, it seems that the effect of catalyst wetting has to be taken into account in the modelling of CWAO processes. Finally, the issue of adiabatic operation in CWAO has not received attention, despite its significance in process economics as pointed out for the well established WAO process.

1.7   Conclusions

At the end of this literature review, we are able to extract some conclusions that are relevant for the work on the CWAO of organic pollutants. First it can be said that the need for effective wastewater recycling has strongly reinforced the research on low cost pollution abatement methods, since the existing techniques cannot offer a global solution. Among the emergent alternative processes, the CWAO process was found to be effective for the treatment of several pollutants like phenols, substituted phenols, carboxylic acids, ammonia, as well as industrial effluents like kraft process liquor and alcohol distillery wastewater at moderate temperatures (100-200$^o C$) and pressures (0.1-5 MPa).

Up to date, industrial scale application of this process is limited mainly because of catalyst deactivation problems and high catalyst costs. The recent development of stable catalysts is expected to realm interest for the process. Among the most promising catalysts, active carbon offers a less expensive alternative with a proven activity in the abatement of several phenol like compounds. Such pollutants are of special interest, because they are increasingly encountered in effluents that cannot be treated in conventional biological treatment plants.

The pathways leading to the complete mineralisation of the treated pollutants during WAO or CWAO processes are complex and far from being well understood. For phenol it has been shown that it is firstly oxidised towards toxic ring compounds, which consequently yield low molecular weight carboxylic acids. Due to the toxicity of the aromatic compounds formed in the first step of phenol degradation, it is important to monitor their production and destruction for the catalysts used.

Kinetic models for CWAO help to understand the elementary mechanisms of the reaction and can be consequently used for process design and optimisation. Kinetic models usually account only for the studied compound degradation rates or lumps of compounds. These models can be useful in predicting COD destruction profiles, but they miss important information concerning the exact composition of the treated effluent. Thus, the development of detailed kinetic models, accounting for the main partial oxidation intermediate products is an emerging aspect of future research work. In addition, these detailed models include more physical features of the reacting system and should be able to better describe the behaviour of the system for a wider range of conditions. Eventually, they can be used to select better mineralisation selectivity as well as to minimise toxic compound production. Existing tools for kinetic parameter estimation may not be powerful enough for the modelling of such complex reaction networks, so the application of more robust algorithms has to be considered.

It becomes evident from the literature that process engineering studies, although required for process design - optimisation, and scale-up, are still extremely scarce in the field of CWAO. Furthermore, the recent trend is to simultaneously develop process chemistry and engineering. The important question of the choice of an adequate CWAO reactor configuration is not trivial and the answer depends on numerous factors. However, in the case of the organic wastewater pollutants, like phenolic compounds, that are prone to undergo homogeneous condensation reactions, the TBR seems to be the priority reactor

candidate, providing a very low liquid to catalyst ratio and partial catalyst wetting. The latter characteristics are sought to reduce homogeneous condensation reactions and to enhance the reactor performance of three phase systems, that suffer from gas - liquid mass transfer limitations. Only comprehensive diffusion - reaction models can describe the complex nature of the such systems and provide thereby useful tools for the design and scale up of CWAO processes. The renewed interest in CWAO should be the incentive for more in depth studies to model the interactions of reaction kinetics, hydrodynamics and heat and mass transfer occurring in multiphase processes. Especially, the study of non-isothermal CWAO has received extremely few attention. As in the case of the well established WAO, process energetic requirements are of outmost importance for process economics. However, this issue is impossible to correctly address up to date because there is a lack of data obtained in non-isothermal conditions. Additional non-isothermal experiments and modelling have to be conducted to assess useful information and to respond to this open aspects of CWAO.

1.8   Objectives

According to the conclusions extracted from the literature review, a combined assessment of the process chemistry and engineering aspects is desirable for the proper establishment of catalytic multiphase reaction systems such as the CWAO. To follow this emerging concept, we have concentrated the process analysis of the CWAO of phenol on three key issues inherent to solid catalysed multiphase reaction system: catalyst choice, detailed kinetic study and reliable reactor modelling to guide process design and scale up. Although it was impossible to treat all of the three topics in the same extend, we attempt to meet with our main goal, that is the development of an economic and effective treatment for the remediation of organic loaded wastewater effluents. In particular we formulated the following specific tasks related to our main goal.

1. The choice of adequate reactor and catalyst is aiming to:

   - Obtain experimentally in a TBR the dependence of phenol degradation with space time for an AC catalyst, under conditions of steady catalyst activity.
   - Compare the performance of AC with that of the $CuO/\gamma - Al_2O_3$ catalyst, through experimental observations obtained in the same reactor and in the same range of liquid flow rates.
   - Define and adequate continuous reactor type and study the influence of the reactor operation mode on the obtained phenol conversion and intermediate compounds formed.

2. The complex kinetic modelling is dedicated to:

   - Identify the main intermediates formed during the process and monitor their evolution.
   - Consider the implementation of stochastic algorithms for the development of kinetic models for complex reaction networks.
   - Develop kinetic models accounting for the complex reaction pathways followed in the CWAO of phenol over AC and $CuO/\gamma - Al_2O_3$ catalysts.

3. The detailed reactor modelling is done to:

   - Develop a transport - reaction TBR model, accounting for reactor hydrodynamics, mass transfer and and non-isothermal operation.
   - Implement the complex kinetic model and validate the TBR model with the experimental data available.
   - Simulate the scale up of a TBR for the CWAO of phenol.

Chapter 2

Methodology

This chapter describes in detail the experimental methods used, as well as the models developed in this work, to study the CWAO of phenol. A laboratory scale TBR, operating either in downflow or upflow mode, was employed to collect data on the CWAO of phenol over Active Carbon. Parallely, a stochastic algorithm (Simulated Annealing) and a gradient based method (Levenberg - Marquardt) algorithm were implemented to proceed a complex kinetic analysis of the experimental data obtained in the downflow CWAO of phenol. Useful information on the reactor model and the optimisation strategy applied in the parameter estimation is also given. Based on the obtained kinetics, a complex transport-reaction TBR model, accounting both for mass transfer and reactor hydrodynamics, is presented. The model dedicates special emphasis to incorporate emergent items in TBR modelling like partial wetting of the catalyst particles and the non-isothermal adiabatic operation with evaporation of water. A last part is dedicated to the proper determination of important physical properties and the reactor operation parameters that are required in the TBR modelling of the CWAO.

2.1 Experimental

The original experimental setup has been designed and constructed by Fortuny [199] to study the CWAO of phenol in a cocurrent downflow TBR, over a commercial $CuO/\gamma - Al_2O_3$ catalyst (Harshaw Cu-0803 Engelhard). In this work similar experimental tests were carried out, but using active carbon as a catalyst. Additionally, the reactor setup was modified to enable comparative tests of reactor performance in the cocurrent upflow mode. In the following sections specific information on materials is given and completed by the description of the experimental setup, procedures and the analytical methods employed.

2.1.1 Materials

Deionised water and analytical grade phenol (Aldrich) was used without any further purification to prepare initial phenol solutions of 53 $mmol/L$ (5 g/L). The gaseous

oxidant was compressed high purity synthetic air (Carburos Metalicos). The Activated Carbon was supplied by Merck (Ref. 2514) in form of 2.5 mm pellets. This AC is manufactured from wood and possesses low ash content (3.75%). The nitrogen B.E.T. method (Micromeritics ASAP 2000) gives a specific surface area of 990 m^2/g, a pore volume of 0.55 cm^3/g and an average pore diameter of 1.4 nm. Phenol adsorption tests performed elsewhere [18] showed a maximum capacity of 370 mg_{Ph}/g_{AC}, at 20^oC in oxic conditions. Phenol oxidation experiments with different AC particle sizes, carried out in a batch slurry reactor showed that internal mass transfer only becomes influent for particle sizes greater than 0.5 mm [107], as shown in Fig. 2.1. Thus, prior to each experimental series, the AC was crushed and sieved to obtain the 0.3 to 0.7 mm fraction (25 - 50 $mesh$). This fraction was washed with deionised water to remove all fines and then dried at 110^oC overnight, allowed to cool and stored under inert atmosphere. Finally, samples of about 6.6 g were loaded in the reactor for each experimental set.
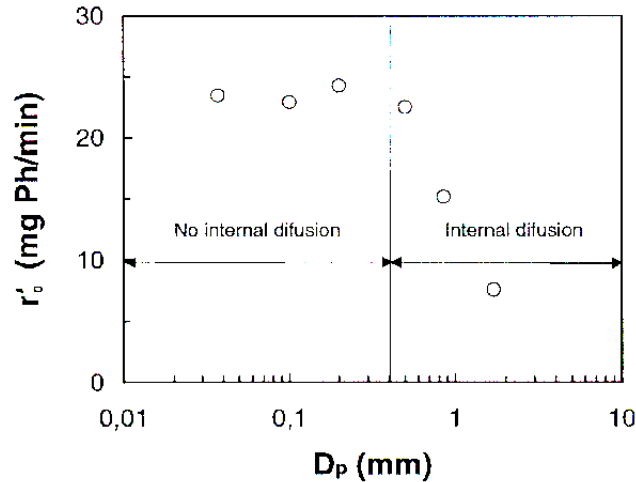
Figure 2.1: Influence of the AC particle size on the initial rate of phenol removal [107] in a semibatch slurry reactor. C_{phen}=5 g/L, m_{AC}=2 g, T=140^oC, P_{O_2}=0.55 MPa.

2.1.2 Apparatus and procedures

The continuous oxidation of phenol was carried out in a packed bed reactor performing either cocurrently downflow in the trickle flow regime or cocurrently upflow in the bubble flow regime. The fixed bed reactor, consists of a SS-316 tubular reactor, 20 *cm* long and 1.1 *cm* i.d., placed in a temperature controlled oven ($\pm 1^oC$). Independent inlet systems for gas and liquid feed allow working at variable liquid to gas flow rate ratios. The liquid feed is stored in a 5 *L* stirred glass tank, which is connected to a high-pressure metering pump (Eldex) that can dispense flow rates between 10 and 300 *mL/h*. The air oxidant comes from a high pressure cylinder equipped with a pressure controller to maintain the operating pressure constant. A flowmeter coupled with a high precision valve is used to measure and control the gas flow rate. The liquid and gas streams are mixed and then pass through a 1 *m* long heating coil placed in the oven to reach the reaction temperature. The mixture then enters the reactor and flows along the AC bed, which is retained between two sintered metal discs. The exited solution goes to a liquid-gas separation and sampling system. Regularly, liquid samples were withdrawn for analysis. A sketch of the experimental set up is also illustrated in Fig. 2.2.
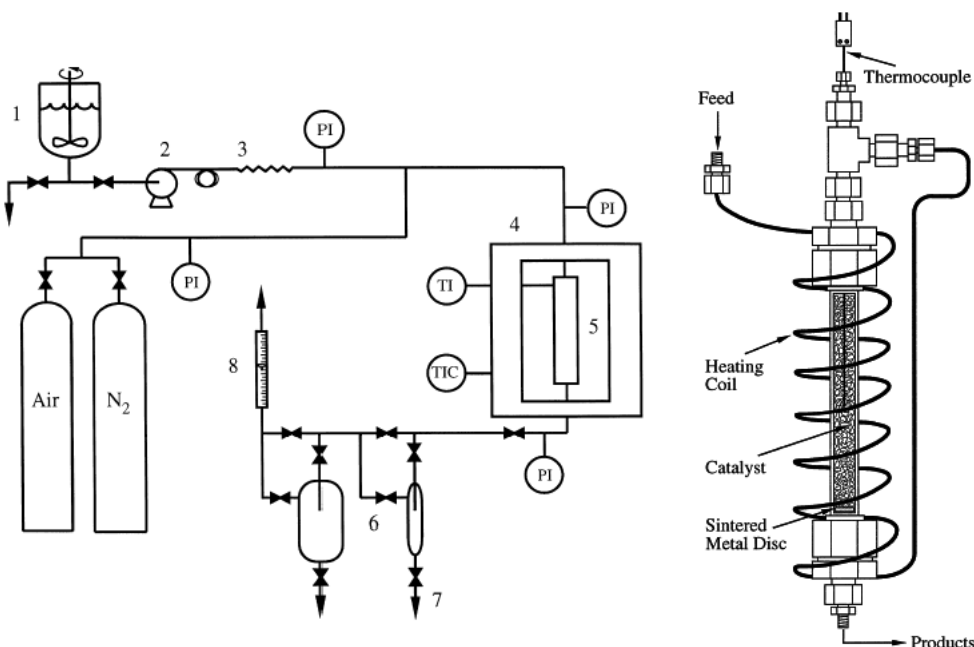
Figure 2.2: Trickle Bed Reactor and experimental set up for the CWAO of phenol. (1) Feed vessel, (2) Pump, (3) Flow regulator, (4) Oven, (5) Trickle Bed Reactor, (6) Gas Liquid Separation System, (7) Sampler, (8) Gas Flow meter

The tests were performed at three different temperatures (120, 140 and 160^oC) and two different oxygen partial pressures (0.1 and 0.2 *MPa*), changing the flow rates at

otherwise similar conditions. The liquid flow rates were ranged from 10 to 160 mL/h. Defining the space time as

$$\tau = \frac{m_{cat}}{\dot{m}_L} \tag{2.1}$$

it can be calculated that the flow rates used correspond to space times between 0.04 and 0.6 h. The air flow rate was always set at 2.4 L/s (STP). Taking into account the phenol conversions and the liquid flow rates, the total oxygen consumption during the runs was kept below 10% of the oxygen fed, except the experiment at 160^oC, 0.2 MPa and flow rate of 160 mL/h, in which an oxygen consumption of 25% was achieved.

Samples were immediately analysed to avoid changes in composition due to homogeneous condensation reactions, catalysed by sun light. In this way it was also possible to monitor the experiment in real time, and to ensure that steady state has been achieved after a new space time was set by changing the liquid flow rate. The reactor was considered to operate in steady state when in three consecutive samples the concentration did not present differences beyond experimental errors. At the end of each experimental set, corresponding to five consecutive days of continuous operation, the AC was dried for 24 h at 400^oC under nitrogen flow to desorb physically adsorbed molecules from the active carbon surface. Subsequently, the AC was weighted to detect any change of carbon mass that occurred during the experiments.

In Table 2.1 the operating conditions for the AC study are summarised. In this table the conditions used by Fortuny [199] for the study of the CWAO of phenol over the Cu0803 catalyst are also presented, since the experimental data obtained in that study will also be considered here.

Table 2.1: Laboratory reactor operating conditions

	Cu0803	AC
Phenol concentration ($mmol/L$)	53.1	53.1
Oxygen partial pressure (MPa)	0.6 - 1.2	0.1 - 0.2
Oxygen concentration ($mmol/L$)	4.6-11	0.77-1.8
Total operating pressure (MPa)	3.2 - 6.6	0.7 - 1.6
Temperature (^oC)	120-160	120-160
Space time (h)	0.1-1.0	0.04-0.6
Liquid superficial Velocity (mm/s)	0.04 - 0.5	0.04 - 0.5
Gas flow rate (mL/s)	2.4	2.4
Gas superficial velocity (mm/s)	0.5-1.2	3.3-7.4
Reactor diameter (mm)	11	11
Reactor height (m)	0.2	0.2
Particle average diameter (mm)	0.5	0.5
Density of catalyst particle (g/L)	1030	400
Catalyst load (g)	14.5	6.6
Bed porosity	0.26	0.13

2.1.3 Analysis

Liquid phase samples were analysed by means of an HPLC (Beckman System Gold) using a C18 reverse phase column (Spherisob ODS-2) to obtain the concentration profiles of phenol and intermediates. To properly separate phenol from the partial oxidation products, a mobile phase of variable composition was programmed at a 1 ml/min flow rate starting from 100% deionised water and ending at a 40/60% mixture of methanol and deionised water. The detection of low molecular weight carboxylic acids was performed with the UV absorbance method at a wavelength of 210 nm, while at the end of the sample analysis the wavelength was switched to 254 nm to detect phenol.

Single compounds were quantitatively identified by injecting pure samples of the expected partial oxidation products. In Table 2.2 the approximate retention times of all the pure compounds injected are given.

Table 2.2: Retention time of possible intermediates during the HPLC analysis.

Carboxylic acids	Retention time (min)	Phenols	Retention time (min)
Oxalic acid	1.8	Pyrogallol	8.1
Glyoxalic acid	2.0	Phloroglucinol	9.3
Formic acid	2.7	Hydroquinone	11.1
Maleic acid	3.2	Catechol	17.5
Malonic acid	3.4	Benzoquinone	17.9
Acetic acid	4.4	4-HBA	21.5
Succinic acid	6.5	Phenol	22
Fumaric	6.9	Salicylic acid	23
Acrylic acid	8.5		

Only some of these compounds were identified in the sample solutions, and were subsequently included in the standard solutions used for calibration. An example of such a standard solution, including the most important intermediate compounds is given in Fig. 2.3a. The correspondance between standard solution peaks and those of a sample obtained at 50% conversion is shown in Fig. 2.3b. However, in the sample solution several significant peaks remain unidetified, as the were found not to correspond to any of the compounds included in the Table 2.2. Calibration curves were established for each intermediate detected using standard solutions that cover the composition range of the detected intermediates. Standard solutions were not only tested before starting the experiment, but also periodically between samples, to correct deviations in retention time and/or peak area, which can be caused by small changes in flow rates, column performance and temperature.

The liquid stream was also immediately analysed for the remaining COD by the closed reflux colorimetric method [200], according to which the organic substances are oxidised (digested) by potassium dichromate $K_2Cr_2O_7$ at 160°C in a sealed tube. When orange colored $Cr_2O_7^{2-}$ is reduced, green colored Cr^{3+} is formed which can be detected in a spectrophotomer set at 600 nm. The relation between absorbance and COD concentration
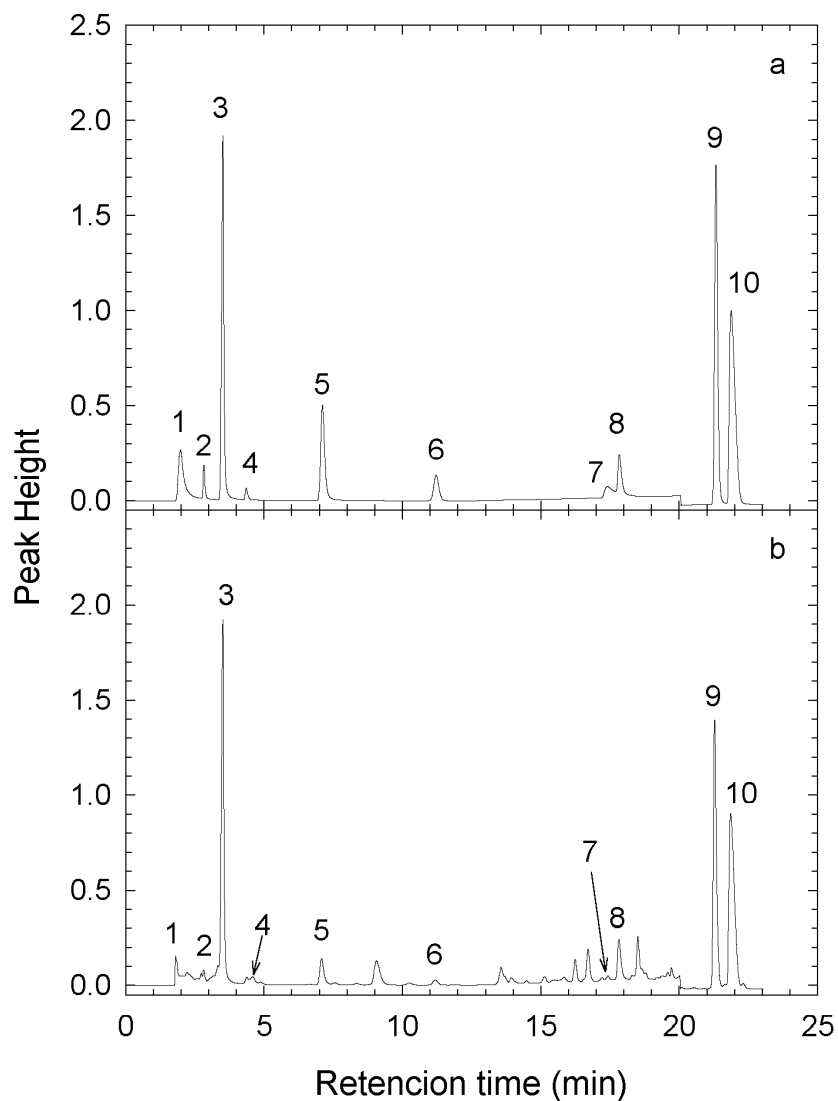
Figure 2.3: Example of (a) standard solution, and (b) sample solution chromatograms. (1) Oxalic acid, (2) Formic acid, (3) Maleic acid, (4) Acetic acid, (5) Fumaric acid, (6) hydroquinone, (7) Catechol, (8) Benzoquinone, (9) 4-Hydroxybenzoic acid, (10) Phenol

is established by calibration with standard solutions of potassium hydrogen phthalate, in the range of COD values between 200 and 1200 mg/l, as shown in Fig. 2.4. As the real sample COD values were up to 10 times higher, prior to digestion all samples were accordingly diluted.
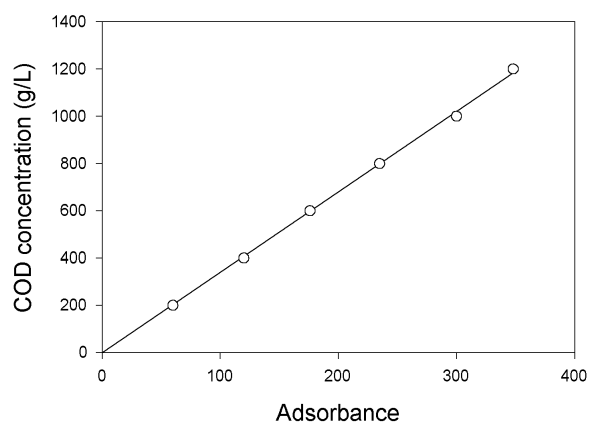
Figure 2.4: Example of calibration curve for COD determination.

2.2   Kinetic Multiparameter Estimation

Nonlinear kinetic parameter estimation methods were used to fit the concentrations predicted by the kinetic model (C_{jkl}^{model}) to the concentrations experimentally observed (C_{jkl}^{exp}), with j running over the number of compounds included in the model (N_c), k over the number of experiments conducted (N_e) and l over the different sample points, i.e. space times (N_p).This gives rise to a minimisation problem of a function $S(x)$:

$$min(S(\mathbf{x})), \quad \mathbf{x} \in \Re^{\mathbf{n}} \tag{2.2}$$

The function S is called objective function and $\mathbf{x}$ is a n-dimension vector containing the n parameters to be obtained. The elements of $\mathbf{x}$ can be restricted to fulfil simple restrictions imposed by the physics of the problem:

$$\mathbf{x_m} \geq \mathbf{0} \quad or \quad \mathbf{x_m} \leq \mathbf{0} \tag{2.3}$$

Three different objective functions were tested in this study. Initially, the Sum of Squared Errors (SSE), or the Sum of Relative Squared Errors (SRSE) were set as objective function:

$$S_{SSE} = \sum_{j=1}^{N_c} \sum_{k=1}^{N_e} \sum_{l=1}^{N_p} \left(C_{jkl}^{model} - C_{jkl}^{exp} \right)^2 \tag{2.4}$$

$$S_{SRSE} = \sum_{j=1}^{N_c} \sum_{k=1}^{N_e} \sum_{l=1}^{N_p} \left(\frac{C_{jkl}^{model} - C_{jkl}^{exp}}{C_{jkl}^{exp}} \right)^2 \tag{2.5}$$

For the S-A algorithm the Sum of Absolute Errors (SAE) was considered:

$$S_{SAE} = \sum_{j=1}^{N_c} \sum_{k=1}^{N_e} \sum_{l=1}^{N_p} \left| C_{jkl}^{model} - C_{jkl}^{exp} \right| \tag{2.6}$$

To solve the resulting problem, the conventional L-M algorithm was first tested to assess its performance, in particular when complex reaction schemes are considered. Then, the simulated annealing algorithm was implemented and compared to the L-M algorithm in the kinetic modelling of the CWAO of phenol.

2.2.1   The Levenberg - Marquardt algorithm

The L-M algorithm was selected from the FORTRAN IMSL libraries, that includes the DBCLSF subroutine, which uses a modified L-M algorithm to solve nonlinear least squares problems with a trust region approach [201].

For the SSE and SRSE criteria, S(x) can be expressed in terms of a vector function $\mathbf{F}(\mathbf{x})$ with the individual components given by Eq. 2.7 and Eq. 2.8 respectively:

$$f_w(\mathbf{x}) = C_w^{exp} - C_w^{model} \tag{2.7}$$

$$f_w(x) = (C_w^{exp} - C_w^{model})/C_w^{exp} \tag{2.8}$$

where w runs over the total number of observations $(N_o = N_c N_e N_p)$. Then, the expresion of $S(\mathbf{x})$ results in:

$$S(x) = \mathbf{F}(\mathbf{x})^\mathbf{T}\mathbf{F}(\mathbf{x}). \tag{2.9}$$

The algorithm used minimises:

$$min0.5S(x) \tag{2.10}$$

For an initial guess of the parameters $\mathbf{x}$, the search direction is calculated as:

$$\mathbf{d} = -(\mathbf{J^T J} + \mu\mathbf{I})^{-1}\mathbf{J^T F} \tag{2.11}$$

where J is the Jacobian of $\mathbf{F}$ with respect to the free variables and μ the L-M parameter. In the following step $\mathbf{x}$ is set to $\mathbf{x} + \mathbf{d}$ and the procedure is repeated untill the gradients become zero, or the parameter space bounds are reached. The L-M parameter μ is a positive number and its value is the minimum for which the matrix $(\mathbf{J^T J} + \mu\mathbf{I})$ can be inverted.

Additionally, the L-M algorithm permits a direct calculation of the variance covariance matrix $\mathbf{V}$. If the experimental errors are independent and normally distributed with a constant variance σ^2 then [153]:

$$\mathbf{V} = (\mathbf{J}\ \mathbf{J}^T)^{-1}\sigma^2 \tag{2.12}$$

In this case an estimator of σ^2 is given by $S_{min}/(N_o - n)$ where n is the number of parameters.

2.2.2 The Simulated Annealing Algorithm

The stochastic algorithm selected in this study is called Simulated Annealing (S-A). A detailed description is given in Goffe et al. [147]. The source code is freeware and was downloaded from *www.netlib.org*. The underlying concept of S-A is a random search method, first applied to thermodynamic calculations for the states of n-body frozen systems [202], and later used in combinatorial optimisation [203, 204]. Recently it has been extended to continuous optimisation problems [145, 147, 146].

Simulated Annealing starts defining an objective function, which for historical reasons is called *energy* (E). E does not have to be a continuous and differentiable function. First, the value of E of an initial parameter set $\mathbf{x}$ is calculated. Afterwards, a new set is generated from the previous by a random perturbation of the parameters, and the new value of E is calculated. If the new value of E is lower than the previous one, the new set is always accepted. In addition a new set that results in higher E values can also be accepted with a probability P if the E is higher. The probability P is a function of an auxiliary parameter termed *temperature* (T) and usually given by the Maxwell-Boltzmann distribution, revealing the thermodynamic root of the method, although other possible criteria exist.

$$P = exp(-\Delta E/kT) \tag{2.13}$$

This acceptance criterion is called the Metropolis criterion and is the basis of the Monte Carlo simulations methods used in statistical physics.

In the S-A version applied here, the new parameter sets are obtained by random perturbations of the actual set. These perturbations are calculated by adding or substracting a random fraction of a quantity termed maximum allowable step for each parameter. This maximum allowed step is a function of the temperature and it is adjusted internally so that half of the movements are accepted.

The procedure, i.e. the generation of a new parameter set, followed by the control of acceptance, is repeated for a certain number of iterations, while maintaining T constant. Subsequently, T is reduced and the procedure restarts, taking as initial parameter set the optimum encountered in the previous temperature. The probability that an uphill movement is accepted decreases and vanishes as T goes to zero. Theoretically, the method converges to the global minimum although this can only be affirmed under several restrictions [205].

To run the algorithm the objective function, an initial parameter set as well as initial values for the T and the maximum allowable step have to be provided. The T is a key parameter in the algorithm performance and its initialisation deserves some consideration. If a too high temperature value is given to the system, then almost all movements are accepted and the algorithm does not progress. Conversely, a very low value leads to *quenching* of the algorithm, which converges rapidly to a local minimum. In the present study, the initial temperature was chosen in such a way that the maximum allowable step was initially in the same order of magnitude of the parameters to be obtained, thus enabling the algorithm to scan the entire range of the possible parameter values. This choice resulted in a satisfactory convergence behaviour of the algorithm.

Obviously when the S-A is used, statistical errors in the parameters cannot be calculated by Eq. 2.12. To overcome this drawback, errors can be estimated by assuming a linear behaviour of the errors in the region near the optimum parameter set. Then, any set of parameters $\mathbf{x}$ that satisfies Eq. 2.14:

$$S(x) = S(x_{opt}) \left[1 + \frac{n}{N_o - n} F(n, N_o - n, 1 - \alpha) \right] \tag{2.14}$$

is not statisticaly different to $\mathbf{x_{opt}}$ for a confidence level of $1 - \alpha$ [138]. Note that in Eq. 2.14 F refers to the $F - distribution$.

An other possibility would be to run the S-A for a high number of different initial parameter set values and calculate directly the mean $\mathbf{x_{opt}}$ and its deviation [204]. This approach would be more adequate for the situation described here, but its application would turn out to be extremely time consuming.

2.2.3   Reactor and kinetic models

The parameter estimation was carried out by a typical integration-optimisation coupling procedure. As the L-M algorithm is optimised for least squares minimisation, the Sum of

Squared Errors (SSE) was chosen as the objective function for the comparison between the two algorithms. The ideal plug flow pseudo-homogeneous model presented in Eq. 1.21 was modified to describe the reactor in terms of the space time, instead of reactor length, yielding:

$$\frac{dC_j}{d\tau} = R_j \rho_l \tag{2.15}$$

Based on the experimental observations, oxygen consumption can be neglected, thus its balance was not incorporated in the model equations.

The reactions were initially considered to follow simple power law kinetics:

$$r_i = k_{0i} \, exp(-E_{ai}/RT) \, x_{O_2}^\alpha \, C_i \tag{2.16}$$

It can be observed that in the above equation all substrate orders are set to unity, in agreement with observations in the literature, while oxygen order was left to be determined by the optimisation algorithm. Furthermore, oxygen concentration was incorporated as mole fraction, to account for the temperature dependence of O_2 solubility. As it will be discussed later P-L kinetics did not perform satisfactory results, thus the application of Langmuir-Hinshelwood kinetics was also tested. The expression selected (Eq. 2.17), considers competitive adsorption of all adsorbed species on the same site and neglects oxygen adsorption, in agreement with the findings in the literature.

$$r_i = k_{0i} \, exp(-E_{ai}/RT) \frac{K_{0i} \, C_i \, x_{O_2}^\alpha \, exp(-\Delta H_i/RT)}{1 + \sum K_0 C_j \, exp(-\Delta H_j/RT)} \tag{2.17}$$

Reparameterisation of the preexponential factor was recommended for convergence, because of the extremely different orders of magnitude that existed in the frequency factor k_0 and the adsorption pre-exponential factor K_0. A simple reparameterisation consisted in estimating the $log(k_{0i})$ instead of k_{0i}, keeping the rest of parameters without any transformation. The S-A algorithm achieved convergence in this way, but the L-M algorithm did not, so, a more sophisticated reparameterisation was implemented, as proposed by Buzzi-Ferraris, [140]:

$$k = exp\left(\alpha_i - b_i \left(\frac{1}{T} - \frac{1}{T^*}\right)\right) \tag{2.18}$$

In this equation T^* is a mean value in the temperature range of the experimental data and was set equal to 140^oC. The new calculated parameters are a_i and b_i. From this expression the frequency factor and the activation energy (or preexponential factor and heat of adsorption in the case of adsorption constants) can be directly deduced. It should be pointed out that in all cases the parameter space was restricted to values with physical meaning. Thus, all parameters were considered positive, except from the heats of adsorption, which take only negative values, because of the endothermic nature of adsorption. This restriction is necessary, for more complex models to exclude the mathematical solutions that give a better value of the objective function, on cost of loosing physical meaning in the parameters optimised.

2.3   TBR model

The developed phenomenological model is based on the previous work of Rajashekharam et al. [178] on the hydrogenation of 2,4 Dinitrotoluene, and of Iliuta and Larachi [198] on the CWAO of phenol. In the present study the calculation of the effectiveness factor was modified to address both the gas limiting reactant and the liquid limiting reactant cases. Also, the heat balance equation was incorporated and extended to account for the evaporation of water. Thus, the model explicitly describes the following processes occurring in the TBR:

- The oxygen concentration variation across the reactor in the gas phase.

- The oxygen, phenol and intermediates concentration variation across the reactor in the dynamic and static liquid portions of the liquid texture.

- The catalyst partial wetting in trickle flow regime at low liquid throughputs.

- The axial dispersion in the dynamic liquid phase.

- The mass transfer across the interfaces between the gas-dynamic liquid, the dynamic - static liquid, the gas-solid, the static or dynamic liquid-solid.

- The intraparticle concentration gradients.

- The heat generation by the oxidation reaction.

- The heat consumption via the valve-effect of water evaporation.

In order to simplify the model equations and numerical treatment it is accepted and reasonable to postulate ideal behaviour of certain physical and chemical contributions because of the conditions at which the CWAO of phenol takes place.

- For the gas phase, ideal gas behaviour is assumed at the given operating conditions.

- The oxygen equilibrium concentration in the liquid phase is described by the Henry law.

- The pressure is constant through out the reactor.

- The dissolved organics are non-volatile and the reaction takes place only in the liquid phase.

- The catalyst operates at stable activity. Catalyst deactivation either by leaching or by carbonaceous deposits does not occur.

- Parallel polymerisation or oxidation reactions in the liquid phase are marginal.

- The catalyst is assumed to be completely wetted internally due to capillary effects.

- The catalyst wetting and liquid hold-up are assumed to be constant through out the reactor depth during non-isothermal operation.

- For the external gas-liquid, liquid-liquid, liquid-solid and gas-solid mass transfer, the two film model is used.

- The static portion of the liquid is not in contact with the gas phase.

- The heat transfer across the different phases (gas-liquid-solid) is rapid so that all phases have the same temperature at the same axial position.

- The water vapour-liquid equilibrium is established instantaneously.

The resulting model equations attempt to describe the whole process on three length scales, i.e. molecular scale (reaction kinetics), pellet scale and reactor scale. As the reaction network and the kinetics depend on the exact case study, so only the pellet scale and the reactor scale models are presented. The reaction network of the CWAO of phenol will be developed and discussed in Chapter 4.

2.3.1 Pellet scale model

To describe the simultaneous diffusion-reaction within the catalyst pellet, the mass balance equation was solved numerically assuming spherical symmetry.

$$\frac{1}{r^2} \frac{d}{dr} \left(r^2 D_j^{eff} \left(\frac{dC_j}{dr} \right) \right) + \rho_p R_j = 0 \tag{2.19}$$

with the following boundary conditions at the center and the surface:

$$\left. \frac{dC_j}{dr} \right|_{r=0} = 0 \tag{2.20}$$

$$\left. \frac{dC_j}{dr} \right|_{r=r_p} = k_{jls}^d f_d (C_j^d - C_j^*) +$$

$$k_{jls}^s f_s (C_j^s - C_j^*) + \left[k_{gs}(1-f)(C_{O_2}^g - H \, C_{O_2}^*) \right]_{only \, for \, O_2} \tag{2.21}$$

Eq. 2.21 accounts for the effect of partial wetting regardless of the limiting reactant. On the cost of superimposing the diffusive fluxes coming from the different zones of the particle, this definition gives a better flexibility as it allows the calculation of systems that lie in-between the asymptotic cases, mainly gas limited or mainly liquid limited reactions.

A partial effectiveness factor can be defined for each of the different zones (dynamic liquid, static liquid and gas), as given below for example for the dynamic liquid:

$$\eta_j^d = \frac{3k_{jls}^d f_d (C_j^d - C_j^*)}{r_p \rho_p R_j^*} \tag{2.22}$$

The overall effectiveness factor can then be described as the sum of the partial effectiveness factors.

$$\eta_j = \eta_j^d + \eta_j^s + \eta_j^g \tag{2.23}$$

Note that the weighting with respect to the fraction of catalyst in contact with each phase has been included in Eq. 2.22 so it is omitted in eq. 2.23

2.3.2 Reactor scale model

The piston dispersion exchange model was used to simulate reactor performance. However, for the gas phase simple plug flow is assumed, because the axial dispersion in the gas phase is usually orders of magnitude smaller than the liquid phase axial dispersion.

$$\frac{u_g dC_{O_2}^g}{dz} + (k_{gl}a)\left(\frac{C_{O_2}^g}{H} - C_{O_2}^d\right) - \eta_{O_2}^g \rho_p R_{O_2}^* = 0 \tag{2.24}$$

The concentrations of reactants and products in the dynamic liquid are described by means of the following mass balance equation:

$$-D^{ad}\epsilon_l^d \frac{d^2 C_j^d}{dz^2} + \frac{d(u_{ld}C_l^d)}{dz} + (ka)_{jll}(C_d^d - C_j^s) - \eta_j^d \rho_b R_j^* -$$
$$\left[k_{gl}a\left(\frac{C_{O_2}^g}{H} - C_{O_2}^d\right)\right]_{only\ for\ O_2} = 0 \tag{2.25}$$

The static liquid is considered to be only in contact with the dynamic liquid and the solid. As there is no movement of this phase along the reactor the mass balance for reactants and products is reduced to the following algebraic equations:

$$(ka)_{jll}(C_d^d - C_j^s) + \eta_j^s \rho_b R_j^* = 0 \tag{2.26}$$

Finally, following the approach of Vav Gelder et al. [193] the energy balance incorporating solvent evaporation was described considering that the gas phase is saturated with water vapor. The following equation results:

$$(u_l\rho_l c_{pl} + u_g\rho_g c_{pg})\frac{dT}{dz} + \frac{\phi}{A}\Delta H^v - \sum \rho_b r_i^{ap}(-\Delta H_i) = 0 \tag{2.27}$$

The apparent rate of the ith reaction (r_i^{ap}) is calculated from the stoichiometry and the overall formation-destruction rates ($\eta_j R_j^*$).

The evaporation rate ϕ per unit of reactor length is determined assuming that the ideal gas stream is saturated in water vapor. Denoting the molar gas flow rate by $\dot{n}_t$ and the vapor molar flow rate by $\dot{n}_{H_2O}$, the following equality must be fulfilled at any time:

$$\frac{\dot{n}_{H_2O}}{\dot{n}_t} = \frac{P_{H_2O^v(T)}}{P_t} \tag{2.28}$$

The total pressure (P_t) is marginally affected by the pressure drop throughout the catalyst bed, thus is considered constant. The gas and the liquid feed are premixed and therefore the gas enters already saturated in the reactor:

$$\dot{n}_{H_2O} = \dot{n}_{H_2O}^{inlet} + \int_0^z \phi(z)dz \tag{2.29}$$

$$\dot{n}_t = \dot{n}_t^{inlet} + \int_0^z \phi(z)dz \tag{2.30}$$

The total molar flow rates and the densities of both gas and liquid phases undergo changes, because of water evaporation and temperature gradients, thus the superficial velocities have to be adjusted.

For the gas phase velocity this axial variation is calculated assuming ideal gas behaviour.

$$u_g = \frac{\dot{V}}{A} = \frac{\dot{n}_t RT}{PA} \tag{2.31}$$

The derivation of Eq. 2.31 gives:

$$\frac{\partial u_g}{\partial z} = \frac{RT}{PA}\phi \tag{2.32}$$

For the dynamic liquid the change in the superficial velocity is both a result of density change and water evaporation. The mass liquid flow rate is then calculated as:

$$\dot{m} = \dot{m}^{(inlet)} - MW_{H_2O} \int_0^z \phi(z)dz \tag{2.33}$$

Defining the dynamic liquid velocity to:

$$u_l = \frac{\dot{m}}{\rho A} \tag{2.34}$$

the derivative is:

$$\frac{\partial u_l}{\partial z} = \frac{\dot{m}}{A}\frac{\partial}{\partial T}\left(\frac{1}{\rho_l}\right)\frac{\partial T}{\partial z} \tag{2.35}$$

The boundary conditions of the reactor model are the following:
At the reactor entrance (z=0):

$$C_{O_2g} = C_{O_2g}^{eq} \tag{2.36}$$

$$u_l C_{jl}^0 = u_l \left. C_{jl}^d \right|_{z=0^+} - D^{ad}\epsilon_{ld}\frac{\partial C_{jl}^d}{\partial z} \tag{2.37}$$

$$T = T_0 \tag{2.38}$$

At the reactor exit:

$$\frac{\partial C_{jl}^d}{\partial z} = 0 \tag{2.39}$$

2.3.3   Numerical solution

The set of algebraic - differential equations was discritisised with the method of orthogonal collocation on finite elements [206, 207]. This method has been applied here to solve differential equations of the form:

$$f(y(x), y'(x), y''(x)) = 0 \tag{2.40}$$

in the interval [0,1], and subject to boundary conditions of the form

$$f_b(y(x), y'(x)) = 0 \tag{2.41}$$

at $x = 0$ and $x = 1$.

In brief, according to this method the unknown solution $y(x)$ of a differential equation can be expressed in terms of an expansion of known orthogonal polynomials $y_i(x)$. In this study the Legendre polynomials were selected. In the interval [-1,1] these polynomials are given by the following relationships:

$$y_1(x) = 1 \tag{2.42}$$

$$y_2(x) = x \tag{2.43}$$

$$y_n(x) = \sum_{m=0}^{int(n/2)} (-1)^m \frac{(2n - 2m)!}{2^n m!(n - m)!(n - 2m)!} x^{n-2m} \tag{2.44}$$

These polynomials can be transformed to be orthogonal in an arbitrary interval [a,b] by substituting

$$x = \frac{b - a}{2}x + \frac{b + a}{2} \tag{2.45}$$

In our case the interval [0,1] was used, since the set of the differential equations can be easily reparameterised to fit in this interval.

The unknown solution can be described as a function of N_{cp} Legendre polynomials:

$$y(x) = \sum_{i=1}^{N_{cp}} \alpha_i y_i(x) \tag{2.46}$$

The first and second derivative of the function can then be calculated as:

$$y'(x) = \sum_{i=1}^{N_{cp}} \alpha_i y_i'(x) \tag{2.47}$$

$$y''(x) = \sum_{i=1}^{N_{cp}} \alpha_i y_i''(x) \tag{2.48}$$

Given that the polynomials $y_i(x)$ are known, if $y(x)$, $y'(x)$ and $y''(x)$ are inserted in the differential equation the only unknown quantity in the resulting algebraic system are the N_{cp} coefficients α_i. To evaluate these coefficients N_{cp} equations are needed. These are obtained by setting the resulting set of equations equal to zero at N_{cp} positions. For the orthogonal collocation method, these positions are defined by the two boundaries, as well as by the routes of the $y_{(N_{cp}-2)}$ polynomial. In this study N_{cp} was chosen to be eight. The solution of Legendre polynomial with degree 6 was taken from Finlayson [206]. The resulting set of algebraic equations was then solved by the Newton method as described by Press et al. [204].

The application of the method in finite elements is straight forward. In this case the space is divided into elements, at which the collocation method is applied. The boundary conditions of each element, appart from that applied in the first and the last one, is simply the continuity of the function, i.e. $y_j(x) = y_{j+1}(x)$ and $y'_j(x) = y'_{j+1}(x)$.

The source code for the descritisation of the differential equation system was programmed in FORTRAN. The number of collocation points was 8 both for reactor and pellet. In most cases with only one element, it was possible to obtain the numerical solution. Nevertheless, for complete wetting or very low effectiveness factors two elements in the reactor model were necessary to achieve convergence.

2.4   Calculation of thermophysical and reactor properties

2.4.1   Thermophysical property calculation

For the bulk liquid solution of phenol, pure water properties have been taken. The water viscosity, surface tension, heat capacity, vapor pressure and heat of evaporation were calculated from standard methods reported by Reid et al. [208]. The density of the gas was calculated by the ideal gas equation of state which was found to agree well with experimental values reported in [209] for the conditions studied. The viscosity of air was calculated by interpolation of experimental data reported also in [209]. Phenol, oxygen and intermediate compound diffusion coefficients in water, were calculated by the Wilke Chang correlation, as described in [208]. Finally, the Henry constants for oxygen in water were obtained from the data of Himmelblau [210]. Table 2.3 summarises the values of these properties for the conditions used in this study.

Table 2.3: Physical properties of the air-water-dissolved phenol reacting system at different temperatures.

	120^oC	140^oC	160^oC
Water density Kg/m^3	943	926	907
Water viscocity $(Ns/m^2)*10^4$	2.41	2.06	1.80
Water surface tension $(N/m)*10^2$	5.86	5.46	5.03
Oxygen diffusion coefficient $(m^2/s)*10^8$	1.10	1.35	1.62
Phenol diffusion coefficient $(m^2/s)*10^9$	5.37	6.60	7.93
Air viscocity $(Ns/m^2)*10^5$	2.30	2.39	2.47
Henry constant $(m^3Pa/mol)*10^{-3}$	130	121	110
Henry constant $(MPa)10^{-3}$	6.83	6.25	5.53
Water vapor pressure (MPa)	1.99	3.61	6.18
Water specific heat(kJ/kgK)	4.24	4.28	4.33
Water heat of vaporisation (kJ/kg)	2212	2153	2091

2.4.2   Hydrodynamic and mass transfer parameters

The determination of the hydrodynamic parameters of the TBR is not trivial for the CWAO operating conditions, because of the high pressure and temperature conditions employed. For this reason it was attempted to implement correlations that include data at such high temperature - pressure conditions. The total external liquid hold-up, ϵ_l, and the pressure drop is calculated using the extended Holub model [186] for trickle beds. This correlation uses a combined phenomenological - NN approach and has successfully correlated data obtained both at low and high pressure - temperature conditions. The static liquid hold-up, ϵ_{ls}, can be estimated from the Sáez and Carbonell correlation [211], or the hydrostatic theory developed by Mao et al. [212]. Both studies have been tested

against low pressure and temperature experimental data and at low values of the Eötvos Number ($E\ddot{o} = \rho_L g d_p^2 / \sigma$) both methods converge to a value of 0.05. The dynamic liquid hold-up, ϵ_{ld}, is obtained by subtracting the static hold-up from the external holdup.

The external catalyst wetting has been shown to significantly influence TBR performance, so the wetting efficiency f is a key factor to correctly assess the reactor performance. For this reason three correlations were employed fo its calculation. In the first place the phenomenological model of Iliuta et al. [213] was employed, which has been tested against the high pressure wetting efficiency measurements of the Al-Dahhan and Dudukovic [168]. Also, the empirical correlation presented by the latter authors for high pressure wetting was also employed. Finally, the correlation of Mills and Dudukovic (cited in [175]) was tested. The static, f_s, and dynamic, f_d, components of the wetting efficiency are obtained from the approximation of Rajashekharam et al. [178], i.e.

$$\frac{f_d}{f_s} = \frac{\epsilon_d}{\epsilon_s} \qquad (2.49)$$

The liquid phase axial dispersion coefficient, D^{ad}, is calculated from the NN correlation presented by Piché et al., [214]. The mass transfer coefficients between dynamic and static liquids, $(ka)_{ll}$, are taken from the plots of Iliuta et al. [177], which have been obtained at low pressure and temperature. The (dynamic) liquid-solid mass transfer coefficient, $(k_{ls}^d a_s)$, is evaluated from the empirical correlation proposed by Goto and Smith [215], obtained at low P-T, and which has been used in many CWAO studies [99, 79, 195], as well as the more recent correlation of Lakota and Levec [219]. In this latter correlation the $(k_{ls}^d a_s)$, is also a function of the liquid hold up. Since the liquid hold up is affected by high pressure [166], this correlation should be more reliable. The (static) liquid-solid mass transfer coefficient, $k_{ls}^s a_s$, is determined using the empirical correlation of Iliuta et al. [192]. The liquid-side volumetric mass transfer coefficient, $(k_{gl}a)$, for oxygen is estimated by the correlation of Iliuta et al. [185], but . The gas-side oxygen mass transfer coefficients, k_{gs}, across the dry pellet region is assumed to be one order of magnitude higher than the liquid-side mass transfer coefficient in agreement with the observations of Herskowitz and Smith [175] and Lu et al. [216]. Finally, the effective diffusion coefficients, D_j^{eff}, are approximated assuming a tortuosity factor equal to 3.

Part II

Results and Discussion

Chapter 3

Catalytic Performance of TBR using AC

A study that aims to assess the intrinsic reaction kinetics obviously should be conducted in a reactor suitable to provide hydrodynamic and mass transfer characteristics that ensure complete control by the reaction kinetics. This is readily achieved in a batch type reactor by means of a rigorous stirring of the reactor mixture and a proper selection of catalyst particle size. However, the high liquid to catalyst ratio can become influent on reaction kinetics through an enhanced contribution of homogeneous side reactions. Phenol is known to form condensation products (dimers) in the liquid phase during CWAO [81], making a solely heterogeneous kinetic study impossible in a batch slurry reactor. The irreversible adsorption of these condensation products additionally causes coke catalyst deactivation as observed by Stüber et al. [107]. The same authors also found out that the reduced extent of homogeneous side reactions do not harm the catalyst performance when the reaction is carried out in a TBR. Thus, the CWAO kinetic study of phenol was undertaken in a laboratory TBR at operation conditions that reduce at maximum the influence of hydrodynamics and mass transfer on the reaction kinetics. This assumption will be discussed in the following by analysing in detail the prevailing hydrodynamics of the gas liquid flow and by experimental comparison of the performance that resulted from either downflow or upflow operation of the cocurrent gas - liquid flow. By doing this, we attempt to check the kinetic model for consistency with respect to the absence of any mass transfer limitations.

3.1 Reactor performance

3.1.1 Hydrodynamics and Mass Transfer

First, all hydrodynamic and mass transfer parameters were estimated by means of selected literature correlations, as described in Chapter 2.4.2. These correlations need both the operation data, such as the gas and liquid flow rates, the type and the size of catalyst particles and the reactor dimensions, and the physical properties of the fluids.

Flow regime: The operating conditions for the laboratory TBR have been already summarised in Table 2.1. For the conditions used the laboratory reactor operates in the trickle regime as can be verified from Fig. 1.10. Similarly, during upflow operation tests the reactor operates in the bubble flow regime as can be verified from the flow maps summarised by Ramachandran and Chaudhari [165].

Catalyst wetting: For the downflow operation the wetting efficiency was calculated to be less than unity independently of the correlation used. Table 3.1 presents the values obtained from three different correlations. It can be seen that the correlations of Iliuta et al. [213] and Al-Dahhan and Dudukovic [168], that have been adjusted including high pressure data, are in close agreement. These correlations give wetting efficiency values that are about half those estimated by the correlation of Mills and Dudukovic (as reported by [175]), which has been obtained at low pressure conditions. Despite these deviations, it is clear that the laboratory reactor should operate under partial wetting conditions, although the exact extend cannot be determined. The possibility that part of the catalyst is not at all in contact with the liquid is not likely. If this was true, conversion at very low liquid flow rates (high space time) would decrease, as observed by Tukac and Hanika [19], but not in our experiments.

Table 3.1: Wetting efficiency calculated with different correlations at $160^o C$ and 0.1 MPa (AC) or 0.6 MPa (Cu0803), for liquid velocities in the range of 0.04 to 0.5 mm/s.

Correlation	AC[1]	Cu0803[2]
Iliuta et al. [213]	0.25-0.35	0.28-0.39
Al-Dahhan and Dudukovic [168]	0.23-0.49	0.23-0.49
Mills and Dudukovic (reported in [175])	0.45-0.82	0.45-0.82

Liquid Holdup: External liquid holdup is also calculated to be low, taking values between 0.06 and 0.1 according to the correlation of Iliuta et al. [186]. These values are in the low limit among the reported values, as can be seen from Fig. 1.13d [156]. However they are not surprising, since the liquid flow rate and viscosity are low, while the gas density is high. All of these factors are known to have a negative effect on liquid holdup. For the static hold up, both Sáez and Carbonell, as well as Mao et al. [212] estimate a value of 0.05. Unfortunately, there are no sufficient data to evaluate the effect of high temperature and pressure on this parameter.

External Mass Transfer: Under the conditions employed in this study, the dissolved oxygen concentration ranges between 0.8 and 11 $mmol/L$, which is much less than the stoichiometrically required for the complete mineralisation of a 53 $mmol/L$ phenol solution. Therefore, the possibility of external mass transfer limitations of oxygen has to be addressed prior to any kinetic analysis of the obtained results. To this purpose, the α_{gl}

and α_{ls} criteria, defined in the introduction in Eqs.1.13 and 1.14 were now calculated in the following way.

$$\alpha_{gl} = \frac{r_{O_2}^{obs} \rho_b}{(k_{gl}a)_{O_2} C_{O_2}^e} < 0.05 \qquad (3.1)$$

$$\alpha_{ls} = \frac{r_{O_2}^{obs} \rho_b}{(k_{ls}a_s)_{O_2} C_{O_2}^e} < 0.05 \qquad (3.2)$$

According to these criteria, mass transfer limitations can be neglected when $a <$ 0.05. The maximum reaction rates are expected to occur at high temperatures and low space times i.e. at high liquid flow rates. When high liquid flow rates are used, phenol conversions are lower, thus phenol concentration is higher through out the reactor, compared to the case of lower flow rates. The $r_{O_2}^{obs}$ can be calculated from the experimentally measured phenol concentration at low space time in the following way:

$$r_{O_2}^{obs} = \frac{7(C_{phen}^0 - C_{phen})}{\tau \rho_L} \qquad (3.3)$$

In Table 3.2 the experimentally obtained phenol concentrations, space times, and the calculated $r_{O_2}^{obs}$ are given, for both catalysts considered here. It can be observed that the initial rates are higher for the AC catalyst confirming the superiority of the AC catalytic activity over the Cu0803 catalyst. Furthermore, for the AC catalyst the initial reaction rate at 0.2 MPa is double that at 0.1 MPa, indicating a first order reaction with respect to the oxygen concentration. This preliminary observation will be confirmed later. On the other hand, when the oxygen concentration changes from 0.6 to 1.2 MPa for the Cu0803 catalyst, there is only slight increase in the observed reaction rate, indicating a lower oxygen order.

Table 3.2: Initial oxygen reaction rates for Cu0803 and AC at 160^oC based on initial phenol conversion measurements (C_{phen}^0.=53.1 $mmol/L$

Catalyst	Pressure (MPa)	Space time (h)	C_{phen} (mmol/L)	$C_{O_2}^e$ (mmol/L)	$r_{O_2}^{obs}$ (mmol/kg_{cat}s)
AC	0.2	0.04	38	1.8	0.81
	0.1	0.06	42	0.91	0.40
Cu0803	1.2	0.09	40	11	0.31
	0.6	0.10	40	5.5	0.28

The gas to liquid volumetric mass transfer coefficients were calculated from the two correlations of Iliuta et al. [185] and Goto and Smith [215], resulting in very different $(ka)_{gl}$ values. It is known that $(ka)_{gl}$ increases at high pressures, thus the former correlation, which has been fitted including high pressure data, gives considerably higher values. This means that the widely used correlation of Goto and Smith is not adequate and will lead to considerable underestimation of the gas - liquid mass transfer at high pressures. The α_{gl} criterion using the Iliuta et al. correlation shows that gas liquid mass

transfer limitations can be slightly influent in the case of the experiments with the AC catalyst (Table 3.3). However, as the reactor operates under partial wetting conditions, the direct gas - solid mass transfer will further diminish the weak influence of gas - liquid mass transfer limitations. For the Cu0803 catalyst these values indicate that the gas - liquid resistance should not be significant.

Table 3.3: Estimation of gas - liquid volumetric oxygen mass transfer coefficients for the Cu0803 and the AC catalysts at 160^oC and criteria for the existence of mass transfer limitations.

Catalyst	Pressure (MPa)	$(ka)_{gl}$ (s^{-1})	α_{gl}	$(ka)_{gl}$ (s^{-1})	α_{gl}
AC	0.2	1.0	0.15	0.016	9.7
	0.1	1.2	0.13	0.016	9.5
Cu0803	1.2	0.82	0.027	0.016	1.4
	0.6	0.87	0.045	0.016	2.5
Ref.		[185]		[215]	

The different correlations used for the liquid to solid volumetric mass transfer coefficient fall within the same order of magnitude. The correlation of Lakota and Levec [219], that takes into account the liquid holdup, is sought be more accurate for high pressure extrapolation than the correlation of Goto and Smith [215]. The calculated values of the α_{ls}, with the former correlation suggest that there should be no significant liquid - solid mass transfer limitations. (Table 3.4).

Table 3.4: Estimation of gas liquid volumetric oxygen mass transfer coefficients for the Cu0803 and the AC catalysts at 160^oC and criteria for the existence of mass transfer limitations.

Catalyst	Pressure (MPa)	$(ka)_{ls}$ (s^{-1})	α_{ls}	$(ka)_{ls}$ (s^{-1})	α_{ls}
AC	0.2	0.53	0.29	3	0.051
AC	0.1	0.53	0.29	3	0.051
Cu0803	1.2	0.53	0.041	1.4	0.016
Cu0803	0.6	0.53	0.074	1.4	0.028
Ref.		[215]		[219]	

Concluding and taking into account the high gas to solid mass transfer rates the oxygen concentration on the catalyst surface should not be affected by mass transfer limitations in the downflow configuration for both catalysts.

Internal diffusion: To account for internal diffusion limitations the Weisz - Prater criterion, modified for n-order reactions defined in Eq. 1.20 can be used:

$$\Phi = \frac{r_{O_2}^{obs} \rho_p d_p^2}{36 D_{O_2}^{eff}} \ll \frac{2}{n+1} \tag{3.4}$$

there are no internal mass transfer limitations as long as $\Phi \ll 2/(n+1)$. The Φ values depend on the effective diffusion coefficient, thus their exact values cannot be precisely calculated. Assuming typical tortuosity values between 2 and 4, the Φ values range between 0.19 and 0.38 for the AC catalyst and 0.06 and 0.22 for the Cu0803 catalyst. It can be seen that Φ values are low, thus internal mass transfer resistances should have only a slight influence. Again, due to the higher reaction rates over the AC catalyst the criteria exhibit higher values for this catalyst. For this catalyst, according to experimental observation of Stüber et al. [107] in a batch agitated reactor at 140^oC and 0.9 MPa internal mass transfer is not influent when for particles with same diameter used here. Furthermore, the reaction kinetics of phenol degradation over AC, that will be presented in a following section, successfully predicted experiments carried out recently [220], at higher temperature (170^oC) and oxygen partial pressure (3.4 MPa), in a different reactor. The good performance of the obtained kinetics at even higher temperatures and pressures, further supports the kinetic control of the phenol degradation in our experiments.

3.1.2 Downflow versus Upflow operation

The application of the available correlations to quantitatively describe the hydrodynamics and mass transfer properties of multiphase reactors, may not always yield reliable and useful information. One has to be aware of the questionable results of the correlations when extrapolating the correlations outside their range of validity. The typical CWAO systems have the advantage of being very close to the well studied Air-Water-Solid multiphase system, thereby avoiding the great uncertainties related to organic and foaming systems. Many correlations exist for this medium, and recent research efforts have been driven to high pressure and temperature systems and more reliable data are now available.

In the case of kinetic studies conducted in a continuous multiphase reactor system, the gas liquid hydrodynamics are imperatively to be selected so that the reaction is completely controlled by the intrinsic kinetics and not by the kinetics of mass transfer. Obviously, one way to guide the selection process is to make use of appropriate correlations to quantify the underlying process physics, as done in the previous section. However, it is recommended to corroborate these findings by a minimum of properly designed experiments. For the study of phenol CWAO, an important information is to determine whether the limiting reactant is in the gas phase or liquid phase and then choose the appropriate reactor configuration. To this purpose, the γ ratio (Eq. 1.10) proposed by Khadilkar et al. [171] is particularly useful.

The γ ratio in our case takes values between 17 and 34 for the AC catalyst and 3 to 6 for the Cu0803, thus the limiting reactant is the oxygen in the gas phase and downflow
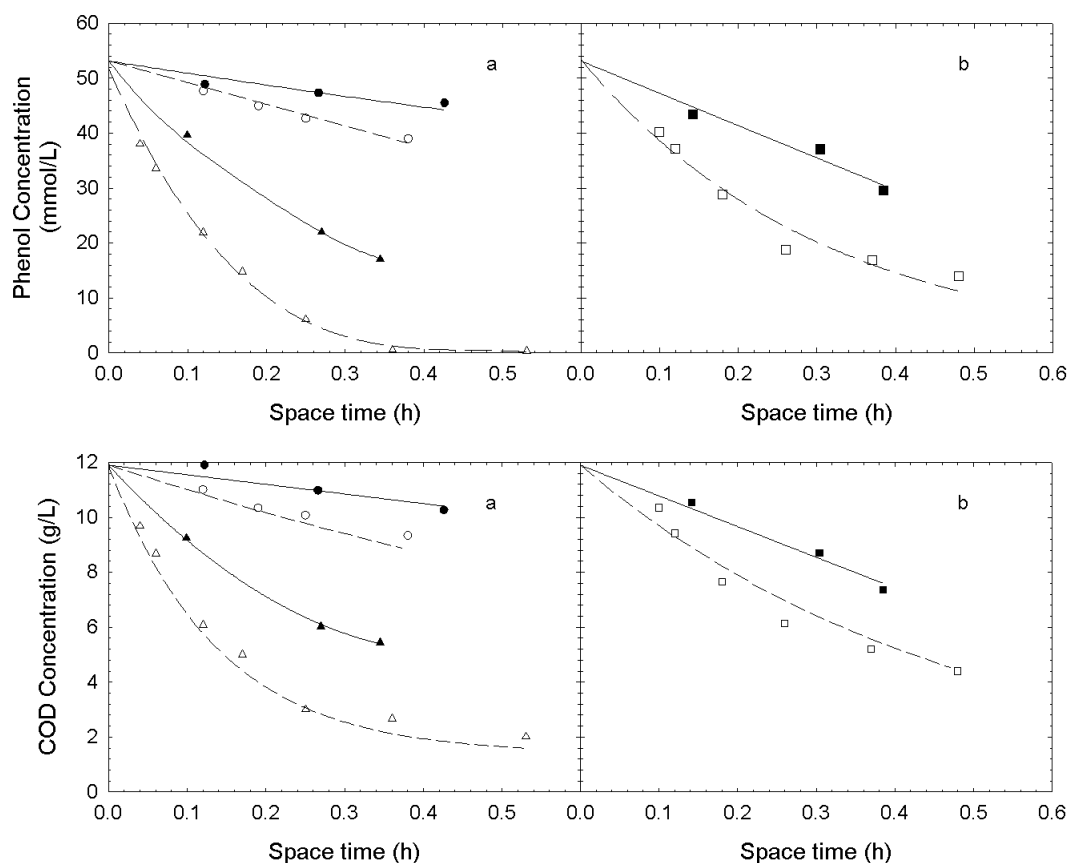
Figure 3.1: Comparison of down flow (empty symbols) and up flow (filled symbols) phenol and COD concentration profiles over AC catalyst at 0.2 MPa of P_{O_2} and : a) 120 and 160^oC b) 140^oC. ($\circ$): 120^oC , ($\square$): 140^oC , ($\triangle$): 160^oC . Lines indicate trends.

operation should be preferred. These results motivated a series of experiments dedicated to assess the reactor conversion for either coccurent downflow or upflow mode. From this experimental data, one can conclude on the effects of reactor hydrodynamics, at least with respect to the wetting efficiency and external mass transfer, which are two key parameters for TBRs.

As predicted, the downflow operation yielded considerably higher phenol conversions than the upflow operation, indicating that the reaction is practically controlled by external mass transfer in the latter operation mode. The phenol concentration - space time profiles measured in both flow directions are plotted in Fig. 3.1. These results are in close agreement with the work of Tukac et al. [195], comparing the phenol conversion obtained in a normal TBR and the same catalytic bed, but diluted with fines, thus operating under complete catalyst wetting as in an upflow fixed bed reactor. These authors also observed that the effect of wetting was not significant at low temperature, conversely to the trends found in our study. This can be attributed to the difference in the γ ratio values between
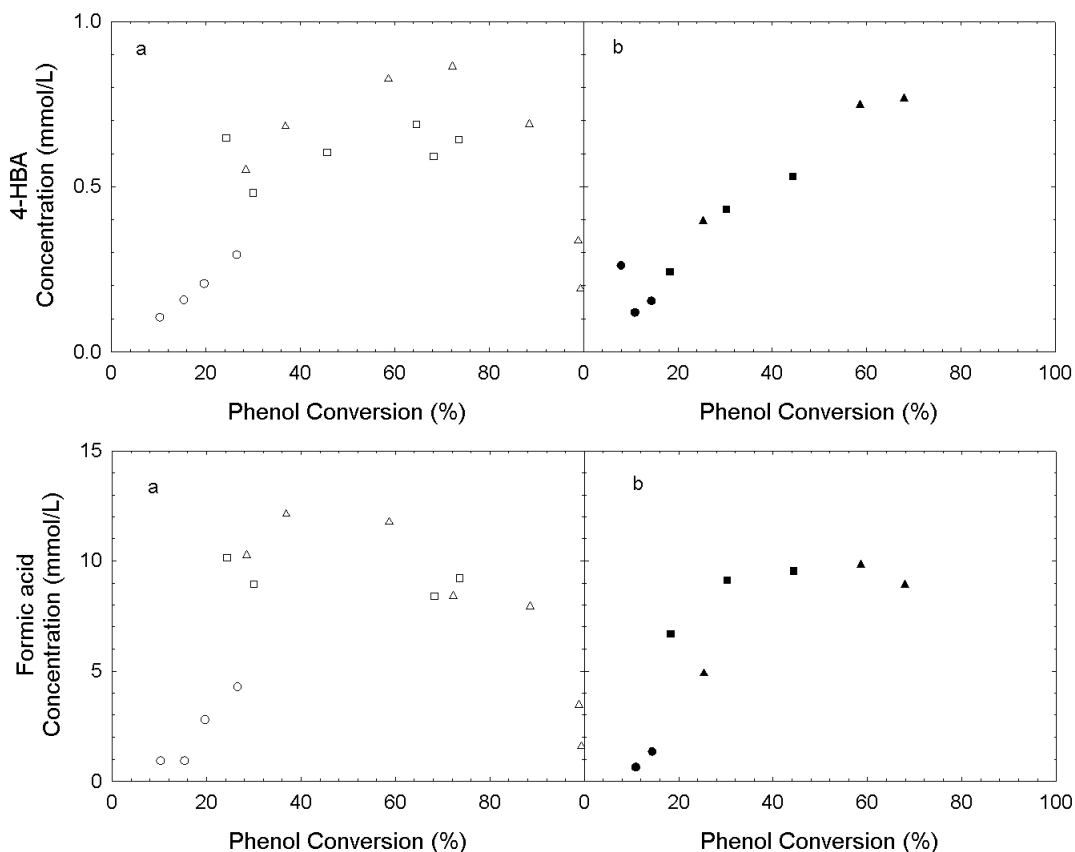
Figure 3.2: 4-HBA and formic acid concentration as a function of phenol conversion over AC at 0.2 MPa with a) downflow (empty symbols) and b) up flow (filled symbols) operation. (○): 120^oC , (□): 140^oC , (△): 160^oC .

17 and 2.5 for our study and the study of Tukac et al. [195] respectively. This means that in our conditions the limitations of oxygen should be much more influent, even at low phenol reaction rates.

The COD degradation profiles follow the same trends established for phenol, as can be also seen in Fig. 3.1. For intermediate compounds, however, differences can be appreciated when their concentration is plotted against the conversion of phenol for the two different operation modes. Exemplarily, in Fig. 3.2 the 4-HBA and formic acid concentration profiles are presented for both operation modes. An important result is that in downflow operation different tendencies can be observed for the different temperatures. For the same phenol conversion at higher temperature higher quantities of 4-HBA and formic acid are formed. This indicates that the activation energy for the formation of 4-HBA is higher to that of its destruction. For upflow operation it is observed that 4-HBA and formic acid concentrations depend only on phenol conversion and not on the temperature employed. Thus the formation and destruction of these compounds have

the same temperature dependence, that must be attributed to mass transfer limitations.

3.1.3   Conclusions

At the employed operating conditions the laboratory scale TBR operates under partial wetting of the catalyst as determined from literature correlations. The calculation of gas -liquid and liquid solid mass transfer volumetric mass transfer coefficients, showed that high pressure correlations predict higher mass transfer coefficients. Then, the available criteria for the diagnostic of mass transfer limitations, based on measured apparent reaction rates, showed that external and internal transport resistances are marginal.

The γ ratio for our reaction system was calculated to be high, taking values of the order of 17. Thus it was expected that partial wetting in downflow operation is advantageous compared to the upflow operation. This was experimentally verified in upflow runs at 0.2 MPa. In the plots of the intermediate compound concentration versus phenol conversion, it can be seen that for downflow operation temperature is influent on intermediate concentration, while for upflow operation the concentration profiles of all intermediates depend only on phenol conversion. The examined results on selectivity give further support to conclude that downflow operation was kinetically controlled, while upflow is partially diffusion controlled.

3.2   Active Carbon Performance

In this section the experimental data for the CWAO of phenol over an AC catalyst are presented. The results were obtained in downflow mode and special care was taken to ensure kinetic regime, because these data are ultimately destinated for a detailed kinetic analysis. Useful details on the transient concentration profiles of the reactants and the products are presented. Then, the behaviour of active carbon is discussed, based on the results obtained from the carbon weight change, and the detected intermediates. The obtained profiles are also compared to those obtained by Fortuny [199] for a commercial copper oxide catalyst. Apparent phenol and COD degradation kinetics are also calculated and discussed.

3.2.1   Transient Profiles

In order to obtain the concentration space time profiles, steady state (concentration) has to be assured for each experimental point, since in the same run different space times were checked by adequately adjusting the pump flow rate. The evolution of concentrations between space times was followed, as shown exemplarily in Fig. 3.3, which reproduces the transition of phenol, COD and maleic acid concentrations resulting from an increase of space time from 0.12 h to 0.36 h at 140^oC and 0.2 MPa. It can be seen that the system needed a relatively large period of four hours to reach the new steady state. Obviously, this time interval became smaller at closer space times, i.e. for a change in space time from 0.12 h to 0.18 h it took about 1.5 h. Therefore, in all runs, analysis of the liquid phase was immediately done to verify steady state conditions and to minimise the total experimental run time. In general, steady state samples were triplicated and the experimental error in the measured phenol and COD concentrations was evaluated to be 5%. Intermediate compounds showed similar error, except for the runs at 140^oC and 0.2 MPa, where scattering in the experimental points for some intermediates was observed, leading to individual errors up to 25%.

3.2.2   Change in active carbon weight

For the Cu0803 catalyst Fortuny [199] did not measure an significant variation on the catalyst weight in 10 days runs of phenol CWAO, when using the same laboratory TBR and similar conditions. On the other hand, the same authors [18, 106] have shown that active carbon weight changes after long term operation. Depending on the time on stream and the operating conditions, this change could be positive or negative. At 140 ^{o}C and 0.9 MPa it was observed that active carbon weight increases in the first 24 h, then reaches a maximum and finally decreases. Furthermore, it was shown that when lower oxygen partial pressures were used the active carbon weight after 10 days on stream increases. In the present study an increase in carbon weight of 33% and 13%, respectively was measured for five day experiments at 0.2 and 0.1 MPa, which is in reasonable agreement
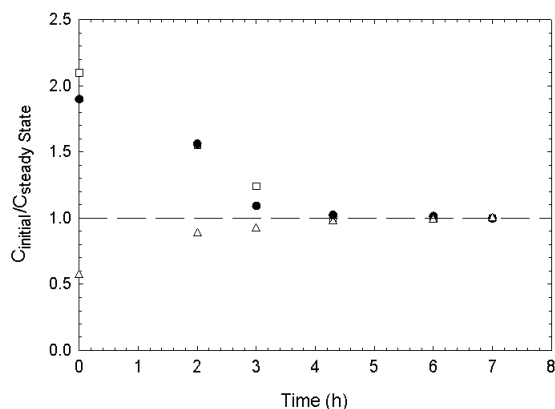
Figure 3.3: Transient concentration for phenol ($\square$), COD ($\bullet$) and maleic acid ($\triangle$), for a change in space time from 0.12 h to 0.36 h at 140^oC and 0.2 MPa.

with the observations of Fortuny et al. [106] for experiments conducted at the same oxygen partial pressure, although at steady temperature (140^oC) and space time (0.12 h). The formation of an active coke layer on the AC surface can thus be also postulated in our experiments.

   In addition, the detailed HPLC analysis of the exiting liquid effluent revealed the presence of up to 60 peaks, many of them having retention times close to quinone like or phenolic compounds. In particular, 4-hydroxybenzoic acid (4-HBA) could be identified in significant amounts, and its formation is difficult to explain by classical phenol oxidation mechanisms. The formation of this compound requires the addition of a carbon atom to the phenol molecule. Since such reaction has not been reported over other catalysts, the formation of this compound may be related to the coke layer formed over the AC catalyst.

3.2.3   Steady state profiles of Phenol and COD

The phenol and COD conversion-space time profiles obtained at different temperatures (120, 140 and 160^oC) and oxygen partial pressures (0.1 and 0.2 MPa), are given in Fig. 3.4. As expected, the increase of either temperature, pressure or space time has a positive effect on phenol conversion and COD destruction. At 160^oC and 0.2 MPa, almost complete phenol destruction ($> 99\%$) was performed for space times greater than 0.3 h. The Cu0803 catalyst gave a 97\% conversion, at the same temperature, but at an oxygen partial pressure of 1.2 MPa and a space time of 1 h. This clearly demonstrates the superior performance of the AC compared to the Cu0803 catalyst, given the higher activity and catalytic stability shown by the AC even at lower pressures.
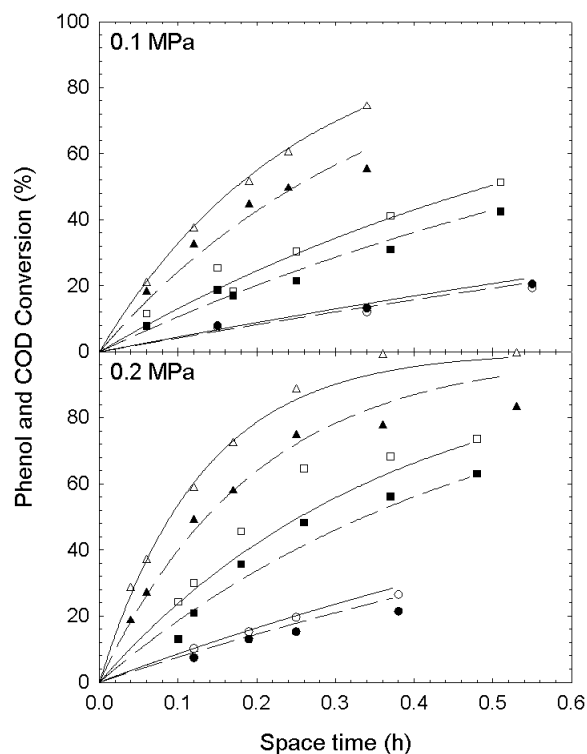
Figure 3.4: Phenol and COD conversions over AC catalyst for different oxygen partial pressures and temperatures. Empty symbols indicate phenol experimental data. Filled symbols indicate COD experimental data. ($\circ$) 120°C, ($\square$)140°C, ($\triangle$) 160°C. Lines indicate kinetic model: ($-$) Phenol, (- -) COD.

A preliminary kinetic analysis of the phenol concentration and COD was made, by means of nonlinear regression, using the reactor model described in Eq. 2.15 and simple power law kinetics (Eq. 2.16). In agreement with the findings of other studies conducted in slurry [90, 81] or TBR [73], a first reaction order for phenol or COD concentration on reaction rate was postulated. The average deviation between experimental and predicted phenol conversions was found to be only 4%. The best parameter fit is given in Table 3.5 with a standard error calculated for a 95% confidence interval. The apparent activation energy for phenol destruction over AC was found to be 70.3($\pm$0.4) kJ/mol, and is in the range of the 85($\pm$2) kJ/mol obtained by [73] in the same TBR using the Cu0803 catalyst. For stirred slurry reactors, intrinsic kinetic values of 85 kJ/mol [82] and 84 kJ/mol [81] for different copper oxide catalysts with similar characteristics. These values suggest that the AC kinetics evaluated in the TBR are very close to the intrinsic kinetics.

An unexpected order of 0.95($\pm$0.02) on dissolved oxygen mole fraction resulted for the

Table 3.5: Kinetic Parameters for Phenol and COD degradation kinetics on active carbon

	k_0 $(L/kg_{cat}\ h)$	E_a (kJ/mol)	α (-)
Phenol	$10^{13.6\pm0.1}$	70.3 $\pm$0.4	0.95 $\pm$ 0.02
COD	$10^{12.0\pm0.2}$	60.9 $\pm$0.6	0.87 $\pm$ 0.03

AC catalyst. A first order oxygen dependence could be readily justified by the presence of strong oxygen mass transfer limitation, although the clear temperature dependence of the phenol conversion and the activation energy found strongly suggests that kinetics governs the process. Pintar and Levec, [80], proposed that dissociative oxygen adsorption is an elementary step during CWAO of phenol over a copper oxide catalyst and reported a 0.5 oxygen order, in agreement with Sadana and Katzer, [90] and Fortuny et al. [72]. On the other hand, according to Sadana and Katzer [90], molecular oxygen also participates in possible elementary steps during CWAO of phenol. Thus, a first order could result from intrinsic kinetic effects involving a molecular oxygen attack of the phenol molecule.

The prediction of COD abatement (dashed lines in Fig. 3.4) are also in good agreement with the experimental COD data. Systematic deviations, i.e. the model over-estimates the COD conversion, are only observed for the highest COD conversions at $160^{o}C$. Accumulation of refractory acetic acid in the system is the cause of this deviation as the model does not account for its effect on COD destruction. This effect can be overcome by means of the complex model that will be discussed later. The activation energy of 60.7($\pm$0.6) kJ/mol found for COD destruction, is lower than that for phenol, although the oxygen order of 0.9 ($\pm$0.03) is close. The lower activation energy of COD reduction can be explained by the fact that most intermediates are less refractory than phenol. Surprisingly, the destruction of phenol and most intermediates seems to depend on oxygen concentration in the same way as the oxygen orders found demonstrate. As expected, phenol is not completely mineralised to water and carbon dioxide and the COD reductions observed are not as large as the phenol conversions (Fig. 2). However, for phenol conversion of 99%, a high COD reduction of about 85% was achieved and it can be expected that the AC shows a high selectivity towards the production of carbon dioxide.

For the same phenol conversion, the Cu0803 catalyst gave a similar COD conversion of 90%, which is related to lower acetic acid formation, as will be discussed later. In order to have a detailed insight of COD behaviour, the exit stream was also analysed to detect the main intermediate compounds from phenol oxidation.

3.2.4 Intermediate compounds

The HPLC analysis detected 15 peaks at low phenol conversions, but this number increased up to 60 for higher phenol conversions. Most of these peaks had no significant areas and could be associated to trace amounts of compounds resulting from the combus-

tion of the coke layer formed or the AC itself. Among all peaks, five principal intermediate compounds were identified, namely 4-HBA, benzoquinone, maleic acid, including its isomer fumaric acid, acetic acid and formic acid. Hydroquinone, catechol and oxalic acid were also detected in trace amounts. The area corresponding to identified peaks decreased from 95% (at low conversions) to 70% (at higher conversions). However, as the different areas are not equally proportional to the concentration, the identified compounds reproduce the directly measured COD with reasonable accuracy, taking into account the complexity of the system and the precision of the COD analytical method. In Fig. 3.5 the measured COD values and HPLC estimated COD are represented in a parity plot. Almost all the data points fall within the $\pm 10\%$ error range, the majority being within the $\pm 5\%$ error band. For high COD values (low phenol conversion), measured and HPLC estimated CODs are distributed uniformly along the equality line. As COD reduction increases, HPLC estimated COD tends to slightly underestimate measured COD, certainly due to the detection of more unknown peaks at higher phenol conversion.
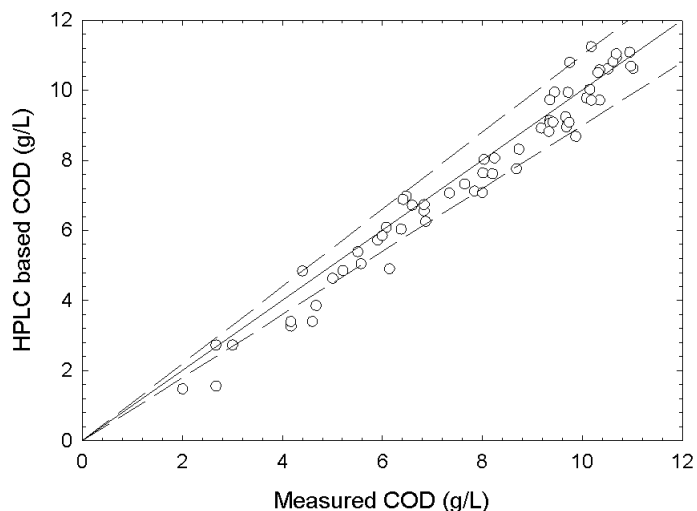
Figure 3.5: Parity plot among HPLC based and chemically measured COD

The obtained concentration-space time profiles for the five main intermediates shown in Figs 3.6 to 3.7, revealing that phenol oxidation follows a complex pathway of parallel and consecutive reactions. With the exception of acetic acid, a maximum concentration appears for all the detected partial oxidation compounds at 160^oC and 0.2 MPa. For benzoquinone and, surprisingly, formic acid this maximum appears fast at space times around 0.1 h, while 4-HBA and maleic acid reach their maximum only at a space time of 0.18 h and 0.36 h respectively. Therefore, a sequential phenol oxidation scheme yielding first 4-HBA and then benzoquinone is not likely. More probably, it seems that phenol

undergoes two parallel oxidation reactions to form benzoquinone and 4-HBA. If these compounds are expected to be the first oxidation intermediate products, they should rapidly reach a maximum. Formic acid, should be formed only after several consecutive oxidation reactions and exhibit its maximum later. This is true in the case of the Cu0803 catalyst, where the formic acid maximum appears at space time twice that of benzoquinone. For the AC, benzoquinone and formic acid form and disappear rapidly, suggesting that there is a direct pathway from phenol, or benzoquinone, to formic acid. On the other hand, 4-HBA and maleic acid are formed and destroyed less rapidly, thus it could be speculated that maleic acid is mainly formed through 4-HBA, rather than benzoquinone. Finally, acetic acid should be formed following maleic acid, according to the Devlin and Harris pathway [119]. Considering these facts the scheme shown in Fig. 3.8 can be proposed. Nevertheless, this scheme has to be reaffirmed by kinetic modelling procedures as will be done later on.
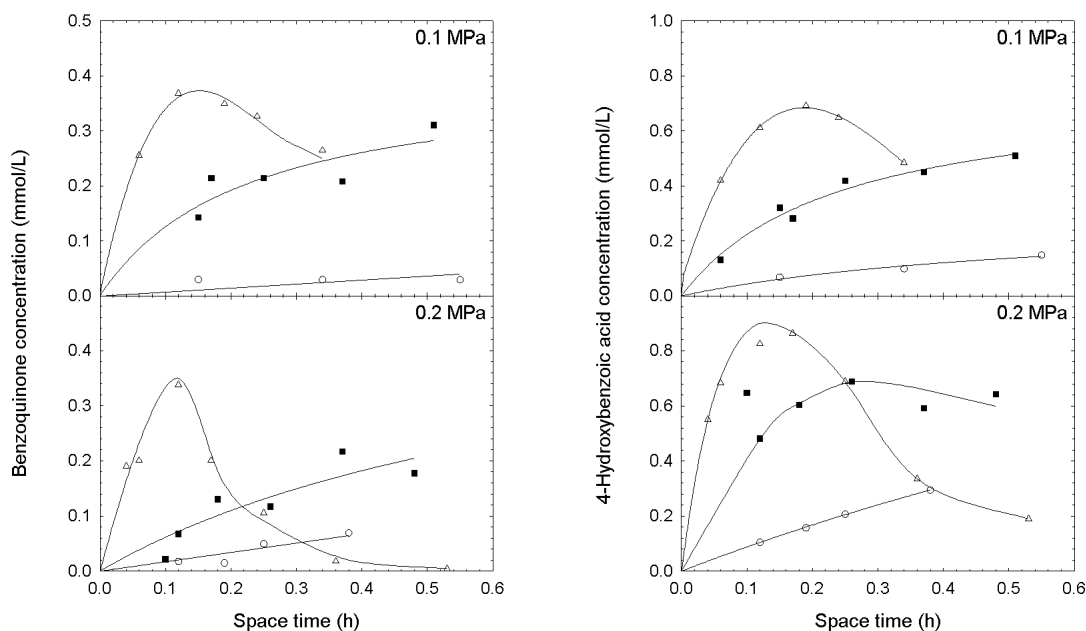
Figure 3.6: Benzoquinone and 4-HBA concentration profiles over AC catalyst for different oxygen partial pressures and temperatures. Empty symbols indicate phenol experimental data. Filled symbols indicate COD experimental data. ($\circ$) 120^oC, ($\square$)140^oC, ($\triangle$) 160^oC. Lines indicate trends

Figure 3.7: Maleic, acetic and formic acid concentration profiles over AC catalyst for different oxygen partial pressures and temperatures. Empty symbols indicate phenol experimental data. Filled symbols indicate COD experimental data. (∘) 120^oC, (□)140^oC, (△) 160^oC. Lines indicate trends
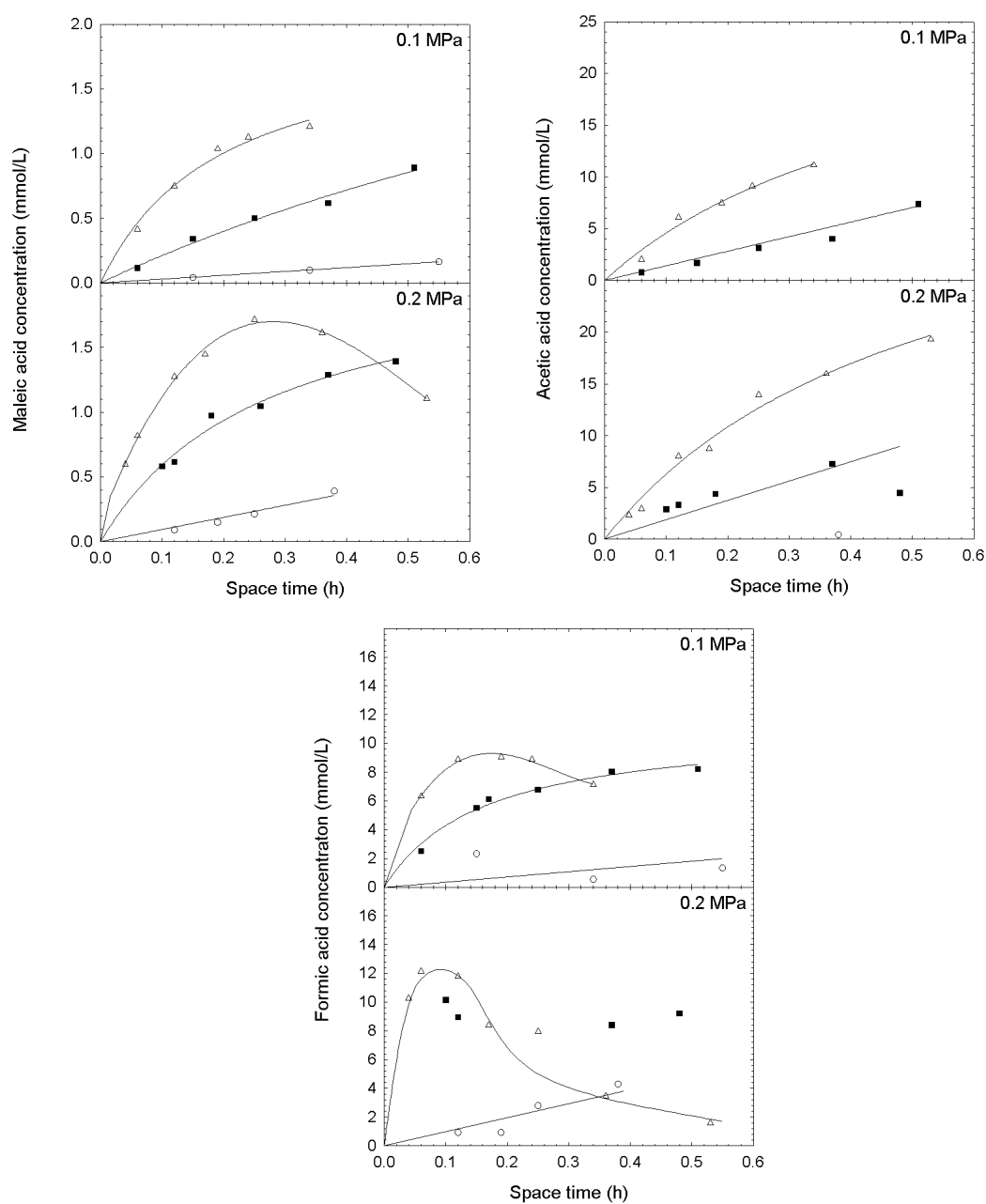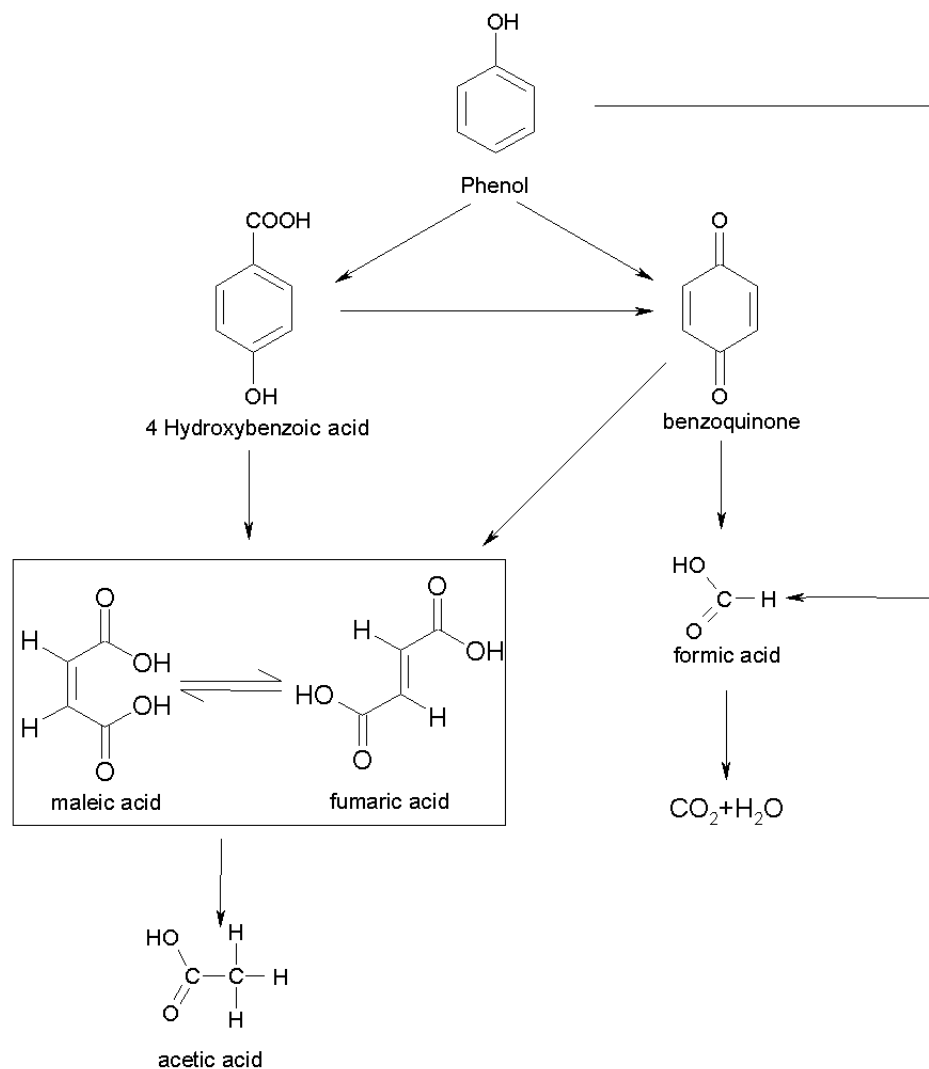
Figure 3.8: Possible scheme proposed for phenol CWAO over AC based on the experimentally observed intermediate compound concentration profiles.

With respect to the kinetic models based on the Devlin and Harris mechanism, a significant difference is that the phenol degradation over AC catalyst seems to occur also through the formation of 4-HBA. The presence of this compound was affirmed by both HPLC retention time and HPLC-MS analysis. The formation of this compound would require the addition of a carboxyl group to the phenol molecule. This suggests that functional surface groups of the AC or the coke layer may react with adsorbed phenol species to form this compound. However, if these groups are not regenerated, only a small part of phenol should be able to follow this route, as in the case that all phenol would react towards 4-HBA a significant AC loss would be produced. Consequently, a constant conversion decline should have been observed in the long-term runs carried out in a previous work, which is not the case.

Also, it must be pointed out that during phenol oxidation over AC, less aromatic compounds are formed as shown in Fig. 3.9. In total, the sum of 4-HBA, benzoquinone and dihydric phenols concentrations never exceeded 1.5 $mmol/L$, while the same compounds could reach more than 3 $mmol/L$ in the case of the copper catalyst. The evolution of 4-HBA and benzoquinone with space time at 0.2 MPa and 160^oC shows that AC is able to efficiently remove both compounds.
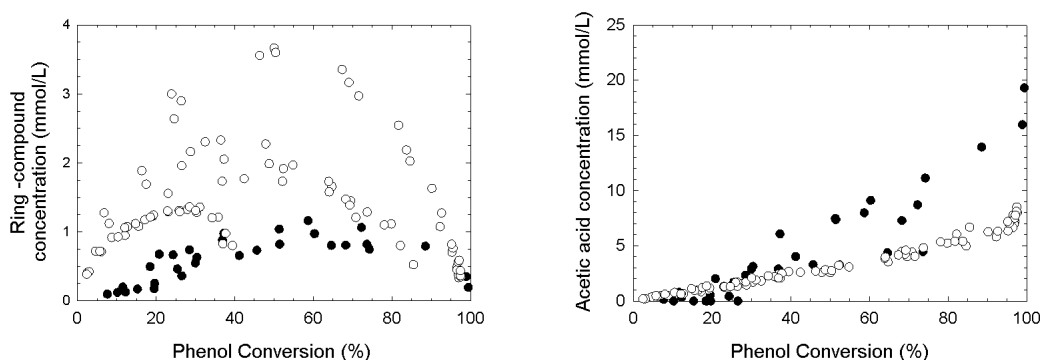
Figure 3.9: Ring compound and acetic acid concentration as a function of phenol conversion for Cu0803 (○) and AC (●).

In agreement with the classical phenol oxidation mechanism proposed by Devlin and Harris, (1984), typical routes for the formation of carbon dioxide or acetic acid are found for both catalysts, although differences do exist. In the route of carbon dioxide formation over AC, oxalic acid is only detected in trace concentrations, which are 20 times lower than those observed for Cu0803. Formic acid is formed in amounts similar to those obtained for the Cu0803 and is easily destroyed at 160^oC with both catalysts. In the formation of acetic acid, maleic and malonic acids appear as common precursors coming mainly from the benzoquinone (Cu0803) or 4-HBA (AC). Although the sum of maleic

and malonic acid concentration is close for both catalysts, maleic acid was produced over AC at a rate 20 times faster, but no malonic acid could be detected. For both catalyst, acetic acid accumulates in the system and it does not undergo further apparent oxidation, since higher temperatures and pressures are usually employed to destroy this well-known refractory compound [46]. For the AC, acetic acid has been detected in quantities up to 20 $mmol/L$, which is 2 to 3 times higher than those obtained for the Cu0803 catalyst, as shown in Fig. 3.9. This rise corresponds to a 7% COD increase explaining the slightly lower COD destruction value observed for the AC catalyst.

3.2.5   Conclusions

Effective phenol conversions exceeding 99% has been achieved in the CWAO of phenol over an active carbon using a continuous TBR at 160^oC and 0.2 MPa of oxygen partial pressures. When compared to a commercial copper oxide catalyst, AC gives not only higher conversion at lower space times and pressures, but also stable catalytic activity beyond 10 days running. The COD removal exceeded 85% in the above conditions and is close to that obtained with a supported copper oxide catalyst. The principal phenol oxidation intermediate compounds were 4-hydroxybenzoic acid, benzoquinone, maleic acid, formic acid and acetic acid. Compared to the copper oxide catalyst, less amount of toxic and non-biodegradable aromatic compounds are formed, while the quantity of refractory, but biodegradable, acetic acid that accumulates in the exited stream is twice that obtained with the copper catalyst.

A kinetic analysis for the phenol removal over AC showed strong dependence of phenol destruction rate on temperature and oxygen concentration. The apparent activation energy (70 kJ/mol) is somewhat lower than that reported for copper oxide catalysts in the kinetic controlled regime. On the other hand, a first order dependence on the oxygen partial pressure was found for AC contrasting the 0.5 order normally observed for other metal supported catalysts. No significant diffusion limitation existing, this dependence should be attributed to a different elementary mechanism involving molecular oxygen in the case of the AC catalyst. In this context, the assumed formation of a coke surface layer, active in the oxidation of phenol, is postulated to play an important role.

Chapter 4

Kinetic Modelling of Phenol CWAO

In this chapter the development and consolidation of complex kinetic modelling for two case studies of phenol CWAO, over a Cu0803 catalyst and over an AC catalyst are discussed. The developed kinetic models are aimed to account for all intermediates that have been detected during the phenol CWAO. For the AC catalyst the experimental data along with a preliminary discussion on the possible reaction network have been given in the previous chapter. The experimental data for the Cu0803 catalyst were obtained in the same experimental set up by Fortuny [199]. Due to the high number of intermediates detected (5 for the AC and 8 for the Cu0803) the resulting reaction networks are of high complexity and the classical kinetic multiparameter approaches, based on local optimisation algorithms, may have difficulties in finding a solution. Thus prior to the discussion of the kinetic results the performance of the classical L-M algorithm and the stochastic S-A algorithm, for the kinetic modelling of the CWAO of phenol over Cu0803 is compared.

4.1 Underlying reaction networks

4.1.1 Copper oxide reaction network development

During the CWAO tests over the Cu0803 catalyst, performed by Fortuny [199], several intermediates appearing in the scheme proposed by Devlin and Harris [119] were detected by following an exhaustive HPLC analysis of the exited stream. The analysis confirmed that the main partial oxidation products are light carboxylic acids such as oxalic, acetic and formic. Malonic acid, maleic acid and its isomer fumaric acid, were detected in trace amounts. For simplicity, fumaric acid was included in the maleic acid concentration. A second clan of products in measurable amounts constitute the following ring compounds of hydroquinone, catechol and benzoquinones. No other possible intermediates could be identified. In order to contrast the goodness of the analytically determined composition, the HPLC based estimated COD or TOC estimates were compared with experimentally determined COD or TOC values. The deviations were found to be less than 5%, indicating an acceptable closure of the carbon mass balance.

The analysis of the concentration histories of these intermediates in front of the space time showed the typical trends of a consecutive-parallel reaction pathway, which favourably agreed with the reaction model stated by Devlin and Harris [119]. Among the intermediates detected by Devlin and Harris, neither succinic nor propionic acids were found in the study of Fortuny [199], so the corresponding pathway that produces propionic acid from maleic acid was directly removed from the proposed scheme. The propionic acid would only appear as a final product if the succinic acid has been formed by hydrogenation of the carbon to carbon double bond in maleic acid. This hydrogenation may occur in some extent only when oxygen is poorly available, which is not the case in the current reaction conditions.

Other of the possible intermediates not detected were acrylic acid, glyoxal and glyoxylic acid. The acrylic acid comes from decarboxylation of maleic acid and is an intermediate in the pathway to form malonic acid and later acetic acid [119]. Since these two latter were obtained, acrylic acid must have been formed in the employed conditions but it is believed to be very reactive, thus leading to concentrations below the HPLC detection limit. On the other hand, since all the oxalic and the formic acid produced might exclusively come from muconic and maleic acid, both glyoxal and glyoxylic acid might not necessarily appear as intermediates. Notwithstanding, it can also be thought that they are short-lived compounds. Glyoxylic acid is reported to be considerably more reactive than oxalic acid [128] so, unlike the latter, it could not accumulate in the system. Oxalic and formic acids were found to further degradate under the conditions studied, thus their mineralisation towards carbon dioxide and water has to be included. In addition, the thermal decomposition of oxalic acid towards formic acid is a further possible step as it has been reported during both non catalytic [129] and homogeneous catalysed [130] WAO. From the obtained profiles, acetic acid seems to accumulate in the reaction system, although a slow degradation reaction cannot *a priori* be excluded.

Even being reduced the complexity of the reaction network compared to the Devlin and Harris mechanism, the number of possible reactions is still undefined since several possible paths exist for the degradation of some partial oxidation products. For instance, benzoquinones can be oxidised via 2,5-dioxo-3-hexenedioic acid, i.e. without passing through maleic acid. The former acid is highly reactive and has not been ever detected as intermediate in phenol oxidation. Thus, benzoquinones could directly yield oxalic acid and/or glyoxal and/or glyoxylic acid. In turn, these two latter can form oxalic acid, formic acid, or even could be directly converted into carbon dioxide. On the other hand, maleic acid could be either decarboxylated to yield acrylic acid or degraded by oxidation to glyoxylic and/or oxalic acid. Acrylic acid was not detected although the subsequent oxidation products, malonic and acetic acid, were indeed obtained. Too, oxalic acid can be directly oxidised into carbon dioxide and water but can also undergo decarboxylation thus yielding formic acid. So, as can be seen, the later steps in the phenol oxidation pathway could follow different ways, some of them even at once, which leads to multiple likely reaction pathways. Over 50 different reaction models were designed and then tested [218]. By means of a robust predictor-corrector method [217], most of the proposed models were eliminated, while the best performning schemes were englobed in

a core reaction scheme presened in Fig. 4.1.
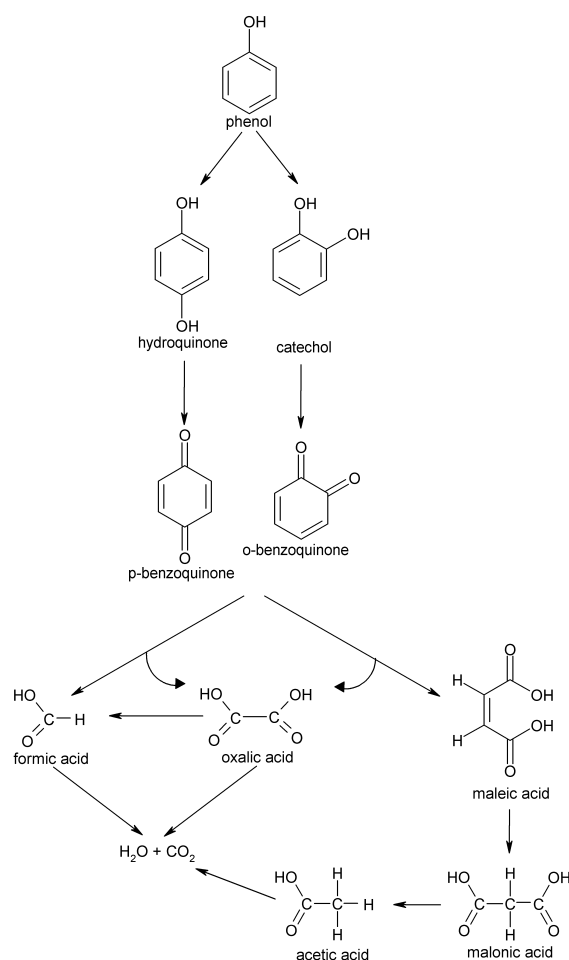
Figure 4.1: Preliminary reaction network for the CWAO of phenol over Cu0803 catalyst

The final model assumes that phenol firstly undergoes a hydroxylation leading to hydroquinone or catechol; a further oxidation yields the corresponding o- and p-benzoquinone. Then, benzoquinones are degraded in two parallel pathways. In the first path, o-benzoquinone is oxidised to muconic acid which, in turn, rapidly decomposes, stoichiometrically yielding maleic and oxalic acid. This reaction has been observed even at room temperature [119]. The subsequent decarboxylation of maleic acid finally produces malonic acid. Oxygen attack to the carbon to carbon double bond of maleic acid to form oxalic acid is not considered here as a significant path. This is in disagreement with some experimental studies [127] where oxidation of maleic acid largely prevails over thermal decomposition, although these results were obtained at more severe conditions under non catalytic environment. In our case, all attempts including an oxidation path-

way from maleic to oxalic acid failed, so this option was finally rejected. The other path to degrade benzoquinones is assumed to occur through a complex reaction network via glyoxal or glyoxylic acid. After checking up several possibilities, we consider lumping both benzoquinones, which degradate yielding one molecule of oxalic acid, one molecule of formic acid, and three molecules of carbon dioxide. Furthermore, direct oxidation steps and thermal decomposition, were initially accepted to be the main path for oxalic acid consumption as both steps have been reported in the literature [119, 128].

Obviously, there is a lack of information to doubtless affirm that this is the true pathway for phenol oxidation in the current experimental conditions. However, the model is consistent with the known oxidation and decarboxylation mechanisms and permits to predict confidently the product yield in the range of conditions studied.

4.1.2   AC reaction network development

In the previous chapter a general reaction network for the CWAO of phenol over AC was proposed (Fig. 3.8) purely based on experimental results. This scheme is particularly useful when selected as a starting point for the subsequent hierarchical model building, as will be shown later on in Chapter 4.4.

4.2 S-A and L-M Performance

The potential of the S-A algorithm in the study of complex kinetic schemes is evaluated, by comparing it to the classical L-M algorithm. The analysis is done using the experimental Cu0803 data and the developed core reaction scheme as a case study. A hierarchical approach of parameter estimation was tested, starting from the study of only phenol degradation (one-reaction network), then including the principle carboxylic acids (five reaction network) and finally incorporating all detected intermediates (eight-reaction network).

4.2.1 One-reaction network (Model 1)

According to this hierarchical approach the first step is to consider only the phenol degradation reaction described by Eq. 4.1:

$$C_6H_5OH \; + \; 7\,O_2 \; \rightarrow \; 6\,CO_2 \; + \; 3\,H_2O \tag{4.1}$$

Preliminary adsorption experiments at room temperature have shown that phenol does not adsorb on the Cu0803 catalyst surface, therefore simple power law expressions (Eq. 2.16) were employed.

$$r_{phen} \; = \; k_0 \; exp(-E_a/RT) \; x_{O_2}^{\alpha} \; C_{phen} \tag{4.2}$$

The total destruction rate for phenol R_{phen} is simply

$$R_{phen} = -r_{phen} \tag{4.3}$$

and can be substituted to the reactor model (Eq. 2.15):

$$\frac{dC_{phen}}{d\tau} = R_{phen}\rho_l \tag{4.4}$$

Then, given an initial guess set of the unknown parameters (k_0, E_a, α) Eq. 4.4 can be numerically integrated, and applying the S-A or the L-M algorithms optimum values of the desired parameters can be obtained. The values of the guess parameters set was chosen from available data in the literure. Fortuny et al. [72], using simple power law kinetics, found an activation energy close to 85 kJ/mol and an oxygen order of 0.5 for this reaction. These values were taken as initial guess for both algorithms. The frequency factor initial guess was set to 10^{11} ($L/kg_{cat}h$). In our case, simple power law expressions were also tested (Eq. 2.16), thus only three parameters were fitted. As expected and due

Table 4.1: Performance of S-A and L-M for Model 1

	S-A	L-M
Minimum	1085	1086
Function evalutations	$\approx 10^5$	$\approx 10^2$
Activation energy (kJ/mol)	77.1	77.1 ± 0.4
Oxygen order	0.37	0.35 ± 0.2
Frequency factor $(L/kg_{cat}h)$	$10^{11.34}$	$10^{11.29 \pm 0.07}$

to the low number of parameters involved, the two algorithms practically converged to the same solution, shown in Table 4.1.

The obtained parameters were found to be statistically significant as can be deduced from the calculated errors for 95% interval of confidence. The L-M algorithm needed only 10^2 function evaluations while S-A needed more than 10^5. This was expected as L-M algorithm is already implemented successfully for similar optimisation problems. The high quality of the fitting is exemplarily illustrated for the S-A solution in Fig. 4.2. The new solution found was not exactly that of Fortuny et al. [72], using the same experimental data set. This is due to the fact that the procedure followed in the present work was different, i.e. all parameters were identified simultaneously. In the former case non-linear regression was applied to obtain the reaction constant for each temperature - pressure set and consequently the activation energy and reaction order were calculated by means of linear regression. This discrepancy is in agreement with the given observation that linearisation results may be different from those obtained by direct nonlinear estimation of all involved parameters [139].
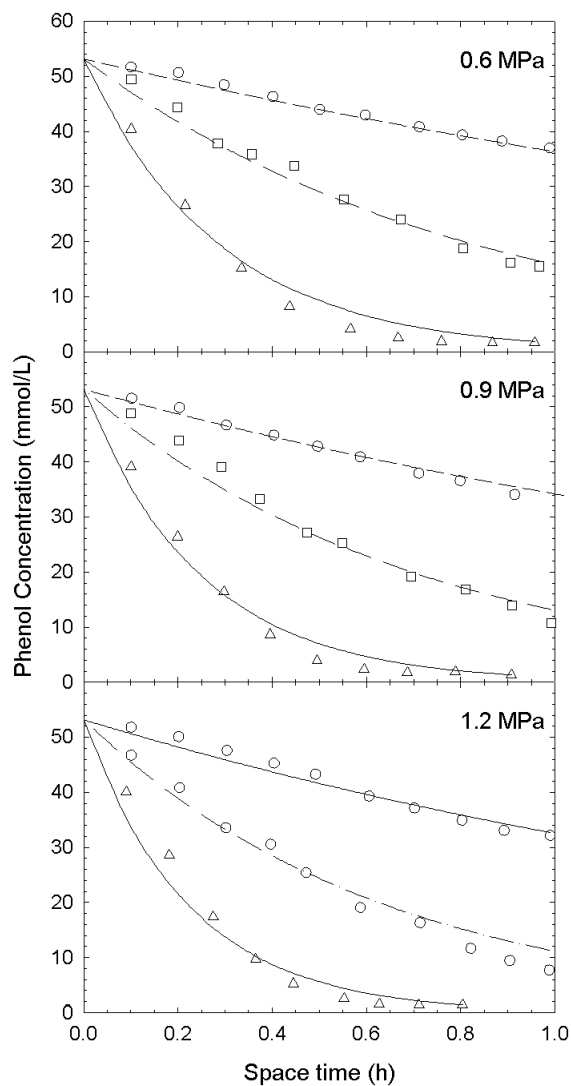
Figure 4.2: Concentration profiles of phenol oxidation over Cu0803 catalyst for different oxygen partial pressures and temperatures for model 1 with the S-A solution. Symbols indicate experimental data: (○) 120°C, (□)140°C, (△) 160°C. Lines indicate model predictions: (- -) 120°C, (- · -) 140°C, (−) 160°C

4.2.2   Five-reaction network (Model 2)

As a result of phenol degradation, a number of intermediate compounds are formed prior to the formation of carbon dioxide. There is no obvious reason why the degradation rates of these compounds are equal to that of phenol. Thus, a model accounting not only for phenol, but also for the main intermediate compounds, should be a significant improvement compared to the previous model.

The first step towards this detailed description of the effluent composition consists in incorporating the main carboxylic acids formed, such as acetic acid, oxalic acid and formic acid. In addition, a lump accounting for all quinone like compounds was included, due to their elevated biotoxicity. The resulting reaction scheme is reproduced in Fig. 4.3.
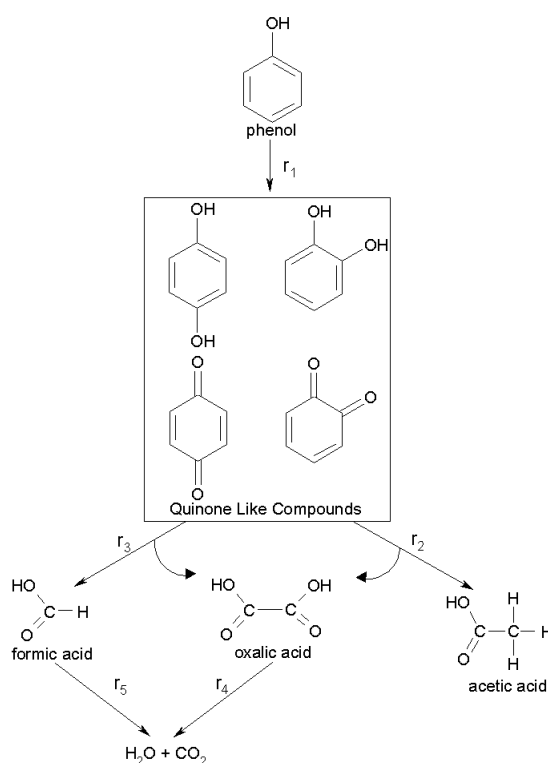
Figure 4.3: Model 2: Five-reaction network proposed for the CWAO of phenol over Cu0803

The very poor fitting obtained when ommiting a direct oxidation step from benzo-quinones to oxalic and formic acid evidents that this pathway has to be included in the model. The reaction of direct oxidation of acetic acid into carbon dioxide and water did not resulted to any considerable improvement, as its reaction rate should be negligible at temperatures below 200^oC [131, 128], so it was excluded from the network. Also the

incorporation of a thermal decomposition of oxalic acid deteriorated model performance. This reaction was only encountered significant at temperatures beyond 180^oC, whereas direct oxidation into carbon dioxide was the most relevant path at lower temperatures [128].

This scheme involves five reactions and five modelled compounds. For phenol destruction (Reaction 1 in the scheme of Fig. 4.3) simple power law equations were chosen again:

$$r_i = k_{0i} \, exp(-E_{ai}/RT) \, x_{O_2}^\alpha \, C_i \qquad (4.5)$$

For the destruction reactions of the intermediate compounds (Reactions 2-5 in the scheme of Fig. 4.3) L-H expressions were recommended.

$$r_i = k_{0i} \, exp(-E_{ai}/RT) \frac{K_{0i} \, C_i \, x_{O_2}^\alpha \, exp(-\Delta H_i/RT)}{1 + \sum K_0 C_j exp(-\Delta H_j/RT)} \qquad (4.6)$$

In this case the number of model parameters increases to 23. The overall destruction/production rates for the five involved compounds can be directly deduced from the reaction scheme (Fig. 4.3) and are as follows:

$$
\begin{aligned}
R_{phen} &= -r_1 & (4.7) \\
R_{quin} &= r_1 - r_2 - r_3 & (4.8) \\
R_{acet} &= r_2 & (4.9) \\
R_{oxal} &= r_2 + r_3 - r_4 & (4.10) \\
R_{form} &= r_3 - r_5 & (4.11)
\end{aligned}
$$

Because of the lack of any specific kinetic data in the literature available for the reactions considered, the same initial guess values used in Model 1 were selected for all five reactions. Furthermore, arbitrary initial values were considered for the adsorption constants. In particular -6 kJ/mol was used for heat of adsorption and $10^{1.5}$ for the respective preexponential factor. The L-M algorithm converged to a SSE value of 2200, while S-A reached a value of 1880, although it needed more function evaluations as shown in Table 4.2. In Fig. 4.4 the profiles obtained with the two algorithms for phenol, oxalic and acetic acid at 0.6 MPa are presented. It can be seen that the profiles obtained by S-A are better than those of L-M, although these could still be accepted.

However, the superiority of the performance of S-A is further supported from the inspection of the calculated parameters, presented in Tables 4.3 and 4.4. L-M obtained a solution in which the oxygen order for all reactions, except for phenol oxidation, as well as the heats of adsorption of oxalic and acetic acid were zero. These results do not have physical sense at all. On the other hand, both algorithms obtained a similar solution for the phenol degradation reaction, which also agrees with the solution obtained in Model

Table 4.2: Performance of S-A, L-M and L-M* for Model 2

	S-A	L-M	L-M*
Minimum	1880	2210	1777
Function Evalutations	$\approx 10^6$	$\approx 5\dot10^4$	10^3

LM*: Solution obained with the L-M algorithm when initialised
from the S-A solution.

1. In addition, the activation energies obtained for the reactions for the degradation of oxalic and formic acid were also close. Finally, the values found by the two algorithms for the activation energies of the reactions corresponding to the destruction of the quinone like pseudocomponent, differed by a factor of 2.

To improve the performance of S-A and to calculate the statistical significance of the S-A solution the L-M algorithm was initialised with the S-A solution (termed L-M*). This led to a decrease of 5% of the objective function. Exemplarily, the corresponding concentration - space time profiles of phenol, oxalic and acetic acid were also given in Fig. 4.4, confirming the close agreement between S-A and L-M*. Some of the obtained frequency and preexponential factors as well as oxygen reaction orders showed however, important differences from the S-A solution, as can be seen from Tables 4.3 and 4.4. It should be pointed out that it was not possible to calculate the statistical significance of these parameters using eq. 2.12. The differences in the orders of magnitude of the included compounds invalid the assumption of constant σ^2 and led to unreasonably small error estimates. Alternatively, the errors reported in Tables 4.3 and 4.4 were calculated using the formulation employed in multivariable linear regression, with 95% confidence interval.

Table 4.3: Frequency Factors, activation energies and reaction orders for Model 2 using S-A, L-M and L-M*

Reaction No	S-A	L-M	L-M*
	Frequency Factors[1]		
1	$10^{10.97\pm0.02}$	$10^{10.84\pm0.02}$	$10^{11.17\pm0.02}$
2	$10^{10.70\pm0.04}$	$10^{4.02\pm0.06}$	$10^{13.25\pm0.06}$
3	$10^{9.67\pm0.03}$	$10^{3.75\pm0.03}$	$10^{12.22\pm0.03}$
4	$10^{12.56\pm0.05}$	$10^{13.87\pm0.05}$	$10^{16.98\pm0.05}$
5	$10^{8.22\pm0.05}$	$10^{10.91\pm0.05}$	$10^{11.18\pm0.05}$
	Activation Energy		
	(kJ/mol)		
1	75.8 ± 0.1	75.7 ± 0.1	76.5 ± 0.1
2	87.5 ± 0.4	40.7 ± 0.4	89.3 ± 0.4
3	78.8 ± 0.4	32.0 ± 0.4	83.0 ± 0.4
4	75.8 ± 0.2	85.8 ± 0.2	80.9 ± 0.2
5	54.3 ± 0.4	62.3 ± 0.4	59.1 ± 0.4
	Oxygen Order		
1	0.31 ± 0.004	0.28 ± 0.004	0.340 ± 0.004
2	0.36 ± 0.01	0	1.08 ± 0.01
3	0.16 ± 0.02	0	0.71 ± 0.02
4	0.79 ± 0.01	0	0.74 ± 0.01
5	0.06 ± 0.01	0	0

[1] The frequency factor has reaction dependent units. For reaction 1 is in $(L/kg_{cat}h)$, while for the rest of the reaction constants is in $(mol/kg_{cat}h)$.

Table 4.4: Adsorption parameters for each adsorbed compound for Model 2 using S-A, L-M and L-M*

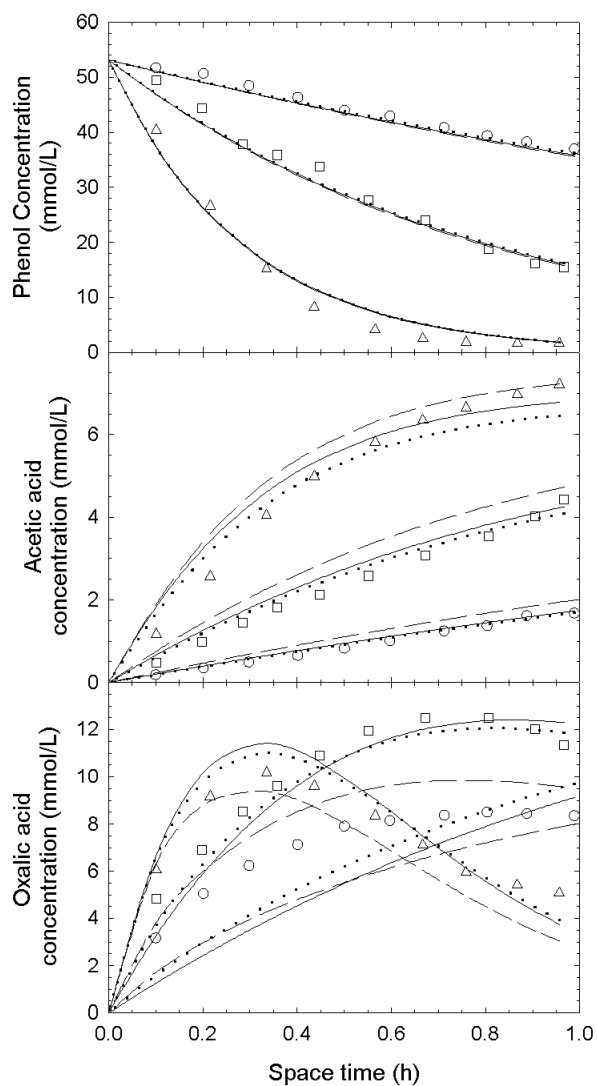| Compound	S-A	L-M	L-M*
	Preexponential Factors		
	(L/mol)		
Lump	$10^{-1.7\pm0.2}$	$10^{-5.7\pm0.2}$	$10^{-3.21\pm0.2}$
Oxalic Acid	$10^{3.94\pm0.05}$	$10^{-1.73\pm0.05}$	$10^{1.65\pm0.05}$
Formic Acid	$10^{2.6\pm0.05}$	$10^{-1.95\pm0.05}$	$10^{-1.86\pm0.05}$
Acetic acid	$10^{4.91\pm0.04}$	$10^{3.15\pm0.04}$	$10^{8.54\pm0.04}$
	Heat of adsoption		
	(kJ/mol)		
Lump	-69 ± 2	-67 ± 2	-95 ± 2
Oxalic Acid	-11.5 ± 0.4	$0. \pm 0.5$	-7.3 ± 0.4
Formic Acid	-13.1 ± 0.4	-1.9 ± 0.4	-8.3 ± 0.4
Acetic Acid	-16.7 ± 0.4	0 ± 0.5	-0.3 ± 0.4

Figure 4.4: Phenol, acetic and oxalic acid concentration profiles at 0.6 MPa for model 2. Points indicate experimental data: (○): 120^oC, (□): 140^oC, (△): 160^oC. (−): S-A, (- -) L-M, ($\cdots$) L-M starting from the S-A solution

4.2.3 Eight-reaction network (Model 3)

After modelling the principal compounds generated by the oxidation of phenol, the last step is to fit all detected compounds. As p- and o- benzoquinones could no be distinguished they were treated as a unique compound. For this reason it was also convenient to join catechol and hydroquinone concentrations. Maleic and malonic acid were inserted in the pathway leading from benzoquinones to acetic acid. The reaction pathway proposed is given in Fig. 4.5. Now, the total number of parameters involved raised to 38, while differences of up to three orders of magnitude existed in the concentration ranges of the compounds to be fitted.
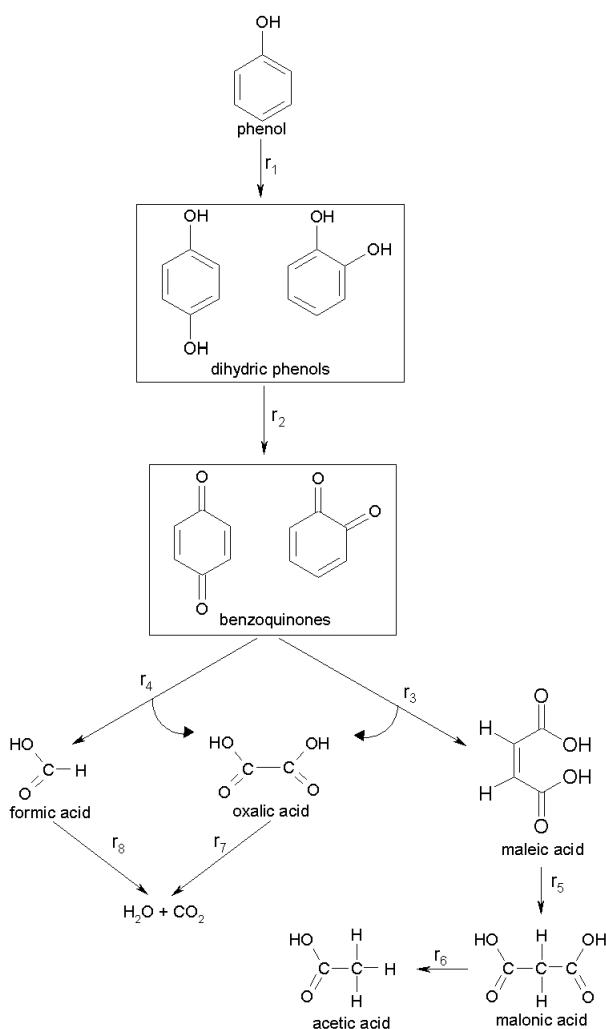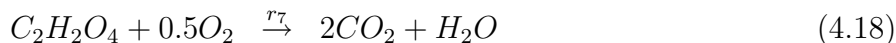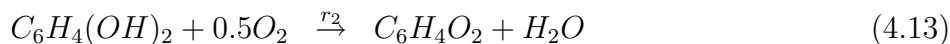

Figure 4.5: Reaction network proposed for the CWAO of phenol over Cu0803 catalyst

This scheme is summarised in the following reactions.

$$C_6H_5OH + 0.5O_2 \xrightarrow{r_1} C_6H_4(OH)_2 \tag{4.12}$$
$$C_6H_4(OH)_2 + 0.5O_2 \xrightarrow{r_2} C_6H_4O_2 + H_2O \tag{4.13}$$
$$C_6H_4O_2 + 2.5O_2 + H_2O \xrightarrow{r_3} C_4H_4O_4 + C_2H_2O_4 \tag{4.14}$$
$$C_6H_4O_2 + 5O_2 \xrightarrow{r_4} CH_2O_2 + C_2H_2O_4 + 3CO_2 \tag{4.15}$$
$$C_4H_4O_4 + O_2 \xrightarrow{r_5} C_3H_4O_4 + CO_2 \tag{4.16}$$
$$C_3H_4O_4 \xrightarrow{r_6} C_2H_4O_2 + CO_2 \tag{4.17}$$
$$C_2H_2O_4 + 0.5O_2 \xrightarrow{r_7} 2CO_2 + H_2O \tag{4.18}$$
$$CH_2O_2 + 0.5O_2 \xrightarrow{r_8} CO_2 + H_2O \tag{4.19}$$

For the degradation of phenol (Reaction 1) a simple power law rate expression (Eq. 2.16) was considered, while for the rest of the reactions L-H expressions (Eq. 2.17) were used. In this case the overall destruction-production rates of the eight involved compounds are given by the following relationships.

$$R_{phenol} = -r_1 \tag{4.20}$$
$$R_{dihydric\,phenol} = r_1 - r_2 \tag{4.21}$$
$$R_{benzoquinone} = r_2 - r_3 - r_4 \tag{4.22}$$
$$R_{maleic} = r_3 - r_5 \tag{4.23}$$
$$R_{malonic} = r_5 - r_6 \tag{4.24}$$
$$R_{acetic} = r_6 \tag{4.25}$$
$$R_{oxalic} = r_3 + r_4 - r_7 \tag{4.26}$$
$$R_{formic} = r_4 - r_8 \tag{4.27}$$

In the first place, the initial guess of Model 1 was extended to this model. In this case L-M did not converged while S-A was progressing very slowly. Thus, in order to improve performance of both algorithms, an initial parameter set was created based on the solution of Model 2. For the reactions that are included in both models the initial guess was the solution previously encountered. For the reaction of dihydric quinone oxidation the parameters were taken as intermediate values of reaction 2 and 3 of Model 2. For the maleic acid and malonic acid the initial guess was the solution for reaction 3 of the Model 2. This was selected because maleic acid and malonic acid destruction reactions are expected to have activation energies lower than the rest of carboxylic acids, given that they appear only as traces. In this case S-A managed to converge to a reasonable solution (objective function of 1970), while the L-M stayed far from a reasonable optimum. Further improvement was achieved when the S-A solution was fed to the L-M algorithm, resulting in a criterion of 1650. The S-A and the improved L-M* solution, mainly differed in the values of frequency and preexponential factors, as observed for model 2. The reported errors have been also calculated by a linear approximation for 95% confidence interval.

When the kinetic data set comprises high concentration compounds, as well as, low concentration compounds, the global quality of te is likely to depend on the criterion imposed on the objective function. This situation is illustrated in Fig. 4.6. The quality of the fitting obtained from S-A using the SSE criterion was acceptable for high concentration profiles (Fig. 4.6a), while predictions of low concentration compounds were unacceptable (Fig. 4.6d). L-M* considerably improved maleic acid profiles, as can be seen from the same figures. In order to improve the low concentration compound estimation, the Relative Least Squares criterion was employed in the optimisation procedure. As a result, this caused a considerable improvement in the fitting of low concentration profile compounds (Fig. 4.6d), but as expected high concentration profiles were poorly predicted (Fig. 4.6b). In this case L-M* could not improve the predicted profiles. In an attempt to balance the counter effects of these two commonly used criterions, the minimisation of the absolute sum of errors was tested. As can be verified from Fig. 4.6c and 4.6f, the predictions of high concentration profiles were then very satisfactory, maintaining the quality of the fit of low concentration profiles.

The calculated parameters with L-M* with the SSE criterion or with S-A with the SAE criterion, are presented for S-A in Tables 4.5 and 4.6. The calculated activation energies clalculated in both cases are close, while oxygen orders where systematically higher for the L-M* than for the S-A solution. The obtained heats of adsorption were considerably different, although this is not surprising, since these constants are less influent in the kinetic model performance, as can be judjed from their corresponding errors. Finally kinetic and adsorption preexponential factors are accordingly adjusted to balance the difference of the rest of the temrs in the kinetic equaiton.

Table 4.5: Frequency factors, activation energies and reaction orders for Model 3 using S-A and L-M*

Reaction	k_0 S-A (1)	k_0 L-M* (1)	E_a S-A kJ/mol	E_a L-M* kJ/mol	α S-A	α L-M*
1	$10^{10.91 \pm 0.02}$	$10^{11.17 \pm 0.2}$	74.9 ± 0.2	76.5 ± 1	0.311 ± 0.005	0.343 ± 0.04
2	$10^{8.4 \pm 0.2}$	$10^{16.76 \pm 0.2}$	52 ± 1	49.6 ± 1	0.52 ± 0.04	0.88 ± 0.04
3	$10^{11.16 \pm 0.03}$	$10^{14.9 \pm 0.03}$	54.9 ± 0.2	49.2 ± 0.2	0.61 ± 0.01	1.13 ± 0.01
4	$10^{8.68 \pm 0.03}$	$10^{13.07 \pm 0.03}$	44.7 ± 0.3	42.4 ± 0.3	0.35 ± 0.01	0.68 ± 0.01
5	$10^{4.72 \pm 0.02}$	$10^{13.03 \pm 0.02}$	27 ± 4	24 ± 4	0.5 ± 0.1	0
6	$10^{4.9 \pm 0.1}$	$10^{2.75 \pm 0.1}$	52.3 ± 0.8	36.1 ± 0.8	0	0
7	$10^{13.9 \pm 0.06}$	$10^{22.79 \pm 0.06}$	91.1 ± 0.6	93.7 ± 0.6	0.80 ± 0.02	1.2 ± 0.02
8	$10^{9.79 \pm 0.04}$	$10^{14.81 \pm 0.04}$	69.9 ± 0.4	75.0 ± 0.4	0.23 ± 0.01	0.43 ± 0.01

[1] For reaction 1 the frequency factor is in $(L/kg_{cat}h)$, while for the rest of the reactions is in $(mol/kg_{cat}h)$.

In Fig. 4.6 can be apreciated that L-M* with the SSE criterion, as well as, S-A with the SAE criterion give equally good prediction for phenol concentration. However, it S-A with the SAE criterion performs slightly better for maleic acid. The same holds for the profiles of the rest intermediate compounds, as can be seen exemplarily in Fig. 4.7, where

Table 4.6: Adsorption paramters for each adsorbed compound for Model 3 using S-A and L-M*

Compound	K_0 S-A L/mol	K_0 L-M* L/mol	ΔH S-A kJ/mol	E_a L-M* kJ/mol
Dihydric Phenols	$10^{-0.2\pm0.2}$	$10^{-7.95\pm0.2}$	-28 ± 1.4	-26.3 ± 1.4
Benzoquinones	$10^{2.3\pm0.2}$	$10^{-4.1\pm0.2}$	-2 ± 1	-13 ± 1
Maleic acid	$10^{0.1\pm0.3}$	$10^{-11.73\pm0.3}$	-40 ± 20	-40 ± 20
Oxalic acid	$10^{2.2\pm0.07}$	$10^{-5.11\pm0.07}$	-11.4 ± 0.5	-1.5 ± 0.5
Malonic acid	$10^{0.7\pm0.2}$	$10^{3.79\pm0.2}$	-28 ± 1	0 ± 1
Formic acid	$10^{0.6\pm0.1}$	$10^{-2.93\pm0.1}$	-8.1 ± 0.4	-5.7 ± 0.4
Acetic acid	$10^{3.7\pm0.1}$	$10^{3.14\pm0.1}$	$-8.6\pm$	0

the concentration profiles for benzoquinone, dihydric phenols, and formic acid at $1.2\ MPa$ are presented. Thus the S-A solution obtained with SAE solution has been considered as the best fit solution. The parameters obtained by the S-A with SSE, corresponding to phenol degradation, are similar to those calculated by Model 2. On the other hand, the parameters of reactions 3, 4, 7, and 8 of Model 3, deviate from the corresponding of Model 2 (reactions 2, 3, 4 and 5 respectively), however, they exhibit similar tendencies. The activation energy for oxalic acid oxidation remains higher than that of formic acid. In the same manner, the activation energy of reaction 3 is higher than that of reaction 4 as in Model 2. Similar behaviour is exhibited by oxygen orders.
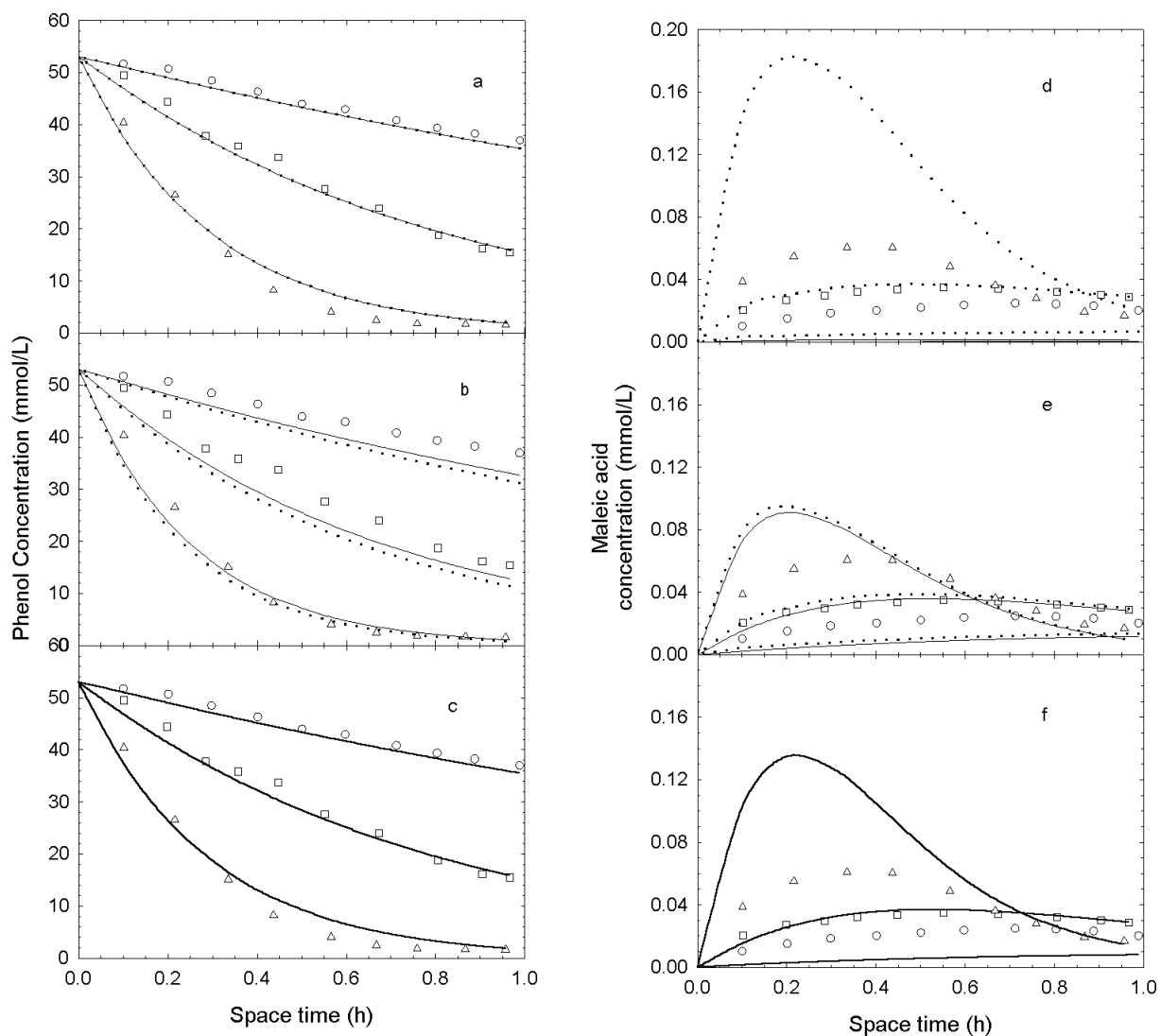
Figure 4.6: Phenol and maleic acid concentration profiles at 0.6 MPa using different objective functions. Experimental data: ($\circ$) 120^oC , ($\square$)140^oC , ($\triangle$) 160^oC . Model predictions: ($-$) S-A, ($\cdots$) L-M*. (a & d): SSEs, (b & e) SRSE, (c & f) SAE.
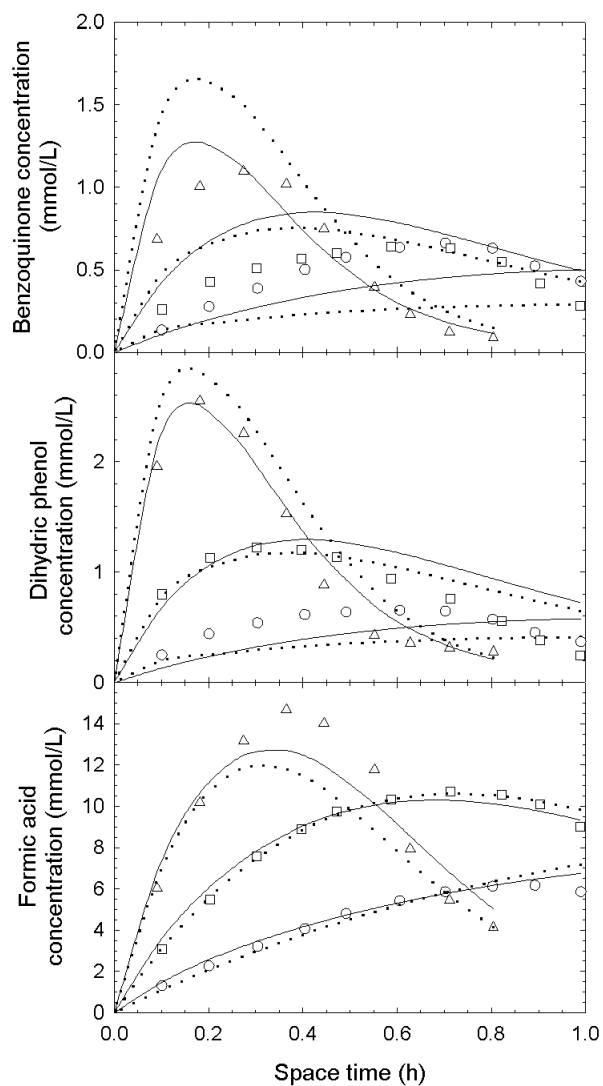
Figure 4.7: Dihydric phenol, benzoquinone and formic acid concentration profiles at 0.6 MPa using different objective functions. Experimental data: (○) 120^oC, (□)140^oC, (△) 160^oC. Model predictions: (−) S-A with SAE, (···) L-M* with SSE.

4.2.4 Conclusions

The Simulated Annealing algorithm was successfully applied to perform complex nonlinear kinetic parameter estimation. The classical Levenberg-Marquardt algorithm was clearly advantageous when only few parameters are to be optimised, and a sound initial estimate can be provided. On the other hand, only S-A was able to fit well experimental data to the most detailed model, for which the L-M algorithm exhibit insuperable problems to converge. Thus, the elevated computational cost of this algorithm is largely compensated by its robustness. For example, the time required on a 700 MHz PC, for the S-A to converge varied from 30 min for the simple model 1, to 10 h for the most complex case. In case of complex reaction networks, a progressive model building was found necessary to achieve convergence within a reasonable computational time. The obtained S-A solution can be further improved by consecutive application of the L-M algorithm. In addition, this approach permits calculation of the statistical significance of the parameters. Also, the form of the objective function may be of importance for the overall quality of prediction when there exist differences in the order of magnitude of the experimental concentrations. In such a case, S-A combined with the sum of absolute errors, or L-M* with SSE criterion have shown to reasonably fit both high and low concentration compounds.

4.3   Kinetics over Copper Oxide

In th previous discussion, the role of progressive model building was demonstrated for the succesfull multiparameter estimation of complex reaction networks. In this context, the potential and easy application of stochastic optimisation algorithm, and in particularly S-A, was clearly highlighted in the case study of the CWAO of phenol over a supported CuO catalyst. Within this discussion, only some representative results were presented, to give support to the data analysis. Thus, we are now going to discuss the entire results from a point of view of reaction kinetics.

4.3.1   Power Law Model

Before using L-H expressions the reaction and the intermediate distribution was modelled in terms of Power Law kinetics. This simpler model had still 24 parameters to be evaluated. To discuss the performance of both types of rate law, Fig. 4.8 shows the estimated and experimental concentration profiles of phenol, malonic acid and formic acid at 0.6 MPa and three different temperatures and compares them to those obtained when using L-H rate expresions. The superiority of the latter expressions is evident, and can be further appreciated in Table 4.7 wher the normalised average error in (%) is given for all compounds involved.

Table 4.7: Average per cent error of the predicted concentrations using power law and L-H expressions

Compound	Power Law	L-H
Phenol	5.8	5.6
Dihydric Penols	25	22
Benzoquinones	45	21
Maleic Acid	45	42
Oxalic Acid	36	20
Malonic Acid	3.9	4.2
Formic Acid	20	14
Acetic Acid	16	6.8
Total	10.6	7.8

It can be noted that the model predicts satisfactory phenol as well as acetic acid concentration, but the deviations for the rest of the carboxylic acids and quinone-like components are significant, thus indicating that the fitting of these compounds is not acceptable. Also, it should be pointed out that some of the estimated parameters were not reasonable. For example, the activation energy for the malonic acid decarboxylation, which should not be limited by any diffusion, was calculated to be 5 kJ/mol, which is in the range of diffusion limited processes.
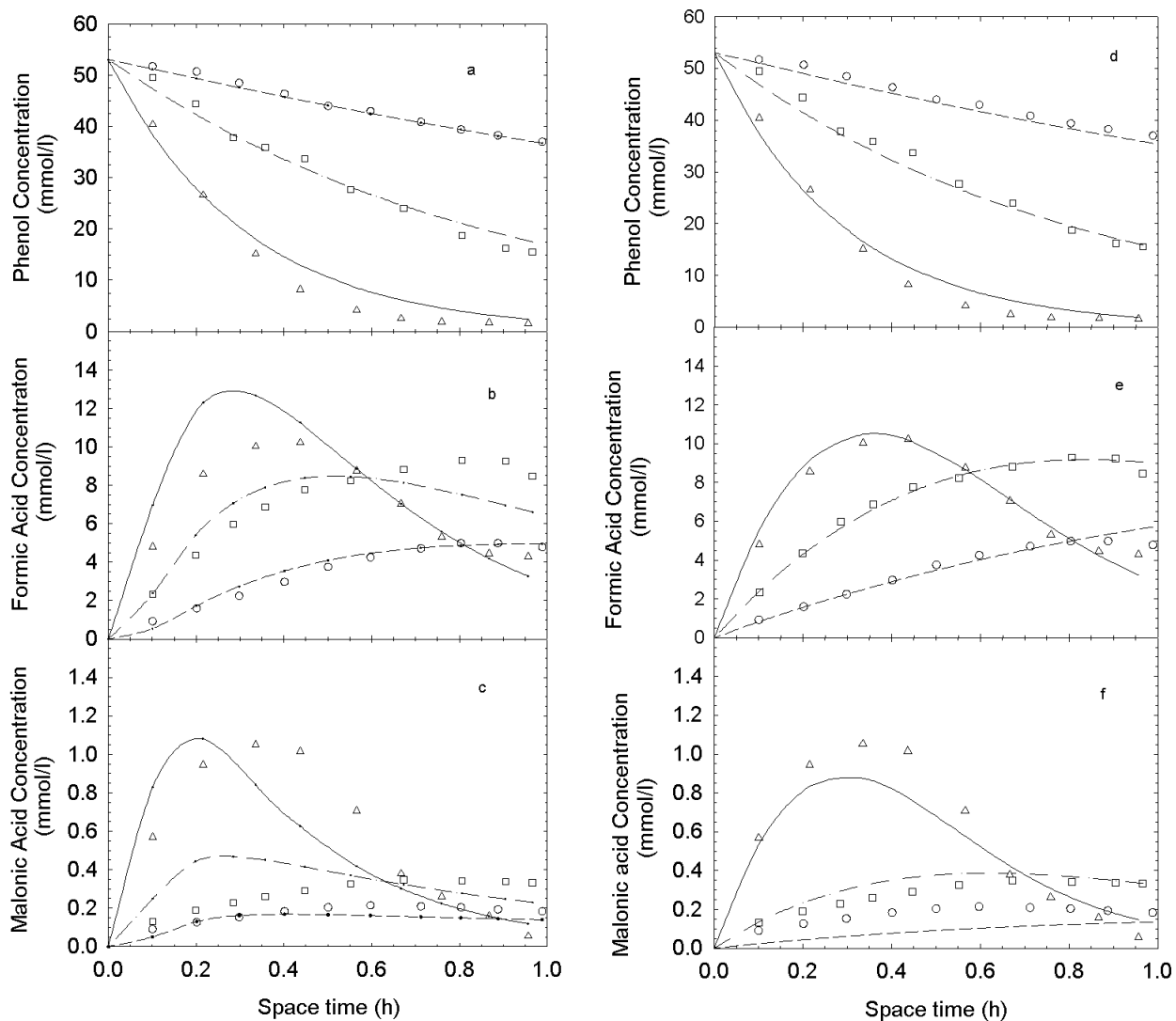
Figure 4.8: Concentration profiles for phenol, formic acid and malonic acid using power law or L-H expresions at 0.6 MPa for the copper catalyst. Symbols indicate experimental data: (○) 120ºC, (□)140ºC, (△) 160ºC. Lines indicate model predictions: (- -) 120ºC, (- · -) 140ºC, (−) 160ºC

4.3.2   Langmuir-Hinshelwood Model

In order to provide a more reliable kinetic model, L-H expressions were implemented in the rate equations. Preliminary experimental data obtained from adsorption experiments, surprisingly show that phenol did not adsorb on the catalyst, contrary to the carboxylic acids and quinone like components. Therefore, the L-H expression was not applied on phenol disappearance. This complex model needed the definition of 38 parameters.

This extended model greatly improves the results as can be seen by comparing the calculated average errors, already presented in Table 4.7 and the concentration profiles shown in Fig. 4.8. The excelent phenol fitting did not improved, but the average error for the rest of the compounds, including acetic acid, decreased significantly. Overall, the total average error reduced from 10.6% to 7.8% when using the L-H expressions.

The resulting concentration profiles of phenol and COD and the detected intermediate compounds are shown in Figs. 4.9 to 4.13, demonstrating the excellent agreement obtained. The CODs of the samples are an indicator for the actual product distribution and were measured independently by a chemical method. The model also allows to calculate, without any fitting, this parameter from the estimated intermediate product distribution. Thus the good correspondence between the measured and the predicted COD values, as illustrated in Fig. 4.9 proves the quality of the general fitting.

It can be pointed out that the model was capable of correctly predicting the profiles of both high, i.e. phenol, acetic acid, oxalic acid, formic acid and low, i.e. dihydric phenols, benzoquinones, maleic acid, and malonic acid, concentration compounds, regardless the three orders of magnitude of difference between them. For quinone like compounds, i.e. dihydric phenols and benzoquinones respectively, the model prediction (Fig. 4.10) loose some precision that certainly has to be related to the difficulty to separate properly these compounds, thus imposing two lumps. Maleic acid was detected in trace concentrations, thus being the component that should be mostly subjected to analytical error. From the Fig. 4.11 it becomes clear that the model could qualitatively predict its concentration scale as well as the general trends of the experimental data. The calculated malonic acid profiles (Fig. 4.11) also match well with the experimental concentrations, describing correctly the sharp peak that appears as the temperature rises from 140 to $160^{o}C$. Acetic acid (Fig. 4.12) is the best fitted components when eliminating its destruction reaction. This is in agreement with experimental findings of other works, that observed negligible oxidation reaction of acetic acid at the given operating conditions. On the other hand, oxalic acid estimates (Fig. 4.13) some deviation only at $120^{o}C$, probably because the lumped reaction to yield carbon dioxide, formic acid and oxalic acid is not accurate enough. Finally, with respect to formic acid (Fig. 4.13) there is only a slight underestimation of the effect of oxygen with respect to the peak, at $160^{o}C$. Globally, given the complexity of the system and concentrations involved the model is capable to predict extremely well the experimental reaction data.
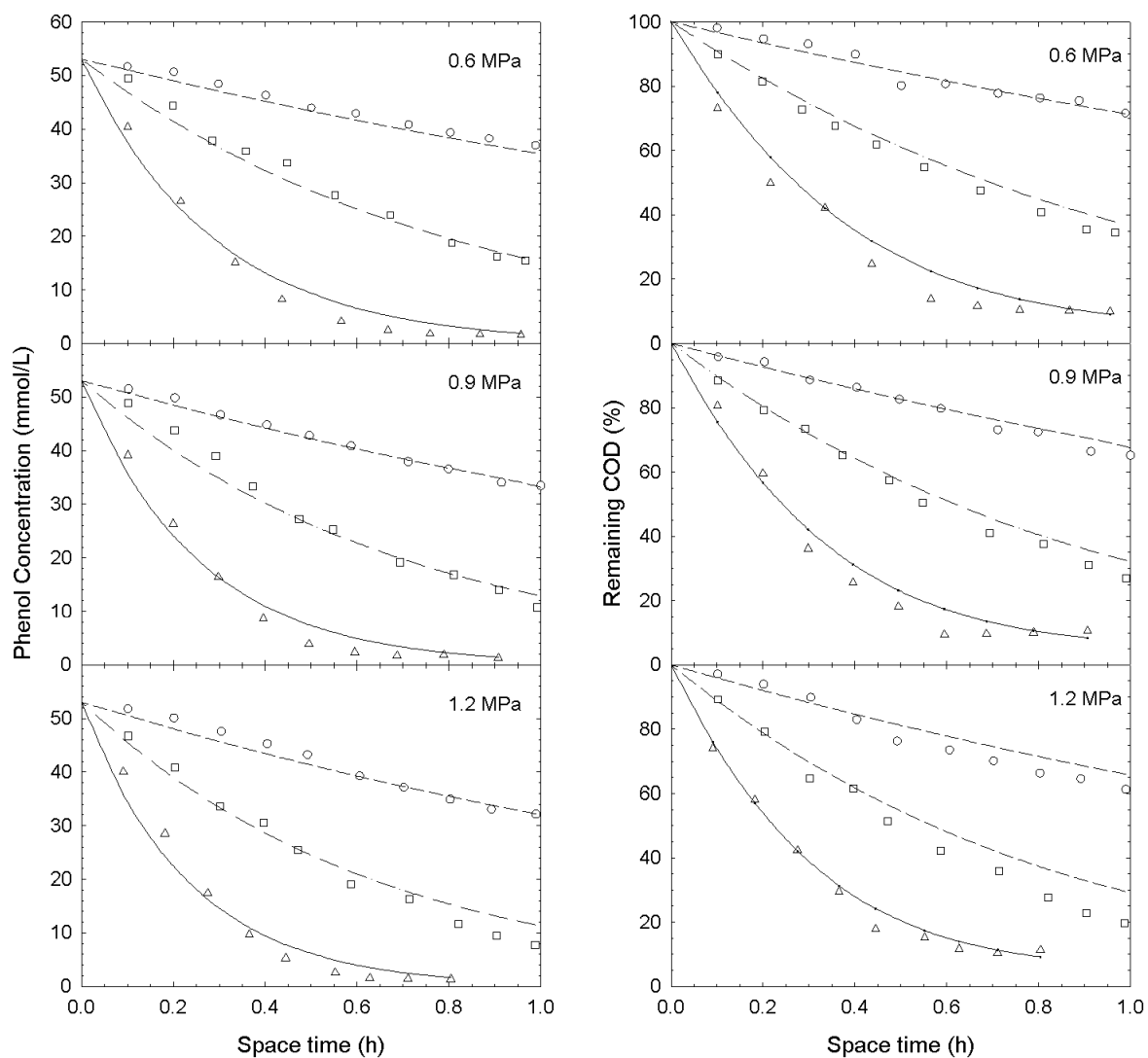
Figure 4.9: Concentration profiles of phenol and COD for different oxygen partial presures and temperatures. Symbols indicate experimental data: (○) 120°C , (□)140°C , (△) 160°C . Lines indicate model predictions: (- -) 120°C, (- · -) 140°C, (−) 160°C
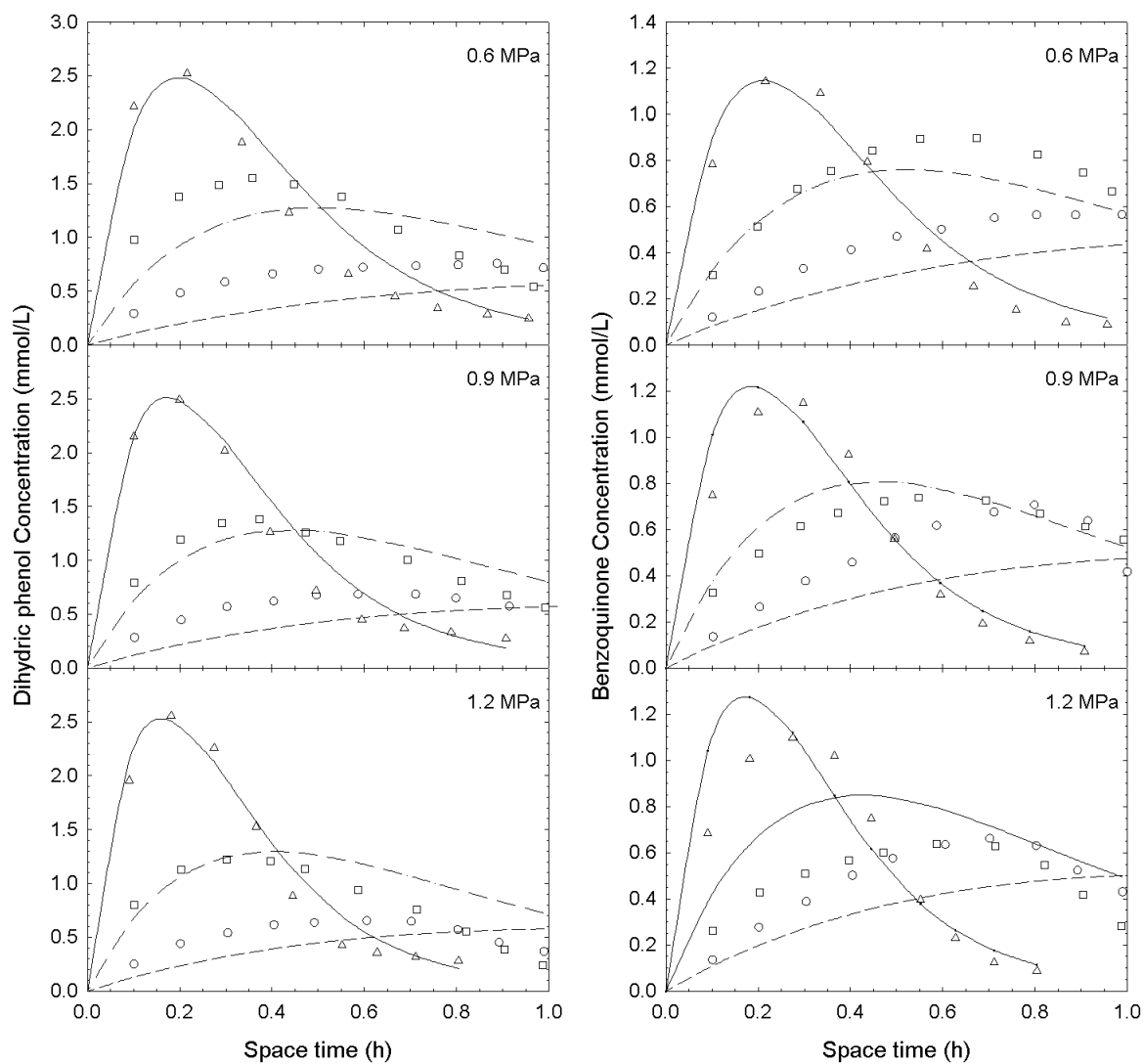
Figure 4.10: Concentration profiles of dihydric phenols and benzoquinone for different oxygen partial pressures and temperatures. Symbols indicate experimental data: (○) 120^oC , (□)140^oC , (△) 160^oC . Lines indicate model predictions: (- -) 120^oC, (- · -) 140^oC, (−) 160^oC
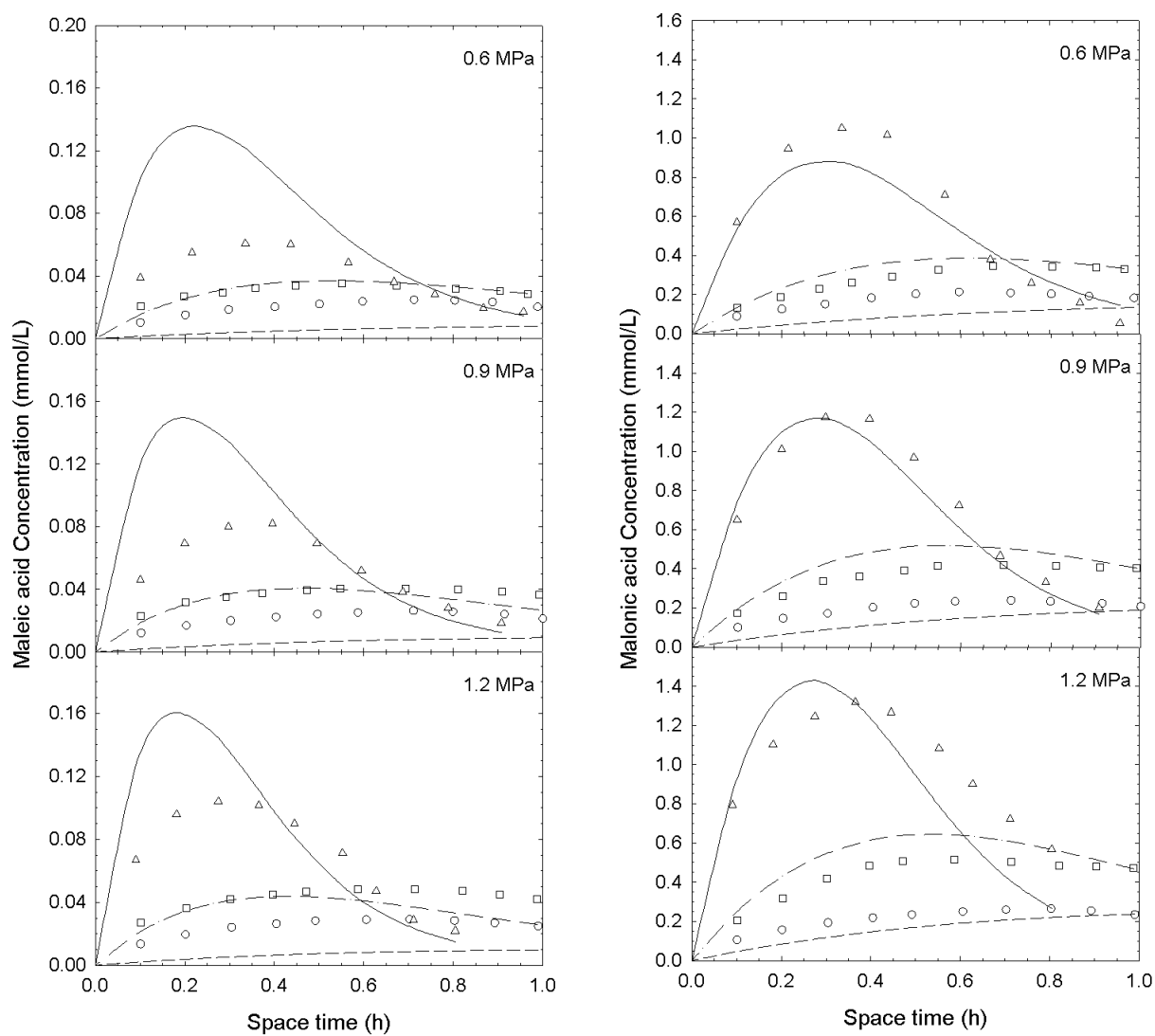
Figure 4.11: Concentration profiles of maleic and malonic acid for different oxygen partial pressures and temperatures. Symbols indicate experimental data: ($\circ$) $120^{o}C$, ($\square$)$140^{o}C$, ($\triangle$) $160^{o}C$. Lines indicate model predictions: (- -) $120^{o}C$, (- $\cdot$ -) $140^{o}C$, ($-$) $160^{o}C$
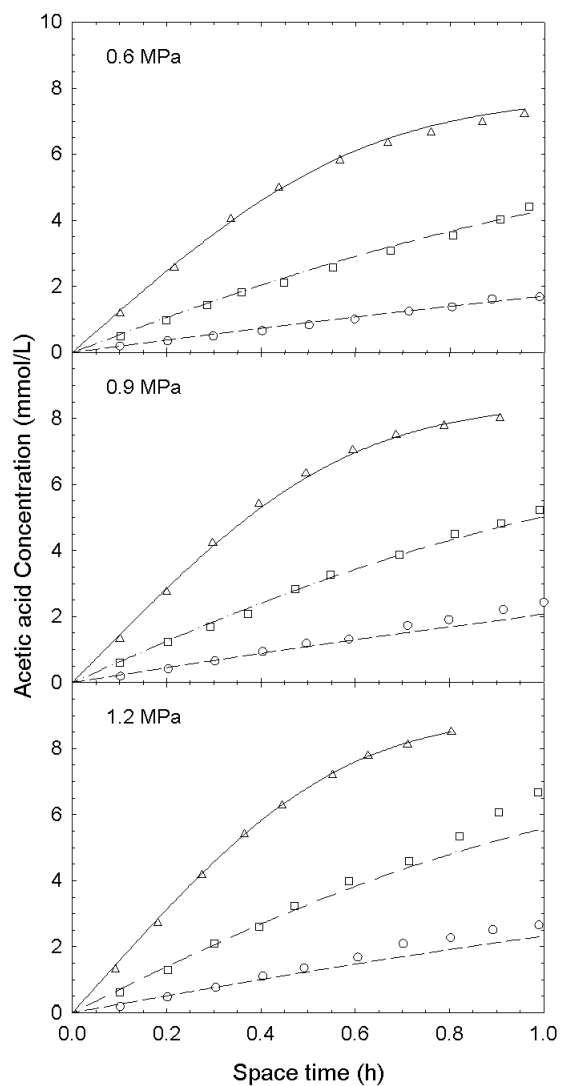
Figure 4.12: Concentration profiles of acetic acid for different oxygen partial pressures and temperatures. Symbols indicate experimental data: (○) $120^{o}C$, (□)$140^{o}C$, (△) $160^{o}C$. Lines indicate model predictions: (- -) $120^{o}C$, (- · -) $140^{o}C$, (−) $160^{o}C$
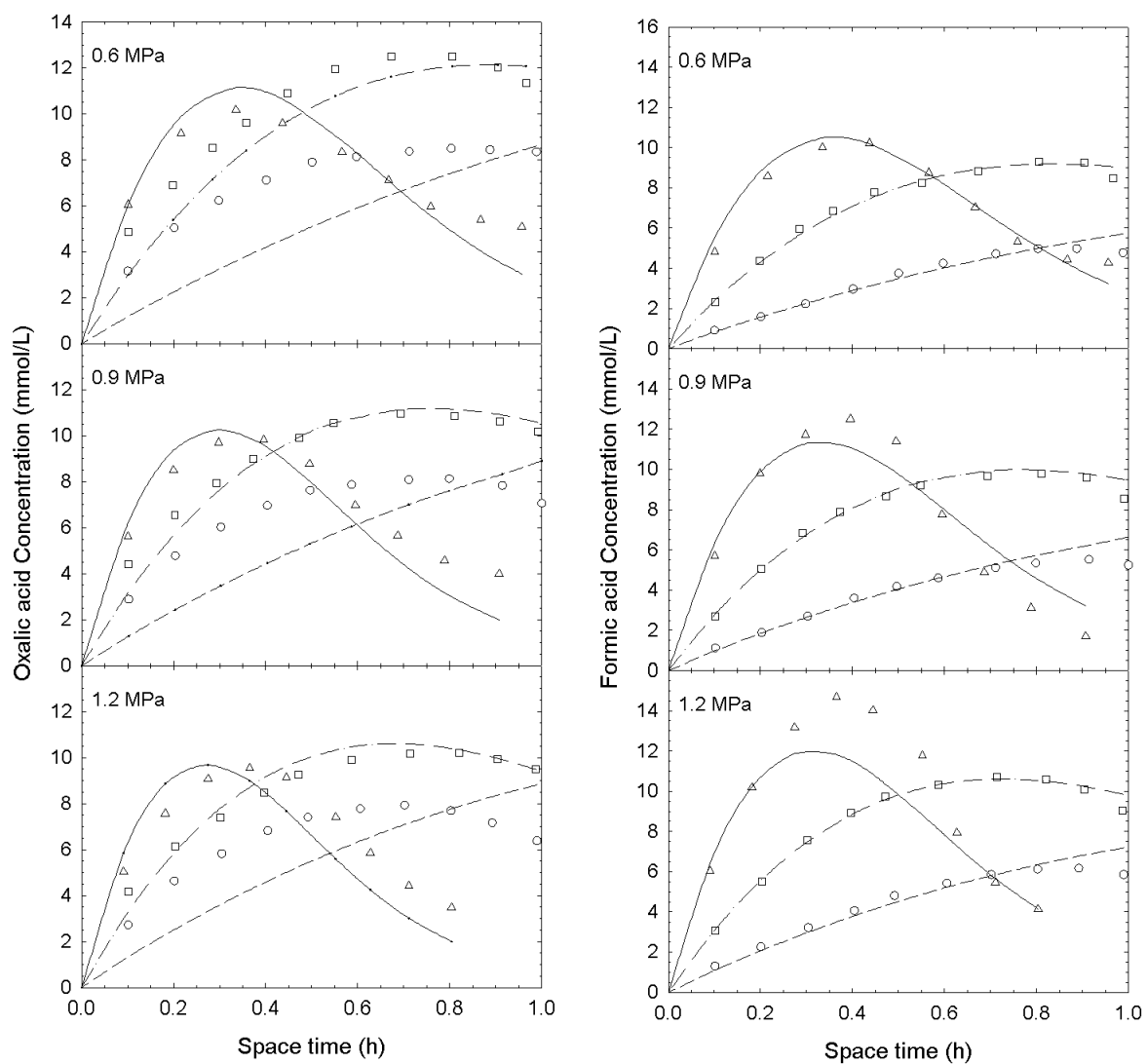
Figure 4.13: Concentration profiles of oxalic and formic acid for different oxygen partial pressures and temperatures. Symbols indicate experimental data: (○) 120°C , (□)140°C , (△) 160°C . Lines indicate model predictions: (- -) 120°C, (- · -) 140°C, (—) 160°C

4.3.3   Model Parameters

In this section our aim is to extend the parameter analysis of the complex model 3 to commend also on the physical meaning that can be attributed to the parameters obtained by the S-A algorithm using the SAE criterion (Tables 4.8 and 4.9).

Table 4.8: Frequency factors, activation energies and reaction orders

Reaction No	k_o (1)	E_a kJ/mol	α
1	$10^{10.91\pm0.02}$	74.9 ± 0.2	0.311 ± 0.005
2	$10^{8.4\pm0.2}$	52 ± 1	0.52 ± 0.04
3	$10^{11.16\pm0.03}$	54.9 ± 0.2	0.61 ± 0.01
4	$10^{8.68\pm0.03}$	44.7 ± 0.3	0.35 ± 0.01
5	$10^{4.72\pm0.02}$	27 ± 4	0.5 ± 0.1
6	$10^{4.9\pm0.1}$	52.3 ± 0.8	0
7	$10^{13.9\pm0.06}$	91.1 ± 0.6	0.8 ± 0.02
8	$10^{9.79\pm0.04}$	69.9 ± 0.4	0.23 ± 0.01

[1] The frequency factor has reaction dependent units:
$L/kg_{cat}h$ for reaction 1, $mol/kg_{cat}h$ for reactions 2-8.

Table 4.9: Adsorption parameters for each adsorbed compound

Compound	K_0 L/mol	E_a kJ/mol
Dihydric Phenols	$10^{-0.2\pm0.2}$	-28 ± 1.4
Benzoquinones	$10^{2.3\pm0.2}$	-2 ± 1
Maleic Acid	$10^{0.1\pm0.3}$	-40 ± 20
Oxalic Acid	$10^{2.2\pm0.07}$	-11.4 ± 0.5
Malonic Acid	$10^{0.7\pm0.2}$	-28 ± 1
Formic Acid	$10^{0.6\pm0.1}$	-8.1 ± 0.4
Acetic Acid	$10^{3.7\pm0.1}$	-8.6 ± 8.6

The activation energy for the destruction of phenol was found to be $74.9\ kJ/mol$. This value falls within the range of values given for the kinetic control, for example close to the $85\ kJ/mol$ [81, 96] and $84\ kJ/mol$ [82]. On the other hand, the oxygen order ($\alpha = 0.311$) differs from the one half order more usually encountered. The values estimated here are also slightly different from those evaluated by Fortuny et al. [72] ($E_a = 85\ kJ/mol$ and $\alpha = 0.5$) using the same experimental data set. This difference can be attributed to the fact that in their study the kinetic parameters were obtained only accounting for the phenol data, whereas in this study phenol and dihydric phenol concentration were matched.

For the rest of reactions included in the reaction network none or few reports of the kinetic constants exist. Furthermore, the available studies have been carried out with pure compounds, and different catalysts, so they cannot be compared in a straight manner with the values reported in the present study. To evaluate the physical sense of the obtained parameters, useful information can be obtained when plotting intermediate compound concentration versus phenol conversion, as shown in Figs. 4.14 to 4.17.
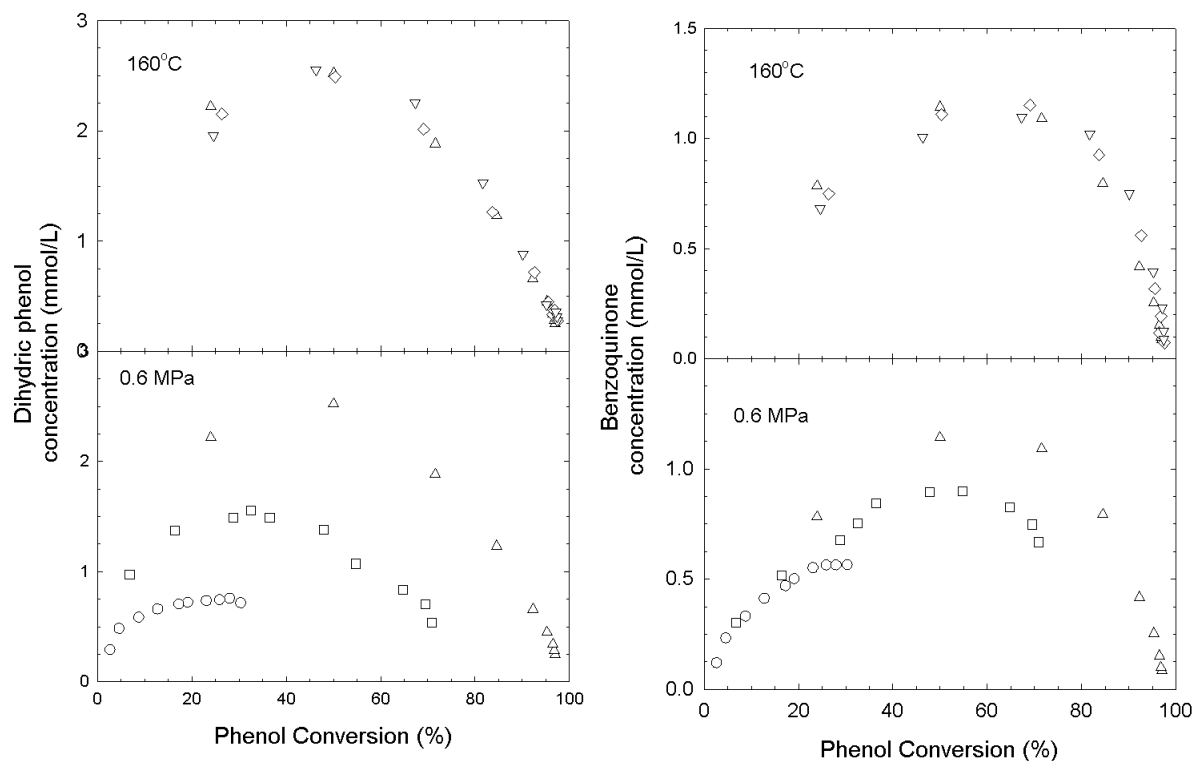

Figure 4.14: Concentration of dihydric phenols and benzoquinone over the Cu0803 catalyst as a function of phenol conversion. (∘) 120°C and 0.6 MPa, (□)140°C and 0.6 MPa, (△) 160°C and 0.6 MPa, (◇) 160°C and 0.9 MPa, (∇) 160°C and 1.2 MPa

Dihydric phenols were considered to oxidise forming benzoquinones. The activation energy for this reaction was found to be 52 kJ/mol, while the oxygen order was 0.5. These values cannot be compared as, to the best of our knowledge, there is no literature reference reporting any kinetic data for this reaction. In Fig. 4.14 it can be observed that for the same phenol conversion dihydric phenol concentration increases with temperature. This clearly indicates that phenol oxidation rate increases more with temperature, than dihydric phenol destruction. Thus a lower activation energy is reasonable for the dihydric phenol oxidation reaction. In the same figure it can be appreciated that the oxygen

partial pressure has only a minor effect on the dihydric phenol concentration, for the same phenol conversion. Therefore, the 0.5 order encountered, being close to the 0.311 found for phenol, seems quite reasonable.

Several benzoquinone degradation reactions can be proposed based on the Devlin and Harris mechanism, here only two of the possible reactions. The first one leads to maleic and oxalic acids, while the second one leads to carbon dioxide, formic acid and oxalic acid. The respective activation energies were found to be 54.9 kJ/mol and 44.7 kJ/mol. This is in agreement with the benzoquinone concentration - phenol conversion profiles, also shown in Fig. 4.14, since benzoquinone concentration increases with temperature. These profiles also indicate that oxygen partial pressure is not significantly influent, so the oxygen orders should be close to the 0.311 value obtained for phenol. However, these were found to be 0.61 and 0.35 for reaction 3 and 4 (see Fig. 4.5), the first one being significantly higher to that of phenol. This high value is dictated from the behaviour of the benzoquinone oxidation products, i.e. maleic acid, oxalic acid, and formic acid, as will be shown in the following paragraphs.

In the first place, maleic acid concentration, for the same phenol conversion, as illustrated in Fig. 4.15, shows strong dependence on both temperature and oxygen partial pressure. It was found that the activation energy for its destruction was very low, (27 kJ/mol), explaining why only trace amounts of this compound were detected. Maleic acid concentration versus phenol conversion, significantly increases with increasing oxygen partial pressure. This is reflected in the obtained kinetic parameters in two different ways. In the first place, due to the oxygen order difference between reaction 3 and reaction 4 more benzoquinones react towards maleic acid at higher oxygen partial pressures, as can seen in Table 4.10, where the percentage of benzoquinone reacting towards maleic acid is presented. Furthermore, maleic acid degradation was found to have a 0.5 oxygen order, i.e. its degradation rate increases less than its formation rate with increasing oxygen concentration. This oxygen order is not in agreement with Rivas et al. [62] who found zero-order dependence on oxygen, both for non-catalytic and catalytic maleic acid oxidation. Furthermore, for the non-catalytic case they state that oxidation reaction become significant only above 170^oC, which is higher than the highest temperature in this study. Shende and Levec [127] report a very low oxygen order for the non-catalytic WAO of maleic acid. Thus, it is likely that the observed 0.5 order dependence corresponds to a limiting oxidation step in the sequence, rather than to the decarboxylation of maleic acid to acrylic acid.

Table 4.10: Percentage (%) of benzoquinones reacting towards maleic acid

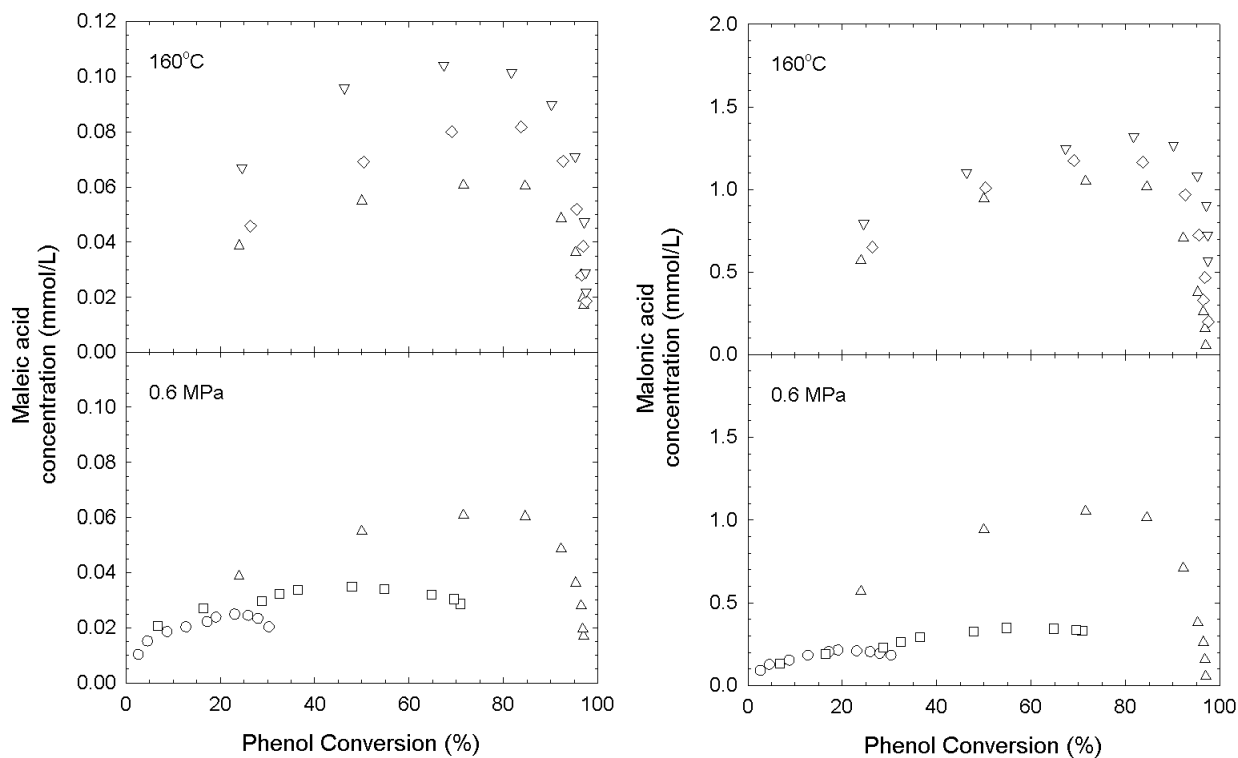| Pressure	Temperature		
(MPa)	120^oC	140^oC	160^oC
0.6	54	58	62
0.9	57	61	65
1.2	58	63	66

Figure 4.15: Concentration of maleic and malonic acid over the Cu0803 catalyst as a function of phenol conversion. ($\circ$) $120^{o}C$ and 0.6 MPa, ($\square$)$140^{o}C$ and 0.6 MPa, ($\triangle$) $160^{o}C$ and 0.6 MPa, ($\diamond$) $160^{o}C$ and 0.9 MPa, (∇) $160^{o}C$ and 1.2 MPa

In the Devlin and Harris reaction scheme maleic acid can be decomposed to form acrylic acid and glyoxalic acid or oxalic acid. Here, only the pathway giving first acrylic acid and, after a large sequence of reactions, leading to malonic acid was taken into account. Malonic acid exhibits a zero-order dependence on oxygen. This was expected as this step is a simple decarboxylation [119]. In Fig. 4.15, it can be appreciated that the influence of of oxygen partial pressure on malonic acid concentration is not as pronounced as to that of maleic acid. The higher malonic acid quantities obtained at higher pressures should be due to the enhancement of this route at higher pressures. The activation energy for this reaction was found to be 52.3 kJ/mol, higher than that for maleic acid. This value is comparable with those reported by Mishra et al. [11] for carboxylic acids.

Oxalic acid destruction was found to have high activation energy (91.1 kJ/mol), which also falls within the reported values for carboxylic acids. Oxalic acid degradation is the only reaction included in the network found to have an activation energy higher to that of phenol. This fact is reflected on the inverse trend exhibited by the initial oxalic

acid profiles with phenol conversion (Fig. 4.16. For low phenol conversions higher oxalic acid concentrations are reported at lower temperatures, leading to the higher activation energy encountered. Nevertheless, this tendency seems to be inverted at higher phenol conversions and the experimental concentrations for lower temperatures show the tendency to become higher with increasing temperature. This could be explained by means of a radical reaction that prevails at higher phenol conversions, although a model including two parallel oxalic acid degradation reactions, oxidation and decarboxylation, was tested without any significant improvement of the obtained profiles and prevailing the oxidation pathway.

This step showed high dependency on oxygen, giving a 0.80 order, indicating that oxalic acid oxidation prevails to decarboxylation. This high value should be expected, since at higher oxygen partial pressures, lower oxalic acid concentrations are obtained. Shende and Mahajani [130], using a homogeneous solution of $CuSO_4$ as catalyst, also report dependence on oxygen, although with a significantly lower exponent, 0.321. The calculated order indicates that oxalic acid is directly oxidised to give carbon dioxide, rather than undergoing a decarboxylation to yield formic acid. This seems reasonable as Shende and Levec [129] state that decarboxylation is a very temperature sensitive reaction, reporting that decarboxylation of oxalic acid only becomes significant at temperatures above 180^oC.

Formic acid was considered to be directly oxidised towards carbon dioxide. The activation energy estimated in this study was 69.7 kJ/mol. This values is slightly lower to that of phenol, thus the temperature dependence of formic acid concentration on phenol conversion is minor (see Fig. 4.16). This activation energy is also lower than that given for oxalic acid, being in contrast with the refractoriness noted by Shende and Levec [129] for non-catalytic WAO, although at temperatures and pressures higher than those studied here. Oxygen was found to have an order of 0.23 in the rate equation, which is lower compared to that of phenol. Thus, even though proportionally less benzoquinones react towards formic acid at lower oxygen partial pressures, still, the formation of formic acid is favoured at high oxygen partial pressures. The 0.23 order found is in disagreement with the first order dependence observed by Baldi et al. [98] and Shende and Mahajani [131]. Different experimental conditions may ex'plain these results, since Baldi et al. [98] conducted the reaction on a similar catalyst (CuO-ZnO), but at significantly higher temperatures (200-240^oC), while the Shende and Mahajani [131] authors not only carried out the reaction at higher temperatures (150-240^oC), but also using a homogeneous $CuSO_4$ catalyst.

Acetic acid is considered as the most refractory of the carboxylic acids [11]. Thus, it was assumed that acetic acid does not undergo any destruction reaction. The excellent agreement between predicted and experimental concentration profiles supports this assumption. This is further confirmed by Fig. 4.17, where it is illustrated that practically acetic acid concentration depends only on phenol conversion. This further evidents that the reactions leading to its formation are very fast compared to the phenol oxidation. The apparent lack of dependence of acetic acid concentration on the temperature or the oxygen partial pressure, is not in disagreement with the previous statements that more
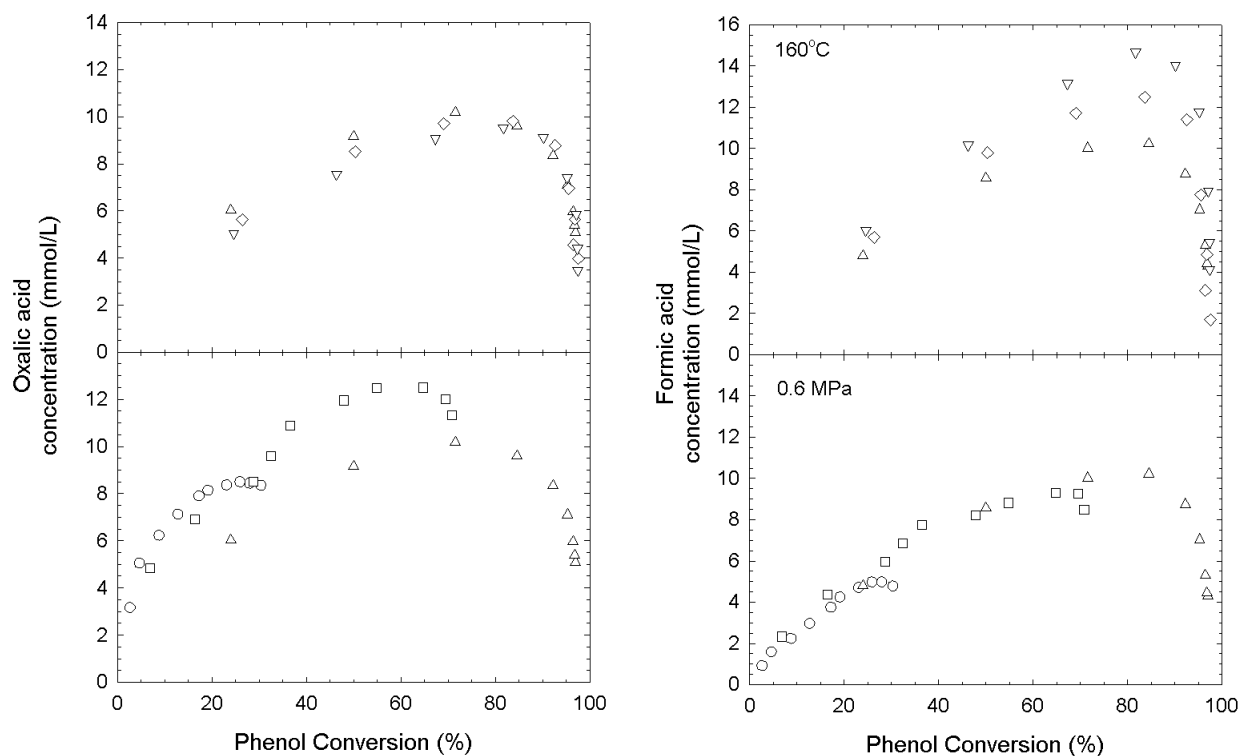
Figure 4.16: Concentration of oxalic and formic acid over the Cu0803 catalyst as a function of phenol conversion. (○) 120°C and 0.6 MPa, (□)140°C and 0.6 MPa, (△) 160°C and 0.6 MPa, (◇) 160°C and 0.9 MPa, (∇) 160°C and 1.2 MPa
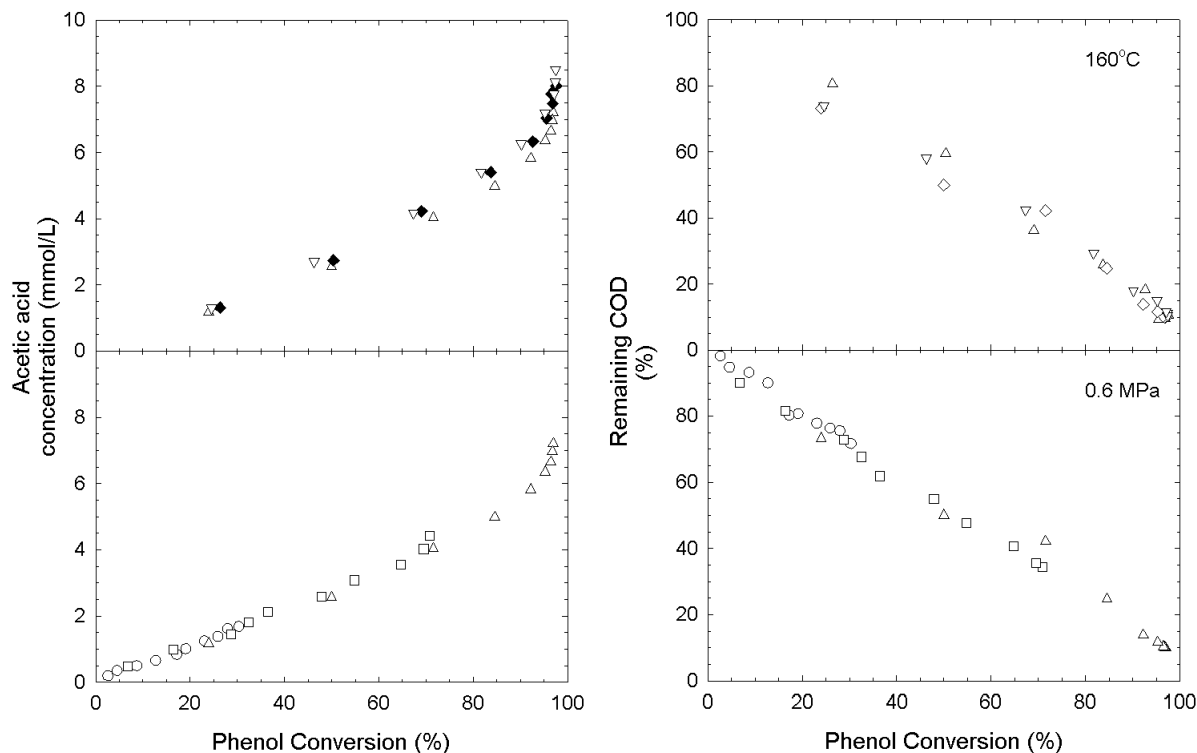
Figure 4.17: Concentration of COD and acetic acid over the Cu0803 catalyst as a function of phenol conversion. (○) 120°C and 0.6 MPa, (□)140°C and 0.6 MPa, (△) 160°C and 0.6 MPa, (◇) 160°C and 0.9 MPa, (▽) 160°C and 1.2 MPa

benzoquinone reacts towards maleic and eventually acetic acid, because the overall deviation shown in Table 4.10 is within the experimental errors for acetic acid concentration. The same observations also hold for the COD profiles, reported in Fig. 4.17.

The corresponding set of optimised adsorption parameters is given in Table 4.9. No values in the literature being available any attempt of comparison is meaningless. However, the following conclusions can be drawn. 1) All ΔH are negative and of the same order of magnitude. 2) Preliminary adsorption experiments have shown that adsorption takes place for carboxylic acids as well as for quinone like compounds, so the results have physical meaning. 3) The statistical confidence is higher to the calculated for the kinetic parameters, thus these parameters are less influent in the fitting than the kinetic parameters.

4.3.4   Conclusions

A detailed reaction network has been proposed and validated for the Catalytic Wet Air Oxidation of phenol over a $CuO/\gamma - Al_2O_3$ catalyst carried out in a Trickle Bed Reactor. The parameters of the kinetic model, 38 in number, involved in the rate equations were obtained by non-linear multiparameter fitting using both S-A and L-M algorithms. The model is capable of matching well experimental concentration profiles not only for phenol, but also for the rest of the detected partial oxidation compounds. The obtained parameters were found to be in reasonable agreement with those reported in the literature and additionally, to match the selectivity features encountered. Overall consistence of the selected network was demonstrated by the excellent prediction of experimental COD data that were not used in the fitting procedure. Thus, a clear progress in kinetic modelling of CWAO was achieved, as modelling is done currently in terms of lumped pseudo compounds.

In particular, the use of L-H expressions had a positive effect on the quality of the fitting, since adsorption phenomena cannot be neglected in the solid catalysed reaction system. The influence of adsorption in the temperature range studied is less pronounced than the effect if temperature on reaction kinetics. This in combination with the lack of any data of adsorption kinetics of the involved intermediates, made it difficult to discuss the physical meaning of the outcoming adsorption parameters. There is a clear need for more detailed experimental studies of CWAO that include quantitative description of the adsorption phenomena involved in the process.

4.4   Kinetics over Activated Carbon

One of the main objectives of the study of the CWAO of phenol over the Cu0803 catalyst was to test and compare the performance of the S-A algorithm against the conventional L-M algorithm in the multiparameter optimisation of complex reaction networks. In this part, we are aiming to assess a reliable kinetic model of the CWAO of phenol over AC, being a stable, active and inexpensive catalytic matter at the same time. We expect the CWAO of phenol over AC to follow more complex mechanism than over the Cu0803 catalyst, because of the formation of an active coke layer, which may lead to the formation of intermediates that were not reported in previous studies.

4.4.1   Phenol degradation kinetics

The preliminary kinetic analysis of the CWAO of phenol over the AC catalyst, presented in Chapter 3 showed that phenol degradation can be described well by simple power law expressions (see Fig. 3.4):

$$r_{phen} = k_0 \, exp(-E_a/RT) \, x_{O_2}^{\alpha} \, C_{phen} \qquad (4.28)$$

As phenol adsorption on the AC surface definetely takes place [18], the application of L-H was also tested. The equation used considers only phenol adsorption on a single catalyst site:

$$r_{phen} = k_0 \, exp(-E_a/RT) \frac{K_{0phen} \, C_{phen} \, x_{O_2}^{\alpha} exp(-\Delta H_{phen}/RT)}{1 + K_{0phen}C_j exp(-\Delta H_{phen}/RT)} \qquad (4.29)$$

Nevertheless, as the P-L fit was already in good agreement with experimental observation, L-H kinetics neither improved, nor deteriorated, phenol concentration profiles. This can be seen in Fig. 4.18, where both L-H and P-L profiles are plotted. The estimated kinetic parameters are presented in Table 4.11.

Table 4.11: Kinetic and adsorption Parameters for Phenol degradation kinetics over active carbon using L-H kinetics

	k_0 (*)	E_a (kJ/mol)	α (-)	K_0 (L/mol)	ΔH (kJ/mol)
P-L	$10^{13.6\pm0.1}$	70.3 ± 0.4	0.95 ± 0.02		
L-H	$10^{13.7\pm0.1}$	75.1 ± 0.4	0.98 ± 0.02	$10^{-0.2\pm0.3}$	-7.4 ± 0.7

* The frequency factor is in $(L/kg_{cat} \, h)$ for power law kinetics and in $(mol/kg_{cat} \, h)$ for L-H.

It is interesting to note that for L-H kinetics the lumped frequency factor $(K_0 \cdot k_0)$, and the lumped activation energy $(\Delta H + E_a)$ are in very close agreement with the respective parameters obtained with P-L kinetics. Then, taking into account that the term $1 +$

$K_0\, exp(-\Delta H/RT)\, C_{phen}$ of the denominator of the L-H expression takes only values between 1 and 1.35, i.e. not significantly influent, it can be concluded that the solution obtained with the L-H kinetic expressions is practically the same with the obtained with simple power law kinetics. It is likely that the phenol concentrations studied are within a range in which adsorption effects cannot be quantified and simple power law kinetics can approximate with the same accuracy the more general L-H expressions. Assuming single site phenol adsorption, deviations from the P-L kinetics should be expected at higher phenol concentrations.
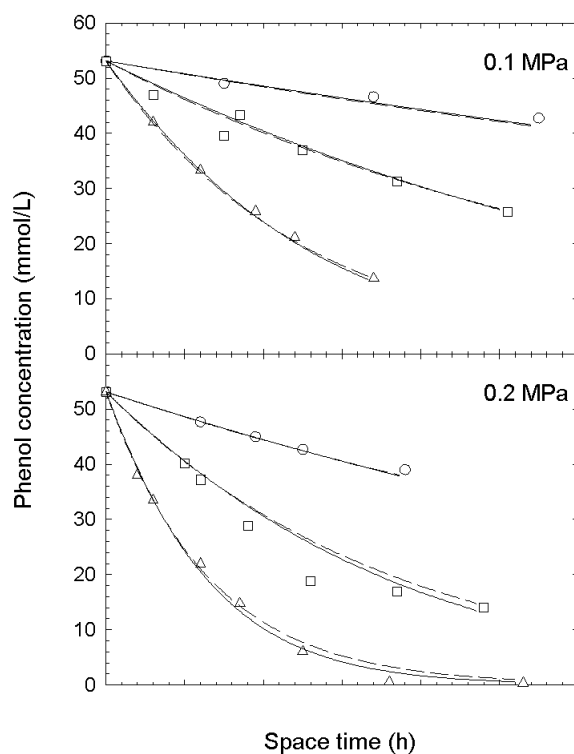

Figure 4.18: Concentration profiles for phenol over the AC catalyst for different oxygen partial pressures and temperatures using P-L (- -) and L-H (—) kinetics. Points experimental data: (○): $120^o C$, (□): $140^o C$, △: $160^o C$.

4.4.2   Ring compound reaction network

A detailed analysis of the experimental data for the AC, suggested that phenol undergoes two parallel reactions to form either 4-Hydroxybenzoic acid (4HBA), or benzoquinone. This assumption is now investigated in terms of kinetic modelling. The parallel phenol degradation (scheme 3) towards benzoquinone and 4-HBA was compared to two consecutive schemes shown in Fig. 4.19
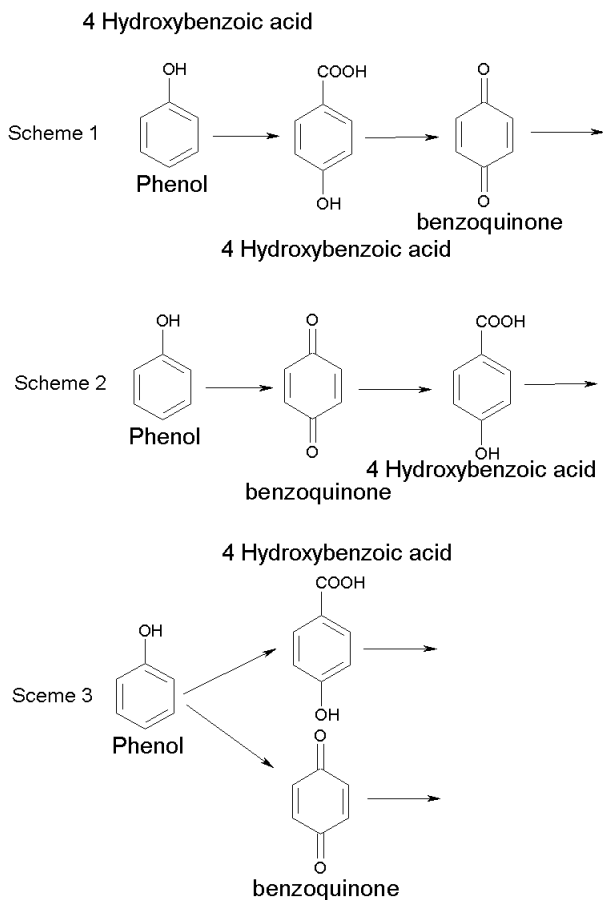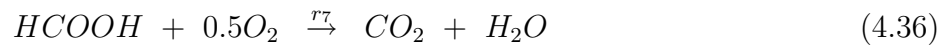

Figure 4.19: Proposed ring compound reaction schemes for the CWAO of phenol over AC.

The Sum of Absolute Errors for each scheme was 40, 67 and 29 for schemes 1, 2 and 3 respectively, indicating that the parallel scheme outperforms the sequential ones. For these calculations P-L expressions were used for phenol, and L-H for benzoquinone and 4-HBA. The application of P-L kinetics for all three compounds did not performed well, as a significant deterioration of the calculated profiles of the intermediate compounds was observed.

4.4.3 Overall Reaction Network

According to the hierarchical approach, several pathways were tested for the CWAO of phenol over AC. In agreement with the observations on the aromatic ring compounds in all models the parallel phenol oxidation scheme was postulated. The first scheme (model AC-1) was build up following the reaction network obtained for the Cu0803 catalyst, and consequently is based on the Devlin and Harris mechanism. Benzoquinone was modelled such as to form both maleic acid and formic acid. For the Cu0803 catalyst in each of these two reactions one mole of oxalic acid is formed, while for the AC catalyst oxalic acid was only detected in trace concentrations and it was omitted in this network. It was observed that the model predictions improved when the formation of 4 moles of formic acid was postulated for each mole of benzoquinone destroyed. Formic acid was consequently considered to further oxidise towards carbon dioxide. Similarly to the Cu0803 reaction network, maleic acid was considered to react forming only refractory acetic acid, which accumulates in the system. 4-HBA was given the possibility to disassociate to forming benzoquinone as well as formic acid. The resulting reaction equations are listed below and the reaction scheme is reproduced in Fig. 4.20.

$$C_6H_5OH \ + \ CO_2 \ \overset{r_1}{\to} \ C_7H_6O_3 \tag{4.30}$$
$$C_6H_5OH \ + \ O_2 \ \overset{r_2}{\to} \ C_6H_4O_2 \ + \ H_2O \tag{4.31}$$
$$C_7H_6O_3 \ + \ 0.5O_2 \ \overset{r_3}{\to} \ C_6H_4O_2 \ + \ HCOOH \tag{4.32}$$
$$C_6H_4O_2 \ + \ 3O_2 \ \overset{r_4}{\to} \ C_4H_4O_4 \ + \ 2CO_2 \tag{4.33}$$
$$C_6H_4O_2 \ + \ 4O_2 \ \overset{r_5}{\to} \ 4HCOOH \ + \ 2CO_2 \tag{4.34}$$
$$C_4H_4O_4 \ + \ O_2 \ \overset{r_6}{\to} \ C_2H_4O_2 \ + \ 2CO_2 \tag{4.35}$$
$$HCOOH \ + \ 0.5O_2 \ \overset{r_7}{\to} \ CO_2 \ + \ H_2O \tag{4.36}$$
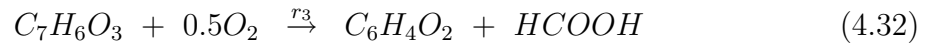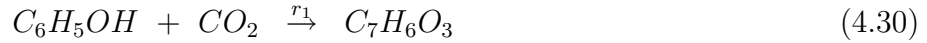
In agreement with the previous observations for the phenol destruction (Reactions 1 & 2) simple P-L expressions were postulated:

$$r_{phen} \ = \ k_{0i} \, exp(-E_{ai}/RT) \, x_{O_2}^{\alpha} \, C_{phen} \tag{4.37}$$

For the degradation reactions of the intermediates (Reactions 3-7), competitive adsorption on the same active site was considered:

$$r_i = k_{0i} \, exp(-E_{ai}/RT) \frac{K_{0i} \, C_i \, x_{O_2}^{\alpha} exp(-\Delta H_i/RT)}{1 + \sum K_0 C_j exp(-\Delta H_j/RT)} \tag{4.38}$$

For this scheme the net destruction or production rates R_j of the involved compounds are given by the following equations:

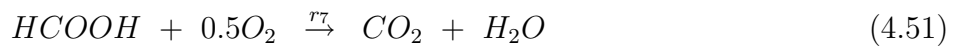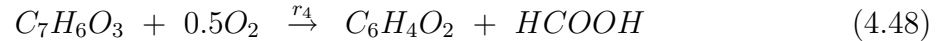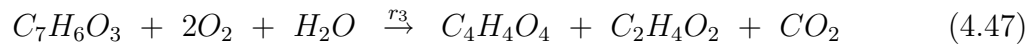$$R_{phen} \ = \ -r_1 - r_2 \tag{4.39}$$
$$R_{4-HBA} \ = \ r_1 - r_3 \tag{4.40}$$

$$R_{benz.} = r_2 + r_3 - r_5 - r_4 \tag{4.41}$$

$$R_{maleic} = r_4 - r_6 \tag{4.42}$$

$$R_{acetic} = r_6 \tag{4.43}$$

$$R_{formic} = r_3 + r_5 - r_7 \tag{4.44}$$

The second scheme (model AC-2) proposed was developed from the analysis of experimental concentration profiles as outlined in Chapter 3. It was observed that benzoquinone and formic acid exhibit a maximum concentration at space times 2 or 3 times lower than 4-HBA and maleic acid. This suggests two different schemes, one going from benzoquinone directly to formic acid and eventually to carbon dioxide and water, and an other going from 4-HBA to maleic acid and finally to refractory acetic acid. This scheme is shown in Fig. 4.21 and the corresponding equations are listed below.

$$C_6H_5OH + CO_2 \xrightarrow{r_1} C_7H_6O_3 \tag{4.45}$$

$$C_6H_5OH + O_2 \xrightarrow{r_2} C_6H_4O_2 + H_2O \tag{4.46}$$

$$C_7H_6O_3 + 2O_2 + H_2O \xrightarrow{r_3} C_4H_4O_4 + C_2H_4O_2 + CO_2 \tag{4.47}$$

$$C_7H_6O_3 + 0.5O_2 \xrightarrow{r_4} C_6H_4O_2 + HCOOH \tag{4.48}$$

$$C_6H_4O_2 + 4O_2 \xrightarrow{r_5} 4HCOOH + 2CO_2 \tag{4.49}$$

$$C_4H_4O_4 + O_2 \xrightarrow{r_6} C_2H_4O_2 + 2CO_2 \tag{4.50}$$

$$HCOOH + 0.5O_2 \xrightarrow{r_7} CO_2 + H_2O \tag{4.51}$$

As for model AC-1, P-L expressions were postulated for reactions 1 & 2 and L-H for reactions 3-7. For this scheme the individual compound production or destruction rates R_j are given by the following relationships:

$$R_{phen} = -r_1 - r_2 \tag{4.52}$$

$$R_{4-HBA} = r_1 - r_3 - r_4 \tag{4.53}$$

$$R_{benz.} = r2_+r_4 - r_5 \tag{4.54}$$

$$R_{maleic} = r_3 - r_6 \tag{4.55}$$

$$R_{acetic} = r_3 + r_6 \tag{4.56}$$
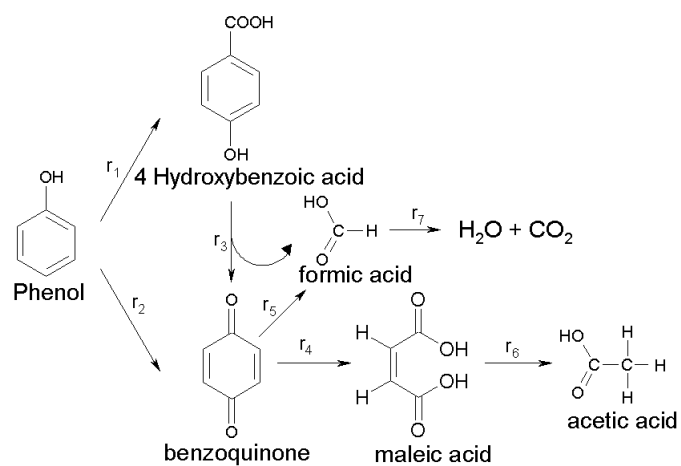
$$R_{formic} = r_4 + r_5 - r_7 \tag{4.57}$$

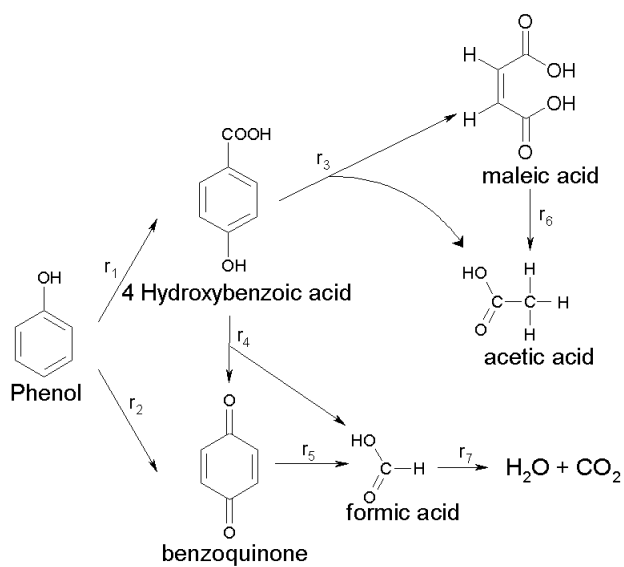**Figure 4.20:** Proposed model for the CWAO of phenol over active carbon (AC-1)

Figure 4.21: Proposed model for the CWAO of phenol over active carbon (AC-2)

Concentration profiles

Both models obtained fits that reasonable agree with the experimental results (see Table 4.12). Model AC-1 reached to a SAE of 96 while Model AC-2 achieved a 10% improved value of 88. This difference in the objective function minimum can also be appreciated on the average % error of the compounds shown in Table 4.12. For the phenol and COD profiles, shown in Fig. 4.22, the differences between model AC-1 and AC-2 is not appreciable and both models can be accepted. The model AC-2 achieves a better or equal fit for all intermediates.

Table 4.12: Average % errors of compounds for the AC catalyst using reaction networks AC-1 and AC-2

Compound	% Error AC-1	% Error AC-2
Phenol	4.2	4.4
4-HBA	12	16
Benzoquinones	45	37
Maleic acid	40	31
Acetic acid	25	16
Formic acid	20	18
COD	4.3	4.5
Total	9.7	8.5

For 4-HBA (Fig. 4.22) Model AC-1 approximated better the experimental points at 120^oC and 160^oC , although model AC-2 slightly subestimates the profiles at 160^oC and overestimates those at 120^oC. This can be attributed to the fact that in model AC-1 the degradation of 4-HBA practically has no influence on the benzoquinone and formic acid production, has less restrictions in adjusting its concentration. For benzoquinone (Fig. 4.22), both models overpredict 120^oC and 140^oC profiles, but agree well with those obtained at 160^oC. Especially at 0.2 MPa of oxygen partial pressure, model AC-1 overestimated benzoquinone profiles compared to the AC-2 model. As stated before, 4-HBA degradation has less influence in model AC-1, because all intermediates are formed mainly through benzoquinone oxidation, therefore large quantities of this compound appear in the model AC-1.

For maleic acid the model AC-2 matches satisfactory by experimental profiles except for 0.2 MPa and 160^oC, where higher experimental concentrations can be observed (See Fig. 4.23). Model AC-1 results in higher maleic acid formation - destruction rates and consequently the peaks appear earlier in the model than experimentally. Acetic acid (Fig. 4.23) is in close agreement with experiments for both model, although the model AC-1 gave less formation at 160^oC. The model prediction at 120^oC cannot be compared to the experimental data, because the peak of acetic acid in the chromatography is very weak, thus at 120^oC the concentrations were so low that it could not be detected. For formic acid (Fig. 4.23) both models show good fitting, although model AC-2 performed slightly better at 0.2 MPa.
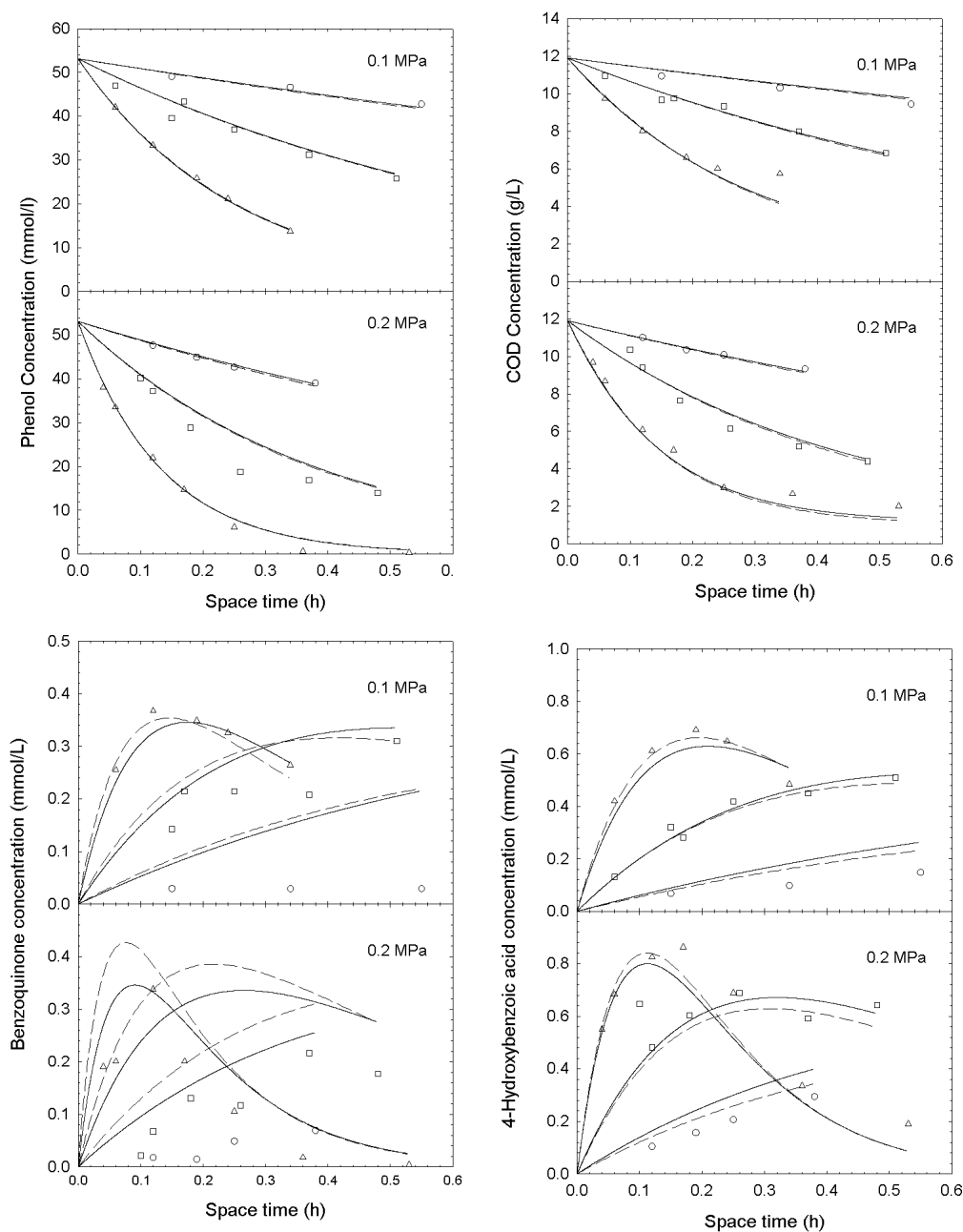
Figure 4.22: Phenol, COD, 4-HBA and benzoquinone concentration profiles over the AC catalyst at different temperatures and pressures for the activated carbon catalyst. Circles: 120^oC , Squares: 140^oC , Triangles: 160^oC . Lines indicate model predictions. Dash: 120^oC , Dash Dot: 140^oC , continuous: 160^oC
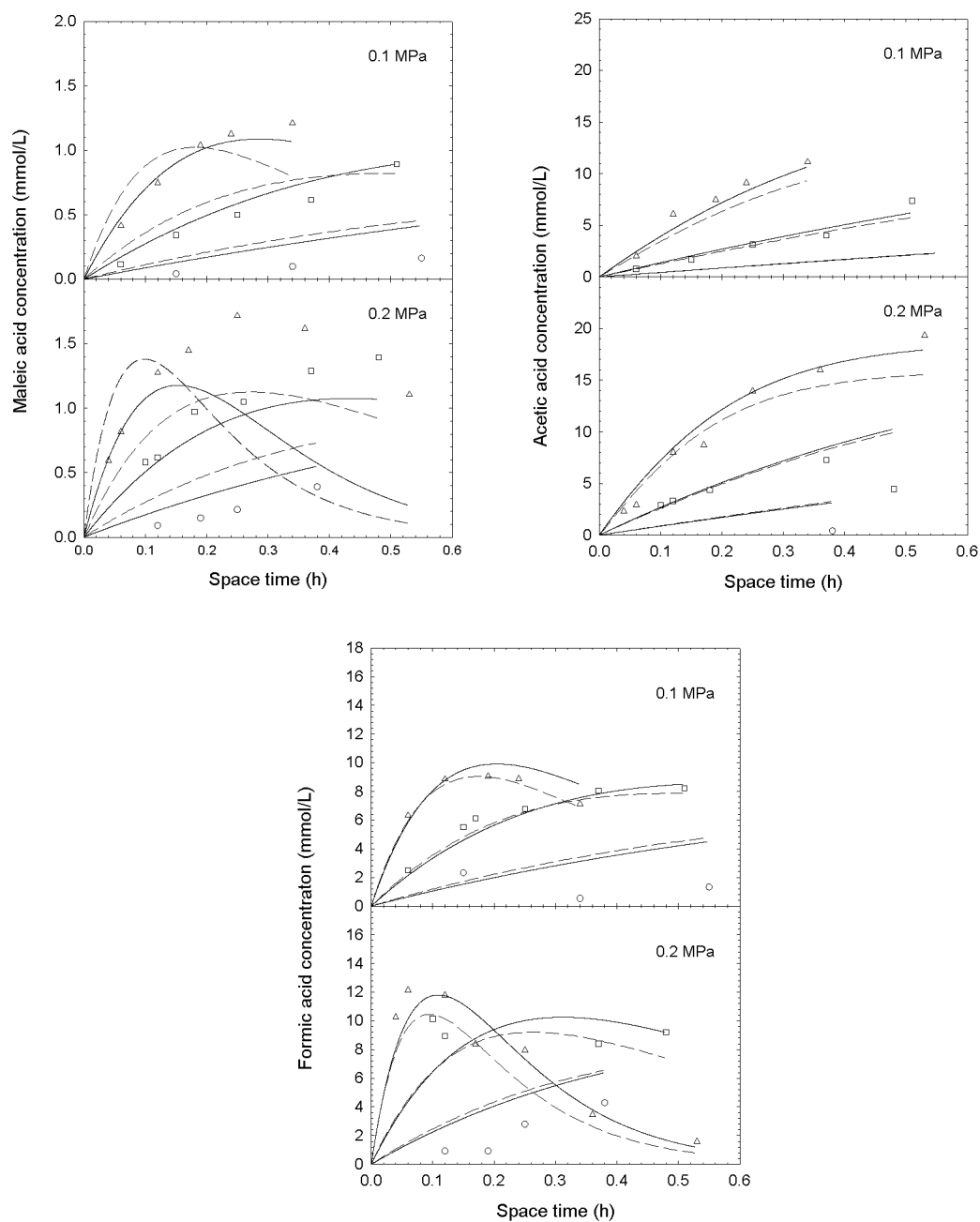
Figure 4.23: Maleic acid, acetic acid and formic acid concentration profiles at different temperatures and pressures for the activated carbon catalyst. Circles: 120^oC , Squares: 140^oC , Triangles: 160^oC . Lines (- -) AC-1, ($-$) AC-2

Kinetic parameters:

Optimised reaction and adsorption parameters for both models are presented in Tables 4.13 and 4.14. There are no specific data available in the literature for most of the reactions considered here, but in general the obtained constants agree reasonably well with typical values for similar reaction systems.

Table 4.13: Frequency Factors, Activation Energies and Heat of adsoption for the CWAO of Phenol over Activated Carbon

Reaction No	k_0 AC-1 (1)	k_0 AC-2 (1)	E_a AC-1 (kJ/mol)	E_a AC-2 (kJ/mol)	α AC-1 (-)	α AC-2 (-)
1	$10^{13.88\pm0.02}$	$10^{13.99\pm0.02}$	83.9 ± 0.6	75.9 ± 0.6	0.86 ± 0.02	1.05 ± 0.02
2	$10^{13.59\pm0.02}$	$10^{13.65\pm0.01}$	69.8 ± 0.6	71.9 ± 0.4	0.97 ± 0.02	0.93 ± 0.01
3	$10^{11.88\pm0.02}$	$10^{11.97\pm0.09}$	70.6 ± 0.6	69 ± 1	0.62 ± 0.02	0.79 ± 0.02
4	$10^{12.25\pm0.02}$	-	68.2 ± 0.6	-	1.02 ± 0.02	-
5	$10^{11.38\pm0.02}$	$10^{13.8\pm0.5}$	67.1 ± 0.6	70 ± 5	0.78 ± 0.02	1.0 ± 0.1
6	$10^{11.53\pm0.02}$	$10^{13.4\pm0.4}$	57.1 ± 0.6	69 ± 4	0.85 ± 0.02	1.0 ± 0.1
7	$10^{11.99\pm0.02}$	$10^{12.1\pm0.1}$	65.2 ± 0.6	67.7 ± 0.8	0.82 ± 0.02	0.77 ± 0.02

[1] The frequency factor has reaction dependent units. For reaction 1 is in $(L/kg_{cat}h)$, while for the rest of the reaction constants is in $(mol/kg_{cat}h)$.

Table 4.14: Adsorption parameters for the CWAO of phenol over Active carbon.

Compound	K_0 AC-1 (L/mol)	K_0 AC-2 (L/mol)	ΔH AC-1 (kJ/mol)	ΔH AC-2 (kJ/mol)
4-HBA	$10^{3.53\pm0.3}$	$10^{4.5\pm0.3}$	-9.6 ± 2	-4 ± 2
Benzoquinones	$10^{5.98\pm0.3}$	$10^{5.2\pm0.7}$	-5.1 ± 2	-1 ± 0.5
Maleic acid	$10^{4.59\pm0.3}$	$10^{4.3\pm0.4}$	-0.8 ± 2	-1 ± 1
Acetic acid	$10^{5.21\pm0.3}$	$10^{5.0\pm0.2}$	-5.2 ± 2	-4 ± 1
Formic acid	$10^{4.51\pm0.3}$	$10^{4.0\pm0.1}$	-45.6 ± 2	-6 ± 2

As done for the Cu0803 catalyst, the experimental intermediate selectivities can be used to verify at least the relation between the values of the obtained kinetic parameters. When plotting intermediate compound concentration against phenol conversion (Figs. 4.24 to 4.26) it can be observed that the temperature and pressure dependencies are not as pronounced as in the case of the Cu0803 catalyst. Thus, it should be expected that the calculated parameters are similar for all reaction. Indeed, it can be observed in Tables 4.13 and 4.14 that both models obtained similar constants, for the reactions in common, and the values do not present the same dispersion as in the case of Cu0803.

The reaction leading to the formation of 4-HBA from phenol has an activation energy of 83.9 kJ/mol for model AC-1 and 75.9 kJ/mol for model AC-2. For both models, this activation energy is higher than the corresponding to the activation energy of the reaction leading to benzoquinone (69.8 kJ/mol and 71.9 kJ/mol respectively). From
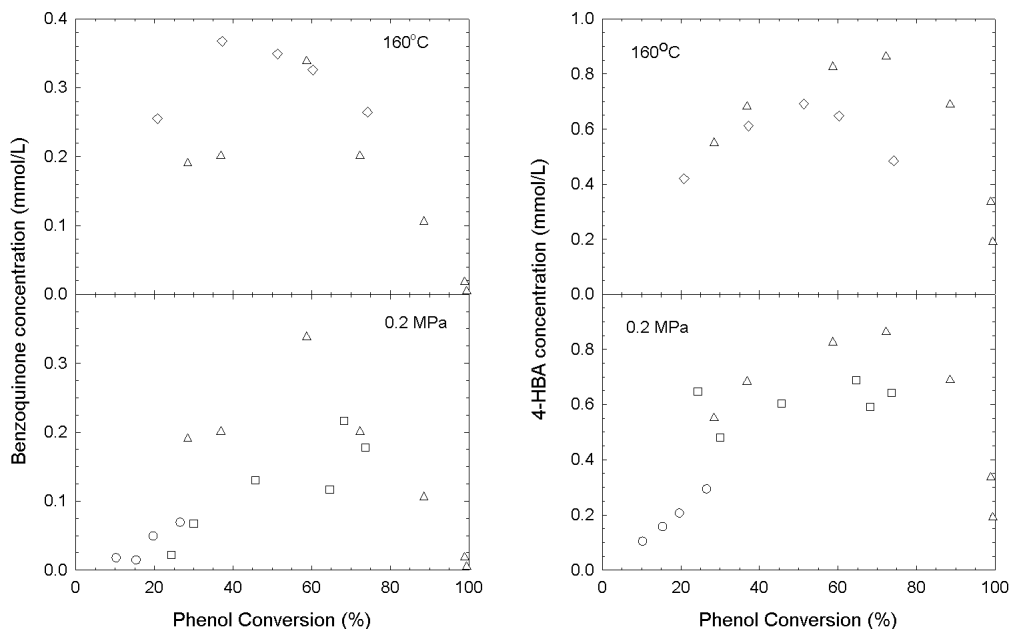
Figure 4.24: 4-HBA and Benzoquinone concentration as a function of Phenol conversion over AC. ($\circ$) 120^oC, (($\square$)) 140^oC, $\triangle$ 160^oC. Filled triangles 0.1 MPa and 160^oC

the obtained reaction parameters, it can be calculated that phenol is mainly destroyed towards benzoquinone, since for model AC-1 only 7-10% of the phenol reacts towards 4-HBA, while for model AC-2 this percentage is between 15-17%. For this reason the kinetic parameters of the reaction of phenol degradation to benzoquinone are very similar to those obtained when only phenol oxidation was examined.

Fig. 4.24 indicates that there is a positive effect of temperature on the obtained concentration of benzoquinone and 4-HBA. So the activation energies of the degradation reactions of these compounds should be lower than those of their formation from phenol. Indeed, both models give slightly lower values for the destruction reactions. In model AC-1 the decomposition of 4-HBA towards benzoquinone and formic acid only slightly influences the rest of profiles. The same reaction was found to be not influent at model AC-2. For this model the maleic and acetic acid profiles exclusively depend on the degradation rate of 4-HBA via reaction 3. The better profiles obtained by the model AC-2 may indicate that the proposed route is more realistic than the classical approach that considers the formation of these compounds mainly through the benzoquine root. Nevertheless, both models fail to predict the degradation rate of maleic acid at 160^oC . The rapid degradation at this temperature is imposed in the model by the high rate of formation of acetic acid. Probably at 160^oC , a different route leading to acetic acid, becomes significant.
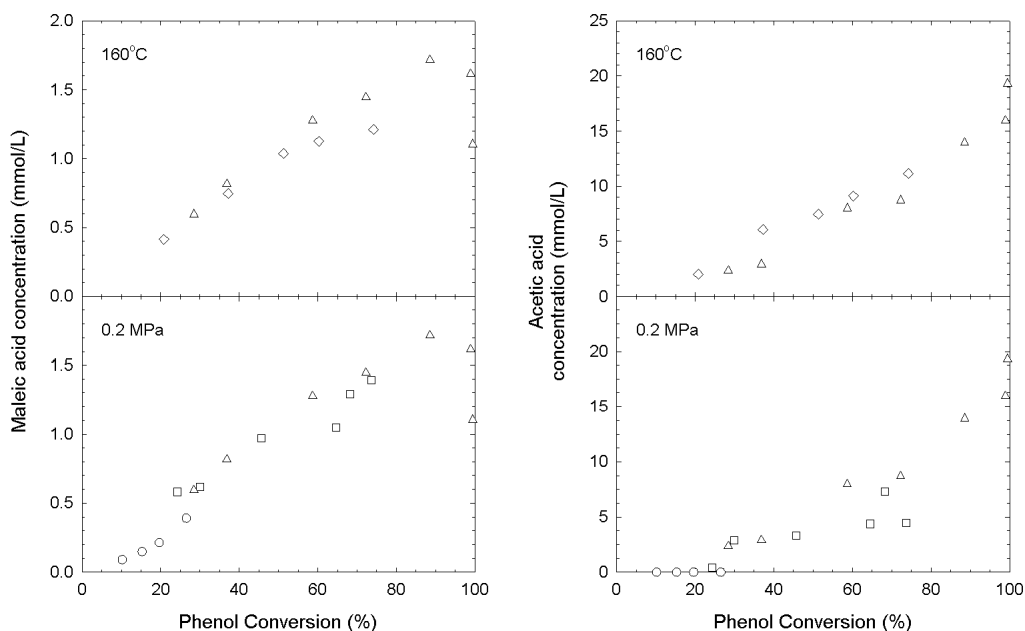
Figure 4.25: Maleic and Acetic acid concentration as a function of Phenol conversion over AC. (○) 120°C, ((□)) 140°C, △ 160°C. Filled triangles 0.1 MPa and 160°C

Maleic to acetic acid activation energy was different in both models, taking a value of 57.1 kJ/mol for model AC-1 and 69 kJ/mol for model AC-2. These values are much higher than that obtained for the Cu0803 catalyst, since this acid is present in higher quantities for the AC catalyst. The dependence of maleic acid concentration with phenol conversion, presented in Fig. 4.25, illustrates that the maleic acid degradation has the same pressure and temperature dependence as its formation. Model AC-1 yields similar oxygen orders for reactions 1 and 6, but significantly different activation energies (83.9 and 57.1 kJ/mol). On the other hand, model AC-2 gives better agreement for the respective activation energies (72 and 69 kJ/mol). Thus, the latter values should be more reliable. Acetic acid concentration for a given phenol conversion, also shown in Fig. 4.25, seems to be only slightly affected by oxygen partial pressure and temperature, indicating that, as also happened for the Cu0803 catalyst, the reactions leading to its formation are fast, compared to the degradation of phenol.

The obtained formic acid degradation reaction parameters are close for both models, the activation energy being 65.2 and 67.7 kJ/mol respectively, while the oxygen order was 0.82 and 0.77 respectively. The positive effect of both temperature and pressure on the formic acid concentration for a given phenol conversion, as can be observed in Fig. 4.26, justifies that both activation energy and oxygen order are lower than the corresponding values of reaction 2. Overall, COD concentration as a function of phenol conversion (Fig.
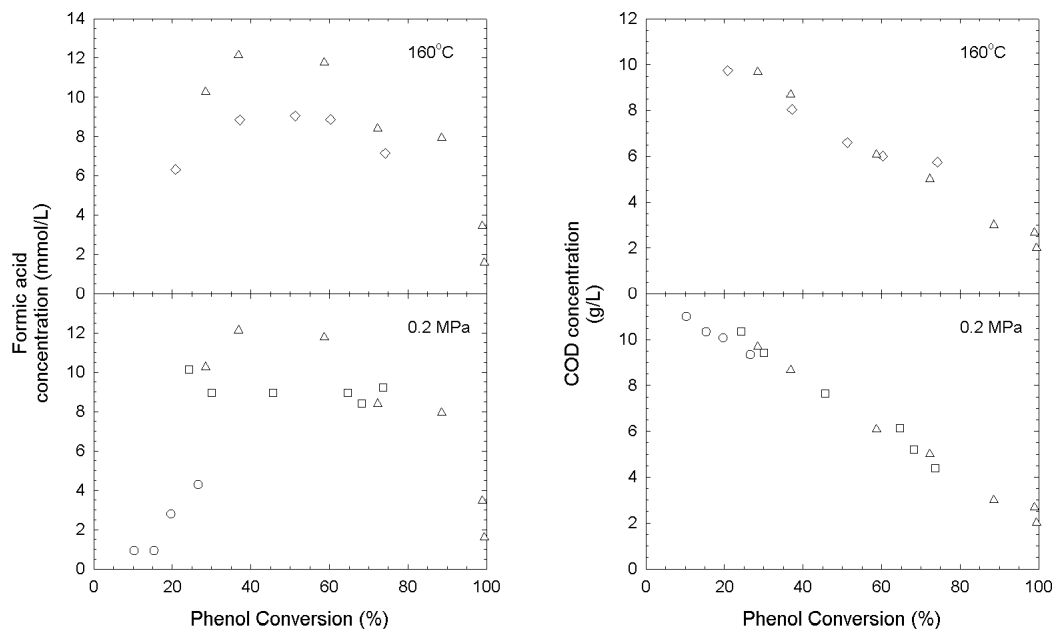
Figure 4.26: 4-HBA and Benzoquinone concentration as a function of Phenol conversion over AC. (○) 120^oC, (($\square$)) 140^oC, $\triangle$ 160^oC. Filled triangles 0.1 MPa and 160^oC

4.26) does not indicate a significant dependence of COD concentration on pressure or temperature, as residual phenol concentration masks the effect of intermediates.

A main difference between AC and Cu0803 is the fact that for the former catalyst most oxygen orders are close to unity, while for the latter most of them are found to be around 0.5. This indicates that there should be a difference in the reaction mechanism. An other interesting result is that the activation energies of aromatic compound degradation were found to have similar values to that of phenol destruction. In contrast, for the Cu0803 catalyst ring compound oxidation reactions exhibited lower values, resulting to a significant difference in ring compound concentration, for the same phenol conversion at different temperatures. On the other hand, for the AC catalyst it was observed that for ring compound concentration was not significantly affected by temperature, at the same phenol conversion.

4.4.4 Conclusions

The CWAO of phenol over AC was also shown to follow a complex parallel - consecutive reaction network. It has been suggested that phenol oxidation over AC proceeds via two parallel reactions. The first and dominating one leads to the formation of benzoquinone, in agreement with most schemes reported in the literature. The second one leads to the formation of 4-HBA and may be related to the active coke layer formed over the AC. The reaction mechanism leading to final products, i.e. water, carbon dioxide and acetic acid needs further investigation, but the results presented here indicate the existence of parallel roots one leading to maleic and ultimately acetic acid, and the other one leading to formic acid which is then mineralised to CO_2 and H_2O.

The complexity of the phenol CWAO over AC requires further in-depth study. Phenol oxidation kinetics using more concentrated feed solution should be assessed, to determine the validity range of the herein reported P-L kinetics, and to obtain more general L-H expressions. It is also important to identify the unknown phenol degradation intermediates to refine the kinetic model. Finally, a study of the AC surface prior to and after reaction, by means of common characterisation techniques, like BET area, TPR-TPO, FTIR, elemental analysis, etc., has to be done to elucidate the formation of the coke layer on the AC surface and its role in the mechanism of the CWAO of phenol.

Chapter 5

TBR Modelling and Scale up

Up to date, the reaction engineering aspects of the CWAO have received little attention, considering the scarce studies available in the open literature. Nevertheless, the successful scale up is one key element for the establishment of any emergent technology. Thus, we ultimately attempt to investigate the operation of a pilot plant reactor through numerical simulations using both the reactor kinetics and the comprehensive TBR, previously established. By doing this, we are aiming to give recommendations for a proper operation strategy of the pilot plant destinated to carry our the CWAO of phenol. Prior to the application of the TBR model for the scale up of the process, a sensitivity analysis is done and the model is subsequently validated against the experimental data obtained in the laboratory TBR. In the following, we then present and discuss simulation results for the pilot plant scale reactor using the kinetics obtained for the Cu0803 catalyst. Similar tendencies can also be observed for the AC catalyst.

5.1   Validation of the complex TBR Model

With respect to the ideal plug flow reactor model used for the kinetic processing of the laboratory TBR data, the comprehensive TBR model accounts for the consumption of oxygen in the gas phase, as well as external and internal mass transfer resistances of reactants and products. The effects of reactor hydrodynamics are also addressed, and special emphasis has been given to the contribution of the dry zones (catalyst wetting) in the oxygen mass transfer to the catalyst surface. The required mass transfer and hydrodynamic parameters for the complex TBR model are calculated from the correlations presented in Chapter 2.4. For the gas - liquid mass transfer the correlation of Iliuta et al. [185] was chosen, while for the liquid - solid mass transfer the correlations of Lakota and Levec [219] was selected. These correlations are based on high pressure data and should be more reliable for the typical operation conditions of CWAO.

5.1.1 Sensitivity analysis

As pointed out in the introduction, the mass transfer and hydrodynamic parameters, when calculated by available correlations, are subjected to some errors. This situation is clearly demonstrated in Fig. 1.13 for different parameters. To assess the influence of the involved parameters in the model prediction, an isothermal sensitivity analysis was performed using the TBR model prediction and operating conditions that maximise the phenol destruction reaction rate. The oxidation of phenol over the AC catalyst at 160^oC, 0.2 MPa and 0.05 h of space time was thus considered. The corresponding set of operating conditions, mass transfer and hydrodynamic parameters are presented in Table 5.1.

Table 5.1: Standard operating conditions, mass transfer and hydrodynamic parameters of the laboratory reactor used for the sensitivity analysis of the comprehensive TBR model.

Operating Conditions	
Temperature	160^oC
Oxygen partial pressure	0.2 MPa
Total pressure	16 MPa
Inlet phenol concentration	53.1 $mmol/L$
Space time	0.05 h
Liquid superficial velocity (u_{ls})	0.42 mm/s
Gas superficial velocity u_{gs}	3.7 mm/s
Reactor characteristics	
Reactor diameter	11 mm
Reactor height	0.2 m
Bed porosity	0.13
Packing specific surface area	1.1 10^4 m^2/m^3
Catalyst characteristics	
Catalyst	AC
Catalyst particle density ρ_p	400 g/L
Catalyst particle diameter	0.5 mm
Catalyst particle porosity	0.8
Tortuosity factor	3 (assumed)
Hydrodynamic parameters	
Axial dispersion coefficient	1.57 10^{-7} m^2/s
Wetting efficiency	0.35
Dynamic liquid hold up	0.05
Static liquid hold up	0.05
Mass transfer parameters	
Effective diffusion coefficients (O_2/Phen.)	4.32 10^{-9}/ 1.8 10^{-9} m^2/s
Dynamic liquid - solid mass transfer coefficients (O_2/Phen.)	4.33 10^{-4} / 2.70 10^{-4} m/s
Static liquid - solid mass transfer coefficients (O_2/Phen.)	3.26 10^{-6} / 2.00 10^{-6} m/s
Static- dynamic liquid volumetric mass transfer coefficient	0.01 s^{-1}
Gas - solid mass transfer coefficient	1.0 10^{-3} m/s
Gas - liquid volumetric mass transfer coefficient	1.0 s^{-1}

When the parameter values presented in Table 5.1 are fed to the TBR model, a reference phenol conversion of 28.5% is calculated, as shown in Table 5.2. In the first place it can be said that the model predictions are insensitive to variations of the hydrodynamic parameters. In particular, the phenol conversion was practically the same as the reference conversion when the axial dispersion coefficient was varied in the range of 1.57 10^{-8} to 1.57 10^{-6}, the wetting efficiency in the rangeof 0.2 to 0.9, the liquid holdup in the range of 0.05-0.1, with different proportions between the dynamic and the static holdup. Secondly, if very high external and internal mass transfer coefficients are postulated (two orders of magnitude higher than in Table 5.1) the phenol conversion tends to a value of 28.8%, which is also close to the reference conversion of 28.5%, indicating that the mass transfer is sufficiently high. The simple kinetic model for the same case predicted 30% phenol conversion, and the slight deviation is mainly attributed to the fact that the kinetic model does not account for the oxygen consumption. Note however, that the sensitivity analysis is performed for the conditions in which oxygen consumption is maximum.

Since there exists the possibility that external and internal mass transfer coefficients are overestimated by the correlations, simulations were carried out with 10 times smaller values. The decrease of phenol mass transfer coefficients did not alter the reference phenol conversion, as phenol is the excess reactant. For oxygen and partial catalyst wetting , only the increase of the effective diffusion coefficients led to significantly lower conversions of 17.0%, whereas the reduction of the gas to solid mass transfer only coefficient slightly affected the phenol conversion, yielding 28.1%, as shown in Table 5.2. The variation of the rest of parameters did not change the calculated phenol conversion.

Table 5.2: Sensitivity analysis of the TBR model, assuming oxygen as limiting reactant, for the AC catalyst at 160^oC and $0.2MPa$, at a space time of 0.05 h.

Parameter varied	Phenol Conversion (%) ($f = 0.35$)	Phenol Conversion (%) ($f = 1$)
none (Table 5.1)	28.5	25.3
$D^{eff}/10$	17.0	15.7
$k_{ls}^d/10$	28.5	20.8
$k_{ls}^s/10$	28.5	20.8
$(ka)_{gl}/10$	28.5	13.5
$(ka)_{ll}/10$	28.5	25.3
$k_{gs}/10$	28.1	-

It can be assumed that the gas-liquid, liquid-solid and liquid-liquid mass transfer coefficients are not influent at partial catalyst wetting conditions, because of the high rates of gas-solid mass transfer, which provides sufficient quantities of oxygen on the catalyst surface, despite the low value of the rest of external mass transfer coefficients. To study the effect of catalyst wetting, calculations were carried out assuming complete catalyst wetting, the rest of parameters being the same. The assumption of complete wetting resulted in a lower phenol conversion of 25.3%, as also shown in Table 5.2. In

this case, however, predictions with decreased mass transfer parameter values lead now to significantly lower conversions, indicating that external mass transfer coefficients become influent. These results clearly highlight the need to account for the effect of the direct gas-solid transport across the dry catalyst surface, caused by partial wetting. As a matter of fact, the correlations for the calculation of catalyst wetting show significant variation giving values in the range of 0.25 to 0.8. However, this inconvenience is not critical in the model prediction, as in our system, partial wetting effects become already maximum for a f below 0.95, and thus phenol conversion does not depend on the catalyst wetting for smaller f values.

5.1.2 TBR Model validation

The close agreement between the complex TBR model, the pure kinetic model, assuming ideal plug flow and the experimental data, obtained in the laboratory reactor, was verified over a wide range of operating conditions. The experimental intrinsic conditions of the TBR runs are set to provide intrinsic kinetic control, thus the complex TBR model and the kinetic model should give the same predictions. This situation is illustrated in Fig. 5.1, where the phenol concentration profiles calculated with the TBR model are exemplarily presented for a) the Cu0803 catalyst at 0.6 MPa and b) the AC catalyst at 0.2 MPa. The quality of the transport-reaction TBR model prediction, reinforces both the assumption of no mass transfer limitations in the laboratory reactor and the confidence in the TBR model.
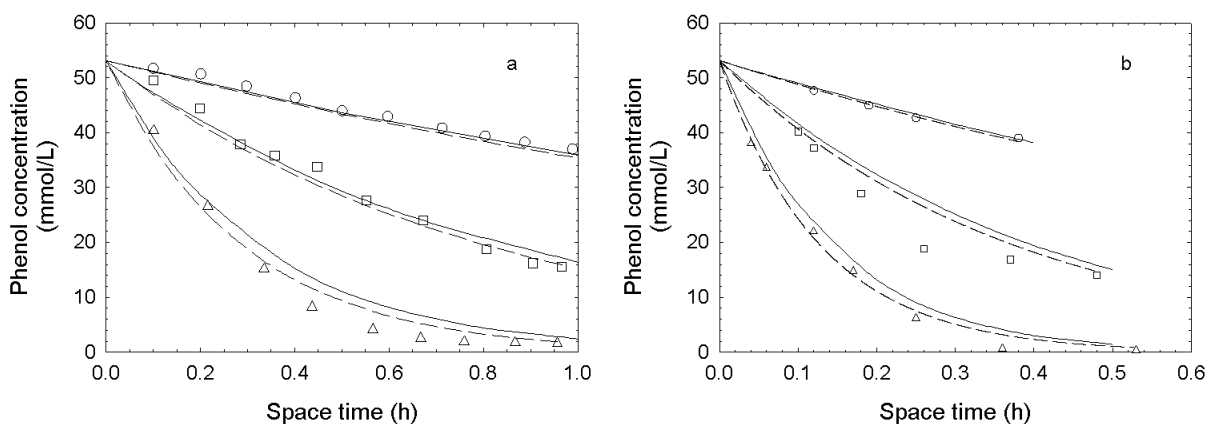

Figure 5.1: Comparison of kinetic (- -) and TBR (−) models for the a) Cu0803 catalyst at 0.6 MPa and b) AC catalyst at 0.1 MPa. Points indicate experimental data: (○): 120^oC , (□): 140^oC , (△): 160^oC .

5.1.3 Conclusions

It was shown that the comprehensive transport - reaction TBR model is capable to match experimental results obtained in the laboratory reactor, indicating that the latter operates in the kinetic controlled regime. A sensitivity analysis demonstrated that the most influent parameters, at typical CWAO conditions and oxygen being the limiting reactant, are the internal diffusion coefficients and the gas-solid mass transfer coefficient. In the case of complete wetting, i.e. for high liquid flow rates, the values of the gas-liquid and liquid solid mass transfer coefficients can also become influent. The entire results show that the comprehensive TBR model can be used with confidence for the scale-up of the CWAO of phenol. However, one has to be aware that the overall quality of the prediction will mainly depend on the accuracy of the key parameters ($f, D^{eff}, k_{gs}, (ka)_{gl}, (k_{ls}a_s)$), as highlighted in the sensitivity study.

5.2 Model Aided TBR scale up

In the following scale up the laboratory TBR for the CWAO of phenol is simulated and discussed, in terms of isothermal operation, to evaluate mass transfer effects, and subsequently of adiabatic operation to account for heat release by the oxidation reaction. The scale up factor was about 40 for the catalyst weight, as well as for the gas and liquid flow rates.

Table 5.3: Standard operating conditions for the pilot plant simulations

Temperature	160^oC
Oxygen Partial Pressure	$0.6\ MPa$
Total Pressure $(P_{O_2} + P_{H_2O})$	$1.2\ MPa$
Phenol concentration	$53\ mmol/L\ (5\ g/L)$
Liquid superficial Velocity	$1\ mm/s$
Gas superficial velocity	$8\ mm/s$
Reactor diameter	$25\ mm$
Reactor Height	$1.5\ m$
Density of catalyst particle	$1030\ g/L$
Bed porosity	0.36
Particle diameter	$3\ mm$

5.2.1 Isothermal operation

The effect of mass transfer and hydrodynamic parameters on phenol conversion was assessed using, for simplicity, the isothermal model.

Catalyst Wetting

As mentioned earlier, catalyst wetting was found to significantly affect reactor performance. To give better insight to this issue, the dependence of γ on phenol concentration for commonly used CWAO oxygen partial pressures and temperatures is presented in Fig. 5.2. It can be seen that γ sweeps out the interval [0.1, 10] indicating that both cases are likely to occur in CWAO within narrow oxygen and phenol concentration windows. The γ values resulting from the operating conditions for the studies of Tukac et al. [195] (empty circle) and Iliuta and Larachi [198] (filled circle) are located in Fig. 5.2. Each of these studies falls in a different γ region, therefore it is not surprising that Tukac et al. concluded that downflow operation is advantageous, while Iliuta and Larachi that upflow is advantageous.
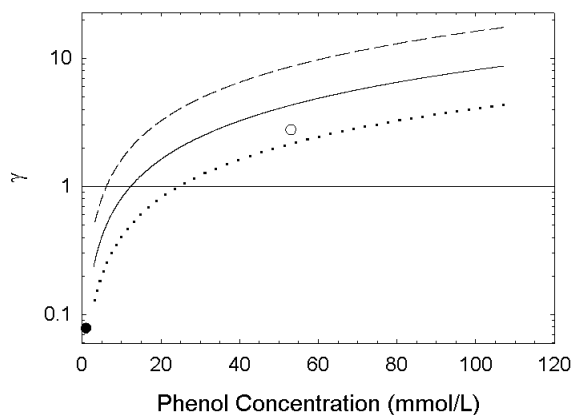

Figure 5.2: γ - ratio variation as a function of phenol concentration for different oxygen partial pressures at $160^o C$. (- -) 0.3 MPa, (−) 0.6 MPa, ($\cdots$) 1.2 MPa. (•) Iluta and Larachi [198], (○) Tukac et al. [195].

In agreement with Fig. 5.2, it would be expected that for 53 $mmol/L$ of phenol, incomplete wetting is to be preferred versus complete wetting as reactant depletion concerns oxygen instead. In Fig. 5.3, phenol conversion bed depth profiles are plotted for three different liquid superficial velocities, assuming full and partial catalyst wetting. For the high and intermediate liquid superficial velocity, partial wetting appears to have a positive effect on phenol conversion. At high superficial liquid velocities (i.e., low conversions), complete wetting would bring about 50% reduction on phenol conversion. For the intermediate liquid velocity, the corresponding conversion decrease would be only 15%. Finally, for the lowest liquid velocity, conversion drop off from partial to full wetting is marginal. Such findings are coherent with the fact that lower pollutant conversion (or higher liquid velocity) leaves higher residual phenol concentration propitious to a higher reaction rate and a deeper consumption of dissolved oxygen. This state of affairs is illustrated under the same conditions in Fig. 5.3 where initial oxygen depletion in the dynamic liquid portion is typically more pronounced the higher the liquid velocity. On

the other hand, for partially wetted catalyst, oxygen concentration in the dynamic liquid remains high, because oxygen enters in the catalyst mainly through the gas-solid interface. It should be mentioned that the axial decrease of oxygen concentration in the gas phase is less than 5% as gaseous O_2 is in excess.
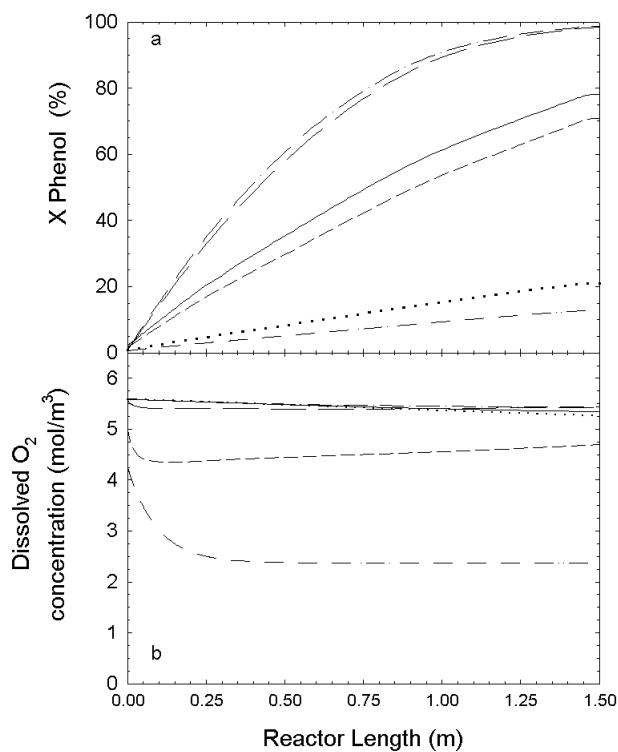

Figure 5.3: Effect of catalyst wetting on (a) phenol conversion, (b) dissolved oxygen concentration, along the reactor for different liquid superficial velocities. $(- \cdot -)$ u_l=0.1 mm/s f=0.8, $(- -)$ u_l=0.1 mm/s f=1, $(-)$ u_l=0.2 mm/s f=0.8, $(- -)$ u_l=0.2 mm/s f=1, $(\cdots)$ u_l=1 mm/s f=0.8, $(-\cdots-)$ u_l=1 mm/s f=1. Rest of operating conditions: Table 5.3

Fig. 5.4 presents the γ ratio bed depth-profile for the case of incomplete wetting. As expected, γ ratio stays almost constant for low conversions, whereas due to stream-wise phenol consumption, it drops off markedly the lower the liquid superficial velocity. For phenol conversions in excess of 90%, γ ratio peaks down to unity while advancing throughout the bed. This suggests that full wetting is the preferred mode due to phenol impoverishment. For such conversion levels to be achieved, the use of fines in the last stages of the reactor, or the use of two reactors, the second being operated up-flow constitute potentially viable strategies.
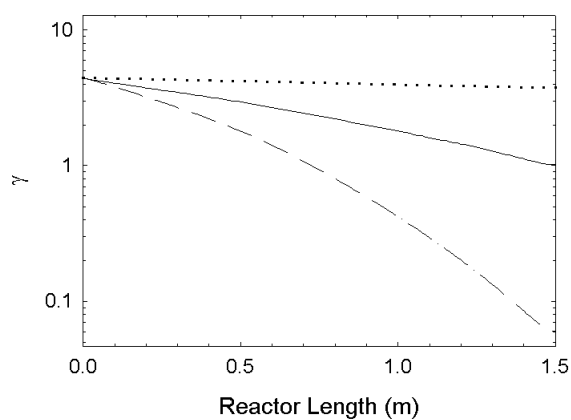

Figure 5.4: Variation of γ-ratio along the reactor for incomplete wetting. $(\cdots)$ u_l=1 mm/s, $(-)$ u_l=0.2 mm/s, $(-\cdot-)$ u_l=0.1mm/s. Rest of operating conditions: Table 5.3

Mass transfer

The importance of all mass transfer parameters was examined for both partial and complete wetting at high liquid superficial velocity to provide high reaction rates and thus, emphasise diffusion limitations, as can be seen in Rajashekharam et al. [178]. Within the range of standard conditions, it was noted from the simulations that only the effective diffusivity and the gas-liquid volumetric mass transfer coefficient influence significantly reactor performance. In the case of incomplete wetting, only a change in effective diffusivity affects the reactor outcome. Contrarily, for complete wetting both resistances are influential, although the gas-liquid mass transfer resistance provokes a decline in phenol conversion that is twice that observed for intraparticle diffusion.

The impact of particle size on reactor performance at high liquid superficial velocity was also evaluated. Phenol conversion (solid line) and pressure drop (dotted line) are plotted in Fig. 5.5 as a function of particle diameter and constant catalyst load. For particle diameter less than 0.5 mm, phenol conversion tends to level off. Considering the sky-high power consumption penalty associated with finer catalyst sizes, 0.5 mm size appears an optimum size for the particular reaction under study.
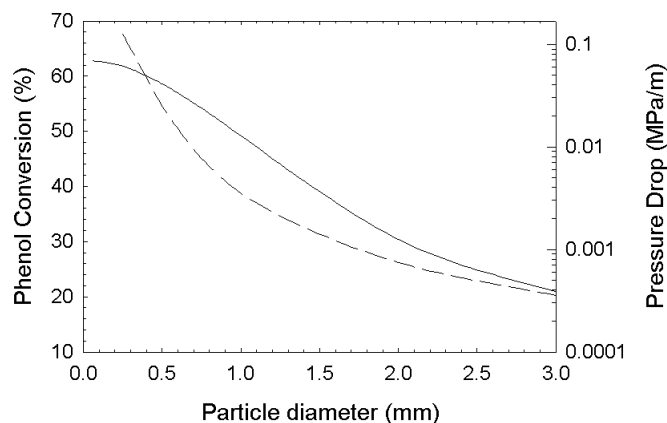

Figure 5.5: Phenol conversion (−) and pressure drop (- -) as a function of particle diameter. Rest of operating conditions: Table 5.3

Intermediate selectivity

Mass transfer limitations can also affect reaction selectivity. In Fig. 5.6, the acetic acid concentration is plotted as a function of the phenol conversion without and with oxygen mass transfer limitations. The first case is calculated directly from the kinetic equations assuming a pseudo-homogeneous model. The second case has been obtained for 3-mm particle size and low liquid superficial velocity (0.1 mm/s). From Fig. 5.6 it is seen that oxygen limitations impede the build up of acetic acid, probably because the reaction pathway route from benzoquinones to maleic and eventually to refractory acetic acid exhibits a higher partial order than that leading to CO_2 via the oxalic and formic acid routes. This result is further corroborated when intermediate COD concentration is plotted as a function of phenol conversion with and without mass transfer limitations (Fig. 5.6b).
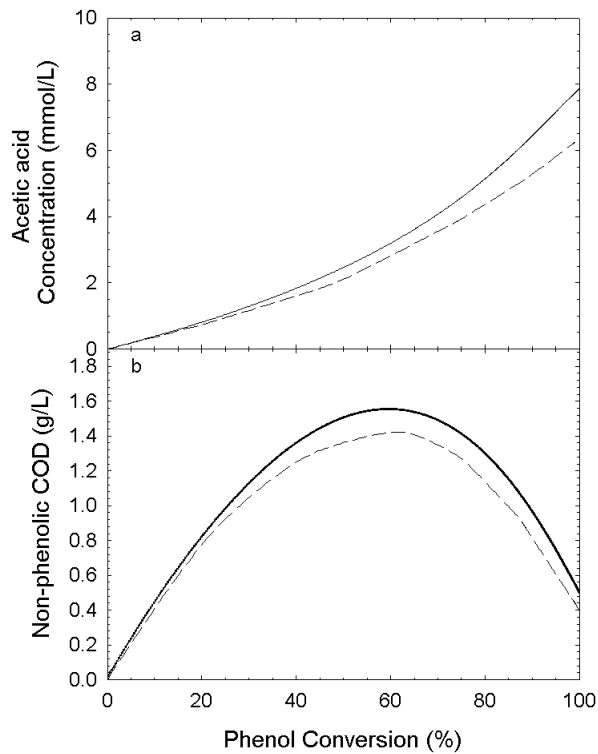

Figure 5.6: (a) Acetic acid concentration and (b) intermediate COD, as a function of phenol conversion calculated in the absence ($-$) and the presence (- -) of mass transfer limitations. (For mass transfer limitation $u : l$=0.1 mm/s. Rest of operating conditions: Table 5.3

Detailed or phenol reaction kinetics

The numerical solution of the comprehensive reaction-transport model when mass transfer resistances are important is obviously much more tedious than that for the single lumping phenol consumption reaction. A simple solution to reduce numerical effort consists in using first the one-equation reaction model to solve for phenol consumption. Then, the corresponding COD reduction and intermediate product distributions, the pseudo-homogeneous model can be obtained for the same phenol conversion that was shown before to result in similar prediction of product selectivity.

Simulations using the detailed kinetic model only slightly affected phenol concentration profiles, because of the slightly lower oxygen consumption due to partial oxidation of the intermediate products, as shown exemplarily in Fig. 5.7. This indicates that considering reaction Eq. 4.1 as a lumping reaction is a reasonable approximation when the focus is only on phenol conversion.
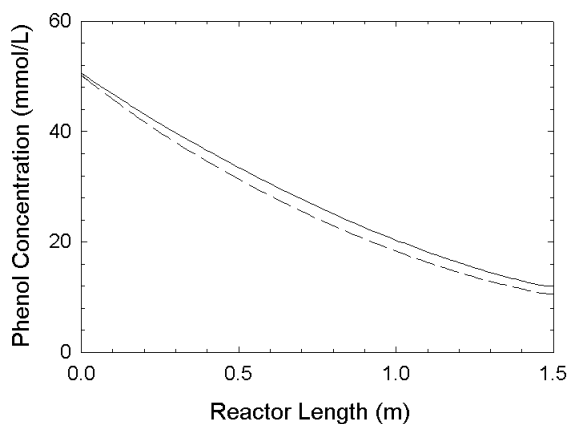

Figure 5.7: Phenol concentration profile along the reactor considering only phenol degradation (−), and the detailed kinetic model (- -). u_l=0.2 mm/s. Rest of operating conditions: Table 5.3

5.2.2   Non-isothermal reactor model

Like other wastewater treatment methods (WAO, incineration etc.), CWAO is carried out above ambient temperature. From a point of view of process economics, it is essential to exploit the heat released by the exothermic oxidation reactions. To do this, adiabatic operation of the reactor is to be preferred, as claimed for the WAO process [38]. In the following, the influence of operating or design parameters, such as inlet phenol concentration, gas superficial velocity, and inlet temperature on the adiabatic temperature rise and phenol conversion is studied.

At first, the influence of water evaporation at adiabatic operation conditions is examined. The simulation of an adiabatic TBR showed that water evaporation can have a substantial effect on reactor performance. In Fig. 5.8 both the adiabatic temperature rise (ATR) and phenol conversion attained with and without water evaporation are plotted as a function of gas superficial velocity. The plots are parameterised for two liquid superficial velocities corresponding to high (a) and low (b) phenol conversions. For a low liquid superficial velocity and phenol conversions above 99% (Fig. 5.8a), a temperature rise of 36 - 39 K is attained neglecting evaporation. When accounting for the evaporation flux required to saturate the gas phase with water at increasing temperature, the predicted ATR and phenol conversion drops down to 8 - 18 K and 90%, respectively. These results provide evidence that water evaporation must be accounted for in CWAO reactor design and scale up calculations. However, for high liquid superficial velocities (Fig. 5.8b), i.e. low phenol conversions, differences in ATR and phenol conversion caused by evaporation effects are minor, the larger difference in phenol conversion being only 5%. Regarding ATR, the differences are lower than those encountered at high phenol conversions and range between 15% and 40% depending on gas superficial velocity.

It is interesting to note that there exists a maximum in the ATR with gas flow rate (see Fig. 5.8). As long as oxygen is fed in quantities up to 110% ($u_g = 0.5 \; mm/s$) of the stoichiometric ratio, ATR and phenol conversion enhance strongly with increasing gas flow rate, both for high (Fig. 5.8a) and low (Fig. 5.8b) liquid superficial velocities. A further rise in gas flow rate only improves slightly conversion, while ATR may decrease considerably, especially when water evaporation is accounted for. This observation agrees well with the strategy employed in WAO where in most plants 110% oxygen excess is used [38]. For high phenol conversions (Fig. 5.8a) ATR peaks at 18 K and then decreases steadily to ca. 8 K at higher superficial velocities. On the other hand, for the high liquid superficial velocity (Fig. 5.8b) the maximum is at 7.5 K and the minimum at 6 K, suggesting that water evaporation is not influential for low phenol conversions. This could explain why Tukac and Hanika [19] did not obtain an ATR lower to that expected without evaporation effects, although it cannot explain why they reported a value even higher.

Another important reaction parameter to be studied is phenol inlet concentration. For first order power law reaction rates with regard to the substrate, typical of CWAO, and no mass transfer limitations, higher phenol feed concentration should result in an increase in both conversion and ATR. When external and/or internal mass transfer limitations occur,
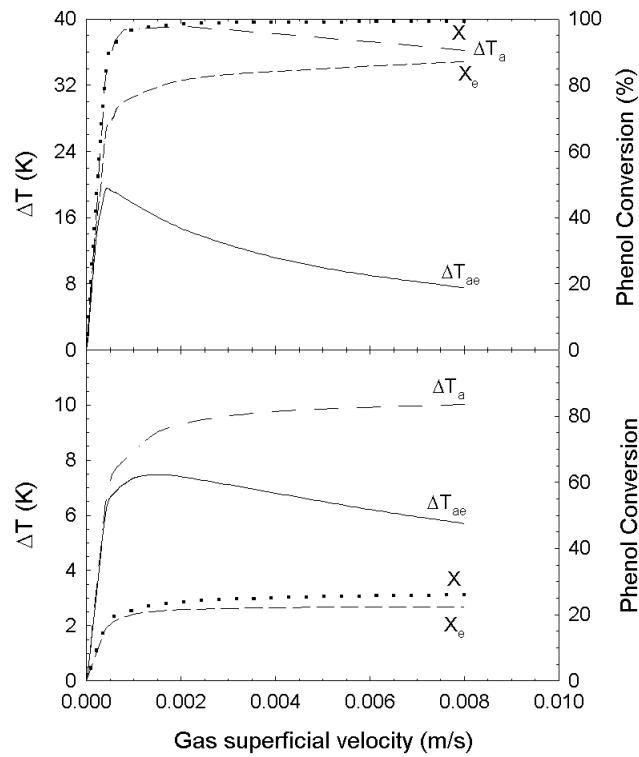
Figure 5.8: Adiabatic temperature rise and phenol conversion as a function of gas superficial velocity. (a) u_l=0.2 mm/s, (b) u_l=1 mm/s, Rest of operating conditions: Table 5.3. (-···-) Temperature rise neglecting evaporation, (···) conversion neglecting evaporation, (--) conversion with evaporation, (−) Adiabatic temperature rise with evaporation.
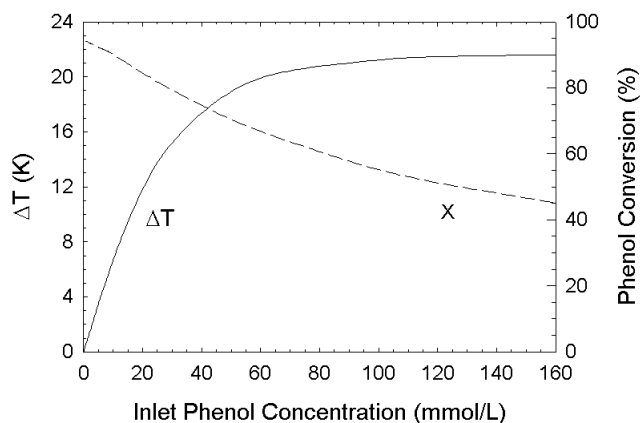
Figure 5.9: Adiabatic temperature rise $(-)$ and phenol conversion (- -) as a function of phenol inlet concentration. $u_l = 0.2 \; mm/s$, $u_g = 0.5 \; mm/s$. Rest of operating conditions: Table 5.3.

this might not be observed. For example in Fig. 5.9, the ATR and phenol conversion are plotted as a function of phenol feed concentration in presence of internal diffusion limitations. In all simulations 110% oxygen excess was set by adequately adjusting the u_g. Phenol conversions decrease with increasing phenol concentration in the whole range studied. On the other hand, ATR increases sharply with phenol concentration up to 30 $mmol/L$, and then starts to level off. This effect cannot be explained solely by the decreasing conversion with increasing inlet phenol concentration, since, as can be deduced also from Fig. 5.9, these magnitudes are not inversely proportional. Therefore, ATR level off should be attributed also to the higher evaporation rates necessary to saturate the increasing gas flow rates used to maintain the 110% oxygen excess.

In Fig. 5.10 the effect of the effluent inlet temperature on ATR and phenol conversion is presented (the remaining operating conditions are kept the same). As expected, higher inlet temperature increases almost linearly phenol conversion. This is not true for ATR that rises linearly between 390 and 410 K, to reach a flat maximum at 425 K and then diminishes. At low inlet temperatures, water vapour pressure is small and heat release due to the reaction dominates in the heat balance, thus producing temperature rise. However, as vapour pressure increases exponentially with temperature, the heat release is progressively compensated by enhanced water evaporation leading to a maximum in ATR and subsequently to its decrease.

Detailed calculation of the heat exchange unit to recover the heat released during the pollutant abatement is beyond the scope of this study. Nevertheless, preliminary calculations considering a simple counter-current double pipe heat exchanger show that CWAO ($T_0 = 433$ K) requires only half of the exchange area required by WAO ($T_0 = 553$ K, [10]), to preheat the inlet stream in the inlet reactor temperature and to auto-thermally operate the plant.
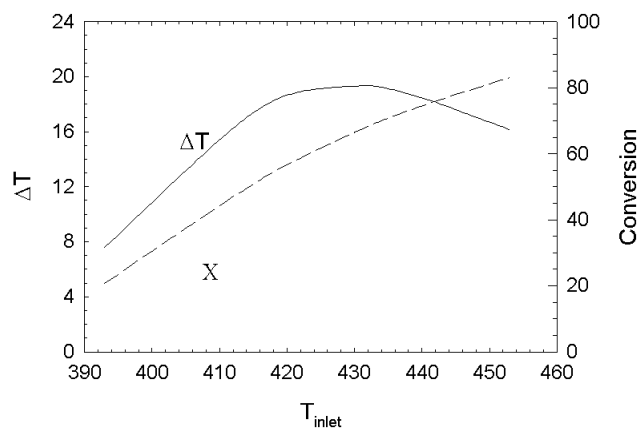
Figure 5.10: Adiabatic temperature rise $(-)$ and phenol conversion (- -) as a function of inlet temperature. $u_l = 0.2 \ mm/s$, u_g=0.5 mm/s. Rest of operating conditions: Table 5.3.

5.2.3 Conclusions

A comprehensive diffusion-reaction TBR model was successfully developed and validated against experimental data obtained in a laboratory TBR. the developed model is capable to coherently predict the effect of the different key parameters involved in the complex CWAO of phenol. This gives support to use the model with confidence in the scale-up of the CWAO of phenol from a laboratory reactor to a pilot plant. The following outcomes from this numerical study can be pointed out.

At typical operating conditions of CWAO the oxidation of phenol may be either gas or liquid reactant limited. A sensitivity study found out that intraparticle diffusion and, under complete wetting, gas - liquid and liquid - solid mass transfer influence the reactor performance. In agreement with experimental results reported in the literature, simulations showed that for a phenol solution of 53 mol/m^3, phenol conversion in a bed with partially wetted particles can double that obtained in a bed with fully wetted particles. Thus, the determination of the catalyst wetting degree is of outmost importance. The build-in of a detailed reaction network, accounting explicitly for the main intermediate phenol oxidation products, only slightly altered phenol degradation profiles. For almost-complete phenol conversion non-phenolic COD can be about 20% lower when strong mass transfer limitations are present.

Non-isothermal simulations evidenced that evaporation must be taken into account in scale up and adiabatic CWAO reactor design. Neglecting evaporation can lead to erroneous calculation of the exit stream temperature and phenol conversion, especially at high conversions. Adiabatic Temperature Rise depends strongly on phenol inlet concentration

and the superficial velocity of the gas stream. In agreement with the observations for the WAO, its is maximum when oxygen excess is around 110%. Furthermore, during CWAO an increase in the inlet substrate concentration can produce a decrease in conversion, without any further increase in the ATR. Finally, the ATR exhibits a maximum with inlet temperature, as with increasing inlet temperature the increased phenol conversion is counterbalanced by the increased water vapour pressure, and the need to evaporate more water to saturate the gas stream.

Chapter 6

Conclusions and Outlook

Conclusions

The ensemble of the outcomings of this work allow responding to the main objective postulated: the experimental and theoretical study of the CWAO of phenol using an adequate catalyst and multiphase reaction and reactor system. As a first milestone, the CWAO process employing active carbon and a TBR was proven to be a very effective treatment for the remedation of moderately concentrated aqueous phenol solutions. In agreement with theoretical consideration, the CWAO of phenol was found to be considerably enhanced when the reactor was operated in cocurrent downflow of gas-liquid. The gas-liquid mass transfer is often a limiting step in solid catalysed multiphase reactions and the partial wetting of the catalyst particles, a characteristic of TBRs operating in the trickle regime, has a significant effect on the reactor performance. However, one should be aware that for non-diluted exothermic reaction systems, the heat control becomes a critical issue and upflow operation may be preferred.

The non metallic and inexpensive catalyst tested, Active Carbon, exhibited both stable and considerably higher activity compared to a commonly used copper oxide catalyst. Almost complete phenol conversion (>99%) along with a COD reduction of 85% were obtained at low space times, 160^oC and low pressures oxygen partial pressures, ranging from 0.1 to 0.2 MPa. Ongoing experimental studies indicate that AC is also active for a variety of toxic organic pollutants, thereby reinforcing the high potential of the CWAO-AC process for its broad application to the abatement of industrial effluents.

The second milestone certainly is the original use of a robust stochastic optimisation algorithm in the development of more realistic kinetic models that are able to describe in detail the complex parallel - consecutive reaction network of the catalytic phenol oxidation in the liquid phase. Up to date, the state of art in CWAO kinetic modelling relies on the use of only simple phenol or COD destruction or lumped intermediate kinetics. In a first case study, using experimental data of phenol CWAO over a copper oxide catalyst, it could be demonstrated that a stochastic optimisation algorithm, termed Simulated Annealing, avoids the problems of local optima frequently encountered in nonlinear multiparameter estimation when using a classical gradient based algorithm like the Levenberg-Marquardt. The selected kinetic model for the copper oxide catalyst

accounted for all the main reaction intermediates detected and precisely predicted their concentration space time profiles, over the whole range of temperatures and pressures studied. For the AC catalyst, the experimental data indicate that phenol degradation proceeds via two distinct routes. One route is in agreement with the classical pathway that leads to the formation of benzoquinone, while a second route should exist to explain the formation of the not before detected 4-HBA. It becomes clear that the mechanism of phenol over AC differs from that over the CuO catalyst. Related results suggest that the phenol oxidation over the AC starts via the formation of a coke layer that probably participates in the reaction through a complex redox cycle. The proposed kinetic model for the AC did not explicitly considered this postulated redox mechanism. However it accounted for all intermediates and successfully described the experimental intermediate - space time profiles.

In the following, the obtained kinetic model was implemented in a phenomenological transport reaction model of the TBR. The model behaviour was tested through a sensitivity study and the reactor model was then successfully validated against the reaction data obtained in the laboratory TBR. It can be pointed out that the correct determination of all the involved key hydrodynamic and transfer parameters is a very delicate task and when improperly done, will wipe off the benefits of a sophisticated description of the underlying process chemistry and physics. The validated model allowed studying numerically the scale up of the laboratory TBR to a pilot scale reactor. In the scale up process, the partial wetting and pore diffusion were highlighted to determine the overall reactor performance at the fixed operating conditions. The feature of non-isothermal reactor operation clearly evidenced that water evaporation at CWAO conditions cannot be neglected. As a result, the adiabatic temperature rise is drastically reduced (by a factor of 2) and thereby the conversion of the target compound. The inclusion of the heat balance revealed that the adiabatic reactor performance is optimal for a feed that contains oxygen in a 110% excess, what is in perfect agreement with the feed conditions typically used in industrial WAO units. Summarising, the behaviour of a catalytic multiphase system is a result of complex interactions between reaction kinetics, hydrodynamics and heat-mass transfer. A correct interpretation of the experimental observation is impossible without an adequate reactor model that will enable to predict the influence of the key operation parameters on the reactor performance. Thus, the disponibility of such a model is a potential tool to correctly guide the design and scale up of multiphase reactors minimising experimental efforts, that are costly, time consuming and often difficult to carry out.

Outlook

The design of multiphase reactors is shown to combine different areas of chemistry and chemical engineering and obviously it is impossible to treat all of them exhaustively in one PhD work. Thus, and in particular for the CWAO of organic pollutants, several open topics are worth to be addressed in detail by future research work in order to improve the understanding and the industrial implementation of CWAO in the remediation of organic pollutants.

One important field of action is certainly extend the kinetic study using both the AC catalyst and a variety of common organic pollutants, to elucidate the complex oxidation mechanism and the role of the formed coke layers in this process. In addition, parallel studies of structural analysis of different ACs should allow characterising the AC surface to provide the means for the optimisation of its catalytic performance either by oxidative surface modification, or by proper manufacturing design.

A second promising option to improve the performance and process economics of CWAO should reinforce the study of combined processes of adsorption reaction cycles and chemical oxidation followed by biological treatment, or the use of dynamic processes like the periodic operation of the TBR. In this context, the development of dynamic non-isothermal reactor model is of outmost importance to aid the design and scale up of such complex processes.

In the context of modelling, one can stress on the general need of more in-depth studies that focus on the determination of hydrodynamic and mass transfer parameters of relevant industrial reaction systems and conditions. Besides the better understanding of multiphase systems, the availability of such parameters would greatly improve the reliability of model aided design and scale up of multiphase processes.

Bibliography

[1] R.B. Jackson, S.R. Carpenter, C.N. Dahm, D.M. McKnight, R.J. Naiman, S.L. Postel, and S.W. Running, Water in a Changing World, http://www.epa.gov/watertrain/step9esa.html

[2] R.K. Turner, D. Pearce, I. Bateman, Environmental Economics, The Johns Hopkins University Press, Baltimore, 1993, p.20

[3] METCALF and EDDY INC., Wastewater Engineering: Treatment, Disposal, and Reuse, 3rd edition, revised by: G. Tchobanoglous, F.L. Burton, McGraw-Hill, New York, 1991, p.17

[4] C.F. Foster, Biotechnology and Wastewater Treatment, Cambridge University Press, Cambridge, 1985, p.303

[5] http://www.epa.gov/tri/

[6] T. C. Voice, Activated carbon adsorption, Standard Handbook of Hazardous Waste Treatment and Disposal, H.M. Freeman (ed), McGraw-Hill, New York, 1988

[7] J.J. Santoleri, Liquid-Injection Incinerators, Standard Handbook of Hazardous Waste Treatment and Disposal, H.M. Freeman (ed), McGraw-Hill, New York, 1988

[8] S. C. Rowat, Medical Hypotheses 52 (1999) 389.

[9] F.J. Zimmermann, Chem. Eng. 25 (1958) 117.

[10] W. M. Copa, W. B. Gitchel, Wet Oxidation, Standard Handbook of Hazardous Waste Treatment and Disposal, H.M. Freeman (ed), McGraw-Hill, New York, 1988

[11] V. S. Mishra, V. V. Mahajani, J. B. Joshi, Ind. Eng. Chem. Res. 34 (1995) 2.

[12] R. Andreozzi, V. Caprio, A. Insola, R. Marotta, Catalysis Today 53 (1999) 51.

[13] F. Luck, Catalysis Today 27 (1996) 195.

[14] J. Barrault, M. Abdellaoui, C. Bouchoule, A. Majeste, J.M. Tatibouet, A. Louloudi, N. Papayannakos, N.H. Gangas, Applied Catalysis B: Environmental 27 (2000) L225.

[15] B. Legube, N. Karpel Vel Leitner, Catalysis Today 53 (1999) 61.

[16] S. Imamura, Ind. Eng. Chem. Res. 38 (1999) 1743.

[17] R.J. Bigda, Chem. Eng. Prog. 91 (1995) 62

[18] A. Fortuny, J. Font, A. Fabregat, Appl. Cat. B: Environ. (1998) .

[19] V. Tukac, J. Hanika, J. Chem. Technol. Biotechnol. 71 (1998) 262.

[20] J. Qin, Q. Zhang, K. T. Chuang, Appl. Cat. B: Environ. 29 (2001) 115.

[21] T. Nunoura, G. H. Lee, Y. Matsumura, K. Yamamoto, Chem. Eng. Sci. 57 (2002) 3061.

[22] Y. Matsumura, T. Urase, K. Yamamoto, T Nunoura, J. Supercritical Fluids 22 (2002) 149.

[23] A. Fortuny, C. Bengoa, J. Font, A. Fabregat, J. Hazard. Mater. 64 (1999) 181.

[24] S. Hamoudi, F. Larachi and A. Sayari, J. Catal. 177 (1998) 247.

[25] Z.Y. Ding, M.A. Frisch, L. Li, E.F. Gloyna, Ind. Eng. Chem. Res. 35 (1996) 3257.

[26] D. R. Grymonpre, W. C. Finney, B. R. Locke, Chem. Eng. Sci. 54 (1999) 3095.

[27] L. Szpyrkowicz, C Juzzolino, S. N. Kaul, S Daniele, M D. De Faveri, Ind. Eng. Chem. Res. 39 (2000) 3241.

[28] C. Dominguez, J. Garcia, M. A. Pedraz, A. Torres, M. A. Galan, Catalysis Today

[29] Y. G. Adewuyi, Ind. Eng. Chem. Res. 40 (2001) 4681.

[30] P. E. Savage, S. Gopalan, T. I. Mizan, C. J. Martino, E. E. Brock, AICHE J. 41 (1995) 1723

[31] M.P. Dudukovic, Catalysis Today, 48 (1999) 5.

[32] H. Schmieder, J. Abeln, Chem. Eng. Technol. 22 (1999) 11.

[33] I. Polaert, A. M. Wilhelm, H. Delmas, Chem. Eng. Sci. 57 (2002) 1585.

[34] A.T. Castellari, P.M. Haure, AIChE J. 41(6) (1995) 1593

[35] V. Tukac, J. Hanika, Unsteady State Wet Oxidation in Trickle Bed Reactor, 3rd European Congress of Chemical Engineering, 26-28 june 2001, Nurenberg, Germany

[36] S. T. Kolaczkowski, P. Plucinski, F. J. Beltran, F. J. Rivas, D. B. McLurgh, Chem. Eng. J. 73 (1999) 143.

[37] F. Luck, Wet Air Oxidation: past present and future, Catalysis Today 53 (1999) 81.

[38] H. Debellefontaine, J. N. Foussard, Waste Management 20 (2000) 2

[39] J. Donlagic, J. Levec, Appl. Catal. B: Environ. 17 (1998) L1.

[40] Y.I. Matatov-Meytal, M. Sheintuch, Ind. Eng. Chem. Res. 37 (1998) 309.

[41] J. E. Atwater, J. R. Akse, J. A. McKinnis, J. O. Thompson, Chemosphere 34 (1997) 203.

[42] S. Hamoudi, A. Sayari, K. Belkacemi, L. Bonneviot, F. Larachi, Catalysis Today 62 (2000) 379.

[43] L. Oliviero, J. Barbier Jr., D, Duprez, A. Guerrero-Ruiz, B. BAchiller-Baeza, I. Rodriguez-Ramos, Appl. Cat. B: Environ. 25 (2000) 267.

[44] S-K Kim, S-K Ihm, Ind. Eng. Chem. Res. 41 (2002) 1967.

[45] P. Gallezot, N. Laurain, P. Isnard, Appl. Cat. B: Environ 9 (1996) L11.

[46] J. Barbier Jr., F. Delanoe, F. Jabouille, D. Duprez, G. Blanchard, P. Isnard, J. Catal. 177 (1998) 378.

[47] P. Gallezot, S. Chaumet, A. Perrard, P. Isnard, J. Catal. 168 (1997) 104.

[48] S. Duprez, F. Delano, J. Barbier, P. Isnard, G. Blanchard, Catal. Today 29 (1996) 317.

[49] J. C. Beziat, M. Besson, P Gallezot, S. Durecu, Ind. Eng. Chem. Res. 38 (1999) 1310.

[50] J. C. Beziat, M. Besson, P. Gallezot, S. Durecu, J. Catal. 182 (1999) 129.

[51] H. T. Gomes, J. L. Figueiredo, J. L. Faria, Appl. Cat. B: Environ. 27 (2000) L217.

[52] H. T. Gomes, J. L. Figueiredo, J. L. Faria, Catalysis Today 75 (2002) 23.

[53] A. A. Klingoffer, R. L. Cerro, M. A. Abraham, Catalysis Today 40 (1998) 59.

[54] J. Barbier Jr., L. Oliviero, B. Renard, D. Duprez, Catalysis Today 75 (2002) 29.

[55] R. Ukropec, B. F. M. Kuster, J. C. Schoten, R. A. van Santen, Appl. Cat. B: Environ. 23 (1999) 45.

[56] H. Takayama, Q. Jiang-Yan, K. Inazu, K. Aika, Chemistry Letters (1999) 377.

[57] W. An, Q. Zhang, Y. Ma, K. T. Chuang, Catalysis Today 64 (2001) 289.

[58] Q. Zhang, K.T. Chuang, Appl. Cat. B: Environ. 17 (1998) 321.

[59] Q. Zhang, K.T. Chuang, Environ. Sci. Technol. 33 (1999) 3641.

[60] A. Pintar, M. Besson, P. Gallezot, Appl. Cat. B: Environ. 30 (2001) 123.

[61] A. Pintar, M. Besson, P. Gallezot, Appl. Cat. B: Environ. 31 (2001) 275.

[62] J. Rivas, S. T. Kolaczkowski, F. J. Beltran, D. B. McLurgh, Appl. Cat. B: Environ. 22 (1999) 279.

[63] L. Oliviero, J. Barbier Jr., D. Duprez, H. Wahyu, J. W. Pnton, I. S. Metcalf, D. Mantzavinos, Apll. Cat. B: Environ. 35 (2001) 1.

[64] D-K Lee, D-S Kim, Catalysis Today 63 (2000) 249

[65] T.-L. Huang, J. M. Maccines, K. R. Cliffe, Wat. Res. 35 (2001) 2113.

[66] J. E. Atwater, J. R. Akse, J. A. McKinnis, J. O. Thompson, Appl. Cat. B: 11 (1996) L11.

[67] Q. Zhang, K.T. Chuang, Ind. Eng. Chem. Res.37 (1998) 3343.

[68] A. Santos, P. Yustos, B. Durban, F. Garcia-Ochoa, Ind. Eng. Chem. Res. 40 (2001) 2773.

[69] A. Santos, P. Yustos, B. Durban, F. Garcia-Ochoa, Environ. Sci. Technol. 35 (2001) 2828.

[70] A. Santos, P. Yustos, A. Quintanilla, S. Rodriguez, F. Garcia-Ochoa, Appl. Cat. B: Environ. 39 (2002) 97.

[71] A. Santos, E. Barroso, F. Garcia-Ochoa, Catalysis Today 48 (1999) 109.

[72] A. Fortuny, C. Ferrer, C. Bengoa, J. Font, A. Fabregat, Catal. Today 24 (1995) 79.

[73] A. Fortuny, C. Bengoa, J. Font, F. Castells, A. Fabregat, Catal. Today 53 (1999) 107.

[74] C. Miro, A. Alejandre, A. Fortuny, C. Bengoa, J. Font, A. Fabregat, Water Research 33 (1999) 1005

[75] A. Alejandre, F. Medina, A. Fortuny, P. Salagre, J.E. Sueiras, Appl. Catal. B: Environ. 16 (1998) 53.

[76] A. Alejandre, F. Medina, P. Salagre, A. Fabregat, J.E. Sueiras, Appl. Catal. B: Environ. 18 (1998) 307.

[77] A. Alejandre, F. Medina, X. Rodriguez, P. Salagre, J. E. Sueiras, J. Catal. 188 (1999) 311.

[78] A. Alejandre, F. Medina, X. Rodriguez, P. Salagre, Y. Cesteros, J. E. Sueiras, Appl. Cat. B: Environ 30 (2001) 195.

[79] A. Pintar, G. Bercic, J. Levec, Chem. Eng. Sci. 52 (1997) 4143.

[80] A. Pintar, J. Levec, Ind. Eng. Chem. Res. 33 (1994) 3070.

[81] A. Pintar, J. Levec, J. Catal. 135 (1992) 345.

[82] H. Ohta, S. Goto, H. Teshima, Ind. Eng. Chem. Fundam. 19 (1980) 180.

[83] S. Hocevar, J. Batista, J. Levec J. Cata. 184 (1999) 39.

[84] S. Hocevar, U. O. Krasovec, B. Orel, A. S. Arico, H. Kim, Appl. Cat. B: Environ.28 (2000) 113.

[85] S. T. Hussain, A. Sayari, F. Larachi, J. Catal., 201 (2001) 153.

[86] S. T. Hussain, A. Sayari, F. Larachi, Appl. Cat. B: Environ. 34 (2001) 1.

[87] S. Hamoudi, F. Larachi, G. Cerrella, M. Cassanello, Ind. Eng. Chem. Res. 37 (1998) 3561.

[88] H. Chen, A. Sayari, A. Adnot, F. Larachi Appl. Cat. B: Environ. 32 (2001) 195.

[89] P. M. Alvarez, D. McLurgh, P. Plucinsky, Ind. Eng. Chem. Res. 41 (2002) 2147.

[90] A. Sadana, J.R. Katzer, J. Catal. 35 (1974) 140.

[91] A. Sadana, J.R. Katzer, Ind. Eng. Chem., Fundam. 13 (1974) 127.

[92] C. J. Chang, C.-M. Ko, K. Shih, Chem. Eng. Com. 156 (1996) 201.

[93] St. Christoskova, M. Stoyanova, Wat. Res. 35 (2001) 2073.

[94] J.F. Akyurtlu, A. Akyurtlu, S. Kovenklioglu, Catal. Today 40 (1998) 343.

[95] C. J. Chang, S-S Li, K. Shih, J. Chem. Technol. Biotechnol., 64 (1995) 245.

[96] A. Pintar, J. Levec, Chem. Eng. Sci. 47 (1992) 2395.

[97] A. Pintar, J. Levec, 49 (1994) 4391.

[98] G. Baldi, S. Goto, C. K. Chow, J. M. Smith, Ind. Eng. Chem. Proc. Des. Dev. 13 (1974) 447.

[99] S. Goto, J. M. Smith, AIChE J. 21 (1974) 714.

[100] J. Levec, J. M. Smith, AIChE J. 22 (1976) 159.

[101] J. Levec, M. Herskowitz, J. M. Smith, AIChE J., 22 (1976) 919.

[102] C. de Leitenbourg, D. Goi, A. Priavera, A. trovarelli, G. Dolceti, Appl. Cat. B: Environ. 11 (1996) L29.

[103] K. Belkacemi, F. Larachi, A. Sayari, J. Catal. (2000) 224.

[104] S. Hamoudi, K. Belkacemi, F. Larachi, Chem. Eng. Sci. 54 (1999) 3569.

[105] S. Hamoudi, K. Belkacemi, A. Sayari, F. Larachi, Chem. Eng. Sci. 56 (2001) 1275.

[106] A. Fortuny, C. Miro, J. Font, A. Fabregat, Catal. Today 48 (1999) 323.

[107] F. Stüber, I. Polaert, H. Delmas, J. Font, A. Fortuny, A. Fabregat, J. Chem. Technol. Biotechnol. 76 (2001) 743.

[108] P.K. Lim, A. John, P. Champakial, Ind. Eng. Chem. Process. Des. Dev. 22 (1983) 477.

[109] R.W. Coughlin, Ind. Eng. Chem. Prod. Res. Dev. 8 (1969) 12.

[110] A. Schraut, G. Emig, H. Hofmann, J. Catal., 112 (1988) 221.

[111] M.F.R. Pereira, J.J.M. Orfao, J.L. Figueiredo, Appl. Cat. A: General 184 (1999) 153.

[112] M.F.R. Pereira, J.J.M. Orfao, J.L. Figueiredo, Appl. Cat. A: General 196 (2000) 43.

[113] M.F.R. Pereira, J.J.M. Orfao, J.L. Figueiredo, Appl. Cat. A: General 218 (2001) 307.

[114] P. M. Alvarez, D. McLurgh, P. Plucinsky, Ind. Eng Chem. Res. 41 (2002) 2153.

[115] Q. Zhang, K.T. Chuang, Can. J. Chem. Eng. 77 (1999) 399.

[116] X. Hu, L. Lei, H. P. Chu, P. L. Yue, Carbon 37 (1999) 631.

[117] Q. Wu, X. Hu., P. L. Yue, X. S. Zhao, G. Q. Lu, Appl. Cat. B: Envorn. 32 (2001) 151.

[118] H.S. Joglekar, S.D. Samant, J.B. Joshi, Wat. Res. 25 (1991) 135.

[119] H.R. Devlin, I.J. Harris, Ind. Eng. Chem. Fundam. 23 (1984) 387.

[120] L. Li, P. Chen, E.F. Gloyna, AIChE J. 37 (1991) 1687.

[121] A. Eftaxias, J. Font, A. Fortuny, J. Giralt, A. Fabregat, F. Stüber, Appl. Cat. B: Environ. 33 (2001) 175.

[122] R.S. Willms, A.M. Balinsky, D.D. Reible, D.M. Wetzel, D.P. Harrison, Ind. Eng. Chem. Res. 26 (1987) 148.

[123] F. Vogel, J. Harf, A. Hug, P.R. von Rohr, Environ. Prog. 18 (1999) 7.

[124] F.J. Rivas, S.T. Kolaczkowski, F.J. Beltrn, D.B. McLurgh, Chem. Eng. Sci. 53 (1998) 2575.

[125] V. Tufano, Chem. Eng. Technol. 16 (1993) 186.

[126] G. Neri, A. Pistone, C. Milone, S. Galvagno, Appl. Cat. B: Environ 38 (2002) 321.

[127] R.V. Shende, J. Levec, Ind. Eng. Chem. Res. 39 (2000) 40.

[128] R.V. Shende, J. Levec, Ind. Eng. Chem. Res. 38 (1999) 2557.

[129] R.V. Shende, J. Levec, Ind. Eng. Chem. Res. 38 (1999) 3830.

[130] R.V. Shende, V.V. Mahajani, Ind. Eng. Chem. Res. 33 (1994) 3125.

[131] R.V. Shende, V.V. Mahajani, Ind. Eng. Chem. Res. 36 (1997) 4809.

[132] L. Li, N. Crain, E. F. Gloyna, Water Environ. Res. 68 (1996) 841.

[133] S. H. Lin, S. J. Ho, C. L. Wu, Ind. Eng. Chem. Res. 35 (1996) 307.

[134] Q. Zhang, K.T. Chuang, AIChE J. 45 (1999) 145.

[135] I. Polaert, A. Fortuny, F. Stüber, A. Fabregat, H. Delmas, Competitive adsorption of phenolic compounds in water on activated carbon, 14th Internacional Congress of Chemical and Process Engineering, 27-31 August 2000, Praha, Czech Republic

[136] M.J. Birchmeier, C.G. Hill Jr., C.J. Houtman, R.H. Atalla, I.A. Weinstock, Ind. Eng. Chem. Res. 39 (2000) 55.

[137] H.S. Fogler, Elements of chemical reactor engineering, New Jersey, Prentice-Hall, 1992

[138] G. F. Froment, K. B. Bischoff, Chemical Reactor Analysis and Design, John Wiley and Sons, New York, USA, 1990, p. 403

[139] S. P. Asprey, Y. Naka, J. Chem. Eng. Japan 32 (1999) 328.

[140] G. Buzzi-Ferraris Cat. Today 52 (1999) 125.

[141] R. Fletcher, Practical methods of optimisation, Great Britain, John Wiley & Sons, 1987

[142] C. Y. Gau, M. A. Stadtherr, 94 AIChE Symp. Ser. (1999) 445.

[143] C. A. Schnepper, M. A. Stadtherr, Comp. Chem. Eng. 20 (1996) 187.

[144] W. R. Esposito, C. A. Floudas, Comp. Chem. Eng. 22 (1998) S213.

[145] A. Corana, M. Marchesi, C. Martini, S. Ridella, ACM Trans. Math. Software 13 (1987) 26 2.

[146] M. F. Cardoso, R. L. Salcedo, S. F. Azevedo, Comp. Chem. Eng. 20 (1996) 1065.

[147] W. L. Goffe, G. D. Ferrier, J. Rogers, J. Econometrics 60 (1994) 65.

[148] Z. Belohlav, P. Zamostny, P. Kluson, J. Volf, Can J. Chem. Eng. 75 (1997) 735

[149] P. Zamostny, Z. Belohlav Computers & Chemistry 23 (1999) 479.

[150] R. Moros, H. Kalies, H. G. Rex, St. Scaffarczyk, Comp. Chem. Eng. 20 (1996) 1257.

[151] D. Wolf, R. Moros, Chem. Eng. Sci. 52 (1997) 1189.

[152] A. Eftaxias, J. Font, A. Fortuny, A. Fabregat, F. Stüber, Comp. Chem. Eng. 26 (2002) 1725.

[153] P.R. Bevington, D.K. Robinson, Data reduction and error analysis for the physical sciences, second edition, McGraw-Hill, New York, 1992

[154] P. Bilardello, X. Joulia, M. Le Lann, H. Delmas, B Koehret, Comp. Chem. Eng. 17 (1993) 517.

[155] R.V. Chaudhari, Challenges in Modelling and Scale-up of Trickle Bed Reactor, Indo-French Workshop on Trickle Bed Reactors for Cleaner and Greener Environment, K.D.P. Nigam (ed.), 7-8 November 2002, Delhi, India

[156] M. P. Dudukovic, F. Larachi, P. L. Mills, Catalysis Reviews 44 (2002) 123.

[157] A. Gianetto, V. Specchia, Chem. Eng. Sci. 47 (1992) 3197.

[158] P.L Mills, R.V. Chaudhari, Catalysis Today 48 (1999) 17.

[159] S. Goto, J. Levec, J.M. Smith, Catal. Rev. Sci.-Eng. 15 (1977) 187.

[160] J. Levec, A. Pintar, Catalysis Today 24 (1995) 51.

[161] J. Levec, Chem. Biochem. Eng. Q. 11 (1997) 47.

[162] F. Stüber, Selctivity in a three phase catalytic reactor, PhD. Thesis, INP Toulouse, 1995 (in french)

[163] G. Biardi, G. Baldi, Catalysis Today 52 (1999) 223.

[164] Y. T. Shah, Gas-Liquid-Solid Reactor Design, McGraw Hill, New York, 1979

[165] P. A. Ramachandran, R. V. Chaudhari, Three Phase Catalytic Reactors, Gordon and Breach science publishers, 1983, New York

[166] M.H. Al-Dahhan, F. Larachi, M.P. Dudukovic, A. Laurent, Ind. Eng. Chem. Res. 36 (1997) 3292.

[167] J. Hanika, K. Sporka, V. Ruzicka, R. Pistek, Chem. Eng. Sci. 32 (1977) 525.

[168] M.H. Al-Dahhan, M.P. Dudukovic, Chem. Eng. Sci. 50(15) (1995) 2377.

[169] Y. Wu, M.R. Khadilkar, M.H. Al-Dahhan, M.P. Dudukovic, Ind. Eng. Chem. Res. 35 (1996) 397.

[170] D. Tsamatsoulis, M.H. Al-Dahhan, F. Larachi, N. Papayannakos, Chem. Eng. Comm. 185 (2001) 67.

[171] M.R. Khadilkar, Y. Wu, M.H. Al-Dahhan, M.P. Dudukovic, M. Colakyan, Chem. Eng. Sci. 51 (1996) 2139.

[172] C. Julcour, R. Jaganathan, R.V. Chaudhary, A.M. Wilhem, H. Delmas, Chem. Eng. Sci. 56(2) 557.

[173] R.V. Chaudhari, R. Jaganathan, P.S. Mathew, C. Julcour, H. Delmas, AIChE J. 48 (2002) 110.

[174] Stüber, H. Delmas, Ind. Eng. Chem. Res.in press.

[175] M. Herskowitz, J. M. Smith, AIChE J. 29 (1983) 1.

[176] F. Stüber, A.M. Wilhem, H. Delmas, Chem. Eng. Sci. 51 (1996) 2161.

[177] I. Iliuta, F. C. Thyrion, O Muntean, Chem. Eng. Sci. 35 (1996) 4579.

[178] M.V. Rajashekharam, R. Jaganathan, V. Chaudhari, Chem. Eng. Sci. 53 (1998) 787.

[179] S. Ishigaki, S. Goto, Catalysis Today 48 (1999) 31.

[180] K.D.P. Nigam, I. Iliuta, F. Larachi, Chem. Eng. Proc. 41 (2002) 365.

[181] C.S.L. Narasimha, R.P. Verma, A. Kundu, K.D.P. Nigam, AIChE J. in press

[182] A. Lakota, J. Levec, R.G. Carbonell, AIChE J. 48(4) (2002) 731.

[183] Y. Jiang, M.R. Khadilkar, M.H. Al-Dahhan, M.P. Dudukovic, AIChE J. 48(4) (2002) 701.

[184] Y. Jiang, M.R. Khadilkar, M.H. Al-Dahhan, M.P. Dudukovic, AIChE J. 48(4) (2002) 716.

[185] I. Iliuta, F. Larachi, B.P.A. Grandjean, G. Wild, Chem. Eng. Sci. 54 (1999) 5633.

[186] I. Iliuta, F. Larachi, B.P.A. Grandjean, Ind. Eng. Chem. Res. 37 (1998) 4542.

[187] A.A. El-Hisnawi, D.Sc. Thesis, Washington University, St. Louis, Missouri, 1981.

[188] Y. Wu, M.H. Al-Dahhan, M.R. Khadilkar, M.P. Dudukovic, Chem. Eng. Sci. 51 (1996) 2721.

[189] C. Julcour, F. Stüber, J.M. Le Lann, A.M: Wilhelm, H. Delmas, Chem. Eng. Sci. 54 (1999) 2391.

[190] C. Julcour, R.V. Chaudhari, J.M. Le Lann, A.M: Wilhelm, H. Delmas, Chem. Eng. Process. 41 (2002) 311.

[191] C.N. Satterfield, AIChE J., 21(2) (1975) 209.

[192] I. Iliuta, F. Larachi, B.P.A. Grandjean, Chem. Eng. Sci. 54 (1999) 4099.

[193] K.B. Van Gelder, P.C. Borman, R.E. Weenink, K.R. Westerterp, Chem. Eng. Sci. , 45 (1990) 3171.

[194] V. Balakotaiah, E.L. Christoforatou, D.H. West Chem. Eng. Sci. 54 (1999) 1725.

[195] V. Tukac, J. Vokal, J. Hanika, J. Chem. Techn. Biotechnol. 76 (2001) 506.

[196] C.B. Maugans, A. Akgerman, Water Research, 37 (2) (2003) 319.

[197] F. Larachi, I. Iliuta, K. Belkacemi, Catlysis Today, 64 (2001) 309.

[198] I. Iliuta, F. Larachi, Chem. Eng. Proc. 40 (2001) 175.

[199] A. Fortuny, Catalytic Oxidation of Phenolic Effluents in a Trickle Bed Reactor, PhD. Thesis, Universitat Rovira i Virgili (in catalan)

[200] L.S. Clesceri, A.E. Greenberg, R.R. Trusell, M.A. Franson, Standard methods for the examination of water and wastewater, 17th edition, American Public Health Association and American Water Works Association, Washington, USA, 1989.

[201] Visual Numerics, IMSL Fortran subroutines for mathematical applications, (1997)

[202] N. Metropolis, A. Rosenbluth, M. Rosenbluth, A. Teller, E. Teller, J. Chem. Phys. 21 (1953) 1087.

[203] S. Kirkpatrik, C. D. Gellat, M. P. Vecchi, Science 220 (1983) 671.

[204] W. H. Press, B. P. Flannery, S. A. Teukolsky, W. T. Vetterling, Numerical Recipes: Fortran Edition, Cambridge University Press, Cambridge, UK, 1986, p. 326

[205] M. Locatelli, J. Opt. Theory and Appl. 104 (2000) 121.

[206] Finlayson, B.A., Nonlinear analysis in chemical engineering, McGraw-Hill, New York, pp. 113, 1980.

[207] Constantinides, A. Applied numerical methods with personal compouters, McGraw-Hill, New York, 1987.

[208] R.C. Reid, J.M. Prausnitz, B.E. Pauling, The properties of gases and liquids, McGraw-Hill, New York, 1987.

[209] Chemical Rubber Company, CRC handbook of chemistry and physics, CRC Press, Cleveland, Ohio, 2000

[210] D. M. Himmelblau, J. Chem. Eng Data, 5 (1960) 10.

[211] A.E. Sáez, R.G. Carbonell, AIChE J. 31 (1985) 52.

[212] Z-S Mao, T-Y. Xiong, J. Chen, Chem. Eng. Sci. 48(15) (1993) 2697.

[213] I. Iliuta, F. Larachi, B.P.A. Grandjean, Chem. Eng. Res. Des. 77 (1999) 759.

[214] S. Pich, F. Larachi, I. Iliuta, B.P.A. Grandjean, J. Chem. Technol. Biotechnol. 77 (2002) 989.

[215] S. Goto, J. M. Smith, AIChE J. 21 (1974) 706.

[216] P.Z. Lu, J.M. Smith, M. Herskowirtz, AIChE J. 30 (1984) 500.

[217] J. Font, A. Fabregat, Comput. Chem. Eng. 21 (1997) 719.

[218] J. Font, Personal Communication

[219] A. Lakota, J. Levec, AIChE J. 36(9) (1990) 1444.

[220] M. Paradowska, PhD Thesis, Universitat Rovira i Virgili, (In progress)

Biographical Note

NAME :   **Athanasios Eftaxias**
Date of Birth : 31/08/1974

EDUCATION:

- 1992-1998: Diploma in Metallurgical Engineering, National Technical University of Athens, Athens, Greece

- 1998-2000: Research Suficiency (Suficiencia Investigadora), Universitat Rovira i Virgili, Tarragona, Spain

PUBLICATIONS

- A. De Jong, **A. Eftaxias**, F. Trabelsi, F. Recasens, J. Sueiras, and F. Stüber, *Solvent Screening for the Supercritical Hydrogenation of Polyunsaturated Hydrocarbons Using VLE Calculations*, Ind. Eng. Chem. Res. 40, 3225-3229 (2001)

- **Eftaxias A.**, Font J., Fortuny A., Giralt J., Fabregat A., Stüber F., *Kinetic Modelling of Catalytic Wet Air Oxidation of Phenol by Simulated Annealing*, Appl. Catal. B: Environm. 33, 175-190 (2001)

- **Eftaxias A.**, Font J., Fortuny A., Fabregat A., Stüber F., *Nonlinear kinetic parameter estimation using simulated annealing*, Comp. Chem. Eng. 26, 1725-1733 (2002)

- **Eftaxias A.**, Font J., Fortuny A., Fabregat A., Stüber F., *CWAO of phenol in a Trickle Bed Reactor using Active Carbon and $CuO/\gamma - Al_2O_3$: Catalytic Performance*, Water Research, Submited

- **Eftaxias A.**, F. Larachi, Stüber F., *Modelling of a Trickle Bed Reactor for the Catalytic Wet Air Oxidation of Phenol*, Can. J. Chem. Eng., Submited

CONTRIBUTIONS IN CONGRESSES WITH PROCEEDINGS

- **Eftaxias A.**, Font J., Fortuny A., Fabregat A., Stüber F., *Catalytic Wet Air Oxidation of Phenol in a Trickle Bed Reactor: A complex kinetic model*, Poster presentation, ECCE-3, Nuremberg, Germany, 2001

- **Eftaxias A.**, , Font J., Fortuny A., Fabregat A., Stüber F., *A detailed kinetic model for the catalytic wet air oxidation of phenol in a trickle bed reactor*, Oral presetation, 3rd Panhellenic Congress of Chemical Engineering, 31/05/2001-02/06/2001, Athens, Greece

- **Eftaxias A.**, F. Trabelsi, F. Recasens, J. Sueiras, and F. Stüber, *Preselection of superciritical solvent for hydrogentation reactions via VLE calculations*, Poster Presentation, II Jornadas de Ingeniería Termodinámica, 7 - 8/ 06/2001, Tarragona, Spain

- Stüber F., **Eftaxias A.**, M. Paradowska, M.E. Suarez, Font J., Fortuny A., Fabregat A., *Tailored oxidation of organic pollutants in wastewater*, Oral Presentation, Indo-French Workshop on Trickle Bed Reactors for Cleaner and Greener Environment (Ed. K.D.P. Nigam), 7-8/11/2002, Delhi, India

- **Eftaxias A.**, F. Larachi, Stüber F., *Modelling of a Trickle Bed Reactor for the Catalytic Wet Air Oxidation of Phenol*, 6th International Congress on Gas-Liquid and Gas-Liquid-Solid Reactor Engineering, 17-20/08/2003, Vancouver, Canada (accepted)

VISITS IN OTHER RESEARCH GROUPS

- 25/11/2001 to 25/02/2002: Visit to the research group of Dr. F. Larachi at the Department of Chemical Engineering, Laval University, Quebec, Canada